Molecular and Mechanical Functions of the Intermediate Filament Protein GFAP

Oscar M.J.A. Stassen

2016

About the cover: The most remarkable characteristic of intermediate filaments is their beautiful structure of ca. 10 nm thick filaments in aligned bundles. One of the intermediate filaments proteins got its name from this structure, as stated in the 1978 paper by Werner Franke: "Vimentin: From the Latin word vimentum, used to describe arrays of flexible rods, both ordered ones (e.g., lattices, filigrees, and wicker-work) and nonordered ones (e.g., brushwood)." But as is described in this thesis, there's more to intermediate filaments than that structure, we have to look beyond the wicker-work.

Cover Design: Heleen Bijkerk

Layout: Oscar Stassen

Molecular and Mechanical Functions of the Intermediate Filament Protein GFAP

Ὁ βίος βραχύς,
ἡ δὲ τέχνη μακρή,
ὁ δὲ καιρὸς ὀξύς,
ἡ δὲ πεῖρα σφαλερή,
ἡ δὲ κρίσις χαλεπή.

Table of contents

Scope and Outline

Scope and Outline

The brain is an extremely complex organ, consisting of a diversity of neuronal and non-neuronal cells. Each cell type plays its specific role, with various classes of neurons specialized in rapid communication, oligodendrocytes providing myelination, and astrocytes involved in maintenance of blood brain barrier, energy homeostasis, neurotransmitter homeostasis, and modulation of neuronal signalling. For all these neural cell types there are stem and progenitor cells in varying degrees of multipotency/differentiation, involved in the maintenance and plasticity of the brain and of great interest for potential therapeutic applications. In addition to these cells of the neural lineage, there are microglia providing the brain's innate immune system and endothelial cells forming vessels for blood perfusion.

This thesis is centred on astrocytes, which is a main type of macroglia. Astrocytes play an important role in the communication between the different cell types in the brain and are considered as integrators of information in the brain. These cells are known to react to brain injury and are activated in neurodegeneration (i.e. reactive gliosis), which coincides with a change in shape and function. It is now recognized that astrocytes are a heterogeneous cell population, and different classes are being identified. A clear subtype are the astrocytes in the neurogenic niches, which are the stem cells of the adult brain. An accumulation of genetic mutations in these cells during cell division is thought to be an origin of astrocytic brain tumours.

A hallmark protein of astrocytes is the cytoskeletal protein Glial Fibrillary Acidic Protein (GFAP), which is highly upregulated in reactive gliosis. GFAP is a member of the intermediate filament family and its gene encodes at least 10 different splice isoforms. One of these isoforms, GFAPδ, is enriched in stem cell niches in the human brain, whereas the canonical GFAPα isoform is expressed in astrocytes throughout the brain. Both isoforms have also been described in astrocytoma, and they have been linked to tumour malignancy. This thesis describes the role of GFAP in astrocyte biology in health and disease from cell biological, molecular biological, and biophysical perspectives.

In **Chapter 1** we reviewed GFAP and other members of the intermediate filament family as integrators of mechanics, cell-cell communication and key molecules in shaping the structure of complex tissues. GFAP is a highly regulated gene and a prominent marker protein of astrocytes in brain injury and pathology.

In **Chapter 2** we studied the transcriptomic changes in an astrocyte cell line in an *in vitro* injury model. Surprisingly, we found that the injury model we applied (stretching cells) only induced minor transient changes in the cell astrocytoma cells. To pinpoint what could be the cause of this low response, we varied the extracellular

matrix coating of the injury model, we attempted to induce injury response by means of purinergic signalling, and we studied primary human astrocyte response to injury. However, none of the conditions showed the expected astrocytosis response.

To gain more insight in the changes in cells induced by modulation of the GFAP network, we performed functional studies on cells with a specific recombinant expression of GFAP isoforms in **Chapter 3.** Here we showed that GFAPδ has a very prominent effect on the state of the IF-network, as at high expression levels the network is disrupted and the intermediate filaments form a juxtanuclear collapse, whereas GFAPα is incorporated into the network. Using GFP-tagged GFAP isoforms, we also showed GFAPδ has a different exchange rate between GFAP in solution and in the network, both when the network had collapsed and when the network was still intact. In addition, an effect of GFAPδ expression on cell shape was shown, and this was linked to a difference in focal adhesion size. Surprisingly, despite the prominent effect on the network, no effect of GFAPδ expression was found on cellular motility or proliferation compared to control, although a distinction was found between the proliferating fraction of GFAPα expressing primary human astrocytes, and GFAPδ primary astrocytes.

In **Chapter 4** we performed an analysis of GFAP isoform expression in relation to astrocytoma malignancy based on the Cancer Genome Atlas patient database. This revealed that the GFAPδ/α ratio increases with increasing astrocytoma grade. To find whether this isoform ratio controls gene expression in astrocytoma, we modulated GFAP isoforms in astrocytoma cell lines by recombinant expression or knockdown and performed transcriptome analysed on a microarray platform. Overlapping these GFAP regulated genes with the genes correlating in astrocytoma with GFAPδ/GFAPα ratio, resulted in 8 GFAP regulated targets relevant for tumour biology and/or prognosis.

In **Chapter 5** we studied the effect of the absences of GFAP and vimentin on gene expression in the healthy mouse brain. We studied the transcriptome of astrocytes, which were acutely isolated from the cortex of wild type, *GFAP$^{-/-}$* (GFAPko), and *GFAP$^{-/-}$ Vim$^{-/-}$* (VIM-GFAPko) mice. Because of the crosstalk between astrocytes and microglia, we also studied the effect of the absence of GFAP on microglia, which surprisingly resulted in more pronounced changes in gene expression than in the GFAPko astrocytes themselves. This showed in a nutshell that GFAP might have more impact through modulation of cell-cell signalling and modulation of cellular interaction with the ECM, than in the astrocytes themselves. This was corroborated by our observation that in the astrocytes the extracellular region and cellular surface/periphery were amongst the most significantly regulated annotations.

The effects of GFAP modulation on the viscoelastic properties of the IF network were studied in **Chapter 6.** Intermediate filaments are implied in cellular mechanics, therefore we anticipated that modulating the GFAP content of the IF network would change the viscoelastic properties of the IF cytoskeleton. We took an approach of extracting the IF network from cells and to remove other major cytoskeletal components to study the network properties in a relatively defined setting. Before extraction we introduced fluorescent beads in the cells, which were captured inside the network structures. The motions of these beads were analysed using particle tracking microrheology. As a proof of method study, we found this procedure is viable, and particles are restricted in their mobility with addition of GFAP isoforms to the network, although further definition, control of the system and more sensitive methods are required to make quantitative statements about the effect of different GFAP isoforms on the network.

Finally, in **Chapter 7**, we discuss the most promising targets from our transcriptome analyses. We highlighted a couple of the recurring targets of GFAP modulations to crystallize which cellular processes are related to GFAP. This shows that GFAP has broad functions in cellular biology, but seems to be most important in cell-cell organization through ECM remodelling and growth factor signalling both in astrocytoma and in astrocytes. We identified two unexpected genes as possible targets downstream of GFAP modulation, and discuss how GFAP modulation might mechanistically exert its downstream effects.

Chapter

1

Glial Fibrillary Acidic Protein and Vimentin - cytoskeletal proteins at the crossroads of astrocyte cellular mechanics and signalling

Oscar M.J.A. Stassen
Elly M. Hol

The brain may well be the most complex system in the universe known to us. Every cell in the brain interacts with a multitude of highly specialized cells involved in either optimal neuronal communication or in the homeostasis of the central nervous system. Each cell has its own specific functions and properties. These individual cells, mainly neurons and glia, create an organized multicellular structure by interacting with and connecting to the extracellular matrix (ECM) and neighbouring cells, creating a structure of over 160 billion networking cells essential for all our conscious and unconscious brain functions (Azevedo et al., 2009). The cells reorganize the matrix and communicate with their direct and distant neighbours through various functional structures and signalling pathways to maintain a healthy organization and functioning of the brain. Much of this organization outside the cells is controlled by the configuration within the cell, provided by a great amount and diversity of proteins and peptides, each protein again with its own molecular structure and one or more functions.

One crucial structure in the organization of the cell is the cytoskeleton (Ingber, 1993). The cytoskeleton not only provides shape, motility, and structural scaffolding to the cell, but is also involved in signalling (outside-in and inside-out) (Jansen et al., 2015). The brain is an organ with highly specialized cell types and shapes, and correspondingly, brain cells contain a highly cell type-specific specialized cytoskeleton. The four main types of neural cells in the brain are the neurons and the several glia subtypes: the astrocytes, the oligodendrocytes, and the microglia. In general terms: neurons are electrically excitable cells highly specialized in rapid communication over long distances, astrocytes have important functions in brain homeostasis and neural communication (Sofroniew and Vinters, 2010), oligodendrocytes provide the brain with the fatty myelin to insulate the neurons (Bercury and Macklin, 2015), and microglia form the brain's innate immune system (Hanisch and Kettenmann, 2007). These cell types derive from distinct progenitors (Zeisel et al., 2015), each with a developmental or functional cell state characterized by a specific and often unique cytoskeletal composition (Bauer et al., 2009; Fanarraga et al., 2009; Gitik et al., 2010; Lariviere and Julien, 2004; Mamber et al., 2013).

Cytoskeleton

Every cell's cytoskeleton can consist of 4 distinct families of cytoskeletal proteins: actin filaments, microtubules, septins, and the intermediate filaments (IFs). Actin filaments and microtubules are ubiquitously present in all cells in the body and have been the subject of intense investigation over the last decades. Their role in cellular migration and intracellular transport makes them crucial components in

cellular survival and function (Gelfand and Bershadsky, 1991; Parsons et al., 2010). IFs have a thickness in between actin filaments (9 nm) and microtubules (25 nm), but were actually named IFs due to their 10 nm intermediate size in between thick (myosin) and thin (actin) filaments of skeletal muscle (Ishikawa et al., 1968). In 1976 glial filaments and neurofilaments were assigned "intermediate filaments" as their size was between microfilaments and microtubules (Yen et al., 1976). IFs were long considered to mainly have a role in the mechanical integrity of cells, but are now shown to have important signalling functions as well (Ivaska et al., 2007). Septins have recently been identified as a fourth cytoskeletal component. They have the ability to form ring- and filament-shaped structures required for organelles with specific membrane-shapes (Mostowy and Cossart, 2012).

IFs are a highly diverse group of proteins, comprising one of the largest protein families in vertebrates. This diversity in IF proteins is linked to cell type specific functions and architecture (Lowery et al., 2015). There are over 70 different mammalian IF members (see www.interfil.org), divided into 6 groups, based on structure and sequence homology. The nuclear Lamins (type V IFs) are represented by 2 genes in humans; Lamin A/C and Lamin B. The Lamins form the inside of the nuclear envelope, and accordingly it has been suggested that they originate from the oldest common eukaryotic ancestor, although it should be noted that plants do not have any IFs at all (Kollmar, 2015). Vertebrate cytoplasmic IFs are organized into the epithelial keratins (type I and II), non-Keratin self-assembling IFs (type III), neuronal self-assembling IFs (type IV), and non-self assembling and lens IFs (type VI) (Guérette et al., 2007). There are also classifications that assign Nestin and Synemin to the type IV category, and consider the lens IFs as a separate type due to the alternate assembly of these IF proteins into beaded filaments.

All of these different proteins are part of the IF family based on their related structure: they have a head domain, a rod domain, and a tail domain. The rod domain is very similar in the different classes of cytoskeletal IFs and can form a coiled coil through an IF-specific multimerization sequence (Herrmann et al., 2009). This structure allows the IF proteins to form a parallel dimer, that organizes into antiparallel tetramers, which will laterally assemble into the unit length filament (ULF) consisting of on average 32 monomers. These ULFs anneal longitudinally and compact to form the 10-nm filaments (Fig. 1). The antiparallel assembly step in the tetramer formation causes IFs to be unpolarized structures, making them unsuitable tracks for directed transport, this in contrast to Actin filaments and microtubules (Chernyatina et al., 2012; Strelkov et al., 2003).

Different tissues in the body have distinct IF expression profiles (Toivola et
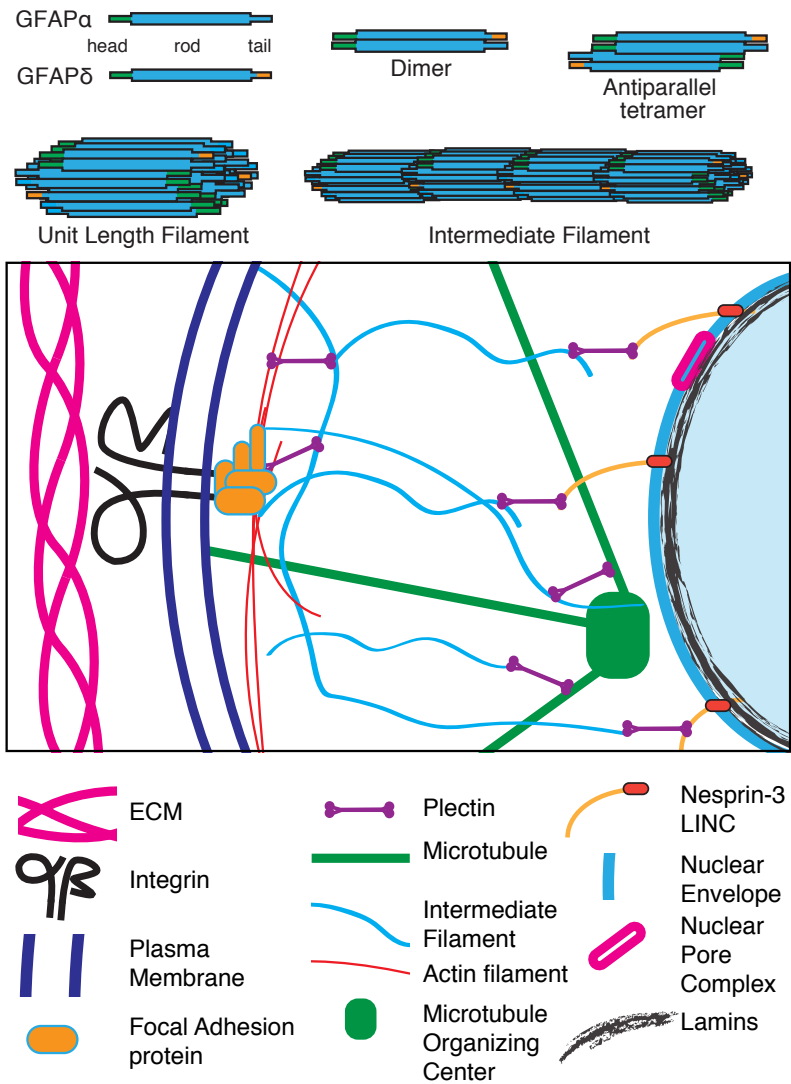
Figure 1. Intermediate filament assembly and integration into the cytoskeleton

Top: The monomers of GFAPα and GFAPδ can assemble into a dimer, that can form a staggered antiparallel tetramer.

Bottom: IFs as a part of the complete cytoskeletal network that physically bridges the extracellular matrix (ECM) outside of the cell to the DNA in the nucleus of the cell. IFs are connected to the ECM through transmembrane Integrins (alpha and beta subunits), that form the anchorage points for focal adhesion complexes. These transmembrane complexes interact with IFs through Plectin, Plectin connects IFs to other cytoskeletal components (microtubules and actin), and ultimately Nesprin-3 connects IFs to the nuclear envelope. Nesprin-3 is a part of the trans-nuclear membrane LINC complex, binding the nuclear IFs, the Lamins. The Lamins subsequently play a role in the organization of heterochromatin and euchromatin, and are likely involved in regulation of transcription.

al., 2005). In neural cells of the central nervous system (CNS), the most common IFs are the Neurofilaments and α-Internexin in neurons and neural progenitors, and GFAP, Nestin, Synemin and Vimentin (Vim) in astrocytes and radial glia. IF proteins in microglia and mature oligodendrocytes, if expressed at all in vivo, typically do not form filaments that are distinguishable by electron microscopy or immunofluorescence, although few reports do describe the presence of Vim positive microglia/macrophages in pathology or in vitro (Graeber et al., 1988; Jiang et al., 2012; Kachar et al., 1986; Massa et al., 1984; Yamada et al., 1992). GFAP is alternatively spliced and 10 isoforms have been described (Kamphuis et al., 2012; Middeldorp and Hol, 2011). GFAPα is the canonical isoform. GFAPδ has an alternative tail domain (Fig. 2), and cannot form homodimers or networks by itself, but can incorporate into GFAPα or Vim networks (Nielsen and Jørgensen, 2004; Perng et al., 2008). GFAPδ levels are typically $1/10^{th}$ of the GFAPα levels (Fig. 1).

The intermediate filament cytoskeleton of astrocytes

Astrocytes express four different IFs, Vim, GFAP, Synemin, and Nestin. Synemin and Nestin are type VI IFs that can not form filaments on their own, but are associated to the IF network (IFN). Although these two proteins are generally considered to be expressed in astrocytes, the expression levels of the proteins are highly heterogeneous in astrocytes throughout the brain, indicating a large molecular variation in astrocyte subtypes (Anderson et al., 2014; Oberheim et al., 2012). We will further focus on the other two, type III IFs. Vim and GFAPα are both able to form a network in a cell free system as well as in cells. Both Vim and GFAP have a distinct contribution to the ultrastructure in astrocytes, as the IFNs in Vim knockout (ko) and GFAPko astrocytes have a different ultrastructure best described as more compacted bundles with high density for VIMko, against lower contrast in electron microscopy, possibly more disperse filaments for GFAPko (Lepekhin et al., 2001; Menet et al., 2001).

Early functional studies on these filaments using either single GFAPko or double VIM-GFAPko mice revealed mild phenotypes (Liedtke et al., 1996; McCall et al., 1996; Pekny et al., 1995; Shibuki et al., 1996; Pekny et al., 1999). GFAPko mice showed enhanced neuronal long term potentiation in hippocampal neurons (McCall et al., 1996), and decreased long term depression in cerebellar parallel fiber-purkinje cell synaptic transmission, in addition to a reduced eye blink conditioning (Shibuki et al., 1996). Old GFAPko mice, over 12-18 months of age, are prone to white matter degeneration, poor white matter vascularization and variable increases in blood

brain barrier permeability (Liedtke et al., 1996).

Mutations in GFAP are the cause of Alexander's Disease (AxD) (Prust et al., 2011). This disease is, in homology to many other IF protein-related or IF associated protein-related diseases, caused by gain of function mutations that induce aggregation. This is the case for lamin, keratin, neurofilaments and GFAP (Opal and Goldman, 2013; Russell et al., 2004; West et al., 2016). The mutations in GFAP result in a GFAP assembly defect and accumulation/aggregation in Rosenthal fibers in the brain, as well as in a cell free system (Perng et al., 2006). AxD is a neurological disease, and the most severe form can have an onset before the age of 4 years, with a severe loss of white matter. Rosenthal fibers can also be found in cases of severe gliosis or pilocytic astrocytoma, and have been described in a mouse overexpressing wild type (wt) human GFAP, indicating that high concentrations of wt GFAP can also induce aggregation (Hagemann et al., 2005; Wippold et al., 2006).

Vim is a widely expressed protein in cells of mesenchymal origin. Surprisingly, despite its wide expression, the initially generated VIMko mice displayed no obvious phenotype (Colucci-Guyon et al., 1994). Further investigations of the VIMko revealed quite diverging phenotypic alterations, ranging from impaired wound healing to decreased dilation of arteries (Eckes et al., 2000; Henrion et al., 1997). In addition, mutations in Vim can cause cataract in the lens (Song et al., 2009).

It is thought that much of the mild effects found in IF ko models are due to redundancy, as often multiple IFs are expressed in a single cell type. However, knocking out GFAP and Vim does not lead to compensatory expression of other IFs and does not lead to severe defects in astrocytes, despite the lack of IF networks as shown by EM. This raises the question: what is then the biological significance of IF proteins? Many data currently point towards IFs as central regulators in different kinds of cellular stress. This includes mechanical (Russell et al., 2004), toxic (Asghar et al., 2015), and hyperglycaemic stresses (Alam et al., 2013). For Vim and GFAP in astrocytes, this has been investigated by exposing the double ko models to a plethora of pathological stimuli and crossing the mice with different mouse models for brain diseases (Hol and Pekny, 2015). The absence of Vim and GFAP resulted in attenuated astrocytosis after injury. Functionally, this attenuated astrocytosis often results in aggravated progression of early injury, although at a later stage the lack of a gliotic scar formation presents the CNS with enhanced capability for regeneration (Hol and Pekny, 2015). However a recent, possibly paradigm-shifting study found that in a model of spinal cord injury, induced regeneration of axons was inhibited by two different methods of astrocytosis ablation, and posed that the glial scar is in fact required, but not sufficient for axonal regeneration, although the contribution of

the IFs in this model was not investigated (Anderson et al., 2016). It has to be noted that astrocytosis or reactive gliosis is a broad and vague term, and has a different meaning in different brain injuries/diseases (Pekny et al., 2016). In the rest of this introduction we will present what is currently known about the function of GFAP and Vim.

Molecular functions of Vim and GFAP

GFAP and Vim are both type III IFs. A wealth of knowledge is available for Vim, as this protein has been most studied. There are many research papers in which GFAP is used as a marker for astrocytes, but studies on the function of GFAP are scarce. We compared the amino acid sequence of GFAP and Vim to get an indication of complementarity or redundancy between these two proteins (Fig. 2). We observed, by using ClustalOmega, a mean sequence homology between human GFAP and Vim of 53%. The most conserved part of the IF proteins is the rod domain, due to the heptad repeat sequence required to form the coiled coil quaternary structure in the dimer stage of the filament formation (Chernyatina et al., 2012). The rod and tail domain have a sequence homology of 64% and 48%, respectively. The head domain only shows 23% homology. The rod has a strictly conserved length for the coiled-coil domains, but head and tail length varies across IFs, although Vim and GFAP have an equal tail length (GFAP (α and δ) head: 62 amino acids (aa), Vim head: 96 aa, Vim and GFAPα tails: 62 aa, GFAPδ tail: 61 aa). Between the other GFAP splice isoforms there are also different tail and even rod lengths (Hol and Pekny, 2015), whether there are variations in the head has not yet been confirmed. The head domain is essential for filament assembly in most IFs, as the heads of IFs (including GFAP) are typically predicted to prefer low solvent exposure, implying a buried state inside the filament (Kornreich et al., 2015). The tail domain is not always required for longitudinal assembly, depending on total IF protein composition in the filament, but the tail can regulate filament assembly (Chen and Liem, 1994). The tail of IFs is often depicted as protruding from the filament, but whether the tail is ordered or disordered in structure, and whether the tail associates to the rod or protrudes and can form crosslinks to nearby filaments is highly dependent on IF type and even specific protein within the IF family (Kornreich et al., 2015). GFAP and Vim are both predicted to have disordered tails with high solvent accessibility (Kornreich et al., 2015).

The tail of Vim is not essential for formation of filaments, but has a stabilizing role. A sequence conserved in the tail of type III IFs (KTXEXRDG) influences lateral

and longitudinal assembly, and can associate with the Vim rod (Kouklis et al., 1991; McCormick et al., 1993). For GFAP, the tail has been shown to be required for homodimer assembly, although the conserved RDG sequence in the tail is not essential (Chen and Liem, 1994). For GFAPδ, the alternative tail domain results in inhibition of assembly, curiously not assigned to the omission of the RDG sequence, but to the gain of tail residues T411 and I412 (Nielsen and Jørgensen, 2004). The high number of serine, threonine and tyrosine residues in the heads and tails are potential targets for kinases, and indeed numerous of these potential phosphorylation sites have been confirmed experimentally. These sites, in addition to other less described post-translational modifications, are important for IF dynamics and interactions with IF associated proteins (IFAPs) (Omary et al., 2006). The observed variability in head and tail domains indicates functional differences between GFAPα, GFAPδ, and Vim (Fig. 2).

To study the cellular and molecular functions of proteins in cell culture, a powerful tool often used is interfering with the protein itself, which can be done by pharmacological agents, by genetically altering the expression level of the protein, or by inducing mutations in the protein to study the role of specific or multiple amino acids. In contrast to Actin and microtubules, there are not yet any specific pharmacological agents available for IFs that have been thoroughly characterized. A compound called Withaferin A induces disruption of the IFN, but also affects other pathways in the cell (Grin et al., 2012). More work on this is in progress and several approaches are becoming available, as recently reviewed (Ridge et al., 2016). Genetic approaches with modified IF proteins with deletions, mutated amino acids, or even domain swaps have been important in determining the domains that are required for the assembly into ULFs and the domains that enable longitudinal annealing into filaments (Chen and Liem, 1994; Herrmann et al., 1996; McCormick et al., 1993). In addition, phosphomutants have been used to study the role of phosphorylation in IF function (Tanaka et al., 2015). As the GFAP and Vim IFs themselves do not have any enzymatic function, we propose they can have two main modes of action. The first mode of action is through the mechanical properties they provide when forming a network, whereas the second is through IFs interacting with other cellular components, such as organelles or proteins and thus modulating the function of these interacting partners.

Mechanical properties of GFAP and Vim networks

Initially IFs were mainly regarded as contributors to cellular integrity. This was based on the multicellular networks that Keratins form in skin, and the fragile

skin and blistering diseases associated with Keratin mutations (McLean et al., 1994). Indeed upon stretching of keratinocytes, a remarkable 2-fold extension of the cells was achieved without rupturing (Fudge et al., 2008). Complete ablation of Keratin filaments in mice results in extensive skin damage, assigned to desmosomal disorganization (Bär et al., 2014). This points towards two different roles in mechanical resilience: IF's role in mechanical strength or intracellular integrity versus IF's role in cellular adhesion. However, in these Keratin mutants effects on mitochondrial composition and activity were also found, again demonstrating that IF function is not limited to mechanical structure, and that diseases due to IF ablation or dysfunction can be due to mechanical as well as signalling changes (Kumar et al., 2015).

In the cell, IFNs can provide mechanical sturdiness, but single filaments also have remarkable mechanical properties. For three different IF proteins probed with atomic force microscopy (AFM) in vitro, it has been demonstrated that the filaments can be stretched on average 2.6 fold with concomitant thinning of the filament, implying structural changes in the filament (Kreplak et al., 2005). In addition to this astonishing mechanical resilience of the single filament, networks of IFs also display remarkable properties in cell free systems. Networks of Vim display stress-stiffening behaviour, increasing their elastic modulus over 100-fold when the network is stressed (Lin et al., 2010a). This makes the IFN highly resilient to deformation. Vim and GFAP also contribute to the mechanical properties of the cell, although in astrocytes they are typically less prominently exposed to mechanical deformation in comparison to the skin (Lu et al., 2010; Mendez et al., 2014). Vim contributes to the elasticity of mouse embryonic fibroblasts as demonstrated by a decrease in the shear modulus G', a measure of mechanical stiffness, from 9 Pa to 4.5 Pa in VIMko fibroblasts as measured by active microrheology (Guo et al., 2013). This mechanical contribution to the cell contributes to the anchoring of organelles and the resistance of the cell to deformation. Induction of GFAP in astrocytes has been reported to have opposite mechanical consequences. In two studies, reactive astrocytes were generated, verified for GFAP increase, and subsequently mechanically tested by AFM. One study reported an increased stiffness, whereas the other reported a decreased stiffness of the astrocytes (Lu et al., 2010; Miller et al., 2009). This discrepancy could be attributed to the differences between the models, with an in vitro mechanical injury of isolated astrocytes in one experiment versus an intraocular pressure induced gliosis in Müller glial cells, followed by an isolation of the cells, in the other approach. In addition, astrocytosis is a complex process where more processes take place in the cell apart from GFAP and Vim upregulation (Pekny

et al., 2016). However, the expected mechanical effect of increased IF density would be an increased stiffness of the cells, based upon semiflexible polymer theory (Lin et al., 2010a). Depending on the IF protein and measurement method the stiffness of in vitro reconstituted IFNs increases with higher IF concentration, scaling with a power ranging from 0.5-2 to IF concentration, and resulting in elasticities of 1-10 Pa at low strains (Block et al., 2015; Lin et al., 2010a). In vivo this is more complex though, as composite networks consisting of multiple cytoskeletal proteins can behave differently depending on component interactions (Jensen et al., 2014).

GFAP networks can also be reconstituted in vitro from recombinant proteins (Perng et al., 2008). This approach has shown that the GFAP isoform GFAPδ induces a collapse of the IF network, but bulk rheological measurements on these in vitro networks have not yet been performed. Interestingly, Liedtke et al and Pekny et al reported softer consistencies of the CNS in the GFAPko and the VIM-GFAPko mice (Liedtke et al., 1996; Pekny et al., 1999).

Molecular interactions of GFAP and Vim in signalling

Driven by the identification of many diseases caused by IF mutations, the emergence of IF function in cell stress, and the correlation between IF expression and developmental state, many studies have proceeded to further clarify the role of IFs at a molecular level. This effort has generated a wealth of information on the biology of IFs, and showed the strikingly broad spectrum of processes that IFs play a role in. For Vim this spectrum extends, but is not limited to, regulation of cell adhesion, vesicle trafficking, migration, autophagy, and regulation of transcription factors, as extensively reviewed before (Ivaska et al., 2007).

Some of these processes have been mapped to specific interaction sites of Vim, which, when aligned to GFAP show practically no overlap (Fig. 2). Still, there is overlap between the functional processes GFAP and Vim are involved in. This will be further demonstrated per biological function in the following section.

Trafficking

Both Vim and GFAP are involved in trafficking of vesicles. A recent review on IFs in vesicle trafficking summarized the various described interactions with the Rab machinery, proteins that are responsible for regulating many steps in trafficking (Margiotta and Bucci, 2016). Direct mechanisms are emerging, as phosphorylation of the Vim head is required for recycling vesicle dependent integrin turnover, dependent on an interaction with PKCε (Ivaska et al., 2005). Another important pathway where Vim and/or GFAP were shown to have a role in, is the activation
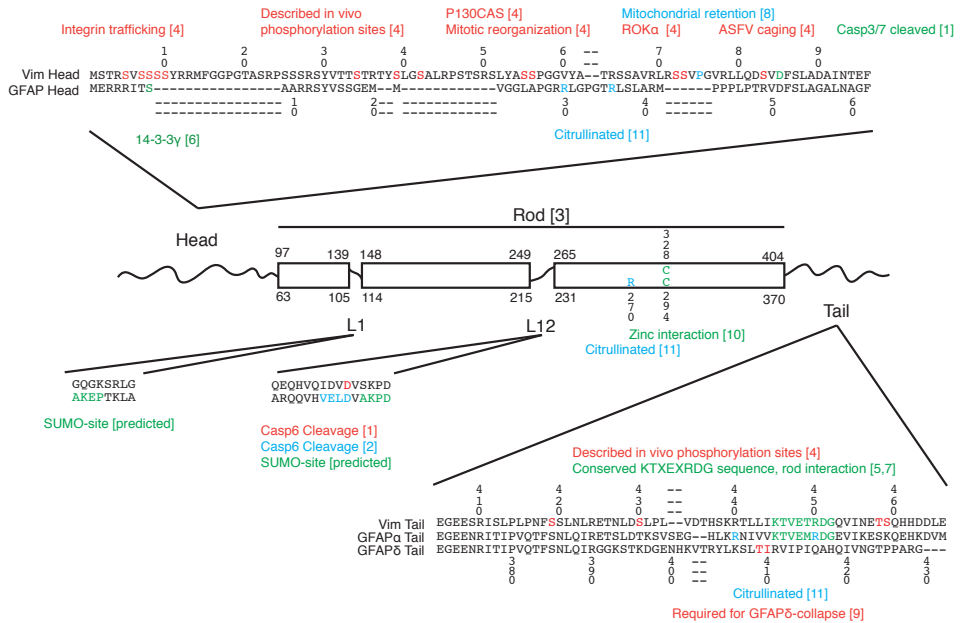
Integrin trafficking [4]   Described in vivo phosphorylation sites [4]   P130CAS [4]   Mitochondrial retention [8]   ROKα [4]   ASFV caging [4]   Casp3/7 cleaved [1]
Mitotic reorganization [4]

```
            1    2      3    4      5    6  --      7        8        9
            0    0      0    0      0    0  --      0        0        0
Vim Head  MSTRSVSSSSYRRMFGGPGTASRPSSSRSYVTTSTRTYSLGSALRPSTSRSLYASSPGGVYA~~TRSSAVRLRSSVPGVRLLQDSVDFSLADAINTEF
GFAP Head MERRRITS---------------AARRSYVSSGEM--M------------VGGLAPGRRLGPGTRLSLARM------PPPLPTRVDFSLAGALNAGF
          ---------------  1    2--  ------------        3        4      5        6
          ---------------  0    0--  ------------        0        0      0        0
```

14-3-3γ [6]   Citrullinated [11]

Head   Rod [3]   Tail

```
        97   139 148      249 265            404
        63   105 114      215 231            370
             L1      L12          328
                                  CC
                                  270 294
                                  R
                                  CC
```

Zinc interaction [10]
Citrullinated [11]

GQGKSRLG
AKEPTKLA

SUMO-site [predicted]

QEQHVQIDVDVSKPD
ARQQVHVELDVAKPD

Casp6 Cleavage [1]
Casp6 Cleavage [2]
SUMO-site [predicted]

Described in vivo phosphorylation sites [4]
Conserved KTXEXRDG sequence, rod interaction [5,7]

```
             4        4    --        4        4        4
             1        3    --        1        4        6
             0        0    --        0        0        0
Vim Tail   EGEESRISLPLPNFSSLNLRETNLDSLPL~~VDTHSKRTLLIKTVETRDGQVINETSQHHDDLE
GFAPα Tail EGEENRITIPVQTFSNLQIRETSLDTKSVSEG~~HLKRNIVVKTVEMRDGEVIKESKQEHKDVM
GFAPδ Tail EGEENRITIPVQTFSNLQIRGGKSTKDGENHKVTRYLKSLTIRVIPIQAHQIVNGTPPARG---
             3        3    4  --       4        4        4
             8        9    0  --       1        4        3
             0        0    0  --       0        0        0
```

Citrullinated [11]
Required for GFAPδ-collapse [9]

Figure 2. Alignment of Vimentin, GFAPα and GFAPδ sequence focussed on head and tail domains, and the L1 and L1-2 region.

Borders of domains are placed as described in (Chernyatina et al., 2015), the region of Vim residue 77 up to the rod is a precoil region of the head, with the ability to form a coiled coil. Various known in vivo phosphorylation sites and interactions or cleavage sites for vimentin are annotated, mainly based upon (Ivaska et al., 2007). For GFAP known annotations, interactions, cleavage sites, and predicted sumoylations are indicated. Two more sumoylation sites were predicted in coil 2 (278-AKHE and 338-LKDE). Interaction between GFAPδ and Presenilin 1 depends on presence of both the GFAPδ tail and rod domain (Nielsen et al, 2002). Colours only used for recognition of annotation text. SUMO: Sumoylation, Casp: Caspase, ROKα: ROCK2, ASFV: African Swine Fever Virus. Refs: [1] Byun et al., 2001; [2] Chen et al., 2013; [3] Chernyatina et al., 2015; [4] Ivaska et al., 2007; [5] Kouklis et al., 1991; [6] Li et al., 2006; [7] mccormick et al., 1993; [8] Nekrasova et al., 2011; [9] Nielsen et al., 2004; [10] Perez-Sala et al., 2015; [11] Jin et al., 2013

mediated endocytosis of Jag1, a component of Notch signalling (Wilhelmsson et al., 2012). Whether this takes place through an interaction with Jag1 or (regulators of) the trafficking machinery, remains to be investigated. Altered trafficking increases differentiation of neural stem cells into neurons and increases engraftment in VIM-GFAPko (Widestrand et al., 2007; Wilhelmsson et al., 2012). Cocultures of neurons and astrocytes revealed that knocking out GFAP results in enhanced neuronal survival, related to increased ECM and adhesion protein expression (Menet et al., 2001). Astrocytes lacking GFAP and stimulated by ionomycin, ATP or interferon-γ, show a difference in the motility of vesicles, depending on vesicle subtype (Potokar et al., 2010; Vardjan et al., 2012). Interestingly, GFAP is enriched in gliosomes,

vesicles excreted by astrocytomas and also containing proteins from the exocytotic machinery. These vesicles play a role in glutamate transport (Milanese et al., 2009). Links for GFAP in receptor trafficking emerge from the accumulation of GLT1 in intracellular vesicles after dibutyryl cAMP treatment in GFAPko astrocytes, whereas in wt this induction results in localization of GLT1 to the membrane (Hughes et al., 2004). Due to the importance of vesicle release and trafficking in astrocytes, it is likely that the scope and importance of GFAP control over trafficking in astrocytes is much larger than so far established and may contribute to gliotransmitter release.

Vim and GFAP also play a role in autophagy, which is related to vesicle trafficking. Autophagy is induced in AxD by the accumulation of GFAP, and the proteasome is inhibited by the mutant form of GFAP (Tang et al., 2010). Mechanistically this may be due to an interaction between GFAP in oligomeric form and LAMP-2A, a lysosomal membrane protein that stabilizes chaperone mediated autophagy. Vim has been shown to interact with the vesicle adaptor complex AP-3. Both LAMP-2A and AP-3 are involved in the formation and sorting of autophagic vacuoles (Bandyopadhyay et al., 2010; Styers, 2004).

Motility

Vim and GFAP are both involved in cell migration and motility (Ivaska et al., 2007). In astrocytes from VIM-GFAPko mice, the loss of GFAP and Vim has an incremental effect on migration in vitro, meaning that the motility is further reduced with loss of each IF (Lepekhin et al., 2001). For Vim various mechanisms and interactions have been discovered that influence migration (Helfand et al., 2011), integrin trafficking (Ivaska et al., 2005), and on a more mechanistic level, migration related kinase modulation (Dave et al., 2013; Havel et al., 2015; Vuoriluoto et al., 2011). This effect on migration has been clearly demonstrated by the injection of Vim protein into the cell, which can induce lamellipod formation and migration (Helfand et al., 2011; Mendez et al., 2010).

The role of GFAP in migration is less straightforward. Loss of GFAP leads to increased invasiveness and reduced adhesion of astrocytoma cells (Rutka et al., 1999). This contrasts with the reported reduction of migration in GFAPko astrocytes (Lepekhin et al., 2001). The effects on migration are not only mediated by the interactions with the focal adhesions, but also by the polarization of cells and positioning of the nucleus (Dupin et al., 2011). Interestingly, the siRNA mediated knockdown of Vim and nestin alone resulted in a loss of cellular control on nuclear positioning, but GFAP by itself did not, although when GFAP is knocked down in the

context of Vim and nestin knockdown, the effect on nuclear positioning is enhanced (Dupin et al., 2011). The interactions GFAP has with the adhesion machinery are not known yet, although first indications for an effect on focal adhesion size have been described by us (Moeton et al., 2016).

Cell-cell adhesion

IFs are also important for cell-cell contacts. This is essential in keratinocytes where Keratins form a network structure spanning multiple cells at desmosomes and hemidesmosome formation. Vim also forms complexes with cell-cell interaction proteins. One of these adhesion proteins is VE-cadherin in endothelium, which is coupled to the IFN via desmoplakin (Vincent et al., 2004). Vim also co-localizes and probably interacts with α-catulin, a novel catenin like protein with roles in migration/adhesion (Bear et al., 2016). For GFAP no interactions have been described with the cell-cell adhesion machinery, but in the following chapters we describe transcriptional effects on proteins from these cell-cell complexes by GFAP modulation.

Kinases targets/scaffolds

GFAP and Vim, like all cytoplasmic IFs, are highly regulated by post-translational modification (PTM). Best understood are the phosphorylations, but also other modifications occur such as sumoylation, ubiquitination, acetylation, and glycosylation (Snider and Omary, 2014). Phosphorylation of Vim has been investigated quite extensively. The PTMs have effects on protein interactions as well as on assembly dynamics of Vim (Ivaska et al., 2007; Sihag et al., 2007). Phosphorylation of GFAP mainly affects dynamics and network organisation during mitosis (Yasui et al., 1998). Other PTMs of GFAP are the modifications of arginines into citrullines (Jin et al., 2013). Interestingly, a bioinformatics screen for sumoylation sites in GFAP using SUMOplot™ (abgent), revealed four unreported high-probability sumoylation target motifs in the rod. Two of these were localized in linker 1 and linker 1-2, regions in the rod where the coiled coil is interrupted (Fig. 2). None of these sites were identified in Vim.

IFs are not only a target for kinases, but they can also act as a scaffold for kinases. Also heat shock proteins can bind to IFs (Perng et al., 1999). These interactions illustrate another function of IFs, namely as protein scaffolds. Heat shock proteins such as αB-crystallin (CRYAB) can bind to the IFs and prevent aggregation of IFs, whereas CRYAB mutations can induce aggregation (Sanbe et al., 2004). Proteins that are not functionally required at all times but should be readily available may be sequestered on the filaments. GFAP binds 14-3-3γ at pSer8, and 14-3-3ε

immunoprecipitates Vim and GFAP (Satoh et al., 2006; Li et al., 2006). The interaction between Vim and 14-3-3ε was suggested to be a sequestering interaction, to prevent 14-3-3ε from binding to other targets (Tzivion et al., 2000). Vim is also required for the dimerization of receptor tyrosine phosphatase β (RPTPβ), which is required for insulin signalling and vascular smooth muscle cell migration (Shen et al., 2015). Various components of insulin signalling are also regulated by GFAP modulation in our experiments, possibly hinting towards a broader role for IFs in this pathway (Chapter 4 and Chapter 5).

Other functions

Vim and GFAP are also implicated in various other functions, e.g. Vim forms cages around aggresomes of accumulated misfolded proteins (Johnston et al., 1998) and captures aggregated proteins in a fishnet like manner (Ogrodnik et al., 2014). Vim can bind collagen mRNA and stabilize it (Challa and Stefanovic, 2011). GFAPδ can interact with a part of the γ-secretase complex, Presenilin 1 (Nielsen et al., 2002), and thereby could potentially affect downstream targets of γ-secretase processing and thus affect APP or Notch signalling.

IFs can interact with transcription factors, either to sequester them or to bring them in position for phosphorylation. Interactions have been found between Vim and Menin, GFAP and Menin, and between Vim and p53 (Lopez-Egido et al., 2002; Virtakoivu et al., 2015; Yang et al., 2005). In the case of Keratin 17, even a functional interaction with transcription factor Aire was found in the nucleus, making Keratin 17 a strong modulator of the cytokine profile of these cells (Hobbs et al., 2015). We also studied the effect on the cytokine profile induced by Alzheimer's Disease in GFAPko astrocytes and microglia, but although quite some factors were differentially expressed, no major anti/proinflammatory profile switch was found (Kamphuis et al., 2015).

IFs not only play a mechanical role in the organization of organelles, but can also functionally interact with them. This is described above for vesicles, but also occurs with mitochondria (Chernoivanenko et al., 2015; Nekrasova et al., 2011). In activated immune cells, Vim can interact with the NLRP3 inflammasome as well as with mitochondria. Activated inflammasomes process pre-cytokines into their mature form, and the interaction with Vim and mitochondria is proposed to control reactive oxygen species levels required for activation of the inflammasome (dos Santos et al., 2015). In addition Vim modulates mitochondria membrane potential and motility, the latter possibly through an anchoring domain (Chernoivanenko et al., 2015; Nekrasova et al., 2011). For GFAP, no interactions have been described

so far with mitochondria, but in astrocytes recently a novel type of very small mitochondria was discovered in the fine processes in the cell periphery, either associated with GFAP or with Ezrin (Derouiche et al., 2015). There are also three case reports describing AxD patients with abnormal mitochondrial function: one with mutation GFAP R88C (and an additional independent mitochondrial mutation), another with GFAP N386I, and a case of a mitochondrial mutation phenotypically resembling AxD (Cáceres-Marzal et al., 2006; Gingold et al., 1999; Nobuhara et al., 2004; Schuelke et al., 1999).

Oligomeric, filamentous, or cleaved Vim and GFAP

Some of the interactions and functions described above have been attributed to the insoluble fully assembled filamentous networks, but oligomeric or cleaved fragments of the IF proteins have also been described to have relevant functions. The recycling of integrin vesicles was attributed to oligomeric Vim (Ivaska et al., 2005). In endothelial cells, Vim cleavage by calpains is an important step in creating a soluble pool for angiogenesis (Dave and Bayless, 2014). GFAP can be cleaved by caspases, such as Casp6. This cleavage leads to an N-terminal domain that has a dominant negative network collapse effect, and a C-terminal domain that forms small particles in vitro, but stays soluble in co-assembly with full length GFAP (Chen et al., 2013). Cleaved Vim can be used in neurons as 'cargo wagons' for carrying AKT to injured sites by binding both AKT and molecular motors (Perlson et al., 2005). IFs are also important targets of Caspases in apoptosis, and Caspase cleaved Vim fragments are pro-apoptotic (Byun et al., 2001).

Ion-IF interactions

GFAP and Vim also have various functional interactions with ions. Zinc was recently shown to be an important factor in Vim assembly through an interaction with C328, a residue important for oxidative stress response in the rod domain, which is conserved in GFAP (C294, Fig. 2) (Pérez-Sala et al., 2015). Divalent cations function as a crosslinker of IFNs, stiffening the network in a cell free system (Lin et al., 2010b). These examples further extend the range of interactions and functions IFs have, and how these can be modulated.

Combining signalling and mechanics, a role in mechanotransduction?

Soon after the discovery of IFs it was clear that they have an important mechanical role in cells. This is now further established by the remarkable mechanical properties of the networks and the filaments and the IF-related diseases that lead to mechanical defects. A 1980s review already proposed that IFs are integrators of cellular space

(Lazarides, 1980). Now in the last 15 years there has been an explosion of findings attributing a central role for IFs in signalling. A logical thought-step to make at this point is to consider whether these mechanical and signalling properties of IFs interact.

The process of translating mechanical cues into biochemical signals is called mechanotransduction. This process can be separated into three steps: mechanotransmission, mechanosensing, and mechanoresponse (Hoffman et al., 2011). Mechanotransmission describes the loading of the force upon structures that relay the force unto the mechanosensing protein. This step is mechanically straightforward and can be considered, very simplified, as a rope pulled on. Mechanosensing is the quintessential step of mechanotransduction, where a force upon a protein typically elicits a steric effect, such as unfolding. Examples include Notch receptor protein exposing an activating cleavage site after an applied mechanical force (Gordon et al., 2015), calcium channels Piezo1 and Piezo2 opening by a mechanical force (Coste et al., 2010), or fibronectin proteins unfolding and displaying complete hidden signalling domains under cell-exerted forces (Klotzsch et al., 2009). The mechanoresponse relates to the downstream cascade of events that are induced by the mechanical cue. This response can be at the molecular level, such as the growing of a focal adhesion under tension (Wolfenson et al., 2009), or at the tissue level, such as the thickening of an arterial wall under hypertension (Hahn and Schwartz, 2009).

A powerful method to find proteins that unfold under mechanical conditions, is cysteine shotgun labelling. This technique uses chemistry that labels cysteines, a residue that can be exposed in a protein that is unfolded under mechanical conditions, and identifies these proteins with mass spectrometry or fluorescence. This has identified spectrins, proteins with multiple buried cysteines, as proteins that unfold under mechanical stress (Johnson et al., 2007). In the same study, Vim was identified as a protein that is 50% more exposed when mesenchymal stem cells are treated with blebbistatin, a compound that inhibits non muscle myosin II, the main molecular motor responsible for cellular contractile forces. This is remarkable considering there is only one cysteine in Vim to be labelled. However this does not automatically imply that Vim filaments expose the cryptic site under cell-exerted tension by unfolding of secondary or tertiary protein structure, as depolymerisation of the filament (unfolding of quaternary structure) would also expose the cryptic cysteine (Johnson et al., 2007). Depolymerisation of the filament can also be a downstream mechanoresponse of a mechanosensitive Vim kinase that phosphorylates and solubilizes Vim. The remarkable elongation of IFs under single

filament stretching however does imply that some form of monomer-shifting can occur (Kreplak et al., 2005). Hypothetically, if this behaviour occurs in vivo, two proteins functionally interacting while associated on the IF scaffold may be pulled apart and can either be activated or inactivated.

A recent methodological paper on Vim also summarizes some of the findings of Vim on contractility measured by growing cells in collagen gels (Ridge et al., 2016). In brief, contractility was initially reported to be reduced in VIMko cells (Eckes et al., 2000), but later it was shown that this was only true at low cell density in the collagen gel. A higher contractility was achieved when VIMko cells were present at higher cell density in the gel (Murray et al., 2014). This effect was attributed to the dominance of cell/matrix over cell/cell contacts. Adding fibronectin to these gels equalized the contractility of the VIMko and the wt cells, further illustrating the complexity of cellular mechanics (Mendez et al., 2014). Similar experiments for GFAPko, VIMko, and VIM-GFAPko astrocytes showed that there was no difference in collagen gel compaction (Pekny et al., 1999). Direct probing of the intracellular forces by force spectrum microscopy, a microrheological technique recently developed, showed that Vim does not have a direct effect on intracellular contractility (Guo et al., 2014), but the effects of Vim on gel compaction can be due to other processes, e.g. through anisotropic effects, meaning forces are differently oriented, or cell-cell signalling dependent processes.

IFs are not only sensors but also targets of the mechanoresponse. The elasticity or pliability of the ECM is felt by cells that continuously probe their adhesion surface. The mechanical properties of the ECM have profound effects on cell differentiation (Engler et al., 2006; Keung et al., 2011; Trappmann et al., 2012). Vim responds to the stiffness of the ECM by shifting the ratio of soluble/insoluble Vim with the highest soluble fraction at the physiological stiffness of cells in tissue (Murray et al., 2014). In a study where LaminA/C was established as a mechanical rheostat, various proteins were screened for a correlation of their expression with the mechanical stiffness of the environment. A U251 xenograft injected into mouse brain (0.5kPa) showed lower GFAP and Vim protein expression than of a U251 xenograft in the flank (4 kPa) (Swift et al., 2013). Similarly, implantation of stiff electrodes in the brain induces gliosis at the interface of tissue and implant. Comparing soft (0.5 kPa) with stiff (30kPa) implants revealed reduced gliosis and reduced GFAP and Vim expression at the border of the softer implant (Moshayedi et al., 2014).

Lastly, IFs can also take part in mechanotransduction by integrating the cytoskeleton as a whole. Actin microtubules and IFs traditionally interact through plectins, and many other crosslinking proteins have been identified. Vim interacts

with and reciprocally organizes actin in lamellipods during migration (Jiu et al., 2015), microtubules link to Vim through APC to keep the IFN spread out (Sakamoto et al., 2013), and Vim and IF-connected plectins play a role in the stability of mechanosensing focal adhesions (Dmello et al., 2016; Gregor et al., 2013; Ivaska et al., 2007). IFs are proteins that bridge the focal adhesions all the way up to the nuclear DNA, as they also interact with the nuclear IFs, the Lamins, via Nesprins and the LINC complex (Linker of Nucleoskeleton and Cytoskeleton) (Fig. 1) (Starr and Fridolfsson, 2010). Lamins subsequently are essential in the organization of chromosomes (Guelen et al., 2008), but whether there is any inside-out or outside-in signalling between the nucleus and the cytoplasm through the IFN is not yet established.

Conclusion

Currently an astounding number of cellular processes has been identified that are related to the presence and structure of IFs. Still, a single IF protein has a limited number of binding sites, for interacting proteins, how is it possible that so many interactions were discovered for this protein class? A plausible explanation is the large amount of IF monomers in the cell and the dynamic nature of the network. One can hypothesize that in an IFN, a protein that both acts on IFs and binds to IFs, such as is the case for some kinases, can bind to one monomer in the filament and perform phosphorylations on the next monomer. The degrees of freedom of protein complexes that can be built upon IFs when tails and heads are both close to one another as well as staggered across the filament are substantial. The number of interactions increases further when heterotypic networks are formed of multiple IF proteins, as is the case in astrocytes, and when non-filamentous soluble IF proteins can expose new domains for interactions. The rod-structure-as-scaffold based functionality allows for immense flexibility in function. The organization of the cell and the high density of IF monomers in a filament allows for localized control of specific interactions and the large complexity of IF functions. The fact that these functions are not essential for survival of a cell or organism, does not relate to survival in a world full of challenges. IFs are called a crisis command center of the cell (Hol and Pekny, 2015), providing an organism with robustness in homeostasis and stress, one of the most important properties in biology for evolutionary success.

In the diseased brain, glia maintain a balance between containment of injury, the inflammatory response, and repair processes. This balance depends for an important part on the interaction between microglia and astrocytes. One of the hallmarks of the diseased brain is the increased expression of IFs in astrocytes. The

extended, dynamic, and extremely flexible IFN, such as in astrocytes, likely plays an important role in the astrocytes' ability to maintain homeostasis. How IFs provide astrocytes with robustness under the stresses that astrocytes are exposed to is a question that will be further investigated in the following chapters.

1

Chapter

2

Mechanical injury is not sufficient to induce a reactive transcriptional program in human astrocytoma cells and human primary astrocytes

Oscar M.J.A. Stassen
Tim A.O. Muntslag
Jacqueline A. Sluijs
Miriam E. van Strien
Willem Kamphuis
Elly M. Hol

Abstract

Traumatic brain injury leads to reactive astrocytes. We aimed to unravel whether the isolated mechanical component of cell stretch in such an injury could induce the reactive phenotype in astroglia. For this purpose we applied a short, but severe, stretch to a culture of a human astrocytoma cell line (U251) and primary human astrocytes. This resulted in a rapid increase in mRNA levels of 2 transcription factors involved in reactive astrocytosis: FOS, which is upregulated in astrocytes by exposure to reactive oxygen species, mechanical pressure, and ATP signalling, and EGR1, which responds to mechanical injury. Subsequently, we performed a genome wide analysis of changes in the transcriptome induced by the stretch at 30 minutes and 24 hours after injury. Unexpectedly, we only found small changes in the transcriptome. The main effect at the 30 minute timepoint was the increase in FOS and EGR1. No significant changes in the transcriptome were detected at 24 hours after stretch application. The FOS and EGR1 signalling were likely not caused by a release of ATP. We further explored the lack of a transcriptional reactive astrocytosis response by studying the effect of stretch on primary adult human astrocytes, by applying a more severe injury, and by applying force on cells grown on different extracellular matrix proteins. Taking all these data together we conclude that a mechanical injury alone can not induce the expression of typical astrocytosis genes both in astrocytoma and primary human astrocyte cultures. These data point towards a high resilience to mechanical injury of the cells studied.

Introduction

Traumatic brain injury (TBI), caused by a mechanical impact, can lead to severe neurological disability, cognitive decline, or even death (Maas et al., 2008). One of the major responses to mechanical injury in the brain is reactive gliosis. In the process of reactive gliosis both microglia and astrocytes undergo a range of molecular changes to restrict the extent of the injury and the secondary consequences thereof. In severe injuries involving damage of the blood-brain barrier it can result in glial scar formation, but only when the tissue is injured beyond repair and ischemia has occurred (Burda et al., 2015; Zamanian et al., 2012). In general, reactive gliosis has short term benefits for the injured brain, but on the long term it inhibits neuronal recovery and functioning (Hol and Pekny, 2015). The most prominent markers of reactive gliosis in astrocytes, refered to as astrocytosis in this work, is the increased expression of the intermediate filament proteins GFAP and vimentin (Middeldorp and Hol, 2011). Various models are used to study the process of astrocytosis, ranging from *in vivo* models of mice suffering from a neurological disease with subsequent

isolation and characterization of the astrocytes (Orre et al., 2014a; Zamanian et al., 2012) to *in vitro* models of chemically or mechanically injured astrocyte cultures (Ellis et al., 1995; Tran and Neary, 2006).

Induction of reactive astrocytosis using *in vitro* mechanical injury models is often done by a short stretch pulse to the substrate on which the cells are cultured, leading to cell swelling, cellular stellation, membrane porosity, mitochondrial and golgi vacuolization, and rupturing of intermediate filaments, all processes depending on the intensity of injury (Ellis et al., 1995). Findings from these systems have identified important signals induced in astrocytes after mechanical injury, including extracellular ATP increase, inositol phosphate signalling, intracellular Ca^{2+} elevation, glutamate release and reuptake early after injury, and eventual increase in chondroitin sulphate proteoglycans (CSPGs), N-cadherin, thrombospondin, and reorganization of the GFAP network (Floyd et al., 2004, 2005; Neary et al., 2005; Wanner et al., 2008). Of these signals, purinergic signalling induces a broad spectrum of reactions in astrocytes and neurons (Franke et al., 2012). By adding apyrases (enzymes that degrade ATP) to injured astrocyte cultures, injury-induced reactivity was abolished (Miller et al., 2009; Tran and Neary, 2006). These findings have led to animal models where the severity of brain injury can be limited after injury by treating with apyrases that catalyse the hydrolysis of ATP (Choo et al., 2013).

Most effects described in *in vitro* mechanical injury models are the direct consequences of the mechanical disruption of the cell, membrane rupture, and the leakage of cytoplasmic ATP and ions, inducing a cascade of events. However astrocytes also express stretch-activated channels, such as Piezo-1, which could mediate an active, more controlled, response to mechanical injury (Blumenthal et al., 2014; Suchyna et al., 2004). Similarly, in neurons there are indications that *in vitro* injury induced signalling is not only due to mechanical disruption of the axons, but also due to active signalling between focal adhesions and the extracellular matrix (ECM) (Hemphill et al., 2011). Also the induction of endothelin-1 in primary astrocyte cultures under continuous cyclic injury indicates the potential for more controlled mechanotransduction responses in this cell type, in contrast to the response to a generic rupture of membranes and cellular structures (Ostrow et al., 2011).

To study the effect of a mechanical stretch on changes in human astrocytes we chose to start with applying a mechanical injury to U251 astrocytoma cells. We observed an injury induced early increase in the immediate early genes FOS and EGR1 mRNA with qPCR. Both genes are known to respond to a mechanical force imposed on astrocytes: FOS expression is induced by reactive oxygen species,

mechanical pressure, and ATP signalling (Bolego et al., 1997; Hashimoto et al., 2005; Hsieh et al., 2010), while EGR1 expression increases in response to mechanical injury and controls transcription of phosphacan, an important glial scar ECM molecule (Beck et al., 2008; Khachigian et al., 1996). Subsequently, we did a genome wide analysis of the injured U251 cell cultures, but remarkably found no other genes responding to injury. We further investigated possible explanations of the lack of this transcriptional reactive astrocytosis response.

Materials and Methods

Astrocytes and astrocyte cell lines

We used U251-MG human astrocytoma cells, which stably expressed mCherry (in this paper referred to as U251 cells) (Moeton et al., 2016). The expression of mCherry was not necessary for this experiment, but used as a control when we compared the effect of GFAP-isoforms on the response to mechanical injury. Since no effect of GFAP-isoforms on our stretch induced effects was detected, we omitted that data from this manuscript. U251-MG cells were maintained in 1:1 DMEM GlutaMAX high glucose: Ham's F-10 nutrient mix, supplemented with 100 U/ml penicillin, 100 μg/ml streptomycin (1% P/S) and 10% fetal bovine serum (FBS; all Invitrogen, Bleiswijk NL).

For primary human adult astrocyte cultures, we obtained freshly dissected post-mortem subcortical white matter from 5 different cases. The tissue was obtained from The Netherlands Brain Bank (NBB), Amsterdam. Informed consent was obtained according to standard NBB procedures. Informed consent is given for the use of the material and clinical information for research purposes. Clinicopathological data of the cases is provided in Table1. Primary cells were isolated as described before (Kreft et al., 2014). Cells were cultured in DMEM/Ham's F12 GlutaMAX medium containing 5% FBS and 1% P/S.

In vitro injury experiments and treatments

U251 cells were plated at a 2% FBS concentration in 6-well flexible bottom Bioflex cell culture plates (Flexcell International, Hillsborough NC, US; Dunn Labortechnik, Asbach, DE) at a density of $5.20*10^4$ cells/centimeter^2 (cm^2). The 6-well plates were either coated with a YIGSR laminin peptide or with collagen type I. The cells were left to attach for 6 hours (h) followed by a replacement of the culture medium with FBS-free medium to stop proliferation, prevent FBS induced signalling activation, and prevent FBS induced GFAP expression. At this point cells were 70-90% confluent. Cells were injured with the Cell Injury Controller II (Custom Design and

Table 1: Clinico-pathological data of white matter brain-donors

NBB	Sex	Age	CD	PMD	Cause of death	Ori
2007-025	M	82	AD	05:15	Cachexia by swallowing problems by advanced dementia syndrome.	Corpus Callosum
2007-050	M	68	AD	05:20	Sepsis by decubitus, cachexia and dehydration	Corpus Callosum
2007-051	M	66	MSA	06:25	Aspiration pneumonia and dehydration	Corpus Callosum
2007-052	M	82	AD	04:15	Pneumonia by marasmus	Corpus Callosum
2010-038	F	79	C	<18h	Cardiac insufficiency	CWM

NBB = Netherlands Brain Bank donor number, M = male, F = female, Age = Age in years, CD = Clinical Diagnosis AD = Alzheimer's Disease, MSA = Multiple System Atrophy, C = Neurological control, PMD = post-mortem delay, (hours:minutes) Ori = Brain area of origin, CWM = Cortical White Matter.

Fabrication, Richmond VA, US), by releasing a 4 pounds per square inch (psi) peak pressure pulse for 50 ms as described in the product manual inducing a 1.55 stretch (where stretch is defined as fold increase of the surface area on which the cells are cultured. A stretch of 1.55 is considered a severe injury). For an even more severe injury, wells were exposed to a 5.7-6.0 psi peak pressure for 50 ms resulting in an estimated stretch of 1.75 (Ellis et al., 1995) (very severe injury). RNA was harvested 0.5h or 24h after a mechanical injury.

Primary cells were seeded at a density of $3.12*10^4$ cells/cm² (NBB donor # 2010-038), or at $1.04*10^4$ cells/cm² for all other NBB donors (Table 1), due to a difference in size, availability and proliferative capacity between the primary astrocytes. Cells were plated in DMEM/Ham's F12 GlutaMAX medium containing 5% FBS, 1% P/S and 0.25% Fungizone. After cells were attached and cultures approached confluency, the cell culture medium was replaced by low serum medium (0.5% FBS). RNA was harvested 0.5 h or 24h after a 4.0 psi injury.

For induction of purinergic signalling, cells were treated with serum free medium supplemented with 250 μM ATP (Sigma-Aldrich; catalogue # 27-2056-01) for 30 minutes (min), to test the same time span of the early time point in the injury experiment. We added 10 μM of the ATP P2 receptor antagonist pyridoxal phosphate-6-azo(benzene-2,4-disulfonic acid) tetrasodium salt hydrate (PPADS, Sigma-Aldrich; catalogue #P178,) to cell cultures 15 min before ATP treatment or injury to inhibit purinergic signalling.

RNA isolation

RNA was isolated by adding TRIsure (Bioline, London, UK; GC biotech B.V., Alphen aan den Rijn, NL) directly to the cell culture wells. RNA was extracted according to the manufacturer's protocol, and precipitated in isopropyl alcohol in the presence of glycogen at -20°C overnight (Roche; Almere) (Kamphuis et al., 2012). Samples were centrifuged at 4°C at a speed of $2.0*10^4$ g for 45 min, washed twice with cold 75% ethanol (in MilliQ), and the RNA pellet was dissolved in MilliQ (Millipore). The 260/280 absorbance ratio was measured by spectrophotometry (NanoDrop; Thermo Scientific) to assess RNA concentration and purity.

Real time quantitative PCR

After treating 500 ng RNA with DNAse for 2 min at 42°C (gDNA wipeout buffer), cDNA was made in 10 μl reactions using Quantiscript® Reverse Transcriptase with a mix of oligo-dT and random primers at 42°C for 30 min. The reaction was stopped by an inactivation step at 95°C for 3 min (Quantitect; Qiagen Benelux B.V., Venlo, NL).

The produced cDNA was diluted 20x in MilliQ and was used as a template in the real time quantitative polymerase chain reaction (qPCR) in 96-wells plates on an ABI7300 (Applied Biosystems, Life Technologies, Bleiswijk, NL). The reaction mix consisted of 1 μl template, 3.5 μl MilliQ, 0.5 μl primer mix (final concentration of 0.1 mM for each primer), and 5 μl SYBR® Green PCR Master Mix (Applied Biosystems, Life Technologies, Bleiswijk, NL). The qPCR program consisted of an incubation of 2 min at 50°C and 10 min at 95°C, followed by 40 cycles of 15 seconds (s) at 95°C and 1 min at 60°C. After the qPCR a dissociation curve was made by ramping from 60°C to 95°C. Curve analysis was performed using the Sequence Detection Software version 1.4 (Applied Biosystems), with a standard threshold of 0.2 (determined to be in the exponential part of the derived curve), and an automatic determination and correction of baseline fluorescence. Primers were designed to target two different exons separated by an intron of over 100 base pairs (bp) of the transcripts of interest (when possible) and to generate 50-125 bp long amplicons. Amplification efficiencies and dissociation curves of all assays were verified using a 1:20-1:320 dilution series of U251 or U373-MG cDNA and the amplicon product size was verified on an agarose gel. Specifications of primers are given in Table 2. Raw data from qPCRs was normalized with two Alu-repeat targeting primer pairs. The Alu-repeat primer pairs target a transposon that is distributed throughout the genome and have been shown to be a reliable measure for total mRNA (Rihani et al., 2013; Witt et al., 2009). For reporting qPCR results we use normalized arbitrary units (n.a.u.).

Table 2: Primer pairs used and their qPCR efficiencies

Genename	E	amplicon	Sequence FW 5'-> 3'	Sequence RV 5'-> 3'
Alu-Sq	1.85	variable	CATGGTGAAACCCCGTCTCTA	GCCTCAGCCTCCCGAGTAG
Alu-J	1.9	variable	CAACATAGTGAAACCCCGTCTCT	GCCTCAGCCTCCCGAGTAG
FOS	1.9	71	CCTTCTCCAGCATGGGCTCGC	GTTGGCACTGGAGACGGCCA
EGR1	1.81	98	AGCCCTACGAGCACCTGACCG	TCGAGTGGTTTGGCTGGGGT
LCN2	2*	104	CAATGTCACCTCCGTCCTGTT	TCTTAATGTTGCCCAGCGTGA
SERPINA3	1.98	80	TGACTCGCAGACAATGATGG	TATCTTGGGGGTCAAAGGGC
CP	1.9	120	CGGAGAGACACAGCAAACCT	CGGAGAGACACAGCAAACCT
TYROBP	2*	92	ACCCGGAAACAGCGTATCAC	CTCTGTGTGTTGAGGTCGCT
GFAPpan	2	50	GCCACCTACAGGAAGCTGCT	GGGAATGGTGATCCGGTTCT
S100B	2*	115	CGAACTGAAGGAGCTCATCAAC	ACATTCGCCGTCTCCATCATT

FW:forward primer; RV: reverse primer; E: Efficiency, *no product on calibration curve or not determined, 2 used for calculations.

Microarray - RNA labelling, hybridization, and scanning

cRNA was made from 100 ng RNA using a Low Input Quick Amp Labelling Kit, two-color (Agilent, Amstelveen, NL), as per manufacturer's protocol. A mix of 825 ng of Cy3 and Cy5 labelled cRNA samples (Unstretched control, N=4; 0.5h after 4.0 psi injury, N=4; 24h after 4.0 psi injury, N=4) was hybridized to Human GE 4x44K v2 Microarrays (Agilent, Amstelveen, NL) according to the manufacturer's protocol. cRNA fluorescence intensity was scanned using an Agilent DNA Microarray Scanner. Scans were made with 100% and 10% photon multiplier tube intensity, at 5 μm resolution.

Microarray - data processing

Data processing was performed as described before (Bossers et al., 2010a; Orre et al., 2014a, 2014b). Briefly, data were extracted from microarray images using Feature Extraction software (v. 9.5.3.1, Agilent). Using the limma package in bioconductor (http://www.bioconductor.org), spot intensities were imported into R software for statistical computing (R version 3.1). Spots labelled by the Feature Extraction software as saturated or non-uniformly distributed foregrounds and backgrounds were omitted. In these cases the statistical analysis of differential expression was based on the remaining spots. Intensities were quantile normalized between all arrays, and sample intensities were extracted for an intensity-based analysis (Bossers et al., 2010b). Redundant probes detecting identical transcripts were averaged and all genes that did not have a condition with an average expression of $\log_2 > 6$ were omitted from the analysis.

Western blotting

Cell cultures were washed, scraped, and collected in cold PBS and stored as pellets at -20°C until protein extraction. Protein extraction was done in loading buffer (50 mM Tris (pH 6.8), 2% SDS, 10% Glycerol, 100 mM DTT) supplemented with protease inhibitor cocktail (Roche Diagnostics)). Protein concentrations were measured using a BCA kit (Pierce, Thermo Scientific), according to manufacturer's descriptions. The samples were supplemented with bromophenol blue, heated for 5 min at 95°C, and run through a 10 or 5% SDS-PAGE. After electrophoresis, proteins were blotted on Whatman Protran membranes (GE Healthcare) using a semi-dry trans-blot system (Biorad) at a current of 100 mA per gel for 60 minutes. Blots were incubated with blocking buffer (50 mM Tris pH 7.4, 150 mM NaCl, 0.25% (w/v) gelatin, and 0.5% triton X-100) for 10 min before they were incubated with primary antibodies at 4°C overnight. Blots were subsequently washed 3 times in TBS-T (100 mM Tris-Hcl pH 7.4, 150 mM NaCl with 0.2% Tween-20), before secondary antibodies (IRdye 800 (1:5000) (LI-COR) and Dylight 649 (1:2000) (Jackson Immune Research), diluted in blocking buffer, were incubated at room temperature for 1 hour. Blots were washed again 3 times in TBS-T before scanning with an Odyssey scanner (LI-COR). GAPDH was used as a loading control. Antibodies used were anti-c-Fos (1:500) and anti-GAPDH (1:5000, Abcam, AB14247).

Statistics

In injury experiments, the FOS and EGR1 expressions at 0.5h after injury and 24h after injury were tested against uninjured control with two-tailed student t-tests and corrected for multiple testing per injury experiment with a Benjamini Hochberg False Discovery Rate correction (FDR). In these confirmation experiments, tests were considered significant if the FDR-corrected p-value was below the α-criterion of 0.05.

For the microarray, statistical significance was tested using a Bayesian linear model fit with an FDR corrected criterion level of $\alpha = .1$ to prevent type II errors (Smyth, 2004). The two injury conditions (0.5h, 24h) were compared versus uninjured control. Microarray probes were considered to report a differentially expressed gene if the statistical test was significant and the fold change showed at least a 1.5 fold absolute change. An FDR correction for multiple testing was applied.

Figure 1. Morphological changes in U251 and human primary astrocytes induced by a 4.0 psi pressure injury
(A-D) U251 cells show tortuous processes (arrowheads) and general retraction or loss of cytoplasm 2 min after stretch (B) compared to unstretched control (A). After 30 mins, tortuous processes have largely been restored and cells begin spreading out again (C).
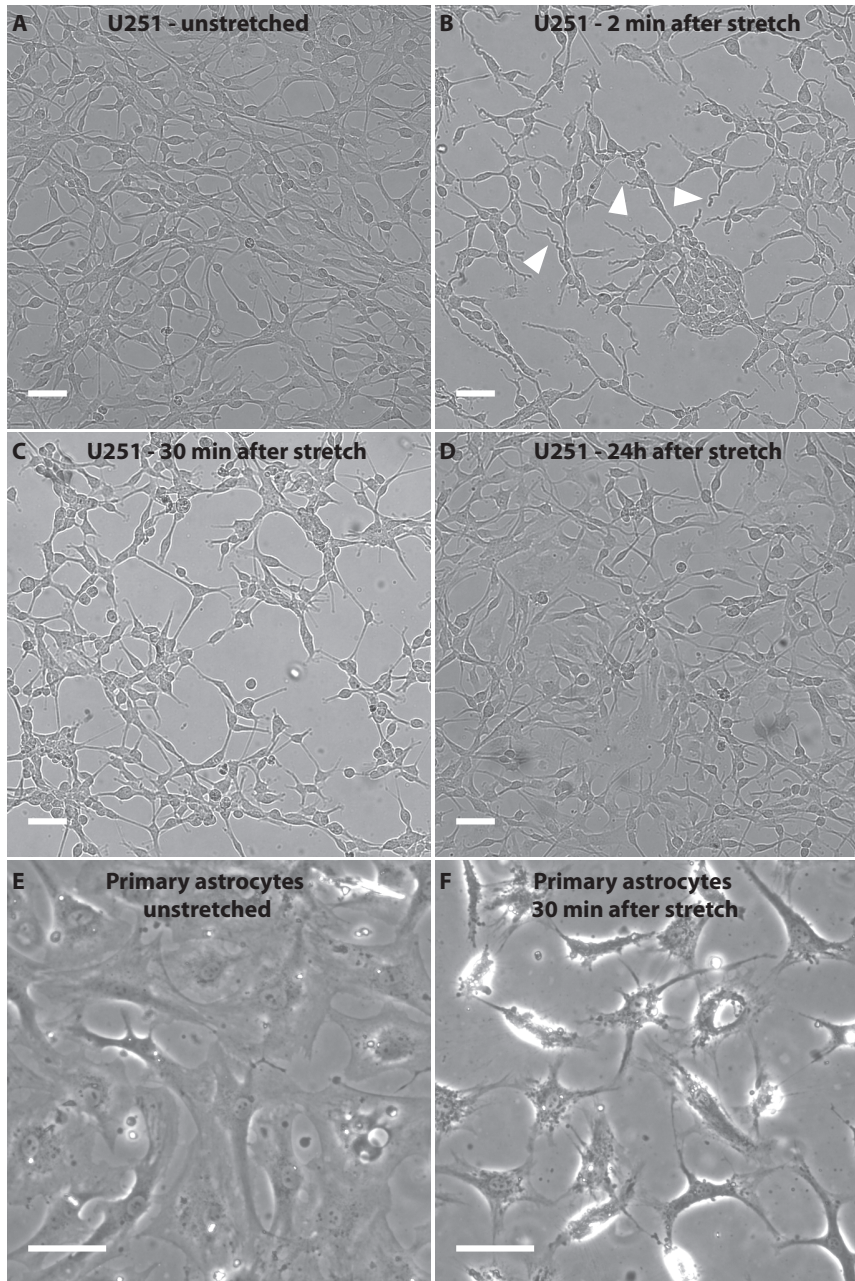
(Figure 1, continued) After 24 hours, cells are back to their original state (D).

(E-F) Human primary astrocytes have a more fibroblast-like morphology when unstretched (E) compared to the U251. After injury they retract or lose part of their cytoplasm, and the granularity of the cytoplasm increases (F).

A-D micrographs were taken with a 10x bright field objective, E-F were taken with a 20x phase contrast objective. Scale bars: 62.5 um.

Results

U251 response to 4.0 psi cell injury

Initial evaluation of the cells response to injury was done by microscopy. U251 cells exposed to a 4.0 psi injury showed a rapid retraction of their cellular processes and injury was visible in the form of tortuous processes when viewed immediately after injury, followed by a recovery from tortuosity 30 mins after injury (Fig. 1A-C). After 24 hours, the cells had morphologically recovered from the injury, but no hypertrophy or stellation, as reported for astrocyte cultures before (Tran and Neary, 2006), was seen (Fig. 1D). Using the same 4.0 psi injury, we assessed changes in transcription of our cells at 0.5h and 24h after injury by qPCR. First, we checked whether our cells reacted to this injury paradigm by evaluating the increased expression of two immediate early genes: FOS (mean uninjured = 0.18 n.a.u., mean 0.5 h = 0.68 n.a.u., FDR < .001) and EGR1 (mean uninjured = 1.2 n.a.u., mean 0.5 h = 2.9 n.a.u., FDR = .01; Fig. 2A&B). We found that FOS and EGR1 mRNA expression were indeed significantly increased at 0.5h after injury, and returned to baseline after 24h. Samples were also tested for expression of GFAP and IL-6, but no mRNA response was found (not shown). Since our main interest was in the early response of the cells to injury, we continued with a whole genome microarray analysis of the mRNA at 0.5h and 24h after injury to obtain a complete image of mRNA transcriptional changes induced by this cellular injury paradigm. Interestingly, microarray identified FOS and EGR1 as the strongest responding genes (around a 2.5-fold increase) (Fig. 2C), although after multiple testing correction these genes were not significantly regulated (Table 3). After 24 hours, none of the 18,893 genes responded significantly to the stretch (Fig. 2D, Table 4). In figure 2C and 2D the red dots represent all genes that are significant before FDR multiple testing correction, but none of these genes are significant after correction. This finding could be due to a lack of statistical power of the study, however we also looked at genes with an average absolute fold change > 2, irrespective of statistics. This resulted in 5 genes or array probes (FOS, EGR1, FAM83F, UMODL1, LOC100293561) affected 0.5 hours after stretch, and 4 genes or probes (IFI27, LOC100293561, LOC100128934, A_33_P3378549) 24 hours after stretch. This shows that there is a limited transcriptional response to the 4.0 psi injury. Due to the known role of GFAP and vimentin in reactive astrocytosis, we specifically looked at the change in transcription of these genes in the microarray. Although vimentin mRNA gave a very strong signal (10th brightest probe, log_2 intensity of 17), the transcript level increased only 13% after 24h (n.s.). For GFAP the expression was lower (log_2 intensity of around 6) with a transcript increase of 27% after 24h (n.s.).
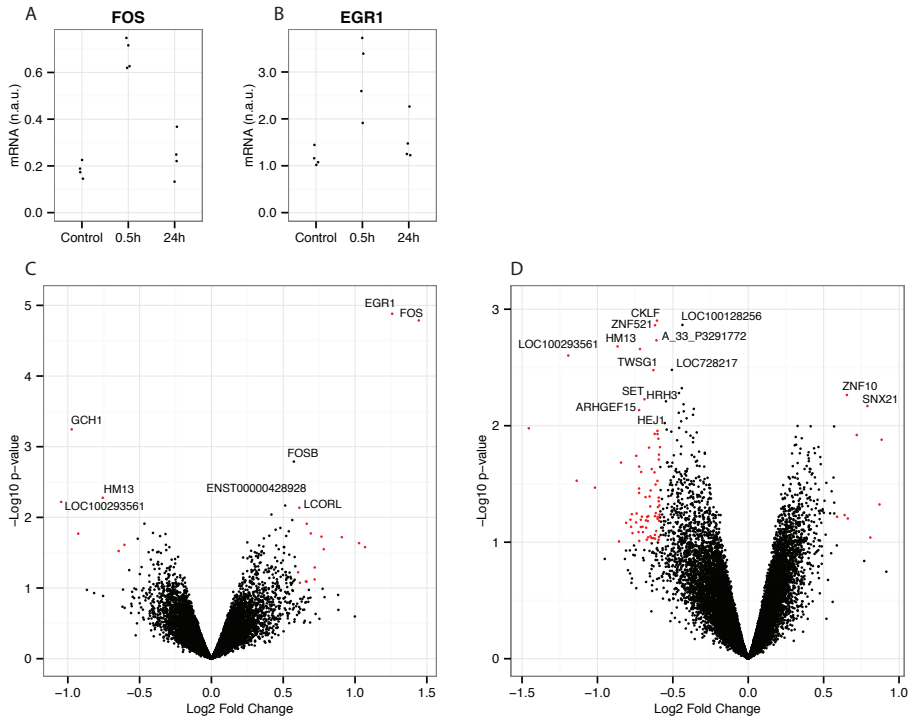
Figure 2. U251 transcriptional changes induced by a 4.0 psi pressure injury.
(A-B) As an initial response to injury, FOS mRNA (3.8 fold) (A) and EGR1 mRNA (2.4 fold) (B) were significantly increased 0.5h after injury. After 24h expression the expression of FOS mRNA and EGR1 mRNA had returned to baseline.
(C-D) Volcano plots showing the distribution of genes affected by mechanical injury 0.5h after injury (C) and 24h after injury (D). Depicted are the $\log_2$-fold changes on the x-axis vs the −log10 of the uncorrected p-values on the y-axis. The dots in red represent genes with an uncorrected p-value below 0.1 and a fold change of over 50% change. After multiple testing correction, no genes were significant.

U251 response to 6.0 psi cell injury

The transient rise in EGR1 and FOS expression is the only transcriptional effect we found in the 4.0 psi condition, although this injury model has been described before to induce molecular hallmarks of reactive astrocytosis (Wanner et al., 2008). Therefore, we varied a number of parameters in our injury paradigm to find a better condition for the induction of transcriptional changes mimicking astrocytosis in response to injury. A possible explanation for the lack of transcriptional changes is that the injury was not severe enough for this particular cell type in our hands, although a 3.2-4.0 psi pulse has been described before to induce injury (Ellis et al., 1995; Wanner, 2012). We next tested U251 cells exposed to a 6.0 psi stretch, to increase the stretch ratio applied to the cells from 1.55 to 1.75, mimicking a very

Table 3: Top 20 genes 0.5h after 4.0 psi pressure injury ranked by absolute highest t-test statistics

Gene Symbol	FC	Int	t	FDR	GenBank accession	Agilent Probe Name
EGR1	2.39	9.92	6.75	0.15	NM_001964	A_23_P214080
FOS	2.72	6.95	6.61	0.15	NM_005252	A_23_P106194
GCH1	0.51	5.96	-4.52	1.00	NM_001024071	A_33_P3311439
FOSB	1.49	6.27	3.96	1.00	NM_006732	A_23_P429998
HM13	0.59	5.53	-3.34	1.00	NM_178582	A_33_P3323448
C8orf17	0.48	5.35	-3.27	1.00	XM_002346128	A_33_P3327888
Unknown	1.43	5.82	3.21	1.00	ENST00000428928	A_23_P4052
LCORL	1.53	5.99	3.17	1.00	NM_153686	A_32_P54242
OR51F1	1.34	6.11	3.06	1.00	NM_001004752	A_33_P3424507
BARHL1	1.48	5.82	2.96	1.00	NM_020064	A_23_P9340
PLA2G2C	0.72	6.13	-2.90	1.00	NM_001105572	A_33_P3344156
DBH-AS1	1.58	5.82	2.90	1.00	AF129263	A_33_P3682006
LOC439911	1.39	7.21	2.83	1.00	AK127450	A_33_P3551349
ATP1A1	1.36	15.99	2.83	1.00	NM_000701	A_23_P1072
Unknown	1.45	7.22	2.77	1.00	A_33_P3292241	A_33_P3292241
CHIC1	0.75	6.80	-2.75	1.00	NM_001039840	A_33_P3215093
FMO6P	1.62	5.78	2.74	1.00	NR_002601	A_33_P3285271
C11orf65	0.53	6.30	-2.73	1.00	NM_152587	A_23_P418485
AP4M1	0.80	6.52	-2.73	1.00	NM_004722	A_33_P3237944
YME1L1	1.32	5.86	2.70	1.00	ENST00000390454	A_33_P3343007

FC = Fold Change >1 = injury induced expression, <1 = injury repressed expression, Int = Mean $\log_2$ intensity, t = t-test statistic, FDR = False Discovery Rate controlled p-value.

severe injury. As no clear astrocytosis markers emerged from the microarray of the samples injured with a 4.0 psi pulse, we chose to analyse by qPCR the expression of genes identified in literature to be highly activated in astrocytosis models, i.e. GFAP, S100B, Lipocalin 2 (LCN2), Ceruloplasmin (CP), Serpin Peptidase Inhibitor, Clade A (SERPINA), and TYRO Protein Tyrosine Kinase Binding Protein (TYROBP) (Orre et al., 2014a; Zamanian et al., 2012). For the early response we again determined the EGR1 and FOS mRNA levels that we showed to be increased in the 4.0 psi injury. Of these selected genes, TYROBP and LCN2 were not detectable in both uninjured and injured U251, and the expression of CP, GFAP, S100B, and SERPINA was not changed (not shown). FOS and EGR1 mRNA levels were again increased early after injury, and the response was stronger in the 6.0 psi condtion, although statistical significance was not reached, the trend was strong and variance was mainly caused

Table 4: Top 20 genes 24h after 4.0 psi pressure injury ranked by absolute highest t-test statistics

Gene Symbol	FC	Int	t	FDR	GenBank accession	Agilent Probe Name
CKLF	0.66	5.92	-4.09	1.00	NM_016951	A_24_P215804
LMNB2	0.74	9.64	-4.05	1.00	NM_032737	A_23_P67725
Unknown	0.65	5.78	-4.04	1.00	XM_001717044	A_33_P3322460
ZNF521	0.66	6.20	-3.89	1.00	NM_015461	A_33_P3219398
HM13	0.55	5.53	-3.82	1.00	NM_178582	A_33_P3323448
NA	0.61	5.66	-3.80	1.00	Unknown	A_33_P3291772
C8orf17	0.44	5.35	-3.73	1.00	XM_002346128	A_33_P3327888
Unknown	0.70	6.42	-3.58	1.00	XR_039169	A_33_P3248580
TWSG1	0.65	7.41	-3.58	1.00	NM_020648	A_24_P202497
Unknown	0.74	7.44	-3.39	1.00	ENST00000420126	A_24_P306469
MORF4	0.73	7.35	-3.34	1.00	NM_006792	A_24_P3461
ZNF10	1.57	7.02	3.32	1.00	NM_015394	A_24_P215475
SET	0.62	7.61	-3.28	1.00	NM_003011	A_24_P917866
HRH3	0.69	6.28	-3.26	1.00	NM_007232	A_24_P301837
IL1RN	0.74	6.11	-3.23	1.00	NM_173842	A_33_P3246829
SNX21	1.73	5.97	3.21	1.00	NM_152897	A_33_P3316683
Unknown	0.78	10.86	-3.18	1.00	Unknown	A_33_P3219105
ARHGEF15	0.61	8.23	-3.17	1.00	NM_173728	A_23_P49674
Unknown	0.74	7.65	-3.16	1.00	Unknown	A_33_P3351775
LOC729732	0.73	5.82	-3.14	1.00	XM_002343155	A_33_P3243500

FC = Fold Change >1 = injury induced expression, <1 = injury repressed expression, Int = Mean log2 intensity, t = t-test statistic, FDR = False Discovery Rate controlled p-value.

by a single experiment (FOS: uninjured N=4, mean = 0.064 n.a.u., 0.5h after stretch N=4, mean = 3.1 n.a.u., FDR = 0.06; EGR1: uninjured N=4, mean = 0.28 n.a.u., 0.5h after stretch N=4, mean = 2.7, FDR = 0.06, Fig. 3A&B).

A western blot was performed on protein of samples isolated from the U251 6.0psi condition, in a time series of 0.5h, 1h, 3h, 6h, and 24h after injury, with uninjured cells as a control, to compare protein levels to the mRNA increase. The intensity of the c-Fos band at 70 kDa, corrected for Gapdh (1.6-fold increase at 0.5h, N=1), did not follow the trend of 48-fold mRNA increase as reported by qPCR (Fig. 3A&C). We tried several Egr1 antibodies, but these did not work on western blot in our hands. A staining to characterize localization of c-Fos did not result in any clear injury induced nuclear localization of c-Fos, due to already relatively high nuclear c-Fos localization in the uninjured control (not shown).
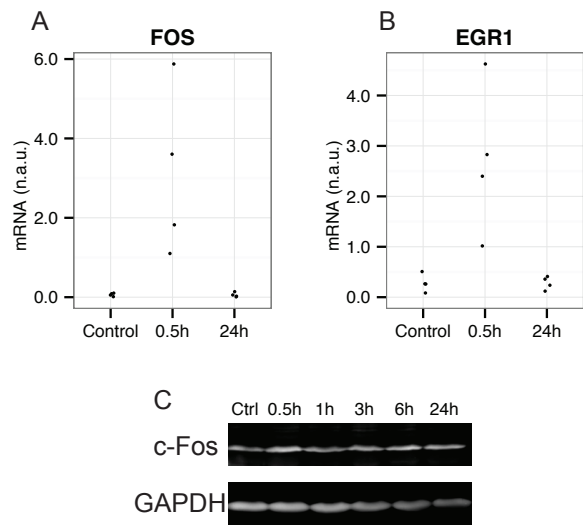
Figure 3. U251 response in immediate early genes induced by a 6.0 psi injury pressure.

(A-B) Injury induced an increase in FOS (A) mRNA (48.4 fold) and in EGR1 mRNA (9.6 fold) after 0.5h. After 24h FOS and EGR1 mRNA levels were back to baseline.

(C) Western blot stained for c-Fos and GAPDH proteins, with samples taken at the indicated time points (Ctrl = uninjured control). C-Fos band migrates at ca 70 kDa, Gapdh at 37 kDa.

Primary human astrocyte response to 4.0 psi cell injury

We anticipated that the lack of injury response, might alternatively be caused by our choice of the astrocyte cell line. Therefore we compared the response of primary human astrocytes to the response of U251 astrocytoma cells by measuring the response to injury with our selected qPCR markers. We isolated astrocytes from several human cases (Table 1). Astrocyte cultures from 4 post-mortem brain isolations proliferated slowly and could only be used for 1 experiment each. The astrocyte culture from isolation 10-083 proliferated quite well and experiments on these astrocytes could be replicated. Cells were subjected to a 4.0 psi pulse and injury evaluated by microscopy and with qPCR. The 10-083 astrocytes showed again a trend for increase in FOS and EGR1 mRNA at the early time point, although, due to the high variation in the samples, this did not result in a statistically significant change (FOS: uninjured N=3, mean = 0.15, 0.5h after stretch N=3, mean = 1.6, FDR=.1; EGR1: uninjured N=3, mean = 0.55, 0.5h after stretch N=3, mean = 1.59, FDR=.1, Fig. 4A-B). Also in these primary astrocytes the mRNA of the astrocytosis marker TYROBP mRNA was below the detection limit, whereas the expression level of GFAP, S100B, LCN2, CP, and SERPINA again did not respond to injury. The primary astrocytes derived from 10-083 were subjected to a 6.0 psi pulse injury (N=1) to test whether the lack of response was caused by the strength of the injury paradigm. Although FOS and EGR1 showed a 88-fold and 15-fold increase by qPCR, respectively, no other genes showed more than a 25% increase or decrease at 24h after stretch. A western blot was performed on protein of samples isolated from the 10-083 primary astrocytes injured by a 6.0 psi pulse, in a time series of 0.5h, 1h, 3h, 6h, and 24h after
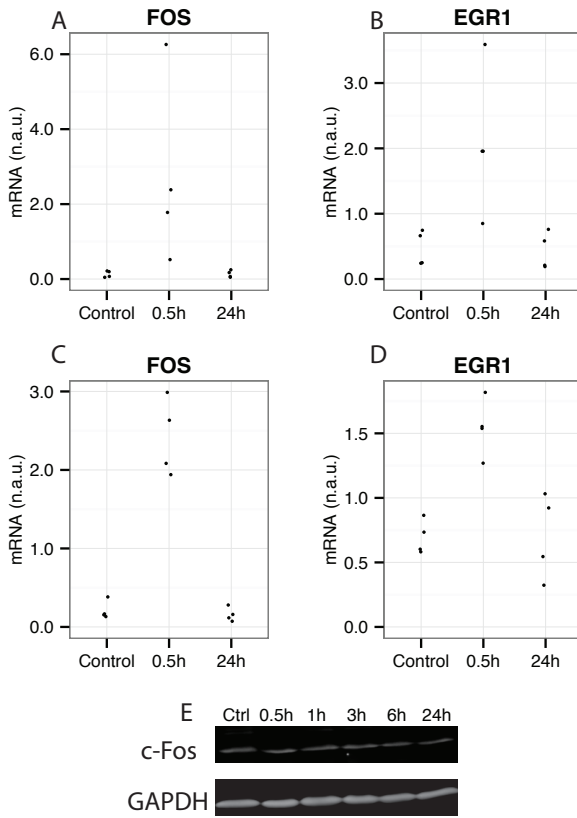
Figure 4. Primary human astrocytes transcriptional changes in FOS and EGR1 induced by 4.0 psi injury
(A-B) In primary human astrocytes (case 10-083 replicated 4 times), a 4.0 psi pressure injury induced a FOS mRNA increase (10.7-fold, not significant; A) and an EGR1 mRNA increase (2.9-fold, not significant; B) 0.5 h after injury. 24h after injury, expression levels were back to baseline.
(C-D) In primary human astrocytes (4 different donors), a 4.0 psi pressure injury induced a FOS mRNA increase (11.5-fold, FDR < 0.001; C) and an EGR1 mRNA increase (2.2-fold, FDR = 0.001; D) 0.5 h after injury. 24h after injury, expression levels were back to baseline. (E) Western blot of protein lysates of human primary astrocytes from case 10-083 injured with a 6.0 psi pressure stained for c-Fos and GAPDH, with samples taken at the indicated time points (Ctrl = uninjured control). C-Fos band migrates at ca. 70 kDa, Gapdh at 37 kDa.

injury and uninjured controls, to compare protein levels to the mRNA increase. The c-Fos band corrected for GAPDH (0.9-fold decrease; N=1) did not show an increase corresponding to the 88-fold mRNA increase reported by qPCR after 0.5h (Fig. 4E).

The other primary astrocyte cultures were only subjected to the 4.0 psi pulse. Microscopy analysis revealed these cells showed a more dramatic morphological change than the U251 cells after 30 min (Fig. 1E-F), but they also responded only with a transient increase in FOS and EGR1 transcription (FOS: uninjured N=4, mean = 0.21, 0.5h after stretch N=4, mean = 2.41, FDR < 0.001; EGR1: uninjured N=4, mean = 0.70, 0.5h after stretch N=4, mean = 1.55, FDR = 0.001, Fig. 4C-D). Transcription of the astrocytosis genes, GFAP, S100B, CP, SERPINA, and TYROBP was neither changed at 0.5h nor at 24h after injury. LCN2 was only detectable in 1 isolation, 2007-052, and showed a 2.6-fold increase 0.5h after injury, returning to baseline 24h after injury.

U251 response to 4.0 and 6.0 psi cell injury on collagen ECM

To test whether active adhesion complex signalling was required for induction
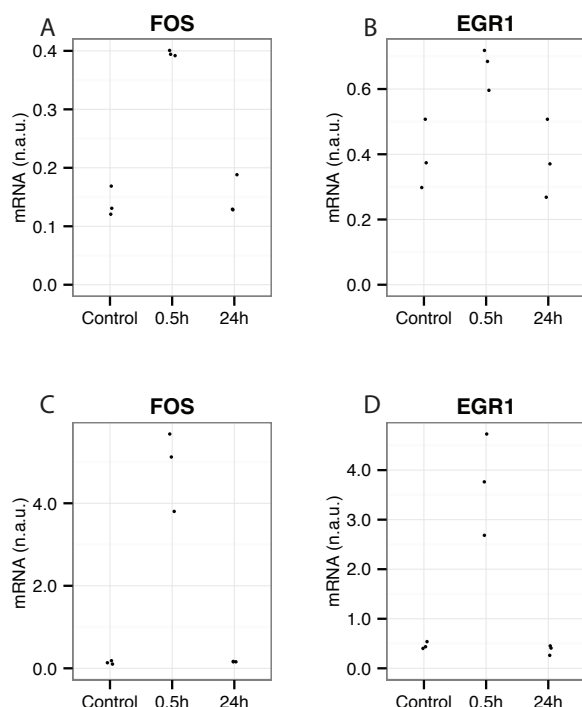
Figure 5. U251 transcriptional changes in FOS and EGR1 induced by a 4.0 psi and a 6.0 psi injury pressure on a collagen ECM

(A-B) U251 plated on collagen reacted to a 4.0 psi pressure injury with a FOS mRNA increase (2.9-fold; FDR < .001; A) and an EGR1 mRNA increase (1.7-fold; FDR = .04; B) 0.5 h after injury. 24h after injury, expression levels were back to baseline.

(C-D) A 6.0 psi pressure injury induced an increase in FOS mRNA (34.8-fold; FDR = .004; C) and an increase in EGR1 mRNA (8.1-fold; FDR = .01; D) 0.5 h after injury. 24h after injury, expression levels were back to baseline.

of genes involved in astrocytosis in our U251 cells, we injured our cells on membranes coated with collagen I instead of the YIGSR laminin peptide. The YIGSR peptide binds cells through the 67 kDa Laminin Receptor/Ribosomal protein SA (RPSA), whereas Collagen I binds cells through integrins, core components of focal adhesions, and mechanical signaling hubs. We applied both the 4.0 and the 6.0 psi pulse injury paradigm and tested for the panel of astrocytosis genes. Similar to the injuries performed on cell grown on YIGSR peptides, injuries with a collagen ECM induced only a FOS and EGR1 response (Fig. 5). Transcription of the astrocytosis genes, GFAP, S100B, CP, SERPINA, and TYROBP was neither changed at 0.5h nor at 24h after injury, whereas LCN2 was not detected in enough samples to quantify (not shown).

Relation of purinergic signaling to astrocytosis

Multiple reports described the role of purinergic signalling in the induction of astrocytosis (Bolego et al., 1997; Choo et al., 2013; Miller et al., 2009; Tran and Neary, 2006). We have performed a single experiment (N=1) on both U251 cells and the 10-038 primary astrocytes (Fig. 6). PPADS, a purinergic receptor inhibitor, treatment by itself did not induce a response in FOS and EGR expression in the cultures, but both cultures showed an increase in FOS and EGR1 after ATP induction and after stretch. Treatment of PPADS prevented the ATP induced response, as expected. However, in
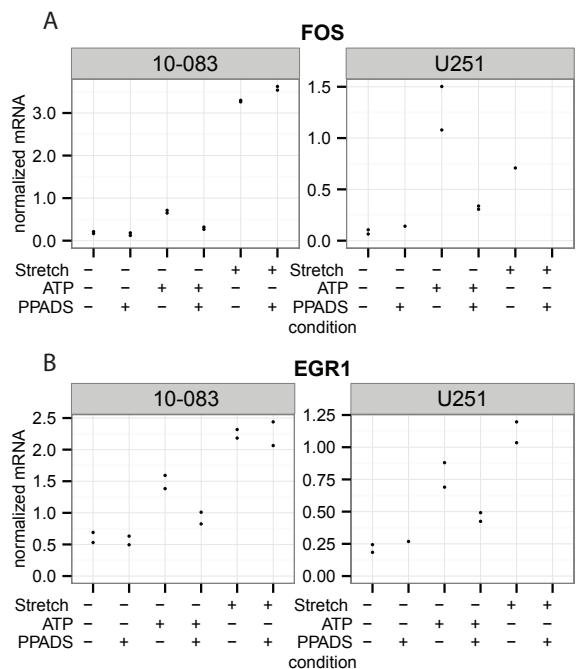
Figure 6. Transcriptional changes in U251 and primary human astrocytes induced by ATP signalling modulation

Primary human astrocytes (10-083) or U251 were injured, treated with ATP for purinergic signalling induction, or treated with PPADS for purinergic signalling inhibition. Expression of FOS (A) and EGR1 (B) mRNA was analyzed by qPCR. Dots represent technical replication of a single biological replicate. PPADS was able to reduce the ATP induced effect on transcription, but not on stretch injury with primary line 10-083. For U251 these data points were lost (A and B).

the primary cells that were mechanically injured, PPADS did not prevent the EGR1 and FOS response. This implies that a different mechanism than ATP signaling via the P2 receptors underlies the increase in FOS and EGR1 after a mechanical injury. The injury of U251 in combination with PPADS failed (last column in Fig. 6A&B) and could not be interpreted. Note that this single experiment needs to be repeated before any conclusive statements can be made, but the observation is interesting nonetheless.

Discussion

To study the response of astrocytes to a mechanical injury, we profiled the transcriptomic changes of the U251 astrocytoma cell line 0.5h and 24h after stretching them by a 50 ms pressure pulse. Although initial qPCR analysis showed a rapid but transient increase in FOS and EGR1 mRNA (Fig. 2A&B), the following microarray analysis unexpectedly found no significant changes in response to the applied mechanical injury (Table 3&4). Subsequently, we investigated a number of conditions in our injury paradigm to find an explanation for the absence of the changes in the transcriptome, but no reactive astrocytosis transcriptomic response to injury could be induced by our paradigm in human astrocytoma cells and in human primary adult astrocytes. The gene targets we employed as markers of

astrocytosis GFAP, S100B, LCN2, CP, SERPINA, and TYROBP, were based on the results of studies in various models (Orre et al., 2014a; Zamanian et al., 2012), but the focused qPCR approach with primers directed against these genes did not result in any evidence for induced astrocytosis. There are several possible explanations as to why we failed to observe a response. We tested: injury severity, astrocyte cell model, the nature of the ECM coating, and started to identify the signaling pathways involved.

Severity of injury

The 4.0 psi injury did not result in an induction of an astrocytosis response in our models (Fig. 2, 4, 5A&B), thus we attempted to increase the response of the cells by applying a larger pressure pulse, leading to a larger deformation, and therefore a more severe injury. Indeed the magnitude of the FOS and EGR1 response increased, but we did not detect a response in the astrocytosis markers GFAP, S100B, LCN2, CP, SERPINA, and TYROBP. The sensitivity of cells for mechanical injury has been described to vary between species, with mouse astrocytes being most sensitive and becoming reactive between 2.4-2.8 psi, rat astrocytes responding around 3.2 psi, and human astrocytes responding between 3.7-4.4 psi injury pressure (Wanner, 2012). Note that these pressures are translated into substrate stretches that injure the cells. Based on the available literature, both the 4.0 and the 6.0 psi injury pressures applied should have been able to induce a astrocytic response, but transcription of astrocytosis genes was not increased in any of the samples. Possibly the cells do not express the proper mechanosensitive receptors, or the cells are incapable of an astrocytic response due to the lack of FBS in the culture medium, or the time point of the increase in expression was missed. Other explanations that we tested, are discussed below.

Injury in different astrocytic models

Of the various human astrocytic cell lines available, we mainly studied the U251 astrocytoma cell line, due to its relative homogeneity for the microarray analysis and ease of use. One of the disadvantages of using astrocytoma for studying reactive astrocytosis, is that GFAP, the hallmark gene, is often downregulated in higher grade astrocytomas. Although U251 is one of the astrocytoma cell lines that does express GFAP (Moeton et al., 2016), GFAP regulation may not behave as in primary astrocytes. We found that the GFAP expression in U251 is quite heterogeneous, as staining for GFAP in a U251 culture reveals a mix of GFAP-positive and GFAP-negative cells (Chapter 4). To circumvent this heterogeneity in GFAP, we also selected a spectrum of reactive astrocytosis markers identified in molecular studies

of astrocytes in pathology (S100B, LCN2, CP, SERPINA, and TYROBP), but also none of these targets responded to the mechanical injury (Orre et al., 2014a; Zamanian et al., 2012). In addition, tumour cell lines have mutations causing altered signalling pathways resulting in the ongoing proliferation (Hanahan and Weinberg, 2011). These alterations could affect the transcription of the reactive astrocytosis genes in U251 cells, and hence the lack of response after injury. We therefore decided to also study primary astrocytes isolated from human post-mortem brains for a reactivity response after injury. Again, also in these cases, increased FOS and EGR1 was observed, but no increased expression of astrocytosis markers (Fig. 4). In the brain, the astrocyte is a cell type in a complex environment, with a highly organized spatial structure with endfeet in contact with the brain's blood vessels, cell regions taking part in tripartite synapses, and many fine processes involved in homeostasis of the brain (Oberheim et al., 2006). The *in vitro* astrocyte is always a gross oversimplification of the *in vivo* astrocyte, and the complex morphology of astrocytes *in vivo* is frequently reduced to a more simple polygonal shape *in vitro* (Puschmann et al., 2013). It has been argued that the *in vitro* astrocyte is already in a reactive state (Puschmann et al., 2013). Nonetheless, there are many reports of primary isolated astrocytes (in most cases from rat) that have been induced to a reactive phenotype through mechanical injury (Ellis et al., 1995; Neary et al., 2005; Tran and Neary, 2006). To study the role of mechanical injury *in vitro* it is of the highest importance that 3-dimensional culturing and injury models are developed where astrocytes can grow in conditions closer to their native state (O'Shea et al., 2015; Puschmann et al., 2013).

Nature of ECM coating

In our injury model, we chose for a YIGSR peptide as ECM coating for the cells to adhere to. Since laminin is a prominent component of the basal membrane in the brain and is produced by astrocytes. The YIGSR-peptide has been identified to be one of the adhesion motifs for cells attaching to laminin, therefore we decided to select the YIGSR peptide as it would better mimic the natural astrocyte environment than e.g. poly-L lysine or collagen (Massia et al., 1993). However, we did not observe any astrocytosis response on this coating, neither with the U251 cells nor with the primary astrocytes (Fig. 2-4). YIGSR and RGD are peptides used as replacements for full length ECM proteins laminin and fibronectin, however, they miss various functional domains of the full length ECM proteins. These peptides do not always induce the same signalling cascades as their full length counterparts (Boateng, 2004). In addition, in contrast to RGD, YIGSR is not a ligand for integrins, but for the ribosomal protein SA (RPSA; 67kDa laminin receptor) (Graf et al., 1987). RPSA is

a protein with both functions in the ribosome, as well as extraribosomal cell-ECM interaction functions (Scheiman et al., 2010). Although RPSA can bind and induce remodeling of laminin, it does not have a described role in mechanotransduction like integrins (Ardini et al., 2002). Since active mechanotransduction signalling can play a role in injury induced response and since most of the reported astrocyte injury studies with the cell injury controller performed so far were done on a collagen coating that integrins can bind to (Ahmed et al., 2000; Ellis et al., 1995; Floyd et al., 2001, 2004; Hoffman et al., 2000; Neary et al., 2005; Tran et al., 2008), we decided to extend our injury experiment of the U251 cells with both the 4.0 psi and the 6.0 psi injury on collagen coated plates. Baseline FOS and EGR1 mRNA expression on collagen did not differ from baseline on the YIGSR-coating. Although the induction of FOS and EGR1 levels after injury were comparable, again no induction of the reactivity targets was observed (Fig. 5). This suggests that the lack of reactive astrocytosis in our injury on YIGSR-coated plates is not due to the lack of integrin-mediated adhesion or omission of other signaling domains of full length laminin.

Signaling pathways of astrocyte injury induced reactivity

Mechanical injury to astrocytes leads to membrane rupture and the release of glutamate and ATP which are involved in injury related signaling (Edling et al., 2007). ATP binds to astrocytic P2Y purinergic receptors, leading to activation of AKT and p38 (ERK) signaling pathways. These cascades induce the release and induction of various hallmarks of astrocytosis, such as thromspondin-1, N-cadherin or altered mechanical properties of the astrocytes (Miller et al., 2009; Tran and Neary, 2006; Tran et al., 2008). We tested U251 and primary astrocytes for their response to ATP and both responded with an induction in EGR1 and FOS after 0.5h. This experiment was a pilot (N=1) and we have not tested the 24h condition yet, but there is an interesting lead in this experiment. On the one hand, considering there is an early induction of FOS and EGR1 by ATP, it would be very interesting to see whether this approach can induce an astrocytosis response on the longer term, for further molecular dissection of the astrocytosis pathway. On the other hand, the response of primary human astrocytes to stretch was not inhibited by the ATP antagonist PPADS (Fig. 6), implying that other P2-receptor independent signalling mechanisms are active in this stretch paradigm (YIGSR coated 6.0 psi injury). It would be an interesting point of investigation for a follow up study, to identify these other mechanisms.

In summary, the various injury paradigms tested did not yet reveal a single condition that could bring about a clear reactive astrocytosis response. Although it

is possible that a combination of primary cells injured on a collagen coating would show an astrocytosis response, there may be other parameters that we have not tested and may be crucial in the process of astrocytosis. Astrocytes are sensitive to the cell culture medium in which they are cultured, e.g. FBS contains components which ensures maturation of astrocytes, although it may also induce a constitutive reactive response. Our experiments were performed after serum depletion, as transcription factors like FOS are known to be transported to the nucleus after serum exposure. Other studies on *in vitro* astrocyte injury experiments use either serum free (Wanner et al., 2008), low serum (Miller et al., 2009; Neary et al., 2005), or high serum conditions (Ellis et al., 1995; Floyd et al., 2001). Although the experiments performed with either 0% or 0.5% serum also did not show an increase in GFAP after injury (Neary et al., 2005; Wanner et al., 2008), other labs working on astrocytes in physiology have used specific batches or species origin of serum to create basal conditions to specifically study non-reactive astrocytes (Puschmann et al., 2013; Wanner, 2012). It is possible that the presence of FBS, in combination with a primary astrocyte model cultured on an integrin interacting coating such as collagen or fibronectin would result in a astrocytosis response. This would be an interesting approach for follow up research.

Specific induction of FOS and EGR1

An interesting observation is the specific and unique induction of FOS and EGR1 transcript levels in the U251 4.0 psi injury model (Fig. 1C&D). Although other genes may also be induced in the other paradigms, a change in the gene expression of these two genes was prominently present in all of our studied conditions. C-Fos is best known for its role as a transcription factor in the AP-1 complex in cell survival and apoptosis and as a marker for neuronal activity (Benito and Barco, 2014; Shaulian and Karin, 2002). Also two of our astrocytosis target genes, GFAP and SERPINA, require AP-1 activation for transcription (Gopalan et al., 2006). Egr1 is a transcription factor best known for its role in neural plasticity (Davis et al., 2003). Interestingly, c-Fos also has a role besides its function as transcription factor, being an activator of various enzymes in the phospholipid synthesis activation, a role which is activated in proliferating cells (Pecchio et al., 2011; Portal et al., 2007). Immediately after mechanical injury, especially the larger cells (primary human astrocytes) display visible membrane disturbances (blebbing and granularity) that the cells repair rapidly (Fig. 1E-F). It is possible that c-Fos is induced in these cells to activate phospholipid synthesis required for membrane repair. Egr1 is also involved in mechanical injury induced transcription programs (Khachigian et al., 1996). Thus it seems our injury model induces just an early injury response, but the cells do not

progress into a full reactive astrocytosis.

Conclusion

In conclusion, we aimed at studying in an unbiased way the transcriptional changes in astrocytes after a mechanical injury, to identify the contribution of mechanical disruption of astrocytes to the events leading to reactive astrocytosis in TBI. Commonly used models to study astrocytes *in vitro* include astrocytes acutely isolated from human or rodent brain by mechanical dissociation or immunophenotypic selection (Foo et al., 2011; Jungblut et al., 2012; Manthorpe et al., 1979), induction of astrocyte differentiation from stem cells (Cuadrado et al., 2013; Williams et al., 2014), or use of rodent or human astrocytoma lines (Cai et al., 2003; Steele et al., 2012). The different models all have their advantages and disadvantages. An important disadvantage of using rodent brain derived astrocytes is that humans have subtypes of astrocytes, which are not present in rodents, and that the astrocytes from each species respond very differently to injury (Oberheim et al., 2009; Puschmann et al., 2010; Wanner, 2012). Therefore a more preferable option to study astrocyte reactivity is to use an astrocyte model of human origin. An advantage of cell lines is that they have been expanded so much over the years that they are usually a homogeneous population and relatively easy to obtain, maintain and experiment on. Well known and widely used human astrocytoma cells are the glioblastomas, e.g. the U251, U343 or U373 cell line (Bigner et al., 1981). A disadvantage of using cell lines is that they are derived from tumours and thus are likely to have mutations causing the ongoing proliferation and have altered their signalling pathways (Hanahan and Weinberg, 2011). Human brain derived astrocyte populations have the disadvantage of often being contaminated by endothelial cells and microglia. Moreover, they rapidly lose their astrocyte properties *in vitro*. For microarray analysis it is important to have a single population of cells, as shifts in cell ratio between cell populations can affect the observed changes in transcription (e.g. cell death of astrocytes only in a mixed population due to mechanical injury, will show a relative reduction of astrocyte transcripts and increase of microglia transcripts). In addition, there may be crosstalk between different cell populations, which in itself can be relevant for biological injury models, but does not answer the question of our study: the response of astrocytes to a mechanical injury in itself. Placing this question in the context of TBI, it is possible that a mechanical injury per se does not induce reactive astrocytosis. *In vivo* TBI models show a peak of reactive astrocytosis 3 days after the injury, a time span that allows for a complex inflammatory reaction to respond to the mechanical neuronal damages.

The findings of our study underline the difficulty of finding a representative *in vitro* astrocyte model, and the future likely lies in the purification of primary populations using sorting techniques, while culturing the cells on 3D materials to maintain the astrocyte phenotype. Although in earlier studies of *in vitro* injury astrocytosis markers increased 6 hours after injury, we only found a transient effect of mechanical injury on our astrocyte cultures. We therefore conclude that the astrocyte models tested by us are mechanically very resilient cells, that can cope quite well with a transient stretch injury.

2

Chapter

3

GFAP isoforms control intermediate filament network dynamics, cell morphology and focal adhesions

Martina Moeton
Oscar M.J.A. Stassen
Jacqueline A. Sluijs
Vincent W.N. van der Meer
Liselot J. Kluivers
Hedde van Hoorn
Thomas Schmidt
Eric A.J. Reits
Miriam E. van Strien
Elly M. Hol

Abstract

Glial fibrillary acidic protein (GFAP) is the characteristic intermediate filament (IF) protein in astrocytes. Expression of its main isoforms, GFAPα and GFAPδ, varies in astrocytes and astrocytoma implying a potential regulatory role in astrocyte physiology and pathology. An IF-network is a dynamic structure and has been functionally linked to cell motility, proliferation, and morphology. There is a constant exchange of IF-proteins with the network. To study differences in the dynamic properties of GFAPα and GFAPδ, we performed fluorescence recovery after photobleaching experiments on astrocytoma cells with fluorescently tagged GFAPs. Here, we show for the first time that the exchange of GFP–GFAPδ was significantly slower than the exchange of GFP–GFAPα with the IF-network. Furthermore, a collapsed IF-network, induced by GFAPδ expression, led to a further decrease in fluorescence recovery of both GFP–GFAPα and GFP–GFAPδ. This altered IF-network also changed cell morphology and the focal adhesion size, but did not alter cell migration or proliferation. Our study provides further insight into the modulation of the dynamic properties and functional consequences of the IF-network composition.

Introduction

Intermediate filaments (IFs) are part of the cytoskeleton. Together with actin filaments and microtubules, they form an integrated system that regulates many cellular processes, such as cell morphology, cell signaling, cell migration, and proliferation (Goldman et al., 2008; Ivaska et al., 2007; Pekny, 2001; Rutka et al., 1994). The main IF protein expressed in astrocytes is glial fibrillary acidic protein (GFAP). The ten different GFAP isoforms, of which GFAPα is the canonical isoform, are formed by alternative splicing (Kamphuis et al., 2012; Middeldorp and Hol, 2011). The function of GFAP and its isoforms is still elusive, but there is emerging evidence that at least one isoform, GFAPδ, alters the properties of the IF network. GFAPδ differs from GFAPα only in its C-terminal tail, and in non-pathological human brains, and is expressed in specific types of astrocytes, including the adult neural stem cells in the human subventricular zone and subpial astrocytes (van Strien et al., 2014; Roelofs et al., 2005; Van Den Berge et al., 2010). The GFAPδ protein has a unique 41 amino acids long C-terminal tail (Middeldorp and Hol, 2011; Roelofs et al., 2005) and is one amino acid shorter than the canonical GFAPα protein (Hol and Pekny, 2015). In pathological conditions, GFAPδ is expressed in certain types of reactive gliosis and glial tumors (Andreiuolo et al., 2009; Choi et al., 2009; Heo et al., 2012; Kamphuis et al., 2014; Martinian et al., 2009). The tail of GFAPδ disables the protein

to form homodimers making it impossible to self-assemble (Nielsen and Jørgensen, 2004). GFAPδ is able to form heterodimers with other type III IF proteins and can, therefore, be integrated in an IF network. Depending on the level of expression and the concentration of other IFs present, GFAPδ is either tolerated in the network or it causes the whole IF network to collapse in the perinuclear region (Perng et al., 2008; Roelofs et al., 2005). Assembly experiments in a cell free environment showed that GFAP networks start to collapse when there is more than 10 % of GFAPδ protein present in the network (Perng et al., 2008).

In the cell, IF proteins are present in a soluble form in the cytoplasm and in filamentous structures that form an important part of the cell's cytoskeleton (Kreplak and Fudge, 2007; Herrmann et al., 2009). These IF networks are highly motile structures that are constantly rearranged. The proteins within the filaments are also dynamic, since there is an active exchange between the filamentous and non-filamentous pool of IF proteins (Blikstad and Lazarides, 1983; Soellner et al., 1985; Lu, 1993; Colakoglu and Brown, 2009). IF networks that are already formed can be actively disassembled by phosphorylation of IF proteins, whereas the lack of dephosphorylation will hamper new IF network assembly (Chou et al., 1989; Ku et al., 1996). It has been shown that phosphorylation of GFAP at the N-terminal head domain by kinases, such as Aurora B or CF kinase, is important for proper dissociation from the filaments during cytokinesis (Izawa and Inagaki, 2006; Omary et al., 2006; Ku et al., 1996; Goto et al., 2000).

Previously, we showed both in vitro and in vivo that physiological levels of GFAPδ are well tolerated in a GFAPα network (Roelofs et al., 2005; Perng et al., 2008; Van Den Berge et al., 2010; Kamphuis et al., 2014), although it has also been shown in a cell free system and in vitro that a high expression of GFAPδ can lead to an IF network collapse (Nielsen and Jørgensen, 2004; Roelofs et al., 2005; Perng et al., 2008). These collapses resemble aggregates of GFAP proteins, which occur when cells are transfected with mutant R416W GFAP (Perng et al., 2006). This is one of the mutations in GFAP that causes Alexander disease (AxD), a fatal neurodegenerative disease characterized by leukodystrophy, macrocephaly, and psychomotor retardation (Brenner et al., 2001). A pathological hallmark of this disease is the presence of Rosenthal fibers, which are astrocytic aggregates that are comprised of GFAP, ubiquitinated proteins, and stress proteins, such as heat shock proteins like αB-crystallin (CRYAB) and heat shock protein 27 (HSP27) (Perng et al., 2006; Iwaki et al., 1989; Tang et al., 2006; Tomokane et al., 1991; Goldman and Corbin, 1988), but also IF-associated proteins like plectin (Tian et al., 2006). AxD mutations in GFAP and the subsequent collapse of the network influence astrocyte viability, morphology,

3

and glutamate transport, and aggregates or accumulations of mutant AxD GFAP have a profound effect on astrocyte biology and physiology (Hagemann et al., 2009; Tian et al., 2010; Chen et al., 2011; Sosunov et al., 2013).

There is increasing evidence that GFAPδ changes IF properties (Perng et al., 2008; Moeton et al., 2014). Here, we studied in more detail the differences in dynamic exchange of GFAPα and GFAPδ with the IF network in vitro. Furthermore, we analyzed the functional consequences of GFAPα or GFAPδ expression by assessing the effect of the altered GFAP network on the dynamics and localization of other IF proteins in the cells, on cell morphology, and focal adhesions. We also determined the effect on cell migration and proliferation, since it has been reported that GFAP affects these processes (Rutka and Smith, 1993; Rutka et al., 1994; Lepekhin et al., 2001; Elobeid et al., 2000). Investigating the dynamic properties of the different GFAP isoforms and the effects of the different GFAP networks on cellular functions will contribute to our understanding of the consequences of modulation of the GFAP network for astrocyte physiology and pathology.

Methods

Cell culturing and transfections

U251MG human astrocytoma cells (gift from A.M.W. van Dam, VU University Medical Center, Department of Anatomy and Neurosciences, Amsterdam, The Netherlands) and U343MG human astrocytoma cells (gift from Prof Dr. R. Quinlan, Durham University, Durham, UK) were cultured in DMEM Glutamax (Gibco) mixed 1:1 with Ham's F10 medium (Gibco) containing 10 % Fetal bovine serum (FBS) (Gibco) and 10-U/mL penicillin streptomycin (P/S) (Invitrogen). Human embryonic kidney (HEK293T) cells were cultured in DMEM/Glutamax with 10 % FBS, 1 % P/S, and 1 % extra Glutamax (all Invitrogen). All cells were cultured in uncoated plastic flasks (Corning) at 37°C in a humidified atmosphere, with 5 % CO_2.

Isolation of primary human astrocytes

Primary human adult astrocytes were obtained from freshly dissected postmortem subcortical white matter of a 79-year-old female control donor (NBB 2010-038), with a postmortem delay of <18 hours (h) and a cerebrospinal fluid pH of 6.30. The tissue was obtained from the Netherlands Brain Bank (NBB), which performs brain autopsies with short postmortem intervals. The brain donors gave informed consent for using the tissue and for accessing the extensive neuropathological and clinical information for scientific research, which is in compliance with ethical and legal guidelines (Klioueva et al., 2015). The tissue was collected in 25-mL cold

Hibernate A (Invitrogen), and mechanically dissociated into small pieces. The tissue was digested with 0.2 % trypsin (Invitrogen) and 0.1 % DNAseI (Invitrogen) at 37°C, while shaking for 30 min (min). Next, 2-mL FBS was added to the mixture, and subsequently, the cells were collected by centrifugation. The pellet was taken up in DMEM without phenol red containing 10 % FBS, 2.5 % Hepes, and 1 % P/S (all Invitrogen), and the suspension was filtered through a 60-μm mesh screen. Then, Percoll (Amersham/GE Healthcare) was added (half of the cell suspension volume), and this mixture was centrifuged at 3220 relative centrifugal force (rcf) at 4°C for 30 min to separate cells, debris, and myelin. The second layer (glial cell containing fraction) was collected and washed with complete DMEM (containing 10 % FBS, 1 % P/S, 2.5 % Hepes, and 1 % gentamycin, all Invitrogen). After centrifugation, the pellet was taken up in complete DMEM, and cells were seeded in a 6-cm uncoated culture dish. Microglia adhered to the dish, and after 6 h at 37°C/5 % CO2, the medium, containing astrocytes, was taken off, centrifuged, and the microglia depleted pellet was seeded onto poly-l-lysine-coated wells [PLL, Sigma-Aldrich, 15 μg/mL in PBS, 1 h at room temperature (RT)] in DMEM/Ham's F12 GlutaMAX medium containing 5 % FBS, 1 % P/S, and 0.25 % Fungizone (all Invitrogen).

Plasmid construction, transient transfection, and virus production

Expression vectors were prepared by cloning human GFAPα and human GFAPδ (Perng et al., 2006, 2008; Roelofs et al., 2005) full length cDNA sequences into the pIRES2EGFP (Clontech). For the GFAPδ constructs, the eGFP sequence was replaced by mCherry.

GFP tagged GFAP constructs were created by cloning human GFAPα and GFAPδ cDNA sequences (Roelofs et al., 2005) in frame after the eGFP sequence in peGFP using BAMHI and HindIII as restriction sites (Clontech) to create N-terminal eGFP tagged GFAPs. The N-terminal side was chosen for the eGFP tag, since GFAPα and GFAPδ differ in their C-terminal tail. All plasmids were sequenced.

Cells for fluorescence recovery after photobleaching (FRAP) experiments were transiently transfected using polyethylenimine (PEI) (Polysciences) or Lipofectamine (Invitrogen) according to manufacturer's descriptions. 2.5 μg of plasmid DNA was used for PEI and 1.6 μg for Lipofectamine (Kamphuis et al., 2012) in subconfluent 24-wells plates.

Subsequently, to produce lentiviral vectors, the constructs were subcloned into a pRRL lenti backbone. Lentiviruses were produced as described before (Naldini et al., 1996a, 1996b) with some alterations. In short, 10×10^6 HEK 293T cells were plated in a 15-cm culture dish and transfected with a total of 90 μg of the envelope (pMD2.G),

packaging (pCMV-dR8.74) and p156RRL plasmid, containing different expression cassettes per dish, using PEI. In total, 90 μg of DNA was mixed with PEI (67.5 ng/μL), incubated for 15 min at RT, and added dropwise to the cell culture. The culture medium was replaced 16 h after transfection, and the medium containing viral particles was collected 24 h after transfection. Supernatants were ultracentrifuged at 22,000 rpm (rotor SW28, Beckman-Coulter) for 2.5 h. The resulting pellet was resuspended in phosphate-buffered saline (PBS) (pH 7.4), aliquoted and stored at −80°C until further use.

To measure viral titers, a dilution series across five orders of magnitude of the viral stock solutions was made and HEK293T cells were transduced. After 2 days of incubation at 37°C, the number of transduced fluorescent cells at the different viral dilutions was counted, and the viral titer was determined in transducing units (TU)/mL.

Creating stable cell lines

For functional experiments, cell lines expressing GFAP isoforms were created. U251 cells were transduced with lentiviral constructs with a multiplicity of infection of 10. Medium was refreshed after 16 h. To maintain a population of transduced cells, cells were sorted on their EGFP or mCherry expression using fluorescent activated cell sorting (FACS ARIA II, BD Bioscience, Franklin Lakes, NJ, USA). In between experiments, U251 cells were stained for GFAP to ensure that more than 70 % of the cells were expressing the construct. The primary human astrocytes were checked for fluorescent reporter expression before any analysis to ensure cells were expressing GFAP isoforms.

MTT assay

To measure cell proliferation, an MTT (3-(4,5-Dimethylthiazol-2-yl)-2,5-diphenyltetrazolium bromide) assay was performed. MTT is reduced into a soluble blue formazan product by mitochondrial enzymes in living cells only. Therefore, the amount of formed formazan is proportional to the amount of living cells present (Mosmann, 1983). MTT assays were performed by plating cells in non-coated plastic 24-wells plates (Greiner). To quantify cells, medium was replaced by 500-μL serum free medium containing 0.5-mg/mL MTT, which was incubated at 37°C for 2 h. Cells were subsequently lysed in 100 % DMSO, which dissolves the purple formazan resulting in a color change of the DMSO. The amount of purple formazan, and therefore the amount of cells able to metabolize the MTT, was measured using a Varioskan Flash (Thermo scientific, USA), measuring the absorbance at

570 nm. Significance was tested with a Kruskal–Wallis test with Dunn's Multiple Comparison post hoc test on 3 independent experiments. Every measurement in the independent experiments was the average of a biological duplicate.

Phospho-histone H3 quantification

To determine the number of actively proliferating cells, U251 cells expressing GFAP isoforms were plated on non-coated coverslips and fluorescently stained for phospho-histone H3 (PHH3) together with the nuclear dye Hoechst (1:1000 dilution) (Invitrogen). Subsequently, micrographs were taken, the number of PHH3 positive, dividing, nuclei was counted using ImagePro software (version 6.3), and the percentage of dividing cells was calculated by dividing the number of PHH3 positive cells by total number of Hoechst positive nuclei. Per experiment, 5 fields of view were analyzed and averaged, each containing at least 50 cells. Data from separate experiments were corrected for inter-experimental variation as stated below. Significance was tested with a Kruskal–Wallis test with Dunn's post hoc test on data from 3 independent experiments.

Migration assay

To measure cell migration, a scratch assay was performed. U251 cells were plated in a 24-wells plate (100,000 cells per well) coated with 20-µg/mL PLL at 37°C for 1 h. The confluent cell monolayer was scratched with a P10 plastic pipet tip. Pictures were taken using an Axiovert 135 M (Zeiss) with a Sony XCD-X700 camera (Sony) at the time points indicated in the results. To quantify cell migration, the surface area not covered by cells was determined at different time points. The migration was calculated as the percentage of uncovered surface area compared with t = 0. A mean of 9 pictures was measured per condition, in at least 3 separate experiments. Significance was tested with a Kruskal–Wallis test with Dunn's post hoc test.

Single cell motility assay

Single cell motility assays were performed on a Zeiss Axiovert 2000 inverted microscope (Zeiss, Jena, Germany). A single cell suspension was plated on PLL-coated glass dishes with four compartments (CELLview, Greiner bio-one, Alphen a/d Rijn, The Netherlands) and allowed to adhere for at least 8 h. Dishes were kept on the microscope in a pre-heated and humidified incubation chamber (OKO labs) at 37°C and 5 % CO_2. Pictures were taken every 10 min with an Axi Aqua camera (Q imaging). Cell motility was measured by tracking single cells throughout all frames of the sequence and measuring the average velocity in µm per min using the manual tracking plugin from ImageJ (Rasband, W.S., ImageJ, U. S. National

Institutes of Health, Bethesda, Maryland, USA, http://imagej.nih.gov/ij/, 1997–2012 version 1.46f). Per experiment, at least 20 cells were analyzed per condition in at least 3 independent experiments. Data from separate experiments were corrected for inter-experimental variation as stated in the "Statistics and factor correction" section below. A Kruskal–Wallis test with Dunn's post hoc test was performed to test for significance. For the primary human astrocytes, which were not sorted, we checked for GFP and mCherry expression to make sure that we only tracked transduced cells.

Quantitative reverse transcriptase PCR (qPCR) analysis

U251 cells were transduced like described before. Medium was refreshed after 16h. RNA was extracted 7 days after transduction. RNA was extracted from cells using TRIsure (Bioline, London, UK) and precipitated in isopropanol overnight (O/N). Five hundred nanograms of RNA was reverse transcribed into cDNA with a QuantiTect reverse transcription kit (Qiagen), as described before (Kamphuis et al., 2012). cDNA was diluted 1:20 before being used as a template in qPCR assays (SYBR® Green PCR Master Mix, Applied Biosystems). qPCR conditions were similar as described before (Kamphuis et al., 2012) and glyceraldehyde-3-phosphate dehydrogenase (GAPDH) and hypoxanthine phosphoribosyltransferase (HPRT) were used as reference genes to normalize gene expression. Data from 4 separate experiments were factor corrected as stated in the "Statistics and factor correction" section below and tested for significance using a Kruskal–Wallis test with Dunn's post hoc test. Primer pairs used are listed in Table 1.

Western blots

Cells were washed and collected with a cell scraper into 100 μL of cold lysis buffer consisting of a suspension buffer (0.1 M NaCl, 0.01 M Tris–Hcl (pH 7.6), 1-mM Ethylenediaminetetraacetic acid (EDTA) with 1 % Triton-x100) and protease inhibitors were added (100-μg/mL phenylmethanesulfonylfluoride (PMSF)(Roche Diagnostics) and 0.5-μg/mL Leupeptin (Roche Diagnostics). Cells were vortexed and incubated for 5 min on ice. Subsequently, samples were spun at 11.7 k rcf for 1 min. Supernatant was taken off and stored at −20°C until further use. Protein concentrations were measured using a BCA kit (Pierce, Thermo Scientific), according to manufacturers descriptions. Proteins were mixed with 2X loading buffer (2X: 100 mM Tris pH 6.8, 4 % SDS, 20 % glycerol, 0.2 M dithiothreitol, and bromophenol blue), heated for 5 min at 95°C, and loaded on a 7.5 % SDS-PAGE reducing gel. After electrophoresis, proteins were blotted on Whatman Protran membranes (GE Healthcare) using a semi-dry Trans-Blot system (Biorad) for 60 min. Blots were

Table 1 qPCR primer pairs of human GFAP isoforms

Transcript	Forward primer	Reverse primer
GFAPα endogenous	CCCACTCTGCTTTGACTGAGC	CCTTCTTCGGCCTTAGAGGG
GFAPδ endogenous	GTGGTAAAGGTGGTGAGTCCTT	AGAGGCTGCTGCTTGCTC
Vimentin	CGTACGTCAGCAATATGAAAGTGTG	TCAGAGAGGTCAGCAAACTTGGA
Nestin	GATCTAAACAGGAAGGAAATCCAGG	TCTAGTGTCTCATGGCTCTGGTTTT
GFAPα	CTTCTCCAACCTGCAGATTCG	CACGGTCTTCACCACGATGTT
GFAPδ	CCGTGCAGACCTTCTCCAA	CGTATTGTGAGGCTTTTGAGATATCT
GFAPκ	GTCAGTACAGCAGGGCCTCG	AGGAGCGCTGCAGTGTCACG
GFAPβ	CGGGCATCGCCAGTCTAG	ATCCTGCTCTGGCTCTGCTC
GFAPγ	CTCAGAAGAGCCTGGACCCA	GGCTTCCAGCCTCAGGTTG
GFAPζ	GCACTGTGCACGTTCCCTG	GGTCCTGCCTCACATCACATC
GFAPΔEx6	TGCGCGGCACGGATC	CACGGTCTTCACCACGATGTT
GFAPΔ135	TCTGCGCGGCACGGAGTA	GGGAATGGTGATCCGGTTCT
GFAPΔ164	GAGGCGGCCAGTTATTCCC	CACGGTCTTCACCACGATGTT
GFAPΔEx7	GCGAGGAGAACCGAAACCAG	CTTCACCACGATGTTCCTCTTG

Endogenous GFAPα and GFAPδ primers are located in the 3'UTR part, which is absent in the plasmid cDNA. The primer sequences used were published before (Kamphuis et al., 2014) GFAP: glial fibrillary acidic protein

incubated with SuMi (50 mM Tris, 150 mM NaCl, 0.25 % gelatine and 0.5 % Triton X-100, pH 7.4) for 10 min before they were incubated with primary antibodies at 4°C overnight. Blots were subsequently washed 3 times in TBS-T (100 mM Tris–Hcl pH 7.4, 150 mM NaCl with 0.2 % Tween-20), before secondary antibodies [IRdye 800 (1:2000) (LI-COR) and Dyelight Cy5 (1:4000) (Jackson Immune Research), diluted in SuMi were incubated at room temperature for 1 h. Blots were washed again 3 times in TBS-T before scanning with an Odyssey scanner (LI-COR). GAPDH was used as a loading control.

Immunocytochemistry

To perform immunocytochemical staining, cells were cultured on uncoated glass coverslips, fixed with 4 % Paraformaldehyde (PFA), washed in PBS, and incubated in SuMi buffer for 10 min. Primary antibodies were diluted in SuMi and incubated at 4°C on a shaker O/N. Cells were washed 3 times in PBS and, subsequently, incubated with secondary antibodies and Hoechst 33258 (1:1000 dilution) (Invitrogen) diluted in SuMi at RT for 1 h. The antibodies used are listed in Table 2. All secondary antibodies were from Jackson Immune Research and diluted 1:1400 in SuMi. Cells were washed again in PBS, before the coverslips with cells were mounted on slides with Mowiol [0.1 M Tris–HCl pH 8.5, 25 % glycerol, 10 % Mowiol

Table 2 Primary antibodies

Antibody	Manufacturer	Dilution	Cat #
Pan GFAP Dako	Dako	1:4000 (1:8000 WB)	Z0334
hGFAPδ	Manufactured in house (10-05-2001 Bleed)	1:1000 (1:1300 WB)	–
GFAP c-term	Santa Cruz	1:4000 (WB)	Sc-6170
Vimentin	Chemicon	1:3000	AB5733
GAPDH	Abcam	1:4000 (WB)	AB14247

GFAP: glial fibrillary acidic protein, WB: western blot, c-term: carboxy terminal, hGFAP: human GFAP, GAPDH: glyceraldehyde-3-phosphate dehydrogenase

(Calbiochem, Merck Millipore)]. The actin network was visualized with acti-stain Phalloidin 670 (Cytoskeleton inc; 1:1000 dilution). All fluorescent images were taken with a Leica SP5 confocal microscope (Leica) with a 63x objective.

Cell morphology measurements

Phase contrast pictures were taken from the U251 cells transduced with GFAP isoforms and mCherry (control) on a Zeiss Axiovert 2000 with an Exi Aqua camera (Q Imaging, Surrey, Canada). Cell outlines were manually drawn using Image J. Area and perimeter were measured in square units. Form factor was calculated as

$$4\pi \times \frac{(Area)}{(Perimeter)^2}$$, where perfectly round cells will have a form factor of 1 (Lepekhin et al., 2001; Thurston et al., 1988). Five independent experiments were performed with 40 cells analyzed per experiment. Data have been factor corrected for inter-experimental variation as stated below. A Kruskal–Wallis test was performed with Dunn's post hoc test to test for significance.

Live cell imaging

U343MG cells were imaged for 48 h using a Leica IR-BE (Leica Microsystems GmbH) inverted wide field microscope at 37°C in a custom built incubator containing 5 % CO_2. Phase contrast and fluorescence images were acquired with a 40x objective at 10 and 30 min time intervals during 48 h. The single images were reconstructed and rendered into a time-lapse using Huygens software (Scientific Volume Imaging) and Image Pro Plus (Mediacybernetics).

Fluorescent recovery after photobleaching (FRAP)

FRAP analysis was performed on transiently transfected U251MG cells. During imaging the temperature was maintained at 37°C in a humidified incubator chamber

(OKO labs). Cells were analyzed 24 h after transfection. To monitor dynamics of GFAP in collapsed networks, we transfected the cells with GFAPδ in combination with either GFP–GFAPα or GFP–GFAPδ. FRAP experiments were carried out on a SP5 Leica Confocal Microscope (Leica) with a 63x objective. The pinhole was set on 209.99 μm, and the scanning speed was at 400 Hz with a resolution of 512 × 512 pixels. Bar-shaped regions of interest (ROI) of 1.5 μm × 10 μm were bleached with a 488-nm Argon laser (full laser power) until at least 50 % of the fluorescence was bleached. Immediately after bleaching, a time-series of capturing 10 frames with a 30 s interval were made. Then, z-stacks were taken manually every 5 min up to 30 min after bleaching. To ensure that the bleached ROI did not drift out of focus, z-stacks were made throughout the whole cell. Three ROIs were bleached per cell at different locations within the IF network. FRAP experiments were performed at different days in at least three separate experiments. This resulted in the following amount of ROIs measured: 33 × GFAPα in a network, 30 × GFAPδ in a network, 8 × GFAPα in a collapse, and 8 × GFAPδ in a collapse.

FRAP analysis

ROIs were positioned in post bleach pictures manually. Per time point, the position of the ROI was corrected for cell movement, and average fluorescence was measured using Image J. The average fluorescence was plotted in time to obtain fluorescence recovery curves for every ROI. The half time was calculated by interpolating the time at 50 % of the fluorescence of the maximum fluorescence at 30 min. The immobile fraction was calculated by comparing the fluorescence in the bleached area after recovery (F_∞) with the fluorescence before bleaching (F_i) and just after bleaching (F_0). The immobile percentage is defined as $(1 - (F_\infty - F_0)/(F_i - F_0)) \times 100$. For F_∞, the average of the last three time points was used for analysis.

Statistics and factor correction

Data obtained from independent experiments were corrected with a factor correction program (version 10.5 2012) (Ruijter et al., 2006) when stated. Kruskal–Wallis, Kolmogorov–Smirnov, or Mann–Whitney tests were performed to test for significance. Differences were considered significant at $p < 0.05$. All statistical tests were performed using Graphpad Prism 5 (version 5.04) (Graphpad Software Inc., La Jolla, CA, USA).

Focal adhesion analysis

To analyze focal adhesions, coverslips were coated with laminin in 24-wells plates. Cells were plated at 10,000 cells per well. After attaching for 2 days, cells

were fixed with 4 % PFA, stained with rabbit anti-phosphorylated-paxillin (pY118; Life Technologies), and counterstained with Hoechst and Phalloidin-488.

Fixed and immunostained samples were imaged on an inverted microscope (Zeiss Axiovert 200) with a Confocal Spinning-disk Unit (Yokogawa CSU X-1) and an emCCD camera (Andor iXon 897). Excitation was accurately controlled by 405 nm (Crystalasers), 514 nm (Cobolt), and 642 nm (Spectra Physics) lasers through an acousto-optic tunable filter (AA Optoelectronics) coupled into the CSU with a polarization-maintaining optical fiber. Images were acquired with Andor IQ 2 software, and further processing and analysis were performed in specifically designed software (Matlab, Mathworks).

Focal adhesions were automatically detected from the 642-nm fluorescence images. Focal adhesion size could be at least 0.4×0.4 μm and at most 4×4 μm. In an image of 512×512 pixels low pass frequency with a cut-off at 2 pixels filtering removed large features. With a subsequent threshold of 3 times the standard deviation of the image, we obtained and characterized the focal adhesions. Focal adhesion size differences were tested using a 2-tailed Kolmogorov–Smirnov test. Differences were considered significant if $p < 0.05$. Per condition, a different amount of cells and focal adhesion were measured, but at least exceeded 30 different cells and a total of more than 700 focal adhesions.

Results

GFAPδ perturbs the GFAP network in astrocytes

Cellular models for studying GFAP isoform function were established by expression of GFAP isoforms in U251 cells and primary human astrocytes. The mRNAs of the different isoforms were highly expressed in the transduced U251 cell lines (Sup. Fig. 1a, b) and primary human astrocytes (Sup. Fig. 1d, e). Western blot analysis showed a clear expression of either GFAPα or δ (Sup. Fig. 1c), while the control (Ctrl) only showed a band with the pan GFAP antibody, representing endogenous GFAPα. The endogenous expression of the other GFAP isoforms was determined with qPCR and is presented as a percentage of the canonical GFAPα expression. GFAPα and GFAPδ were the most abundant isoforms expressed, followed by GFAPκ. Other isoforms were expressed at a very low level (Sup. Fig. 1f).

First, we confirmed whether GFAPδ-induced cytoplasmic collapses of GFAP also occurred in the transduced U251 cells and primary human astrocytes, as we have shown before in SW13 human adrenal carcinoma cells and U343 astrocytoma cells (Kamphuis et al., 2012; Perng et al., 2008). We investigated the IF network

morphology by immunostainings for GFAP, and we observed that the different GFAP isoforms gave similar results in both the primary human astrocytes (Fig. 1a) and the human U251 astrocytoma cells (Fig. 1b). The endogenous GFAP network was stained in the control condition, in which cells were transduced with mCherry. The GFAP network was present throughout the cytoplasm up to close proximity of the cell periphery, which is visualized by actin staining. Expression of recombinant GFAPα in human astrocytes, or in U251 cells, resulted in a GFAP network which was morphologically similar to astrocytic IF networks, indicating that the recombinant GFAPα was incorporated into the endogenous IF network of the cells. In contrast, expression of GFAPδ led to a collapse of the GFAP network mostly in a perinuclear fashion (Fig. 1a, b). This perturbing effect of GFAPδ on the GFAP network in these cells is concentration dependent and is a gradual process (data not shown), as has also been described before (Nielsen and Jørgensen, 2004; Perng et al., 2008).

Vimentin and nestin co-collapse with GFAPδ, while actin and microtubules stay intact

To assess whether GFAPδ induces a collapse of the complete cytoplasmic IF network, we also studied the distribution of vimentin (Fig. 2a) and nestin (Fig. 2b), which were both present in the IF network in primary human astrocytes. Transduction with GFAPα had no effect on the intracellular location of these proteins, but transduction with GFAPδ led to a condensation of vimentin and nestin, mostly around the nucleus. The same effect was observed in the U251 cell line (not shown). The actin and microtubule cytoskeletal networks did not co-collapse with the IF network upon GFAPδ expression (Fig. 2a, b, Sup. Fig. 2a, b). The staining intensity of actin was very variable between cells and between conditions, but the overall morphology of the actin network showed no actin collapse induced by GFAPδ.

To examine whether the additional expression of GFAPα or GFAPδ would lead to effects on transcription of other IFs, we analyzed the change in mRNA expression of vimentin, nestin, and endogenous GFAPα and GFAPδ in U251 cells using quantitative PCR. GFAPα mRNA (Sup. Fig. 3a), GFAPδ mRNA (Sup. Fig. 3b), vimentin mRNA (Sup. Fig. 3d), and vimentin protein (Sup. Fig. 3e) levels were not significantly changed due to an increase in either GFAPα or GFAPδ. However, we noticed a small but significant upregulation of nestin transcript in GFAPα expressing cells (p = 0.03) (Sup. Fig. 3c).

GFP tagged GFAP incorporates into the endogenous IF network

Next, we assessed the dynamic properties of GFAP isoforms using N-terminally GFP tagged GFAP fusion proteins for live cell imaging. The transduced cells express
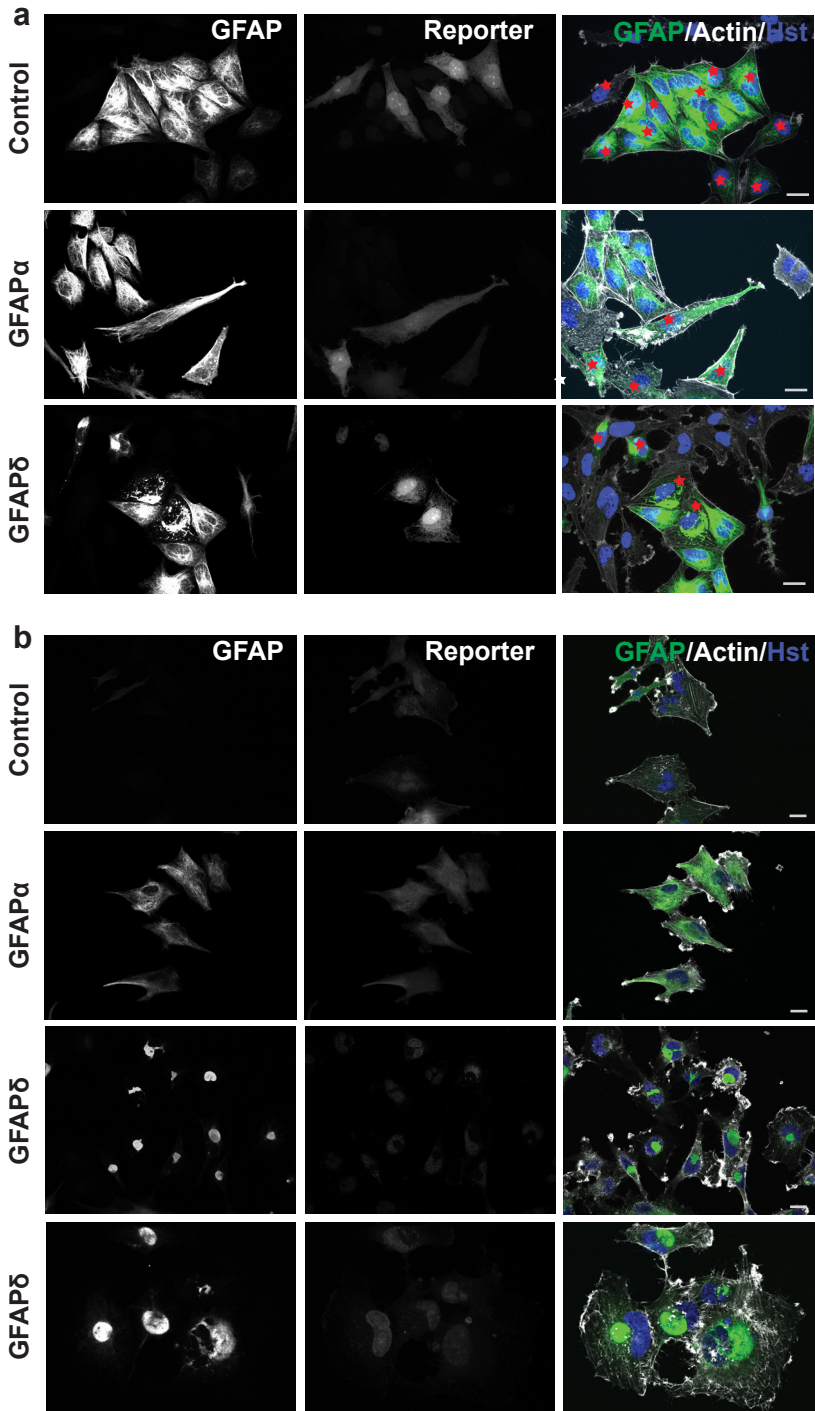
GFP-labeled GFAP isoforms, and thereby, transduced cells can be directly identified based on the reporter GFP. Both GFP–GFAPα and GFP–GFAPδ did incorporate into the endogenous IF network of U251 cells (Sup. Fig. 4a, b). Since a high expression of tagged GFAP also led to a collapse of the network, a relatively low expression was needed to image a non-collapsed network, which was established by analysis 24 h after transient transfection using U251 cells for a reasonable transfection efficiency. 24 h after transfection, the GFP–GFAPα transfected cells showed a spread out network (Sup. Fig. 5a), and GFP–GFAPδ expressing cells showed a mixture of cells with either a spread out network (Sup. Fig. 5b) or a collapsed IF network (Sup. Fig. 5c). The endogenous IF network is visualized by the vimentin staining. About 30 % of the GFP–GFAPδ expressing cells in our cell culture condition showed a collapse at this time point, although the exact percentage varied between experiments and was dependent on the transfection efficiency.

Live cell imaging of the GFAPδ dynamically shows the collapse of the network

To visualize the dynamics of the collapsing network over time, U343MG astrocytoma cells transfected with GFP–GFAPδ were imaged for 48 h, starting 4 h after transfection. U343MG cells were used here, since they are less motile than U251MG cells, which enabled us to image the IF network for a long period of time. First, GFP–GFAPδ was distributed throughout the IF network in the whole cell (arrow in Fig. 3a t = 12 h). GFP–GFAPδ started to condensate around the nucleus, as the expression of GFP–GFAPδ increased over time (Fig. 3a and Sup. Movies 1 and 2). Sometimes small aggregates or condensations were seen, which joined the already collapsed GFAP proteins (arrowheads Fig. 3a t = 30 and Sup. Movies 1 and 2). During and after the process of the accumulation, cells were still migrating, and the collapsed IF network was a motile structure in both stationary and moving cells. These experiments showed that GFP–GFAPδ, in small amounts, is incorporated into the endogenous IF network before it causes a collapse of the IF network. Images

Figure 1. GFAP isoform expression in primary human astrocytes and U251 astrocytoma cells. a Human primary astrocytes transduced with GFAPα, GFAPδ, or mCherry (control). Cells were stained with pan GFAP Dako antibody (GFAP) together with phalloidin (Actin) and Hoechst (Hst). The reporter showed in the middle panel which cells were transduced cells, and these are additionally highlighted in the right panel with red stars. Expression of GFAPα resulted in a dense GFAP network, which was spread throughout the whole cell. Expression of GFAPδ showed a drastic redistribution of the GFAP network, which collapsed in a perinuclear fashion. **b** Human U251 astrocytoma cells transduced with GFAPα, GFAPδ, or mCherry (control) also showed a collapse of the GFAP network in GFAPδ transduced cells only. In this panel, all cells were transduced, as these were stably transfected cell lines. A close up of the collapsed network is shown in the lowest panel. Scale bars represent 20 μm
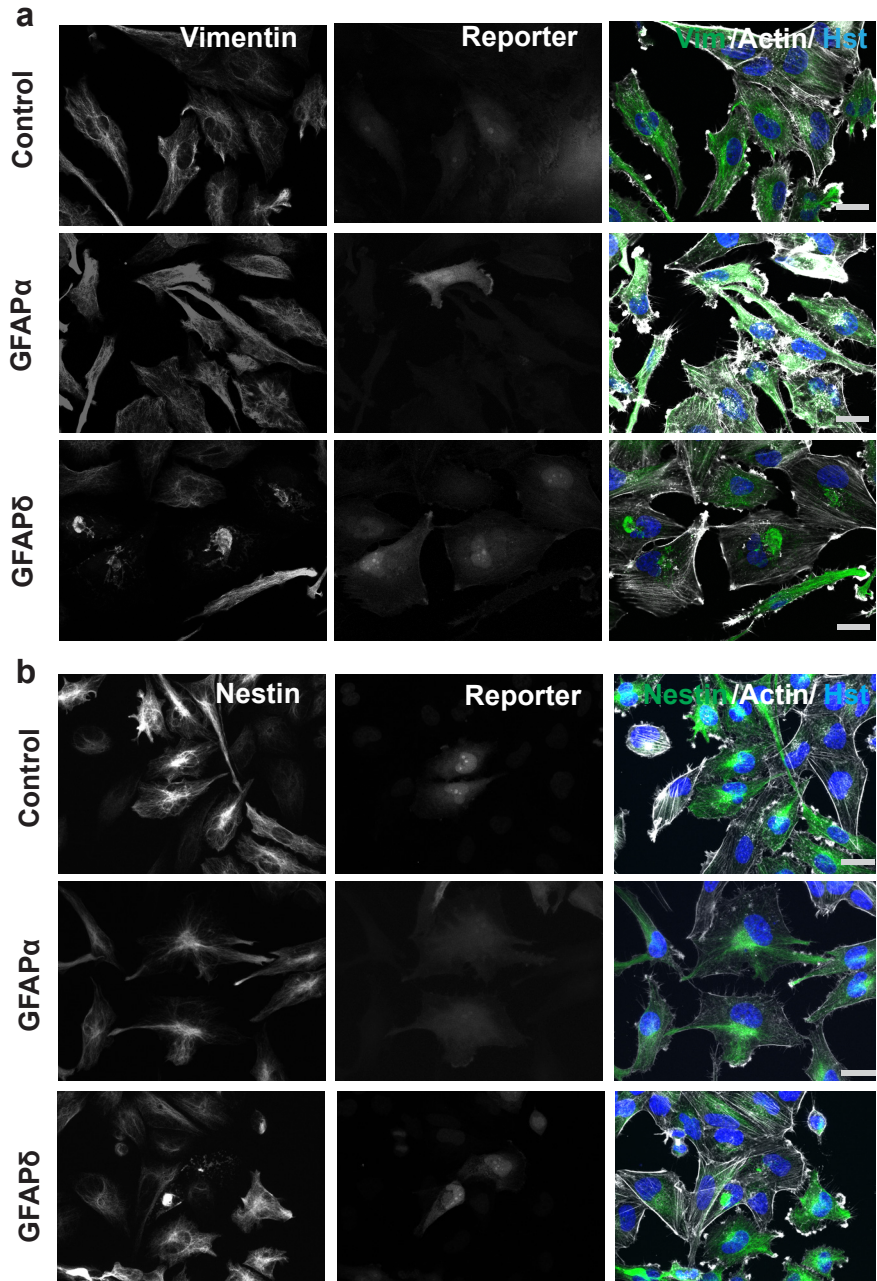
Figure 2. GFAPδ collapses the whole IF network. a Primary human astrocytes transduced with GFAPα, GFAPδ, or control plasmid stained for vimentin and actin or **b** nestin and actin. Astrocytes expressing ectopic GFAPα or mCherry had a network that was spread throughout the whole cell while GFAPδ expressing cells showed a perinuclear collapse of both vimentin and nestin in cells positive for the reporter only. GFAPδ transduced cells with relative low expression, as seen by lower reporter expression, do not show a collapsed IF network yet. Scale bar represents 20 µm

from fixed cells stained for GFP, GFAP, and vimentin showed that the squiggles (short filaments) of GFP–GFAPδ sometimes co-localized with vimentin and were not part of larger filaments (Fig. 3b, arrow).
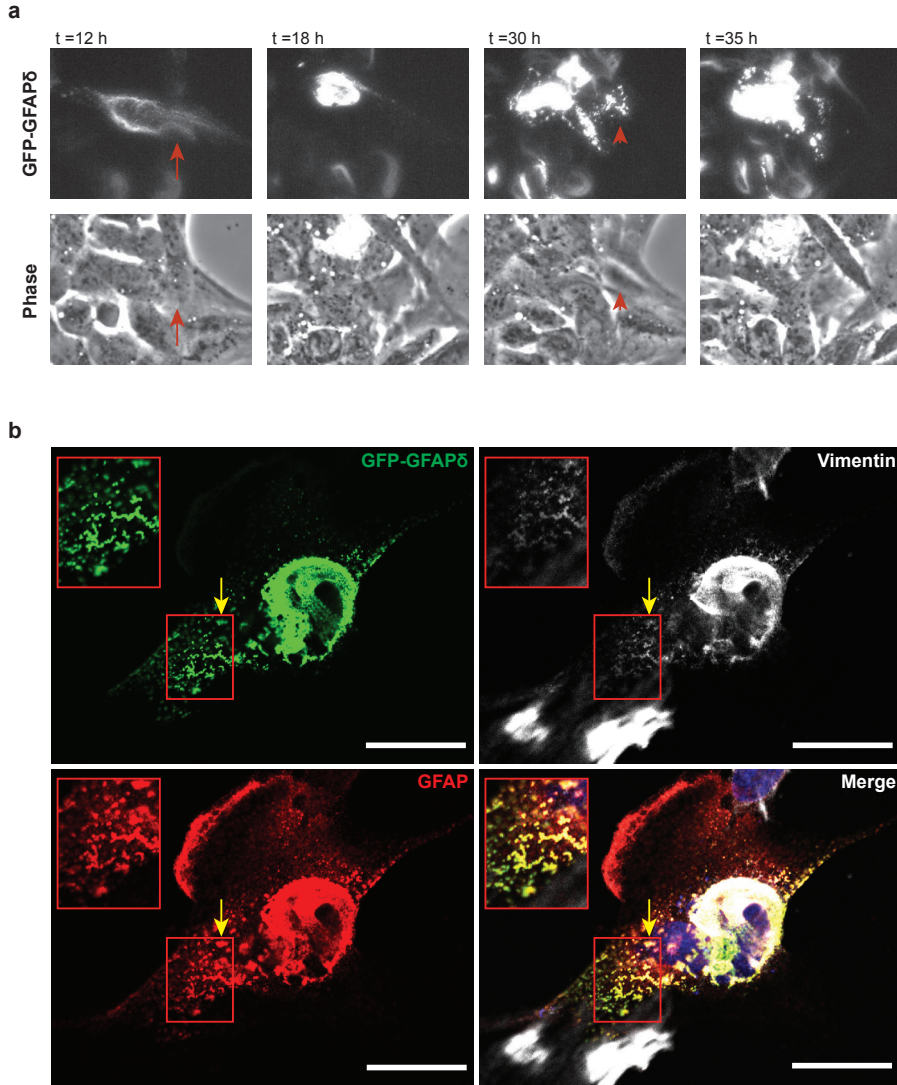
Figure 3. Collapse of the IF network due to high GFP–GFAPδ expression. a Stills from a representative live cell imaging experiment. U343MG cells were transfected with GFP–GFAPδ and imaged for 48 h. The GFP–GFAPδ was initially incorporated into the IF network (arrows at t = 12 h), but as the amount of GFP–GFAPδ increased over time, it eventually caused a collapse of the network (t = 18 h). During the process of collapsing, thicker and shorter filamentous structures are visible in the cell, which are moving into the direction of the collapsed network (arrowheads in t = 30 h). b These small filaments sometimes co-localized with vimentin in U251MG cells as well (yellow arrow). Scale bars represent 20 μm. See also supplemental Movie 1 and 2

Dynamic properties of GFP–GFAPα are different from GFP–GFAPδ

To assess the dynamic properties of GFAPα and GFAPδ, FRAP experiments were performed on U251 astrocytoma cells in which small boxed regions of fluorescent cells were photobleached, and recovery of fluorescence was measured over time. Cells were transfected with the GFP–GFAP isoforms, and the FRAP analysis was started 24 h later. Cells with non-collapsed and collapsed networks were measured and analyzed separately. Regions of fluorescent GFAP networks were bleached, and the fluorescence recovery was imaged up to 30 min after bleaching. A typical example is shown in Fig. 4a. The median of all FRAP recovery experiments for GFAPα and GFAPδ in an extended network and GFAPδ in a collapsed network are shown in Fig. 4d. The half time t½ (the time needed to recover to 50 % of the final fluorescence) and the immobile fraction (the percentage of fluorescence which is not recovered) were calculated. The median t½ value of GFAPδ in extended, non-collapsed networks was 2.3 min, and this was significantly (p < 0.05) longer than the median t½ of GFAPα, which was 1.1 min (Fig. 4b). Since high GFAPδ expression leads to a collapse of the IF network, we next investigated the dynamic properties of GFAPδ in a collapsed network. Although not significant, there was a clear trend visible that GFAPδ had a longer t½ (median = 3.8 min) when in a collapsed network compared with GFAPδ in a spread out network (Fig. 4b), indicating a slower on/off rate from the IF network. We also calculated the immobile fraction of the GFP–GFAPs, which is the percentage of fluorescence that did not recover from the FRAP curves. We observed that the immobile fraction did not significantly differ between GFAPα (median = 40.3 %) or GFAPδ in extended network (median = 49.1 %). There was, however, a significant difference between the immobile fraction of

Figure 4. Different dynamics between GFAPα and GFAPδ. a FRAP experiments consisted of bleaching ROI and measuring the fluorescence recovery up to 30 min after the bleach in U251MG cells. Within 150 s, most of the fluorescence was recovered, but recovery was never complete. **b** FRAP experiments were performed for GFAPα, GFAPδ, and GFAPδ in a collapsed network, and half times were calculated. There is a significant difference in half time between GFAPα (median = 1.1 min) and GFAPδ (median = 2.3 min) (p < 0.05; n = 33, n = 30), and between GFAPα and GFAPδ in a collapsed network (median = 3.8 min) (p = 0.000; n = 32). There was no significant difference in the half time of GFAPδ in spread out or collapsed network, although there was a trend that a collapse decreased the half time of GFAPδ. **c** The immobile fractions were not significantly different between GFAPα (40.2 %), GFAPδ (49.1 %) (p = 0.7; n = 29 and n = 30). GFAPδ in a collapse did have a significantly different immobile fraction (56.3 %; n = 32) compared with GFAPα (p = 0.03) and GFAPδ (p = 0.04) in a network. Graphs b and c show median values with interquartile range. **d** Medians of FRAP curves for GFAPα, GFAPδ and GFAPδ in a collapse show the recovery after bleaching. Non-parametric tests were performed on the data extracted from the FRAP measurements, so non-overlapping curves do not equal significant differences in this graph
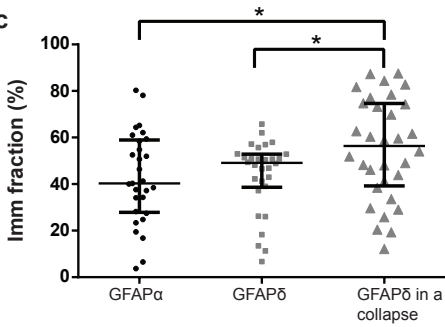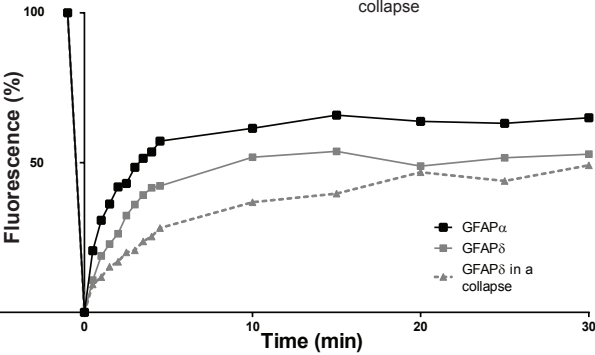
a

3

b

c

d
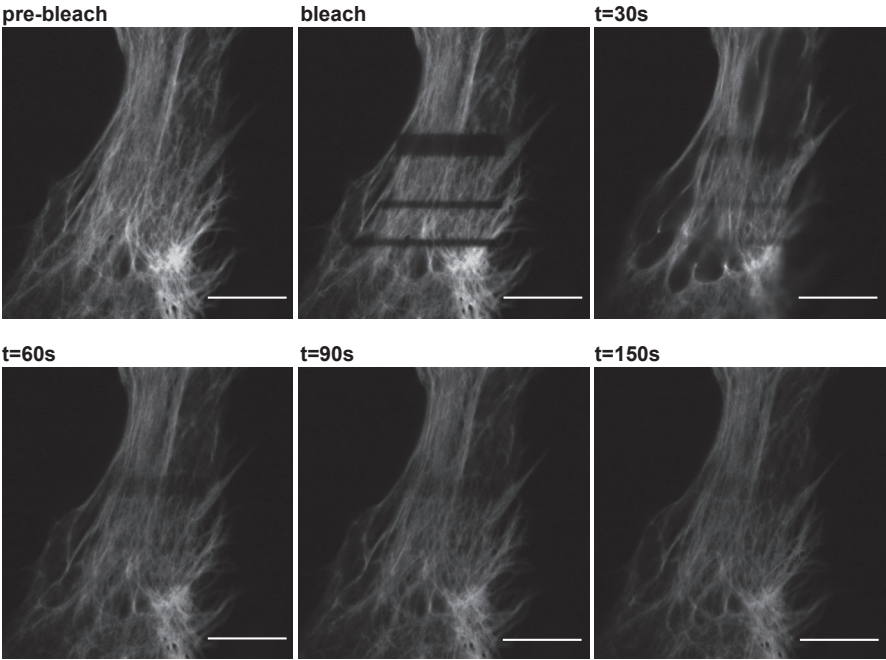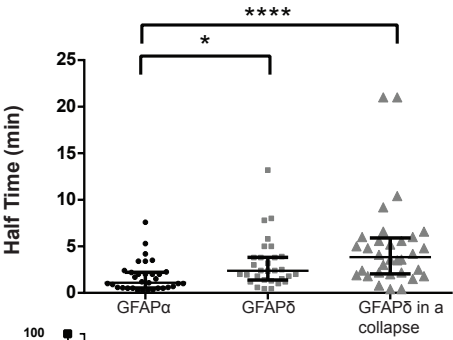
GFAPδ when the majority of the GFAP was in a collapsed network (median = 56.4 %) compared with the immobile fraction of GFAPα and GFAPδ when GFAP was in a spread out network (Fig. 4c).

To assess whether the change in dynamic properties between GFAPδ when in a network and when it has collapsed was due to the collapse of the network and not GFAPδ itself, we performed experiments in which we also measured the dynamics of GFAPα in a collapsed network. To study this, we transfected cells with untagged GFAPδ to induce the collapse, and co-transfected either GFP–GFAPα or GFP–GFAPδ to visualize the fluorescent isoform dynamics. Both GFP–GFAPα (Sup. Fig. 5a) and GFP–GFAPδ (Sup. Fig. 5b) were incorporated into the collapse as can be seen by staining for vimentin, which is highly expressed in U251 cells and shows the endogenous IF network. A representative example of a bleached collapsed network and the subsequent recovery is shown in Fig. 5a. The median t½ for GFAPα (4.4 min) and GFAPδ (5.5 min) did not differ significantly (p = 0.8) (Fig. 5b). The t½ measured for GFAPα was remarkably increased due to the collapsed network (Fig. 5b). The fluorescence had not yet reached plateau after 30 min of recovery. Taken together, this indicates that GFAPα and GFAPδ have different exchange dynamics (as measured by t½) and the dynamics show a trend for higher t½ when the IF network is collapsed.

A collapsed IF network changes cell morphology

Next, we aimed at defining whether the IF network collapse and changes in dynamics also result in a change in morphology, since IF expression has been linked to cell morphology (Lepekhin et al., 2001; Moeton et al., 2014). Morphological parameters of living U251 cells expressing different GFAP isoforms were determined by measuring the cell surface area and the perimeter. From these parameters, we calculated the form factor, as described in the methods section. Forty cells were analyzed per experiment in five independent experiments. GFAPδ expression caused the cells to become rounder (0.56 ± 0.006; mean ± SEM) in comparison with the control (0.49 ± 0.005, p = 0.009) (Fig. 6a). We also observed significant differences in perimeter (Fig. 6b) and area (Fig. 6c) between cells expressing GFAPδ and GFAPα.

To assess whether the morphological changes we observed were due to changes in cell-extracellular matrix interaction, the sizes of focal adhesions were assessed by phosphorylated paxillin stainings in cells plated on a laminin substrate. In both GFAPα and GFAPδ expressing cells, the size of the focal adhesion was increased (mCherry: 1.13 µm2 ± 0.02; GFAPα: 1.34 µm2 ± 0.03; GFAPδ: 1.37 µm2 ± 0.03 (Fig. 6e, f). There was, however, no transcriptional regulation of the main laminin-binding

integrins expressed in these cells (data not shown).

GFAP overexpression does not affect cell motility or cell proliferation

Focal adhesions are tightly regulated during cell migration, and GFAP has been linked to in vitro migration by others (Rutka et al., 1994; Lepekhin et al., 2001). To
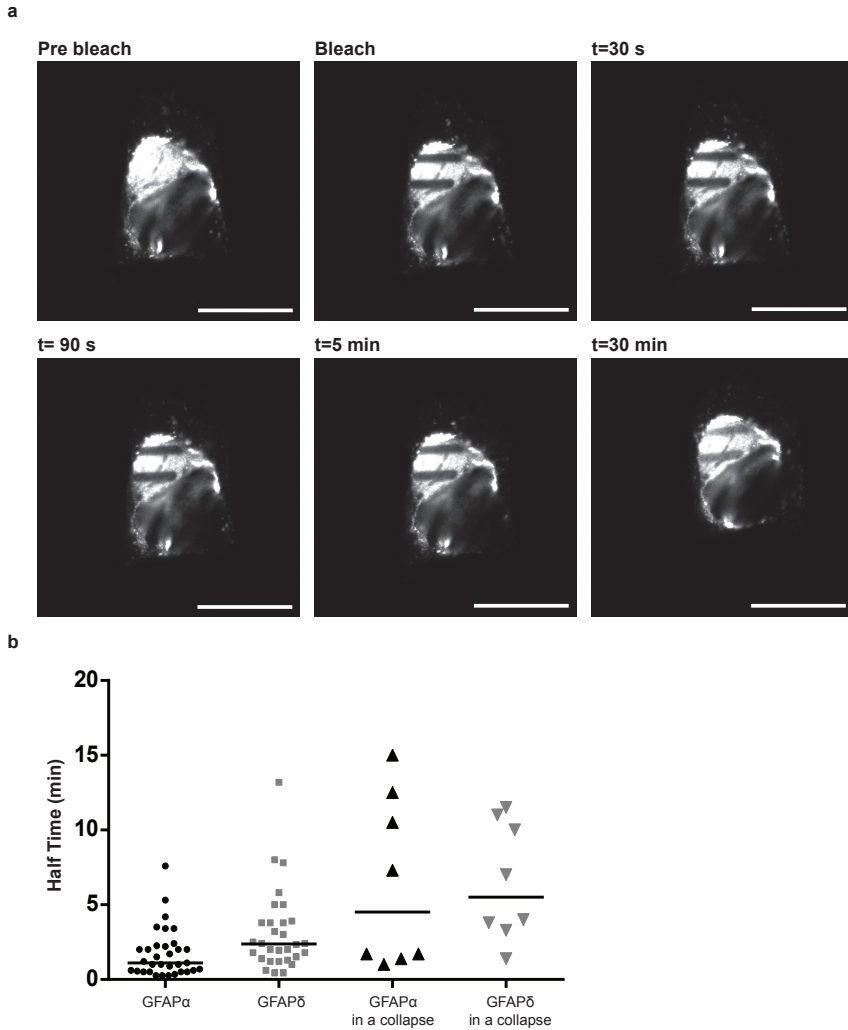
Figure 5. Dynamics of GFAP isoforms in a collapsed IF network. a A representative still of a FRAP experiment on U251MG cells with a collapsed IF network. ROIs were bleached and the fluorescence recovery was measured for up to 35 min. Even after 30 min, the bleach area was still clearly visible. **b** Half times were calculated as described in the materials and methods section. There were no significant differences between the half time of GFAPα in a collapse (median = 4.5 min) or GFAPδ in a collapse (median = 5.5 min) (p = 0.8; n = 8). There was a clear trend showing that a collapse caused a longer half time (4.5 vs. 1.1 min for GFAPα and 5.5 vs. 2.3 min for GFAPδ) of the GFAP isoforms
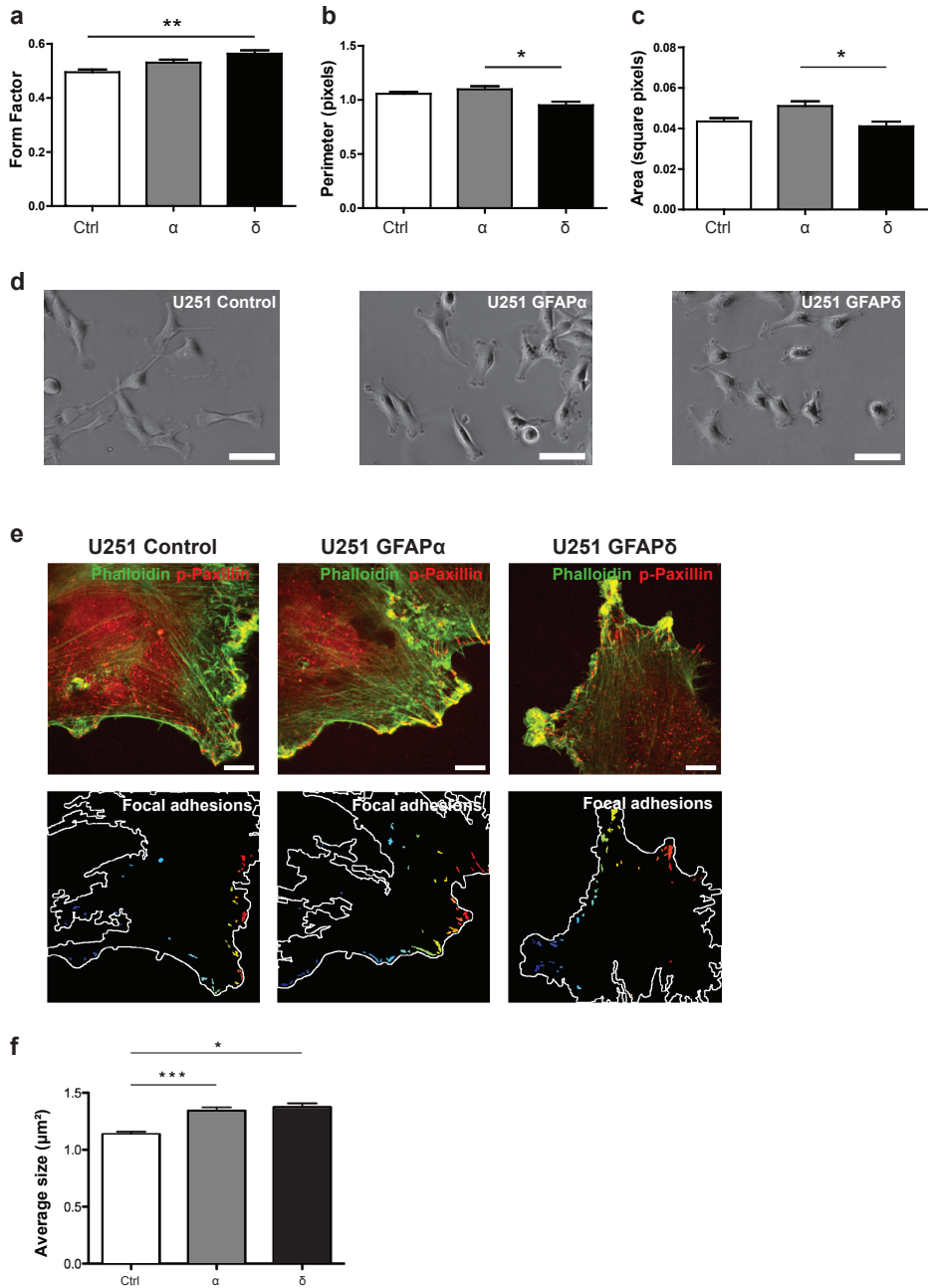
Figure 6. Morphology of U251 cells with different IF networks. a GFAPδ expressing cells showed a more round morphology in comparison to the control (p = 0.009) as is measured by the form factor of these cells. Significant differences between GFAPα and GFAPδ were found in **b** perimeter (p = 0.02) and **c** area (p = 0.03). Bars show mean and SEM (n = 5). **d** Phase contrast pictures showing the more round morphology of the GFAPδ expressing cells in comparison with the control vector and GFAPα. Scale bars represent 100 μm. **e** U251 cells expressing different GFAP isoforms are stained
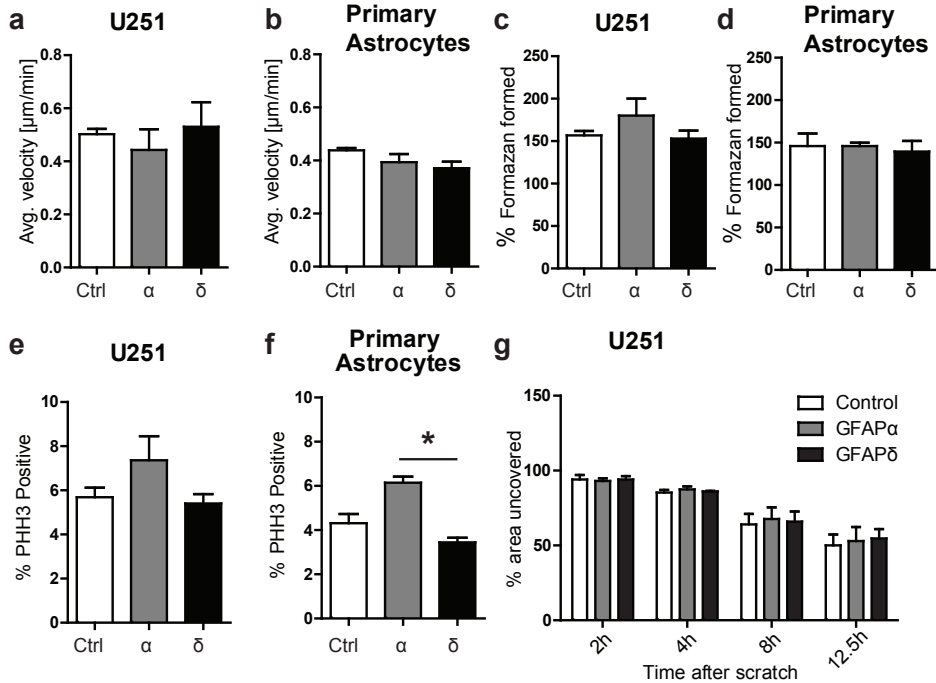
Figure 7. Migration and proliferation is not affected by GFAPδ. a Single cell motility was measured as the average velocity in μm/min of a single cell, in a sequence of images, which were taken overnight. Average velocity did not differ significantly between GFAPα, GFAPδ, and control cells (p = 0.9) (n = 3) in U251 cells or in **b** primary astrocytes (p = 0.15) (n = 3). **c** Proliferation was measured by metabolic conversion of MTT, which was measured by absorbance of light. The absorbance at t = 24 h was put at 100 %. There was no significant difference between GFAPδ, GFAPα, and control (p = 0.56) (n = 3) at 48 h in U251 cells or **d** primary astrocytes (p = 0.56) (n = 3). **e** Cells were stained for PHH3, indicating dividing cells. The average percentage of dividing cells per condition at one time point is not significantly different in cells with GFAPα, GFAPδ, and control in U251 cells (p = 0.21) (n = 4) **(f)**. In primary astrocytes, there was a significant difference in proliferation between GFAPα and GFAPδ (p = 0.04) (n = 3). **g** Scratch assays were done by scratching a monolayer of cells and measuring the area uncovered by cells, over time. The area of the scratch at t = 0 was put at 100 %. The bars represent the area where there are no cells at different time points. There was no significant difference (p = 0.7) (n = 3) between GFAPα, GFAPδ, and the control after 12.5 h. All graphs show mean with SEM

(Figure 6, Continued) for actin with phalloidin (green) and phosphorylated paxillin (red). Scale bars represent 10 μm. The lower panel shows focal adhesions (overlap of phalloidin and phosphorylated paxillin). **f** Quantification of focal adhesion shows larger focal adhesion size in GFAPα (p = 0.0001) and GFAPδ (p = 0.001) expressing cells compared with the control mCherry (mCherry: 1.13 μm2 ± 0.02 n = 735; GFAPα: 1.34 μm2 ± 0.03 n = 994; GFAPδ: 1.37 μm2 ± 0.03 n = 828

check for changes in cell motility, we analyzed single cell motility and scratch wound healing speed. Single cell motility assays were performed on U251 cells expressing GFAPα, GFAPδ, or mCherry. Cells were seeded on PLL coated glass coverslips, and thirty cells were analyzed per experiment in 3 independent experiments. There were no statistically significant differences in average velocity between U251 cells expressing GFAPδ (0.53 μm/min ± 0.09), GFAPα (0.44 μm/min ± 0.08), or control (0.50 μm/min ± 0.02) (p = 0.9) (Fig. 7a). Similar results were found in a wound healing assay where a monolayer of cells was scratched and the wound healing speed was measured over time (Fig. 7g). Wound healing speed of U251 cells expressing GFAPα (52.9 % ± 9.3), GFAPδ (54.7 % ± 6.2), or the control (50 % ± 7.3) was not different at 12.5 h (p = 0.7). To study the effects of GFAP isoform expression on primary cell motility instead of on tumor cells, single cell motility assays were also done on primary human astrocytes. Again, we found no statistically significant difference between cell motility of cells expressing GFAPα (0.39 ± 0.03), GFAPδ (0.37 ± 0.02), and control cells (0.43 ± 0.009) (p = 0.15) (Fig. 7b).

Since GFAPδ is highly expressed in proliferating astrocytes, i.e., neurogenic astrocytes (Roelofs et al., 2005; Van Den Berge et al., 2010) and astrocytoma cells (Choi et al., 2009; Heo et al., 2012), we determined the effect of GFAPδ expression on proliferation by performing a 3-(4,5-Dimethylthiazol-2-yl)-2,5-diphenyltetrazolium bromide (MTT) assay (Mosmann, 1983). We observed no significant difference between proliferation of GFAPδ (153 % ± 9.2), GFAPα (180 % ± 19.8), and control (mCherry) (156 % ± 5.3) (p = 0.56) over a period of 48 h in U251 cells (Fig. 7c). The MTT assay in primary astrocytes also did not show significant differences between GFAPα (146 % ± 3.8), GFAPδ (139 % ± 12.5), and control (146 % ± 14.7) (p = 0.56) (Fig. 7d). To confirm these results, proliferation was also assessed by staining for the proliferation marker Phospho histone H3 (PHH3). U251 cells transduced with the GFAP isoforms were plated, fixed 48 h later, and stained for PHH3 (Fig. 7e). We observed no significant difference (p = 0.21) in the percentage of PHH3 positive cells between GFAPα (7.3 % ± 1.1), GFAPδ (5.4 % ± 0.4), and control (5.6 % ± 0.4). PHH3 staining in primary astrocytes did, however, show a significant difference between GFAPα (6.1 % ± 0.3) and GFAPδ (3.4 % ± 0.2) (p = 0.04) (Fig. 7f). Taken together, these data show that GFAPδ expression did not alter cell proliferation or motility, while GFAPα led to a slightly higher proliferation rate compared with GFAPδ.

Discussion

Astrocytes and astrocytoma cells tightly regulate the expression of at least 10 different GFAP isoforms (Middeldorp and Hol, 2011). GFAPα and GFAPδ are the

two most highly expressed isoforms. The functional consequences of changes in the IF network in astrocytes and astrocytoma cells are still elusive. In this study, we have investigated the effect of GFAPδ on cell proliferation, migration, motility, and shape but also the intracellular effects on IF network dynamics. We here show that GFAPα and GFAPδ have different intrinsic dynamic properties, but that expression of GFAPδ does not affect cell proliferation or migration when there is a collapse of the IF network.

Dynamic properties

GFAPδ is assembly compromised by itself (Nielsen and Jørgensen, 2004) and causes a collapse of the whole IF network. We here show that even before a collapse, GFAPδ changes the dynamics of the the IF network. Dynamic properties of IF proteins differ between IF family members (Yoon et al., 1998, 2001; Li et al., 2006; Gilchrist et al., 2004). These differences are likely due to phosphorylation or structural properties that affect the assembly. The latter is for instance reflected in higher FRAP recovery half time values by the nuclear lamins (~140 min) (Gilchrist et al., 2004; Moir et al., 2000), which forms IgG-like folds during assembly (Kreplak et al., 2004). In contrast, GFAP and vimentin, which are both located in the cytoplasm, have half times between 1 and 5 min (Yoon et al., 2001; Li et al., 2006). In this study, we showed that GFAPδ incorporates and dissociates slower from an IF network than GFAPα. Since the C-terminal tail is the only difference between GFAPα and GFAPδ, the differences in dynamics must be due to this specific sequence. IF protein motility and exchange are mediated through interactions with microtubules and actin to regulate transport (Yoon et al., 1998), and IF protein phosphorylation to regulate filament stability (Ku et al., 1996; Nakamura et al., 1992; Skalli et al., 1992). In the part of the C-terminus, where GFAPα and GFAPδ differ, the same amount of putative phosphorylation sites are present (7 residues). However, the position of these residues is different, possibly leading to a different availability of phosphorylatable residues in the protein tertiary structure. In the tail of GFAPδ is a coil 2B binding site, which lacks in the GFAPα tail (Nielsen and Jørgensen, 2004). It has been proposed by Nielsen and Jorgensen (Nielsen and Jørgensen, 2004) that this domain results in a gain of coiled-coil binding activity of GFAPδ, which might explain the slower dissociation of GFAPδ from an IF network. Earlier experiments have shown that ablation of the whole C-terminal tail of IF type III proteins inhibits IF assembly (Chen and Liem, 1994; Chen et al., 2011), but phosphorylation of vimentin at the C-terminal side did not affect its assembly (Chou et al., 1996). Mutant GFAP isoforms, with mutated phosphorylation sites, will help to elucidate the effects of

3

GFAP phosphorylation on network dynamics.

Effect on proliferation, motility, and migration

In this study, we showed that a GFAPδ-induced collapse of the IF network results in a reorganization of the whole IF network. This is in contrast with a knockout or knockdown of GFAP, which does not severely affect vimentin or nestin localization (Moeton et al., 2014). GFAP, as well as other IFs, has been linked to changes in proliferation and astrocyte motility, but it has to be noted that the studies on the role of GFAP in cell proliferation are inconclusive. A GFAP knockdown has been shown to lead to an increase in proliferation in some studies (Rutka et al., 1994; Ding et al., 1998), but not in others (Weinstein et al., 1991). On the other hand, astrocyte cultures of transgenic mice overexpressing human GFAPα showed a decrease in proliferation (Cho and Messing, 2009). Since GFAPδ is expressed in cycling cells in the human brain (Choi et al., 2009; Van Den Berge et al., 2010; Heo et al., 2012), we expected an effect of GFAPδ on cell proliferation. Unexpectedly, we observed that not the expression of GFAPδ, but an enhanced expression of GFAPα resulted in a significant increase in proliferation of primary astrocytes. We detected a similar trend in the U251 astrocytoma cells. Our data show that the increase in proliferation is caused by the mere increase in GFAPα and that there is no direct role of GFAPδ in cell proliferation in cells with a collapsed IF network. Lowering the ratio of GFAPα:GFAPδ making sure that there is still an intact network also did not change cell proliferation in vitro (Moeton et al., 2014).

Several studies have found that a knockdown or knockout of GFAP increases cell motility (Rutka et al., 1994, 1998; Lepekhin et al., 2001). In addition, we recently showed that a specific knockdown of GFAPα leads to a reduced motility in astrocytoma cells (Moeton et al., 2014). Here, we show that an overexpression of GFAPα or GFAPδ has no effect on cell motility, even if the IF network is collapsed by high GFAPδ levels. Regulation of motility by GFAP is rather complex. Mutations in the rod domain of GFAP that causes collapses of the network, and thus mimics our GFAPδ condition, have been shown to increase cell motility. In contrast, mutations in the tail domain of GFAP had no effect on motility (Yoshida et al., 2007, 2009). GFAPα and GFAPδ only differ in the C-terminal tail, thus this might explain why we do not see differences in cell motility.

Effect on ECM interaction

GFAP has been linked to cell morphological changes in astrocytes in vitro, where a correlation was observed between the level of GFAP expression and the number of cell protrusions (Weinstein et al., 1991; Rutka and Smith, 1993; Rutka et al., 1994;

Lepekhin et al., 2001; Elobeid et al., 2000). In reactive gliosis, the production of GFAP as well as other IF proteins is upregulated. This results in a more pronounced, GFAP-positive, IF network (Buffo et al., 2010; Sofroniew, 2009; Wilhelmsson et al., 2006). Here, we show that the collapse of the IF network due to GFAPδ expression resulted in more round cells with longer focal adhesions in vitro. This change resembles the morphological change in astrocytes devoid of IFs in vitro (Weinstein et al., 1991; Rutka and Smith, 1993; Rutka et al., 1994; Lepekhin et al., 2001). Thus, an intact IF network is important for the formation or stabilization of processes of cells. In our earlier study, we showed, however, that a pan-GFAP knockdown in U373 cells did not result in a rounder morphology (Moeton et al., 2014). This is probably due to the presence of an intact vimentin and nestin IF network, which is lacking in the cells with a GFAPδ-induced collapse.

The change we observed in cell morphology in cells with a GFAPδ-induced collapsed IF network shows that the IF network distribution per se can affect the shape of the cell. The way GFAPδ alters shape is likely to occur through integrins. Integrins are the main linkers between the extracellular matrix and the cytoskeleton in vivo and, together with other proteins, they form the focal adhesions. Focal adhesions can be present in different sizes and maturation states, ranging from small structures, of less than 1 μm, to larger focal adhesions. Focal adhesion size is dependent on actomyosin generated tension (Bershadsky et al., 2003; Wolfenson et al., 2011). Indeed, interactions between the IF protein vimentin and mature focal adhesions have been shown to be essential for proper cell spreading (Lynch et al., 2012). Vimentin can regulate adhesion and focal contact size under shear stress (Tsuruta and Jones, 2003) and controls cell adhesion strength through plectin and β3 integrins (Bhattacharya et al., 2009). Thus, GFAP could have a similar function in adhesion of astrocytes to the ECM and in this way alter cell shape. Our data confirm a direct effect of the IF constellation on focal adhesions and cell–matrix interactions, as both GFAP isoforms increase focal adhesion size. Since only GFAPδ expressing cells showed altered morphology, this implies a difference in the effect GFAPα and GFAPδ has on the functionality of focal adhesions. This might partly be due to differences in production of ECM molecules, such as laminin, as we have shown before (Moeton et al., 2014). Although the exact interaction of GFAP with focal adhesions is still elusive, interactions between other IFs and focal adhesions have been described, as is nicely reviewed by Leube et al. (Leube et al., 2015).

Conclusion

To summarize, we have shown that a GFAPδ-induced collapse of the IF network

has a profound effect on IF network morphology, increases focal adhesion size, and changes the IF network dynamics, without altering astrocyte motility or proliferation. Although GFAPδ is expressed in more proliferative cell types with a higher migration potential, GFAPδ itself does not directly influence proliferation or migration when there is a collapse of the IF network. The changes in IF network dynamics could hold clues to GFAP isoform specific functions.

Acknowledgments

Legend Supplemental Materials

Supplemental materials can be found on www.ellyhollab.eu, with the published version of this chapter, or will be made available upon request.

Supplemental Figure 1
GFAP isoform specific overexpression models. GFAP mRNA levels were determined in U251 cells (a, b) and in primary human astrocytes (d, e), 7 days after transduction with GFAPα or GFAPδ lentiviral constructs. The transduced GFAP isoforms gave the highest expression in both U251 (n = 4) and primary human astrocytes (n = 3). The overall expression levels of GFAP are higher in primary human astrocytes compared with U251 cells. Overexpression is confirmed at protein level with Western blot. In U251 cells, the specific upregulation was shown with isoform specific antibodies, the GFAP c-term antibody distinctively recognizes GFAPα and the hGFAPδ antibody recognizes GFAPδ. The band in the control condition was recognized by a pan GFAP antibody and reflects the endogenous presences of mostly GFAPα. Due to less sensitivity of the C-term antibody, this band is not visible when blots are stained with this antibody. (f) Endogenous expression levels of GFAP isoforms in U251 astrocytoma cell lines and primary human astrocytes show that GFAPα and GFAPδ are the most abundant isoforms expressed. (TIFF 1722 kb)

Supplemental Figure 2
Cytoskeleton in primary human astrocytes with a collapsed IF network. Primary human astrocytes transduced with GFAPα, control plasmid, and GFAPδ, as indicated by the fluorescent reporter,

showed that microtubules (a) and actin filaments (b) were not co-collapsing with the IF network. Microtubules and actin filaments were still present throughout the whole cells in GFAPδ transduced cells. Hst = Hoechst. Scale bar represents 20 μm. * indicate the transduced cells in the GFAPα condition of 2b. (JPEG 1918 kb)

Supplemental Figure 3
mRNA expression of IFs in GFAP isoform expressing U251 cells. In U251 cells transduced with GFAP isoforms, mRNA was measured for the other IFs. There is no significant regulation of endogenous GFAPα (a), GFAPδ (b), or vimentin (d mRNA and e protein). The nestin mRNA expression (c) was significantly regulated only in cells ectopically expressing GFAPα protein (p = 0.03). (TIFF 976 kb)

Supplemental Figure 4
Incorporation of GFP–GFAP isoforms in a collapsed IF network. U251MG cells expressing GFAPδ showed a collapse of the IF network, as seen in a and b by analyzing GFAP and vimentin fluorescence. When co-expressed with GFAPδ, both GFP–GFAPα and GFP–GFAPδ were incorporated into the collapse (arrows). GFP fluorescence co-localized with GFAP and vimentin immunostaining, showing that the dynamics measured in these experiments reflect GFAP in a collapsed network. Cells transfected with GFP–GFAPδ showed a similar collapsed structure as the GFP–GFAPα cells. Scale bar represents 20 μm. (TIFF 5999 kb)

Supplemental Figure 5
GFP–GFAP incorporates into the endogenous IF network. (a–c) U251 cells transfected with GFP–GFAPα or GFP–GFAPδ showed incorporation of the fusion protein into the endogenous IF network. Cells were fixed 24 h after transfection and stained for GFP, GFAP, and vimentin. (a) After 24 h, GFP–GFAPα transfected cells showed the presence of GFP in the endogenous spread out network, indicating that this fusion protein assembled with endogenous IF proteins. After 24 h, GFP–GFAPδ transfected cells showed both cells with spread out networks (b), as well as with collapsed IF networks (c). In both cases, the GFP fusion protein co-localized with the endogenous IF network. Scale bar represents 20 μm. (JPEG 2056 kb)

Supplemental Movie 1
U343MG cells were transfected with GFP–GFAPδ and imaged for 48 h. As the expression of GFP–GFAPδ comes up the GFAP network becomes faintly visible. As the expression increases, the GFAP network collapses and condensates near the nucleus. The collapsed network remains motile within the cell. Scale bar represents 20 μm. (AVI 10,327 kb)

Supplemental Movie 2
This movie is a zoom in on one of the cells shown in Sup Movie 1 where U343MG cells were transfected with GFP–GFAPδ and imaged for 48 h. Here, it is clear to see that small parts of fluorescent GFP–GFAP move around in the cytoplasm before they condensate near the nucleus. Scale bar represents 20 μm. (AVI 1349 kb)

Chapter

4

GFAPδ/GFAPα ratio correlates with astrocytoma grade and directs astrocytoma gene expression towards a more malignant profile

Oscar M.J.A. Stassen*
Emma J. van Bodegraven*
Fabrizio Giuliani
Martina Moeton
Regina Kanski
Jacqueline A. Sluijs
Miriam E. van Strien
Willem Kamphuis
Pierre A.J. Robe
Elly M. Hol

* Authors contributed equally

Abstract

Astrocytomas are the most common malignant brain tumours and are to date incurable. It is unclear how astrocytomas progress into higher malignant grades. The intermediate filament cytoskeleton is emerging as an important regulator of tumour malignancy. The majority of the astrocytomas express the intermediate filament protein Glial Fibrillary Acidic Protein (GFAP). Several GFAP splice variants have been identified and the main variants expressed in human astrocytoma are the GFAPα and GFAPδ isoforms. Here we show a decrease of only GFAPα in astrocytomas with increasing grade, and a significant downregulation in glioblastoma (WHO grade IV), resulting in an increased GFAPδ/α ratio. Mimicking these changes in astrocytoma cell lines and comparing the transcriptomic changes with the changes in the patient tumours, we have identified a set of GFAPδ/α ratio-regulated tumorigenic and anti-tumorigenic genes. These genes are involved in cell proliferation and protein phosphorylation, and their expression correlated with patient survival. We additionally show that changing the ratio of GFAPδ/α, by targeting GFAP expression, affected expression of tumorigenic genes, suggesting that GFAP splicing is an attractive therapeutic target for astrocytoma.

Introduction

Astrocytomas are the most common malignant brain tumours, with an incidence of 5.9 per 100,000 in the Netherlands (Ho et al., 2014). Astrocytomas are malignant brain tumours that develop from either astrocytes, adult neural stem cells, or glia progenitors (Chen et al., 2012). These tumours are classified into different grades of malignancy based on histological assessment. Grade I (pilocytic astrocytoma) are slowly growing, localized tumours that only very seldom become anaplastic. Grade II (diffuse astrocytoma) are slowly growing tumours that tend to invade the brain more diffusely and sooner or later progress to more anaplastic grade III, or develop hyperplastic neovessels and areas of necrosis and become grade IV (glioblastoma multiforme (GBM)) tumours (Louis et al., 2007). Glioblastomas can also arise *de novo* (Ohgaki and Kleihues, 2013) and are by far the most common and most malignant variant of astrocytoma. Resection surgery, followed by additional radio- and chemotherapy increases survival, but disease recurrence is inevitable. The current median survival time after diagnosis is between 4 and 20 months, depending on the age, the clinical condition of the patient and the treatment (Ho et al., 2014). One of the key factors in the poor response to treatment is the heterogeneity of the cells within a single tumour, with different signalling pathways active. This makes it extremely challenging to target the entire tumour with a single-pathway drug (Patel

et al., 2014). However, a better knowledge of the molecular mechanisms of tumour cells interacting with their cellular and proteinaceous environment proves to be highly valuable to improve treatment strategies (Verhaak et al., 2010) and patient prognosis (Cancer Genome Atlas Research Network et al., 2015; Charles et al., 2012).

The intermediate filament (IF) protein family is a large family of cytoskeletal proteins that are central in the integration of cellular structure and cell signalling (Coulombe and Wong, 2004). IF proteins are involved in cellular differentiation processes (Yang et al., 2011), and are involved in the tumour biology of various malignancies. For instance, keratin 14 is essential for the metastasizing invasive front of breast cancer (Cheung et al., 2013), keratin 17 is an important transforming protein in Ewing Sarcoma (Sankar et al., 2013), whereas vimentin is a marker of the epithelial to mesenchymal transition and induces the characteristic cellular changes of this transition (Mendez et al., 2010; Thiery et al., 2009). Vimentin regulates lung cancer cell adhesion through focal adhesions and activates Slug, a transcription factor involved in epithelial mesenchymal transition in breast carcinoma (Havel et al., 2015; Virtakoivu et al., 2015). Thus, in several tumours a change in the composition of the IF-network induces the progression towards a more invasive tumour.

A loss of GFAP - the typical astrocyte IF protein - in higher grade astrocytomas was described more than 40 years ago (Velasco et al., 1980). The GFAP locus encodes for multiple GFAP isoforms, and at least 10 different splice variants are now known to be expressed in the human brain (Kamphuis et al., 2014; Middeldorp and Hol, 2011). There are several indications that a change in the stoichiometry of these isoforms correlates with astrocytoma grade. Staining with two different antibodies for either all GFAP isoforms or for GFAPδ shows a negative correlation of astrocytoma grade with total GFAP but a positive correlation with GFAPδ immunoreactivity (Brehar et al., 2014; Choi et al., 2009; Heo et al., 2012). GFAPα and GFAPδ are the most abundantly expressed isoforms in the central nervous system and differ only in their C-terminal 41 amino acids, a signalling hotspot in IF proteins due to the high content of phosphorylatable residues (Moeton et al., 2016). Both isoforms are expressed in several astrocytoma cell lines (Middeldorp et al., 2009; Moeton et al., 2014; Perng et al., 2008). GFAPα encodes the canonical GFAP-isoform and is expressed in astrocytes and highly upregulated in reactive gliosis, whereas GFAPδ is enriched in neural stem cells and subpial astrocytes in the human brain (Kamphuis et al., 2014; van Strien et al., 2014; Roelofs et al., 2005). The two isoforms differ in their 3'UTR and GFAPδ contains the alternative exon 7+, which is part of intron 7 and is not present in GFAPα (Nielsen et al., 2002; Roelofs et al., 2005).

Since various members of the IF protein family are described to be involved

4

in cell-extracellular matrix (ECM) interactions as well as in signalling and differentiation processes involved in tumour malignancy (Cheung et al., 2013; Ivaska et al., 2007; Leduc and Etienne-Manneville, 2015), we investigated the expression of GFAP isoforms in astrocytoma. We first analysed GFAP isoform expression in a large RNA sequencing dataset of the Cancer Genome Atlas (TCGA) and observed different levels of GFAPα expression in astrocytomas of different grade as well as a different GFAPδ/α ratio. Subsequently, modulation of GFAPα and the GFAPδ/α ratio in an astrocytoma cell model resulted in transcriptional changes, which we related to the observations in patients, and resulted in the identification of a set of tumorigenic and anti-tumorigenic genes that are regulated by GFAP.

Methods

Sample selection from The Cancer Genome Atlas

The cancer genome atlas (TCGA) contains data of 528 astrocytoma grade IV cases (also known as GBM) and 516 lower grade glioma cases. Of the latter group 168 were classified as astrocytoma grade II or grade III cases. RNA sequencing data was available for 165 GBM and the 168 astrocytoma grade II and III cases. We excluded recurrent tumours from this study and we averaged the results of the analysis on the same tumour samples (same vial). The final cohort, included in our analysis, consisted of 55 grade II, 105 grade III, and 150 grade IV astrocytoma samples (Table 1).

RNA sequencing data and statistics

An explorative differential gene expression analysis between astrocytoma patients of different grade was performed in R software for statistical computing using the limma package in bioconductor (http://www.bioconductor.org). Expression data of grade II, III, and IV patients containing normalized gene and RNA isoform expression levels were obtained from TCGA data portal (Level 3 released data downloaded June, 2015), and expression levels were extracted as upper quartile normalized RSEM (RNA-Seq by Expectation Maximization) count estimates (normalized counts). Statistical significance was tested using a Bayesian linear model fit with a Benjamini-Hochberg False Discovery Rate (FDR) corrected criterion level of $\alpha = .1$. Genes were considered differentially expressed if the test reached statistical significance and showed at least a 1.5 fold absolute change. Normalized isoform expression level 3 data was used to determine GFAPα and GFAPδ expression levels and for each patient sample, the GFAPδ/α ratio was calculated. Statistical difference in the GFAPδ/α ratio and the GFAPδ or GFAPα expression level between grade II, III,

Table 1. Clinical Characteristics of included astrocytoma patients

Astrocytoma	grade II	grade III	grade IV
N (number of patients)			
Total	55	105	150
Age			
Median (LQ, UQ)	36 (30, 66)	42 (34, 74)	60 (52, 89)
Average	37.16	44.17	59.61
Survival, daysi			
Median (LQ, UQ)	230 (114.5, 3283)	300 (155, 6423)	280.5 (146.5, 1642)
Censored, %	94.64	77.36	34.67
Karnofsky score			
100	13	16	12
90	8	27	2
70-80	8	18	67
<70	2	5	30
NA	24	39	39
Gender			
male	31	61	97
female	24	44	53

Age, survival, Karnofsky score and gender specifications of included patients as provided by the The Cancer Genome Atlas (TCGA) database. LQ: Lower quartile, UQ: Upper Quartile, NA: Not Available, [i] survival data was available for 41 grade II, 91 grade III and 150 grade IV astrocytoma patients

and IV was tested using the non-parametric independent 2-group Mann-Whitney U Test, since the criteria for normal distribution were not met (Shapiro-Wilk test). The p-values were corrected with an FDR correction.

GFAP isoform modulation in astrocytoma cell lines

To explore the transcriptional changes induced by GFAP isoform levels in astrocytoma, we performed *in vitro* GFAP isoform modulation experiments. For these experiments we used two different human astrocytoma cell lines. U251-MG has a lower endogenous level of GFAP and was used to study the effect of inducing GFAPα and GFAPδ expression. U373-MG has a high endogenous level of GFAP and was used to knockdown (KD) specific GFAP isoforms and modulate the ratio between the different isoforms. U251-MG cells were transduced with lentiviral vectors containing recombinant-mCherry (referred to as "control"), recombinant human GFAPα-IRES-eGFP (referred to as "GFAPα⁺") or recombinant human GFAPδ-IRES-mCherry (referred to as "GFAPδ⁺") as described before (Moeton et al., 2016). U251-MG cells were maintained in 1:1 Dulbecco's modified Eagle medium (DMEM) GlutaMAX high glucose : Ham's F-10 nutrient mix, supplemented with 100 U/ml

penicillin, 100 μg/ml streptomycin (1% P/S) and 10% (v/v) fetal bovine serum (FBS; all Invitrogen, Bleiswijk NL).

U373-MG human astrocytoma cells were transduced with lentiviral vectors containing shRNAs targeting either GFAPα (referred to as "GFAPα-"; shRNA targeted to the 3'UTR in exon 9), GFAPpan (referred to as "GFAPpan-", shRNA targeted exon 2 which is present in all known GFAP isoforms), or with a non-targeting control shRNA construct (referred to as "NTC") as described by Moeton et al (Moeton et al., 2014). U373-MG cells were maintained in DMEM GlutaMAX high glucose supplemented with 1% P/S and 10% FBS. Transduction efficiency was maintained by culturing cells with puromycin (2 μg/ml).

The serum concentration in the cell culture medium was changed from 10% to 2% FBS three days before an experiment. For the microarray analysis, GFAPα^+ and GFAPδ^+ cells or GFAPα^- or GFAPpan$^-$ cells were plated in medium with 2% FBS in 6-well flexible bottom Bioflex plates coated with the laminin derived peptide YIGSR (Flexcell International, Hillsborough NC, US; Dunn Labortechnik, Asbach, DE), at a density of 5E4 cells/cm^2.

For maintenance, all cells were split twice a week and cultured in uncoated tissue culture plastics at 37°C, under a humidified 5% CO$_2$ / 95% air atmosphere.

RNA isolation

RNA was isolated by adding TRIsure (Bioline, London, UK; GC biotech B.V., Alphen aan den Rijn, NL) to the cell culture wells. RNA was extracted according to the manufacturer's protocol, and precipitated in isopropyl alcohol in the presence of glycogen at -20°C overnight (Roche; Almere) (Kamphuis et al., 2012). Samples were centrifuged at 4°C and at a speed of 2.0*10^4 g for 45 minutes (min), washed twice with cold 75% ethanol (in MilliQ (Millipore)), and the RNA pellets were dissolved in MilliQ. The 260/280 absorbance ratio was measured by spectrophotometry (NanoDrop; Thermo Scientific) to assess RNA concentration and purity.

Real time quantitative PCR

After treating 500 ng RNA with DNAse for 2 min at 42°C (gDNA wipeout buffer), cDNA was made in 10 μl reactions using Quantiscript® Reverse Transcriptase with a mix of oligo-dT and random primers at 42°C for 30 min. The reaction was stopped by an inactivation step at 95°C for 3 min (Quantitect; Qiagen Benelux B.V., Venlo, NL).

The produced cDNA was diluted 20x in MilliQ and was used as a template in the real time quantitative polymerase chain reaction (qPCR) in 96-wells plates and

the reaction was analysed with an ABI7300 (Applied Biosystems, Life Technologies, Bleiswijk, NL). The reaction mix consisted of 1 μl template, 3.5 μl MilliQ, 0.5 μl primer mix (final concentration of 0.1 mM for each primer), and 5 μl SYBR® Green PCR Master Mix (Applied Biosystems, Life Technologies, Bleiswijk, NL). The qPCR program consisted of an incubation of 2 min at 50°C and 10 min at 95°C, followed by 40 cycles of 15 seconds at 95°C and 1 min at 60°C. After the qPCR reaction, a dissociation curve was made by ramping the temperature from 60°C to 95°C. Curve analysis was performed using the Sequence Detection Software version 1.4 (Applied Biosystems), with a standard threshold of 0.2 (determined to be in the log linear part of the derived curve), and an automatic determination and correction of baseline fluorescence. Primers were designed to target intron-spanning exons (when possible) of the transcripts of interest and to generate 50-125 bp long amplicons. Primer efficiencies and dissociation curves were verified using a 1:20-1:320 dilution series of U251-MG and U373-MG cDNA and the amplicon product size was verified by agarose gel electrophoresis. Specifications of primers are given in Sup. Material 1. A set of 3 reference genes was identified based on the microarray analysis (PPP3CB, CNOT10, CLNS1A), of which the geometric mean was used to normalize the data.

RNA labelling, hybridization, and scanning

cRNA was made from 100 ng RNA using a Low Input Quick Amp Labelling Kit, two-colour (Agilent, Amstelveen, NL), as per manufacturer's protocol. A mix of 825 ng of Cy3 and Cy5 labelled cRNA samples was hybridized to Human GE 4x44K v2 Microarrays (Agilent, Amstelveen, NL) according to the manufacturer's protocol. The recombinant expression samples (N=8 per condition: control, GFAPα^+, GFAPδ^+) and the GFAP KD samples (N=5 for GFAPα^-, N=5 for GFAPpan$^-$, N=6 for NTC) were hybridized to the microarrays. cRNA fluorescence intensity was scanned using an Agilent DNA Microarray Scanner. Scans were made with 100% and 10% photon multiplier tube intensity, at 5 μm resolution. The microarray data have been submitted to the Gene Expression Omnibus (GSE74567).

Microarray data processing

Data processing was performed as described before (Bossers et al., 2010a; Orre et al., 2014a, 2014b). Briefly, data were extracted from microarray images using Feature Extraction software. Using the limma package in bioconductor (http://www.bioconductor.org), spot intensities were imported into R software for statistical computing. Spots labelled by the Feature Extraction software as saturated or non-uniformly distributed foregrounds and backgrounds, as well as visually identified artefacts on the array were omitted. In these cases the statistical

analysis of differential expression was based on the remaining spots. Intensities were quantile normalized between all arrays, and sample intensities were extracted for an intensity-based analysis (Bossers et al., 2010b). Redundant probes detecting identical transcripts were averaged. All genes that did not have a condition with an average hybridisation intensity of $\log_2 > 6$ were omitted from the analysis.

Microarray statistics

Statistical significance was tested using a Bayesian linear model fit with an FDR corrected criterion level of $\alpha = .1$ to prevent type II errors (Smyth, 2004). The analysis of U251 and U373 cells were performed independently of one another. For recombinant expression, all three conditions (control (N=8), GFAPα^+ (N=8), and GFAPδ^+ (N=8)) were compared. For knockdown, contrasts between the two KD conditions (GFAPα^- (N=5), GFAPpan$^-$ (N=5)) versus NTC (N=6) were made. Microarray probes were considered to report a differentially expressed gene if the statistical test was significant and the fold change showed at least a 1.5 fold absolute change.

Linear regression analysis

In vitro differentially expressed genes (our microarray data) induced by changes in GFAP isoforms (FDR <0.1; FC > 1.5) were compared to transcriptomic (TCGA data) differences between astrocytoma of different grade (FDR <0.1; FC > 1.5). A comparison was made between *in vitro* GFAPα regulated genes (observed in the
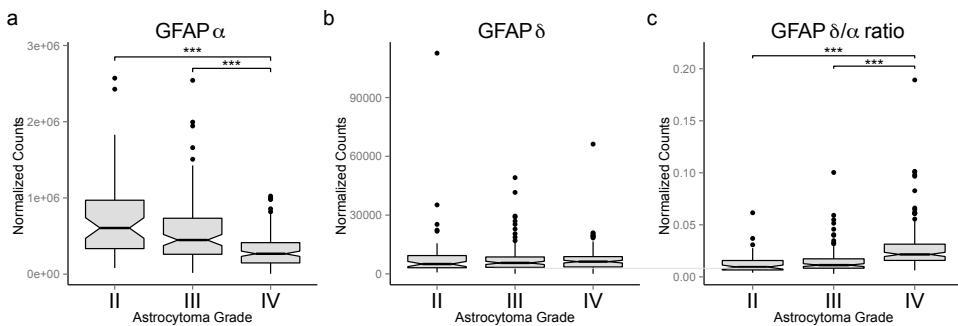
Figure 1. GFAP-isoform expression in astrocytoma
Box plots showing **(a)** GFAPα, **(b)** GFAPδ, and **(c)** GFAPδ/α levels in grade II (n=55), III (n=105) and IV (n=150) astrocytomas (*whiskers:* **±1.5 × IQR;** *notch:* **95% CI; ***: FDR < 0.001). Expression levels of GFAP-isoforms were obtained from RNAseq level 3 released normalized isoform expression data of the TCGA database. The GFAPδ/α ratio was calculated for each patient. A significant decrease in GFAPα expression in grade IV astrocytoma compared to grade II and III (a) and no difference in GFAPδ expression between astrocytoma of different grade (b) resulted in a relative increase in GFAPδ expression compared to GFAPα (c), which we define as the GFAPδ/α ratio.**

GFAPα^-, GFAPpan$^-$, GFAPα^+ conditions) and differentially expressed genes between grade II and grade IV, and grade III and grade IV, analysed as described above. The same comparison was made for *in vitro* GFAPδ/α ratio regulated genes (observed in the GFAPδ^+, GFAPα^-, and GFAPα^+ conditions). The TCGA gene expression levels of the overlapping genes were tested for a significant correlation to GFAPα, GFAPδ, and GFAPδ/α ratio in patients by fitting a linear regression model to the data. P-values were FDR adjusted. At FDR < 0.01 genes were identified as strongly correlating genes. Gene expression of the final set of (anti)-tumorigenic genes was correlated to GFAPα, GFAPδ and GFAPδ/α ratio within each astrocytoma grade in the same way. Correlation was considered significant at FDR < 0.05.

Gene ontology

To detect gene ontology (GO) clusters that were overrepresented in our datasets we used the topGO R package (Gene Ontology Consortium, 2015). We used a Fisher statistical test to test for overrepresentation, with a weighted algorithm to correct for dependency between parent-child relations between ontology clusters (Alexa et al., 2006). The test for overrepresentation of our genes of interest was performed in the context of all Entrez gene IDs considered in the statistical test for differential expression on the RNAseq data. Databases used to search for overrepresentation were the GO domains 'Cellular compartment' (CC), 'Biological Process' (BP) and 'Molecular Function' (MF). Annotation was performed using an annotation build of 10-Aug-2015 (org.Hs.eg.db, ID = entrez) for the analysis on our RNAseq data set.

Survival Analysis

To test whether survival and progression free survival estimates for patients with below or above median expression of a gene of interest were significantly different, we calculated survival and progression free survival probabilities with a Kaplan-Meier survival analysis using the Survival package in R. Survival and progression free survival data were available for 41 grade II and 91 grade III astrocytoma patients. Survival data was available for 150 grade IV astrocytoma patients (downloaded from TCGA January, 2016). Estimates were compared using the log rank regression analysis and were considered different at an FDR adjusted significance level of 0.05. A trend for a difference between estimates was determined at FDR < 0.1.

Immunocytochemistry

For immunocytochemical stainings, cells were fixed in 4% (w/v) paraformaldehyde (4% PFA) dissolved in phosphate buffered saline, pH 7.4 (PBS) for 15 min. Cells were washed with PBS and incubated overnight at 4°C with the primary antibody diluted in blocking buffer (50 mM Tris pH 7.4, 150 mM NaCl,

e

f
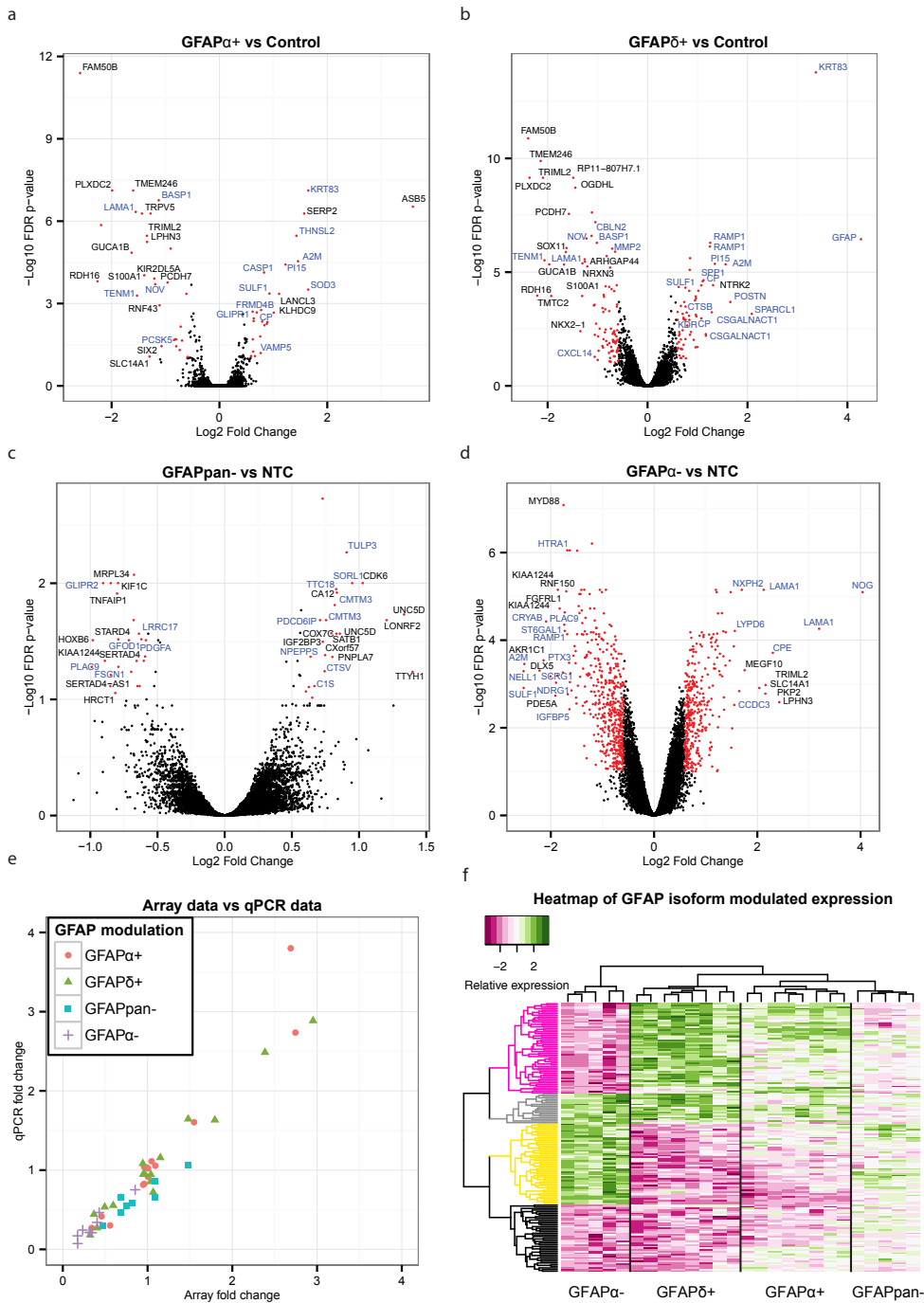
0.25% (w/v) gelatine, and 0.5% triton X-100). Cells were then washed three times with PBS and incubated with the secondary antibodies and the nuclear counterstain Hoechst 33258, diluted in blocking buffer, at room temperature for 1 hour. Cells were then washed three times with PBS, dipped in MilliQ and mounted with Mowiol (0.1 M tris-Hcl pH 8.5, 25% glycerol, 10% Mowiol (Calbiochem, Merck Millipore, Darmstadt, Germany)). Micrographs from the fluorescent stainings were taken with a Leica epifluorescent DMRD microscope. The antibody used was polyclonal anti-GFAP (1:2000; DAKO, #Z0334) and the nuclei were counterstained with Hoechst 33258 (1:1000; invitrogen).

Results

GFAP isoform expression differs between low and high grade astrocytoma

To get insight into the biological processes that determine the malignancy of astrocytoma and to investigate the potential role of GFAP isoforms in regulating these processes, we performed a differential gene expression analysis on RNA sequencing (RNAseq) data of low- and high-grade astrocytoma obtained from TCGA. The final cohort used in our analysis included 150 grade IV, 105 grade III, and 55 grade II astrocytoma. Normalized gene expression data was used to analyse differential gene expression between low- (II and III) and high-grade (IV) astrocytoma. GFAP expression was significantly decreased in grade IV compared to both grade II (46%, FDR= 1.58E-10) and grade III (58%, FDR= 3.92E-7) astrocytoma. Interestingly, the absolute difference in normalized gene expression of all genes analysed between low- and high-grade astrocytoma was the largest for GFAP. Grade II versus IV showed an absolute difference in GFAP expression of 3.57E5 normalized counts and grade III versus IV of 2.20E5 normalized counts. In order to determine the expression levels of the GFAP isoforms, TCGA derived RNA sequencing data

Figure 2. Differential expression analysis of astrocytoma cell lines with modulated GFAP networks Volcano plots showing the −log10 of the FDR p-value of each gene plotted against the $\log_2$ fold change (a-d). This visualizes the general effect of GFAPα$^+$ (a), GFAPδ$^+$ (b), GFAPpan$^-$ (c), and GFAPα$^-$ (d) on the transcriptome. Differentially expressed genes selected for analysis with GO are represented with red dots. Names of the genes with the highest fold change have been added in black, and names of genes in GO-clusters "ECM disassembly", "ECM organization", "ECM", "ECM binding" and "Extracellular Region" in blue (a-d). Validation of the microarray results by qPCR of selected genes (THNSL2, LINGO2, A2M, BASP1, OGDHL, PIEZO2, SOX11, PI15, GLUL, LAMA1, GAPDH, GFAPα, SULF1, CNOT10, PPP3CB, CLNS1A, SERP2, RAMP1, and CRYAB) showed that the fold change assessment of microarray and qPCR were correlated, ϱ=0.93 (e). Clustering of the scaled expression changes revealed 4 main clusters of genes, dominated by parallel or opposite changes in expression of these genes between GFAPδ$^+$ and GFAPα$^-$, as indicated by different colors in the dendrogram (purple, gray, yellow, black) (f).
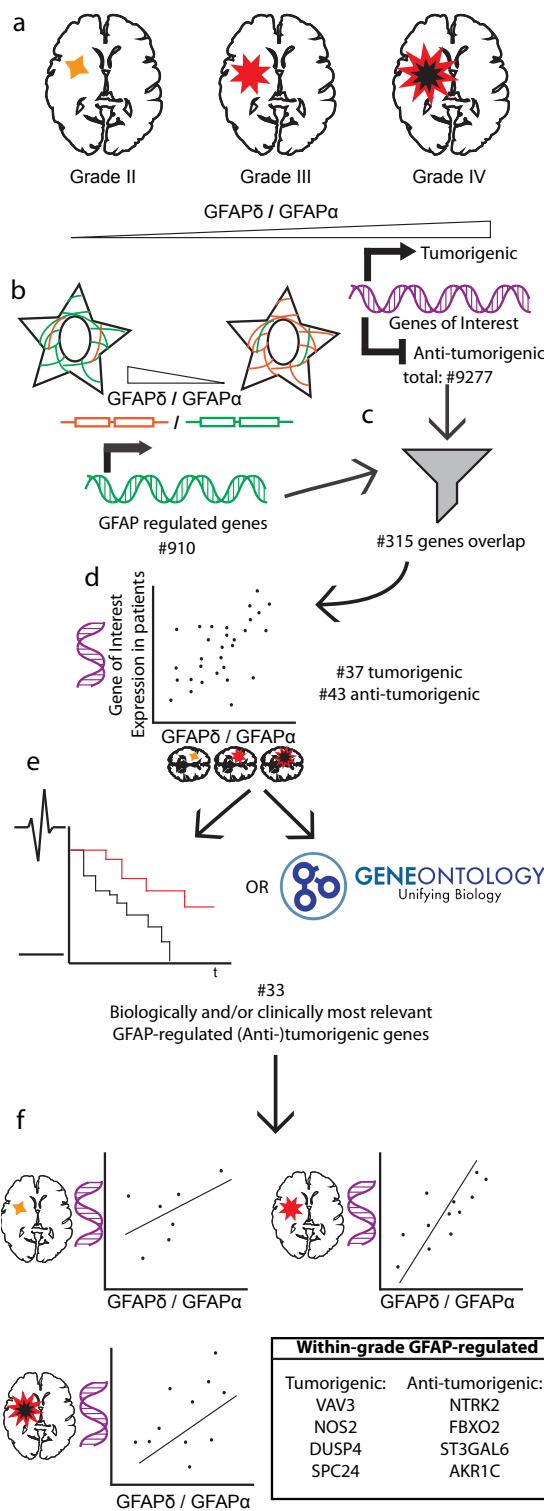
Figure 3. Processing steps of the data in this study

After finding that GFAPα and GFAPδ/GFAPα ratio correlate with astrocytoma grade (Fig. 1), all genes that were differentially expressed across astrocytoma grades in patients were identified from the TCGA database (a). To select genes that are regulated by GFAPα and GFAPδ/GFAPα ratio, we modulated the GFAP network in astrocytoma cell lines *in vitro* and identified differentially expressed genes regulated by GFAP (b). The cell line dataset was used to filter the astrocytoma data (c). From these combined patient/*in vitro* genes we calculated initial correlations between GFAP-isoforms/GFAP-ratio and target genes in the patient data and identified a set of GFAP-regulated tumorigenic and anti-tumorigenic genes. These sets are GFAP-regulated based on their *in vitro* regulation by GFAP isoforms. Gene sets are tumorigenic or anti-tumorigenic based on their expression pattern in astrocytoma patients (d). To identify the subset of genes relevant for astrocytoma progression and biology, the filtered genes were analyzed for survival, progression free survival, and gene ontology (e). To further reduce the risk of confounding by astrocytoma grade, a linear regression was performed between the most interesting GFAP-regulated (anti-)tumorigenic genes and GFAP expression within the different astrocytoma grades (f). Finally, 8 genes passed all these criteria and emerged as the most probable GFAP-regulated (anti-)tumorigenic genes with biological or clinical relevance in astrocytoma.

consisting of normalized isoform expression data was used. The only known GFAP isoforms that were annotated in this dataset were GFAPα and GFAPδ. Interestingly, while canonical GFAPα expression is indeed significantly decreased in grade IV astrocytoma compared to grade II (45%, FDR = 1.20E-4; Fig. 1a) and to grade III (55%, FDR = 8.4E-4; Fig. 1a), the expression of the alternative splice variant GFAPδ is not different between astrocytoma grades (Fig. 1b). This results in a relative increase in GFAPδ compared to GFAPα, which we report as the GFAPδ/α ratio. Importantly, the GFAPδ/α ratio was significantly increased in grade IV astrocytoma compared to both grade II (220%, FDR = 5.87E-08; Fig. 1c) and grade III (177%, FDR = 4.16E-08; Fig. 1c).

*Extracellular matrix genes are overrepresented in transcriptome changes due to GFAP modulation in astrocytoma cell lines **in vitro***

To get insight into the function of these GFAP isoforms in astrocytoma and to investigate a potential role for GFAPα and the GFAPδ/α ratio in astrocytoma malignancy, we modulated GFAP isoform expression in U373 and U251 cells by recombinant expression or silencing with shRNAs of the isoforms. We analysed the GFAP isoform induced transcriptomic changes. We generated microarray-based whole-genome gene expression profiles of GFAPα+, GFAPδ+, GFAPpan-, and GFAPα- astrocytoma cell lines. For validation of the cell lines see Sup. Material 2. The results of the microarray are represented in volcano plots (Fig. 2a-2d). Differentially expressed genes (FC>1.5, FDR<.1) are represented with red dots. GFAPα+ expression induced a differential expression of 57 genes and GFAPδ+ expression induced differential expression of 158 genes compared to control. GFAPpan- and GFAPα- cells were compared to the NTC. These resulted in 48 and 848 differentially expressed genes, respectively. Lists of the top 50 most significant hits (1.5 fold upregulated or downregulated) in the GFAPα+, GFAPδ+, GFAPpan-, or GFAPα- cells are provided in Sup. Materials 3-6.

The array data were validated by qPCR. Targets were selected to verify various fold changes and directions of change of expression patterns: THNSL2, LINGO2, A2M, BASP1, OGDHL, PIEZO2, SOX11, PI15, GLUL, LAMA1, GAPDH, GFAPα, SULF1, CNOT10, PPP3CB, CLNS1A, SERP2, RAMP1, and CRYAB. The original RNA samples that were used to generate the labelled cRNA probes for array hybridisation were used to make cDNA and analysed by qPCR (Fig. 2e). The qPCR confirmed the findings of the microarray. Overall, the array and qPCR data were highly correlated (ϱ = 0.93, p-value<.001).

Genes with an FDR adjusted p-value of <.1 in both the recombinant expression

and the knockdown models were clustered and evaluated in a heatmap. This analysis showed that GFAPα- and GFAPδ+, which both had the largest impact on the GFAPδ/α ratio, had the highest contribution to the clustering of the heatmap. These two conditions led to four main emerging patterns, that either showed an effect in the same direction or in an opposite direction for GFAPα- and GFAPδ+ (Fig. 2f). The other experimental groups, GFAPpan- and GFAPα+ had a lower effect on GFAPδ/α ratio, and had a less prominent effect on the clustering. The individual genes and their patterns are shown in Sup. Material 7. We conclude that not the change in GFAP per se but the change in GFAPδ/α had the most pronounced effect on the transcriptome in astrocytoma cells.

The differentially expressed genes were tested for overrepresentation in a gene ontology analysis, to reveal potential functional differences related to the changes in the GFAP-network. This analysis of both the recombinant expression and knockdown cells resulted in a recurring overrepresentation of gene ontology clusters related to the cell periphery, such as "extracellular matrix", "extracellular space" (everything extracellular except the matrix) or "plasma membrane" (Sup. Materials 8-11). Remarkably, the 80 differentially expressed genes between GFAPδ+ and GFAPα+ were also overrepresented in the same clusters (Sup. Material 12). These results show that both GFAP modulation per se, as well as modulation of the specific isoforms individually, affected genes involved in the composition of the extracellular matrix and the extracellular space. These findings corroborate our earlier work, where we showed that silencing GFAPα in astrocytoma cells led to a strong increase in LAMA1 expression (Moeton et al., 2014).

GFAPδ/α ratio correlates to tumour malignancy and regulates tumorigenic genes

To identify those GFAP isoform induced transcriptomic changes that are relevant for astrocytoma malignancy, we compared our *in vitro* transcriptomic data to the TCGA derived patient transcriptomic data (Fig. 3a-b). In patients, GFAPα expression and the GFAPδ/α ratio was significantly different between grade II and III versus grade IV astrocytoma (Fig. 1). Therefore we compared transcriptomic changes induced by *in vitro* modulation of GFAPα (GFAPpan-, GFAPα-, GFAPα+) or the GFAPδ/α ratio (GFAPδ+, GFAPα+, GFAPα-) to transcriptomic differences between grade II and III versus grade IV astrocytoma (Fig. 3c).

Fig. 4a shows a Venn diagram for the comparison of genes regulated by a change in GFAPα *in vitro* and genes differentially expressed between astrocytoma of low and high grade. Of the 865 genes that were regulated by a change in GFAPα
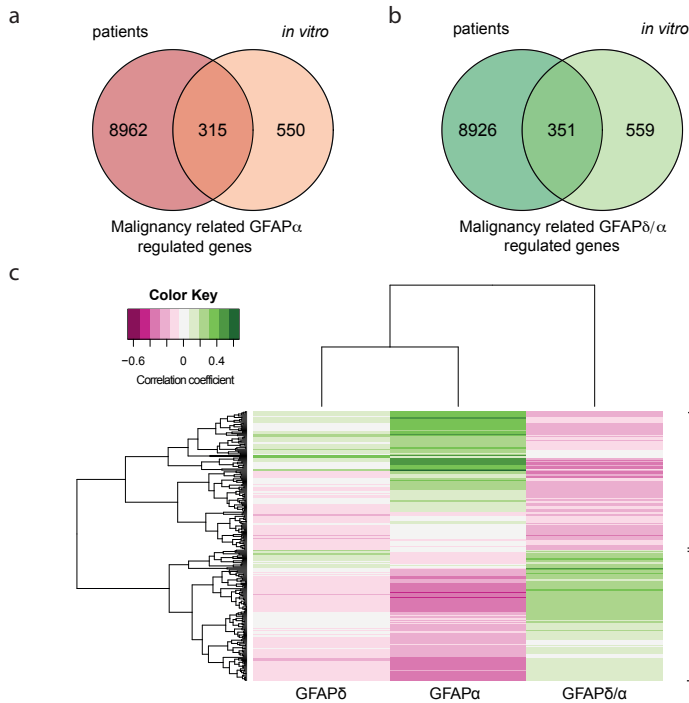
Figure 4. Comparison between GFAP-regulated genes in astrocytoma cells and patients
Venn Diagrams show the overlap of genes differentially expressed between low and high grade astrocytoma in patients (left circles) and genes regulated by a change in the GFAP network in vitro (right circles) (a,b). 315 genes are both differentially expressed between astrocytoma of low and high grade as well as regulated by a change in GFAPα expression in vitro (a). 351 genes are both differentially expressed between astrocytoma of low and high grade as well as regulated in vitro by a change in the GFAPδ/α ratio (b). The intersect of both diagrams represent the genes identified as malignancy related GFAPα or GFAPδ/α regulated genes. For these genes, a linear regression analysis was performed. Correlation to GFAPα and GFAPδ expression, and the GFAPδ/α ratio in patients ranging from grade II to grade IV was determined. The heatmap shows the genes that significantly correlated to either GFAPα or the GFAPδ/α ratio (FDR < 0.01) (c). The colour key indicates the correlation coefficient (ρ). Hierarchical clustering on the absolute correlation coefficient results into the identification of two main clusters. Cluster 1 consists of genes that positively correlate to GFAPα but negative to the GFAPδ/α ratio, cluster 2 shows the opposite pattern with genes negatively correlating to GFAPα and positively to the GFAPδ/α ratio. A larger version of this figure is provided in Supplemental Material 13.

expression *in vitro* (FDR < 0.1, FC >1.5), 315 genes were differentially expressed between astrocytoma of low and high grade (FDR < 0.1, FC >1.5) and showed a similar direction of change as GFAPα. The comparison between genes regulated by a change in the GFAPδ/α ratio *in vitro* and differentially expressed genes between astrocytoma of low and high grade is visualized in Fig. 4b. Of the 910 genes regulated by a change in GFAPδ/α, 351 were found to be differentially expressed between astrocytoma of low and high grade and showed a similar direction of change as the

GFAPδ/α ratio.

We classified the overlapping genes between our *in vitro* and patient data set as malignancy related GFAPα regulated genes or malignancy related GFAPδ/α regulated genes. A linear regression analysis was performed on the overlapping genes (Fig. 3d), to test their correlation to GFAPα, GFAPδ and GFAPδ/α within grade II to IV astrocytoma. Genes that significantly correlated to either GFAPα or the GFAPδ/α ratio (FDR < 0.01) were clustered in a heatmap (Fig. 4c). This hierarchical
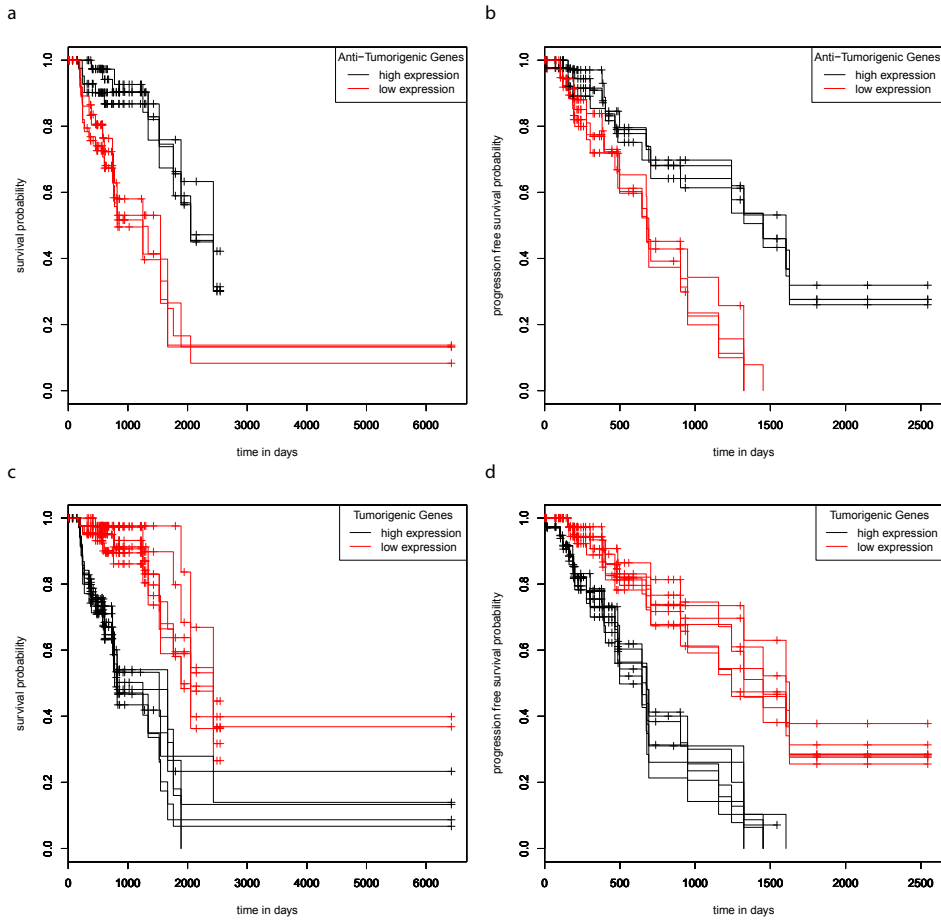
Figure 5. Kaplan-Meier survival and progression free survival curves grade III astrocytoma
The graphs show survival and progression free survival curves of below and above median expression of GFAP regulated anti-tumorigenic (a, b) and tumorigenic genes (c, d). Survival and progression free survival curves are shown for genes of which a high expression predicts both a significantly shorter survival and a progression free survival compared to low expression, or vice versa (FDR < 0.05). Low expression of the anti-tumorigenic genes AKR1C3, ARHGEF10L, SMAD7 and ST3GAL6 predicts a significant shorter survival (a) and progression free survival (b). High expression of the tumorigenic genes C7orf46, DUSP4, HS3T3B1, ODZ1, TTL, VAV3 and ZDHHC23 predicts a significant shorter survival (c) and progression free survival (d).

clustering resulted in the identification of two large gene clusters, i.e. genes that correlated positively to GFAPα and negatively to the GFAPδ/α ratio and genes that correlated negatively to GFAPα and positively to the GFAPδ/α ratio. These genes were classified as GFAP-regulated, since their expression level was also significantly regulated in the *in vitro* cells with modulated GFAP-networks. Based on their astrocytoma correlation, genes were classified as tumorigenic or anti-tumorigenic genes (Fig. 3a).

We observed a positive correlation for GFAPα, a negative correlation for GFAPδ/α ratio, and no correlation for GFAPδ between astrocytoma of low and high grade (Fig. 1). Therefore, we selected genes that show a strong correlation to both GFAPα and GFAPδ/α ratio in opposite directions (FDR < 0.01), but do not correlate to GFAPδ (FDR > 0.1) as the most relevant tumorigenic or anti-tumorigenic genes regulated by GFAP (Sup. Material 13 gives detailed information of the gene clusters in Fig. 4c). This resulted in 43 genes that were identified as GFAP-regulated anti-tumorigenic genes due to their positive correlation to GFAPα and negative correlation to GFAPδ/α (Sup. Material 14). The 37 genes that correlated negatively to GFAPα while they correlated positively to GFAPδ/α were identified as GFAP-regulated tumorigenic genes (Sup. Material 15).

GFAP-regulated genes are involved in tumour biology

The GFAP-regulated tumorigenic and anti-tumorigenic genes were tested for overrepresentation in a GO analysis to gain an insight in the function of GFAPα and the GFAPδ/α ratio in astrocytoma (Fig. 3e). Table 2 shows significant GO clusters overrepresented by a minimum of 5 of these genes. Interestingly, three biological processes highly related to tumour malignancy, 'mitotic cell cycle', and 'regulation of cell proliferation' related to tumour growth and 'regulation of phosphorylation' involved in the activation or deactivation of many tumour malignancy related signalling pathways, were significantly overrepresented. As shown in Table 2, both GFAP-regulated anti-tumorigenic and tumorigenic genes were overrepresented within these GO clusters. These results show that the GFAPα and GFAPδ/α ratio levels regulate cellular expression patterns of genes that are involved in regulating biological processes known to be different between astrocytoma of low and high grade. This supports a role for GFAP isoforms and the GFAPδ/α ratio in astrocytoma malignancy.

GFAP-regulated tumorigenic and anti-tumorigenic genes are associated with patient survival

In order to test whether differences in GFAPα and GFAPδ/α levels contribute to

4

patient outcome, we performed Kaplan-Meier analyses for patient survival within each astrocytoma grade patient group (Fig. 3e). No significant differences were found between survival and progression free survival estimates for grade II, III, or IV astrocytoma patients with below (low) or above (high) median GFAPα expression or a below or above median GFAPδ/α ratio. These results indicate that GFAPα and the GFAPδ/α ratio per se do not directly modulate tumour characteristics that affect survival of patients within one astrocytoma grade. However, the survival estimates for below and above median expression of the GFAP-regulated tumorigenic or anti-tumorigenic genes were significantly different for 32 of these genes in astrocytoma grade III patients. Interestingly, high expression of the tumorigenic genes and low expression of the anti-tumorigenic genes was associated with a worse survival probability (FDR < 0.05) (Sup. Material 16). Moreover, high expression of 7 of the tumorigenic genes (C7orf46, DUSP4, HS3ST3B1, ODZ1, TTL, VAV3, ZDHHC23) or low expression of 4 of the anti-tumorigenic genes (AKR1C3, ARHGEF10L, SMAD7, ST3GAL6) was associated with a lower progression free survival probability of grade III astrocytoma patients (Fig. 5).

To further investigate the regulation of these genes of interest by GFAP, we calculated the strength of correlation to GFAPα and the GFAPδ/α ratio within astrocytoma grade (Fig. 3f). This reduces the influence of astrocytoma grades on the correlation of GFAP with expression levels of a gene. For this analysis, we only considered genes that were overrepresented in one of the gene ontology clusters or that were associated with a worse progression free survival probability. We found that 4 of the genes that we identified as GFAP-regulated tumorigenic genes: i.e. NTRK2, FBXO2, ST3GAL6, and AKR1C3, also correlated with GFAPα or GFAPδ/α ratio within astrocytoma grade (Fig. 6a-h, corresponding statistics in Sup. Material 17). The set of genes identified as GFAP-regulated anti-tumorigenic genes, also contained 4 genes which showed the GFAP-dependent pattern within one or more of the astrocytoma grades (NOS2, SPC24, VAV3, and DUSP4; Fig. 7a-h, corresponding statistics in Sup. Material 17).

The genes that emerged from this final analysis are the genes we consider most likely to be regulated by a change in GFAP-isoforms in astrocytoma. We show that the regulation of their expression could influence astrocytoma malignancy through alterations in biological processes highly involved in the regulation of tumour malignancy (mitosis, proliferation, phosphorylation). In addition, regulation of these genes by a change in GFAP-isoforms could alter the biology of the tumour in such a way that it influences disease progression and survival of astrocytoma grade III patients.

Table 2. Overrepresented GO clusters by GFAP-regulated (anti)-tumorigenic genes

GO ID	GO Term	# sig gene	p-value	GFAP-regulated Anti-Tumorigenic Genes	GFAP-regulated Tumorigenic Genes
Biological Processes					
GO:0000278	mitotic cell cycle	8	3.2E-4	TTYH1	SPC24, CENPP, CENPQ, PRIM1, RBBP8, RFC4, E2F8
GO:0042127	regulation of cell proliferation	9	0.020	EDNRB, SGK3, FBXO2, NTRK2, PURA, AKR1C3	VAV3, IGFBP5, NOS2
GO:0042325	regulation of phosphorylation	10	0.043	DMD, EDNRB, SASH1, SMAD7, NTRK2	VAV3, DUSP4, ECT2, BARD1, PDGFD
Cellular Compartment					
GO:0005829	cytosol	20	0.006	DMD, CYS1, SGK3, FBXO2, SMAD7, NTRK2, FMN2, MID1IP1, AHNAK, AKR1C3, GTPBP1	VAV3, POLR3G, IGF2BP3, SPC24, ECT2, CENPP, NOS2, CENPQ, DCTPP1
GO:0031090	organelle membrane	17	0.026	ST3GAL6, CPE, EDNRB, CYS1, TMEM59L, FBXO2, NTRK2, FMN2, SLC44A2, TTYH1, AHNAK, EFHD1	ECT2, MANEA, MYO19, PDGFD, HS3ST3B1
GO:0045121	membrane raft	7	5.6E-6	DMD, EDNRB, CYS1, FAIM2, MAL AHNAK	CXADR
Molecular Function					
GO:0042803	protein homodimerization activity	6	0.006	NTRK2, MYOM1	ECT2, NOS2, BARD1 E2F8

Genes identified as GFAP-regulated (anti-)tumorigenic genes were analyzed for gene ontology overrepresentation, in the Biological Processes, Cellular Compartment, and Molecular Function domain. GO ID: Gene ontology identifier, # sig gene: Number of significant genes in the GO term.

4
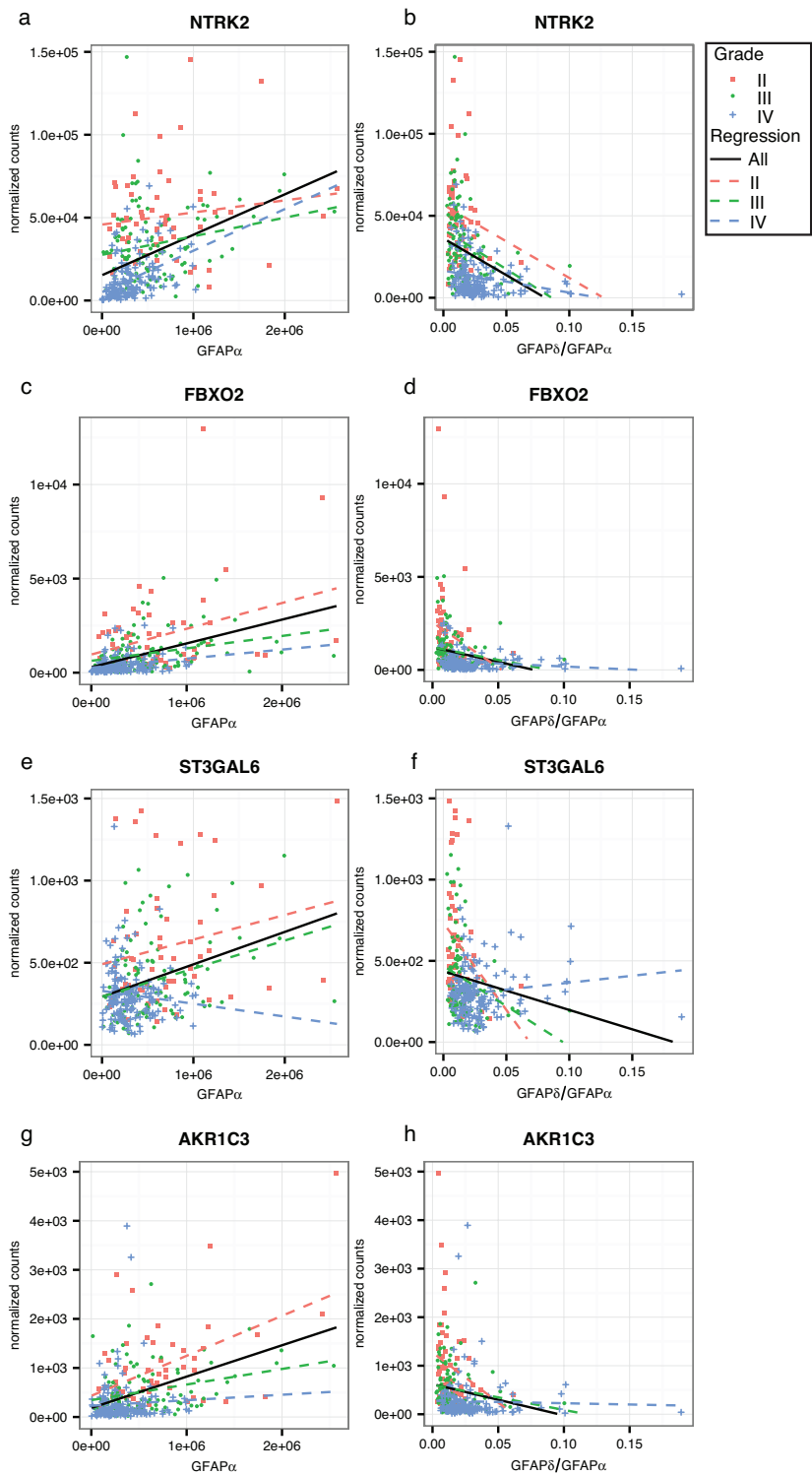
Discussion

Intermediate Filament proteins, such as vimentin and keratin, emerge as important regulators in various malignancies (Cheung et al., 2013; Mendez et al., 2010). GFAP is the signature IF of astrocytoma cells, nevertheless the function of GFAP in astrocytoma biology is still unclear. In order to gain new insights into astrocytoma biology, we studied GFAP-isoform expression in resected astrocytoma from patients (TCGA database) and the downstream transcriptional changes in astrocytoma cells caused by modulation of these GFAP isoforms. With this approach we identified anti-tumorigenic and tumorigenic genes that are regulated by GFAP. These genes regulate cellular processes highly related to tumour malignancy as apparent from our GO analysis, and the expression levels have a prognostic value for astrocytoma grade III patients.

Our earlier work shows that an experimentally induced shift in the GFAPδ/α ratio leads to changes in cellular motility and morphology (Moeton et al., 2014, 2016). Therefore, we hypothesized that the stoichiometry of the GFAP-isoforms determines specific molecular and functional changes in astrocytoma cells related to their malignancy. Indeed the most pronounced transcriptional changes in our study were induced by the largest increase in GFAPδ/α ratio. More importantly, the increase in this ratio correlated with an increase in astrocytoma malignancy. Although GFAP immunoreactivity is decreased with increasing astrocytoma grade (Velasco et al., 1980), it is also known that a complete lack of all GFAP-isoforms, as in the GFAP$^{-/-}$ mice, is not sufficient to increase tumorigenicity (Wilhelmsson et al., 2003). We here show that it is the ratio between different GFAP-isoforms, and not the mere expression level of GFAP, that contributes to malignancy. In fact, a positive correlation between GFAPδ and the degree of astrocytoma malignancy was described earlier in a small number of patients (Brehar et al., 2014; Choi et al., 2009;

Figure 6. Linear regression analysis within astrocytoma grades for GFAP-regulated anti-tumorigenic genes

Scatterplots show the distribution of GFAPα normalized isoform expression and the GFAPδ/α ratio (=GFAPδ/GFAPα normalized isoform expression) plotted against the normalized gene expression of each gene of interest. The black line shows the regression line for a correlation when all patients are included in the analysis. Red squares depict astrocytoma grade II patients, green dots astrocytoma grade III, and blue crosses depict astrocytoma grade IV patients. Dotted lines show the regression line for a correlation within grade II (red), grade III (green), and grade IV (blue) astrocytoma. (a-h) GFAP regulated anti-tumorigenic genes that significantly correlated to GFAPα or GFAPδ/α (FDR < 0.05) in either grade II, III or IV, and were related to patient survival and progression free survival (AKR1C3, ST3GAL6) and/or were present in one of the three significantly overrepresented GO Biological Processes clusters (NTRK2, FBXO2, AKR1C3) are shown here. The results of the linear regression analysis are reported in Supplemental Material 17.

Heo et al., 2012).

GFAP-regulated tumorigenic genes in tumour biology

We identified four GFAP-regulated tumorigenic genes, i.e. VAV3, NOS2, DUSP4 and SPC24, that are most relevant for astrocytoma malignancy and that are induced upon an increase in the GFAPδ/α ratio both *in vitro* and in astrocytoma patients (Fig. 6a-h).

VAV3 is a guanine nucleotide exchange factor (GEF) that is more expressed in high grade astrocytoma compared to lower grade tumours (our analysis and (Liu et al., 2014a; Salhia et al., 2008)). High VAV3 expression in grade IV astrocytoma patients has been linked to a worse survival probability (Liu et al., 2014a; Salhia et al., 2008) while we find this link in grade III astrocytoma patients. Interestingly, VAV3 is a marker for glioma-initiating cells (GICs) (Liu et al., 2014a). These cells are therapy resistant, highly invasive, and, because of their self-renewing capacity, they can initiate tumour recurrence stimulated by VAV3 expression (Liu et al., 2014a). In addition, in GICs and in different astrocytoma cell lines, VAV3 modulates cell migration and invasion (Liu et al., 2014a; Salhia et al., 2008), probably by targeting the Rho-GTPase Rac1 (Kwiatkowska et al., 2012; Movilla and Bustelo, 1999; Salhia et al., 2008). In patients, Rac1 protein expression is increased in high-grade astrocytoma (Kwiatkowska et al., 2012; Salhia et al., 2008). Our data suggest that this pathway is regulated by a change in the GFAP-IF-network composition. Interestingly, an interaction between the IF protein vimentin, VAV2, and Rac1 controls the formation of focal adhesions via FAK, and together they regulate the invasive capacity of lung cancer cells (Havel et al., 2015). Such an interaction between focal adhesion components and IFs is a recurring theme in IF biology (Leube et al., 2015). Changes in the expression of GFAP-isoforms regulate expression of genes involved in focal adhesion formation (Moeton et al., 2014) and the size of focal adhesions in

Figure 7. Linear regression analysis within astrocytoma grade for GFAP-regulated tumorigenic genes

Scatterplots show the distribution of GFAPα normalized isoform expression and the GFAPδ/α ratio (=GFAPδ/GFAPα normalized isoform expression) plotted against the normalized gene expression of each gene of interest. The black line shows the regression line for a correlation when all patients are included in the analysis. Red squares depict astrocytoma grade II patients, green dots astrocytoma grade III, and blue crosses depict astrocytoma grade IV patients. Dotted lines show the regression line for a correlation within grade II (red), grade III (green) and grade IV (blue) astrocytoma. (a-h) GFAP regulated tumorigenic genes that significantly correlated to GFAPα or GFAPδ/α (FDR < 0.05) in either grade II, III or IV, and were related to patient survival (VAV3, DUSP4) and/or were present in one of the three significantly overrepresented GO Biological Processes clusters (DUSP4, SPC24, VAV3, NOS2) are shown here. The results of the linear regression analysis are reported in Supplemental Material 17
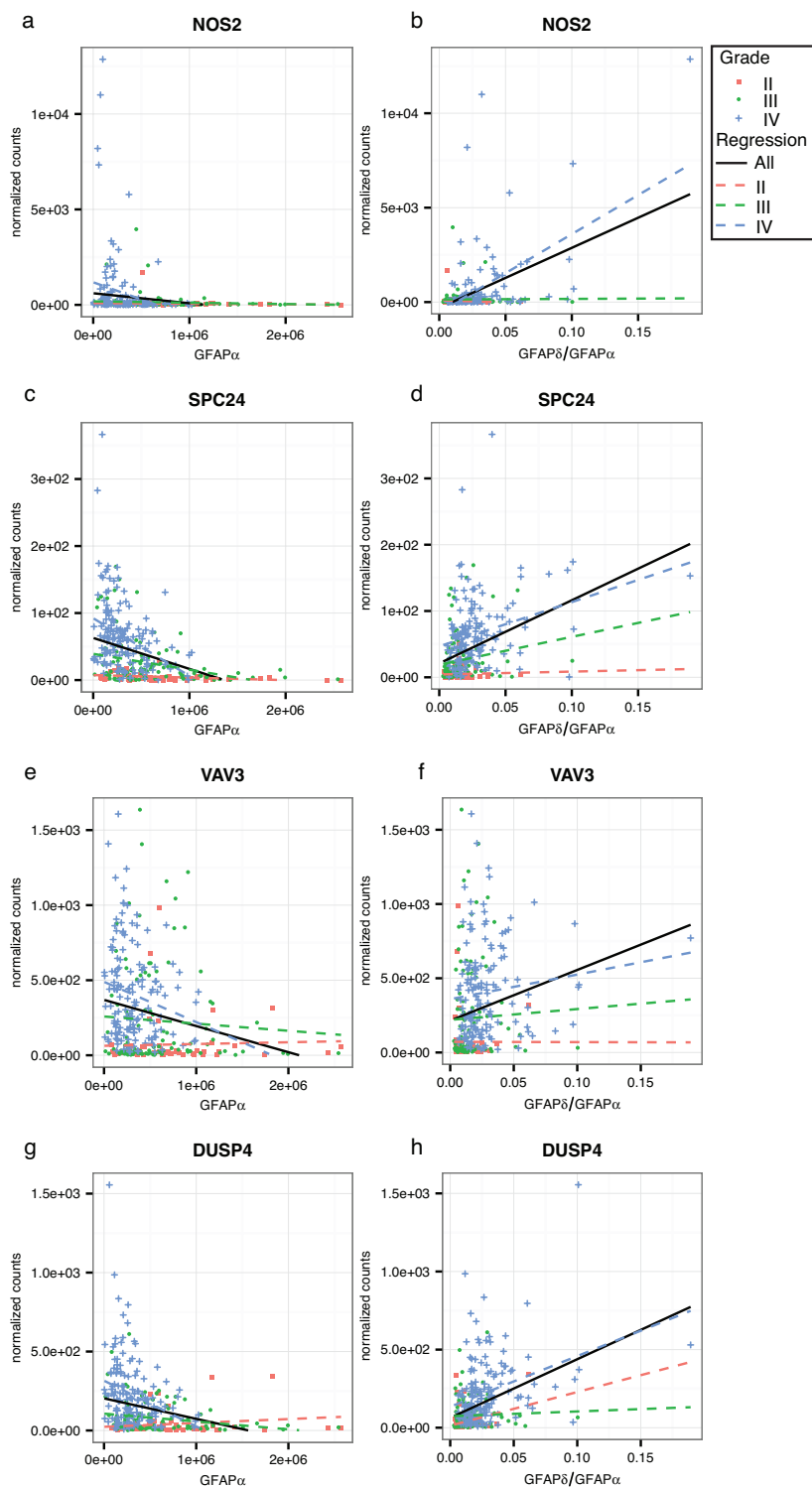
astrocytoma cell lines (Moeton et al., 2016). These findings and the observations in our study indicate that a change in the GFAP-network could influence the invasive capacity of astrocytoma cells by regulation of VAV3.

NOS2 encodes for the inducible nitric oxide synthase 2 that metabolizes L-arginine into the short-lived free radical nitric oxide (NO$^-$). NOS2 is higher expressed in brain tumours compared to healthy tissue and in highly malignant brain tumours compared to tumours of lower malignancy, in line with our findings (Ellie et al., 1995; Hara and Okayasu, 2004; Hara et al., 1996; Lin et al., 2008). We confirmed that NOS2 expression in grade IV astrocytoma was higher than in both grade II and III. In addition, we associated high expression of NOS2 in grade III astrocytoma patients to a lower survival probability. Previous analysis using the REMBRANDT dataset has linked high NOS2 expression to a worse survival probability in grade IV astrocytoma patients supporting the tumorigenic role of NOS2 (Eyler et al., 2011). This role is furthermore supported by studies that link NOS2 expression to GICs (Eyler et al., 2011), maintenance of tumour growth (Eyler et al., 2011), invasive capacity of tumour cells (Lin et al., 2008), radiation resistance (Kim et al., 2013), and angiogenesis (Kostourou et al., 2011). More evidence exists for a role of NOS2 in the acquisition of chemoresistance (Yang et al., 2004; Yin et al., 2001) and in the attenuation of the anti-tumour inflammatory response in the brain, thereby preventing tumour cell death (Badn et al., 2007; Hara et al., 1996). Hence NOS2 has a tumorigenic function at different levels of astrocytoma biology. Interestingly, induction of NOS2 expression by another identified GFAP-regulated tumorigenic gene, dual specificity phosphatase 4 (DUSP4) has been previously described (Al-Mutairi et al., 2010).

DUSP4 is part of a larger family of DUSPs that has been implicated in different types of tumours. DUSPs are known to modulate the MAPK pathway by their dephosphorylating activity (Al-Mutairi et al., 2010; Prabhakar et al., 2014) and can have both tumour suppressive and tumour promoting functions depending on the context (Prabhakar et al., 2014). DUSP4 is either up- or down-regulated in different types of tumours (Prabhakar et al., 2014). In our analysis, we found an increased DUSP4 expression in high-grade astrocytoma and a lower survival and progression free survival probability for grade III astrocytoma patients with high DUSP4 expression. This is in line with the reported significantly better clinical outcome of patients with increased methylation of the DUSP4 gene promoter (Waha et al., 2010) and the worse prognoses of oligodendrogliomas with an increased expression of DUSP4 due to a CIC mutation (Gleize et al., 2015). It is however possible that the effect of DUSP4 in astrocytomas could vary between tumours, as forced DUSP4

expression *in vitro* has been reported to inhibit the growth of an astrocytoma cell line (Waha et al., 2010).

The function of kinetochore-associated Ndc80 complex subunit SPC24 (SPC24) has not been studied in astrocytoma before, but findings in other types of tumours and healthy tissue identify SPC24 as a tumorigenic gene (Kaneko et al., 2009; Zhu et al., 2015) that has a negative prognostic effect in liver tumours (Zhu et al., 2015). We report an increased expression in high-grade astrocytoma compared to low-grade and the presence of SPC24 in our overrepresented GO cluster of regulation of proliferation. SPC24 is a component of the kinetochore complex and is essential for proper chromosome segregation and mitotic checkpoint control (Janke et al., 2001). *In vitro*, targeting SPC24 with siRNA inhibits cell proliferation and invasion and induces apoptosis in liver tumour cells (Zhu et al., 2015). These studies indeed indicate a tumorigenic role for SPC24, which supports our findings in astrocytoma.

GFAP-regulated anti-tumorigenic genes in tumour biology

NTRK2, FBXO2, ST3GAL6 and AKR1C3 are the GFAP-regulated anti-tumorigenic genes that we identified as most relevant for astrocytoma malignancy (Fig. 6e-h). The expression of these genes is inhibited by an increase in the GFAPδ/α ratio *in vitro* and in patients with high-grade astrocytoma.

Neurotrophic Tyrosine Kinase, Receptor, Type 2 (NTRK2) encodes for the receptor tropomyosin receptor kinase B (TrkB). A lower expression of NTRK2 in high-grade astrocytoma compared to low-grade has been reported previously (Palani et al., 2014) but inconsistently (Assimakopoulou et al., 2007), (Xiong et al., 2015). In tumours, TrkB receptor activation is described to stimulate cell proliferation, cell invasion, and angiogenesis, and to contribute to tumour chemoresistance and metastasis (Desmet and Peeper, 2006; Thiele et al., 2009). Thus, TrkB activation is mainly associated with stimulation of tumour aggressiveness and growth, which is in contrast with our identification of TrkB as an anti-tumorigenic gene. However, as reviewed by Desmet *et al.,* studies on different tumours do suggest a possible anti-tumorigenic function (Desmet and Peeper, 2006). In addition, expression of the truncated TrkB isoform, TrkB-T1, is associated with a more anti-tumorigenic function due to inhibition of full-length TrkB effects (Garofalo et al., 2015; Ohira et al., 2006), an effect that could be mediated by the direct binding of the Rho-GTPase inhibitor GDI1 to TrkB-T1 (Ohira et al., 2005, 2006). Interestingly, as described above, one of our identified tumorigenic genes, VAV3, is also known to increase Rho-GTPase activity and can induce morphological changes and invasivity in astrocytoma cells (Liu et al., 2014a; Movilla and Bustelo, 1999; Salhia et al., 2008). These results indicate

4

that similar downstream targets are influenced upon a decrease or an increase in the GFAPδ/α ratio in opposite directions.

The aldo-keto reductase 1 family member C3 (AKR1C3) is thought to protect the cell against aldehyde and oxidative cytotoxicity. We found increased expression in low-grade astrocytoma, although others reported no different expression between tumours of different grade (Park et al., 2010). Increased expression of AKR1C3 has been reported before in low-grade glioma with a specific 1q19p co-deletion (Ducray et al., 2008) which corroborates our findings of a better prognosis for grade III astrocytoma patients with high AKR1C3 expression (Bredel et al., 2009). In contrast, a high AKR1C3 expression has been linked to worse prognosis for grade IV patients (Bredel et al., 2009). *In vitro* findings in astrocytoma cells and oesophageal carcinomas suggest a tumorigenic function (Ragel et al., 2007; Xiong et al., 2014). Future studies will have to determine how AKR1C3 expression changes the biology of astrocytoma cells and leads to a better outcome for grade III astrocytoma patients.

Finally, we identified the genes encoding the F-box protein 2 (FBXO2) and the ST3 beta-galactoside alpha-2,3-sialyltransferase (ST3GAL6), as GFAP-regulated anti-tumorigenic genes. Both showed an increased expression in low-grade astrocytoma compared to high-grade and high ST3GAL6 expression in astrocytoma grade III patients is associated with a lower survival and progression free survival probability. To our knowledge, these genes have not been studied in astrocytoma. However, their described function in healthy tissue and other tumour types combined with our observations imply a role for them in astrocytoma. ST3GAL6 is a sialyltransferase that modulates glycosylated proteins such as N-glycans by adding sialic acid to their oligosaccharide chain. In different tumours, glycosylation is altered and ST3GAL6 is a modulator of this process in breast cancer cells. Increased ST3GAL6 expression leads to changes in interactions with the tumour cell environment and in cell adhesion and migration (Glavey et al., 2014). Furthermore, ST3GAL6 expression is a negative prognostic factor in a specific subtype of breast carcinoma (Milde-Langosch et al., 2014). To the contrary, decreased ST3GAL6 expression is observed in hepatocellular carcinomas compared to non-tumour liver tissue (Souady et al., 2011). Our data suggest an anti-tumorigenic role of ST3GAL6, but how ST3GAL6 modulation of glycan proteins could lead to a less malignant astrocytoma subtype is unknown. More support has been published for an anti-tumorigenic role of the f-box protein 2 (FBXO2). This gene encodes an F-box protein that is part of a ubiquitin ligase complex that specifically targets N-glycosylated proteins for proteasomal degradation (Yoshida et al., 2002). FBXO2 is thought to be responsible for the elimination of the N-glycosylated integrin β1 precursor protein, important

for adhesion, migration, and invasion (Yoshida et al., 2002). In addition to this, FBXO2 regulates protein degradation of cell cycle regulators. Increased expression of FBXO2 in different cell types induces growth arrest (Erhardt et al., 1998; Wen et al., 2010), related to the presence of FBXO2 in the overrepresented GO cluster of regulation of proliferation. These observations support an anti-tumorigenic role for FBXO2.

GFAP-isoform stoichiometry and astrocytoma biology

Our data show that the stoichiometry of GFAP-isoform expression is important for determining astrocytoma malignancy related molecular and functional processes. The gene ontology analysis on the GFAP-regulated (anti-)tumorigenic gene sets suggests a role in the regulation of tumour growth. Previous studies have suggested an important role of the IF network in astrocytoma cell migration and interaction with the ECM (Moeton et al., 2014, 2016). Moreover, a GO analysis on all GFAP-isoform induced transcriptional changes observed in our astrocytoma cell lines revealed the cell's interaction with its environment through adhesion, ECM composition, and ECM remodelling as the major targeted modules regulated by GFAP modulation (Sup. Material 8-11). For brain tumours to grow and metastasize, ECM remodelling is an essential step. On the one hand tumours have to degrade the ECM barrier to allow for infiltration. On the other hand the ECM environment of the tumour itself has to meet requirements for maintenance of the various heterogeneous populations of tumour cells present in the tumour, ranging from a tumour stem cell population to the vasculature of the tumour (Wang et al., 2010). Remarkably, the 80 differentially expressed genes between GFAPδ^+ and GFAPα^+ are also overrepresented in the same clusters representing interaction with environment (Sup. Material 12) suggesting a role of the isoforms in these processes. In addition, analysis of annotations and function in physiology and pathology in an Ingenuity Pathway Analysis with a focus on cancer, more specifically indicated a role of GFAP-isoform regulated genes in tumour invasion *(data not shown).* Together, our data and previous observations suggest that GFAP-isoforms in astrocytoma could regulate the malignant phenotype of the cells both by regulating their growth as well as their invasive capacity by modulating the cell's interaction with its environment and the ECM.

In conclusion, our data supports an important role for the IF-network in astrocytoma malignancy. Astrocytoma of low and high grade consist of a different network composition induced by altered levels of GFAP-isoforms, leading to changed expression of genes that are involved in tumour growth and invasion and

4

are associated with survival and progression of disease in patients. We identified VAV3, NOS2, DUSP4, and SPC24 as tumorigenic, and NTRK2, FBXO2, ST3GAL6, and AKR1C3 as anti-tumorigenic genes that are all regulated by the GFAP network. Thus, GFAP isoforms have an important function in astrocytoma malignancy and the GFAP-network and GFAP alternative splicing are novel targets that await further exploration as a potential novel treatment for astrocytoma.

Acknowledgements

Legend Supplemental Materials

Supplemental materials can be found on www.ellyhollab.eu or will be made available upon request.

Supplemental Material 1
Primer pairs used and their qPCR efficiencies for microarray validation.

Supplemental Material 2
Modulation of GFAP-network in U373 and U251 astrocytoma cells
To get insight into the function of these GFAP-isoforms in astrocytoma and to investigate a potential role for GFAPα and the GFAPδ/α ratio in astrocytoma malignancy, we modulated GFAP-isoform expression in U251 (a-e) and U373 (f-l) cells by recombinant expression or silencing with shRNAs of the isoforms and analysed the GFAP-isoform induced transcriptomic changes. U251 cells were transduced with GFAPα (GFAPα+) or GFAPδ (GFAPδ+). Staining the control U251 cells showed some cells positive for endogenous GFAP, but predominantly GFAP-negative cells (a) GFAPα+ cells showed a GFAP-network throughout the cytoplasm (b), whereas GFAPδ+ cells showed the characteristic juxtanuclear accumulation of GFAP (c), as we have described before (Moeton et al., 2016). At the RNA level, using primers that recognize all (pan) GFAP-isoforms, a significant increase of pan-GFAP expression in GFAPα+ (FC = 9.6, FDR<.001) and GFAPδ+ (FC = 16.3, FDR<.001) cells was observed (d). GFAPδ mRNA was only increased in GFAPδ+ cells (FC = 1534, FDR<.001) (e). Depicted is the median (horizontal line) with quartiles (box), N=8. These finding are in agreement with western blot results showing that the amount of GFAP protein is increased in these cell lines

as shown before (Moeton et al., 2016).

U373 cells were transduced with shRNA directed against pan-GFAP (GFAPpan-) or against GFAPα (GFAPα-). Both the GFAPpan- (FC = 0.46, FDR=.063) and the GFAPα- (FC = 0.15, FDR=.027) U373 cells showed a decrease in GFAPα mRNA (f). GFAPα- cells shifted their ratio of GFAPδ/α mRNA more towards GFAPδ, due to a strong decrease in GFAPα (ratio of GFAPδ/α (arbitrary units) the ratio for NTC = 0.42; GFAPpan- = 0.51, FDR=.31; GFAPα- = 1.73, FDR=.077) (g), while the GFAPδ was stable (h) N=5, depicted is the median (horizontal line) with quartiles (box)). The knockdown of GFAP was confirmed by western blot, and was more efficient in the GFAPα- than in the GFAPpan- cells (i) depicted is median with quartiles (box), N=4. Stainings confirmed the less efficient knockdown of GFAP in the GFAPpan- (k) than the GFAPα- (l), compared to NTC cells (j). Scale bars in the micrographs represent 50 um.

Supplemental Material 3

Top 50 of most significant probes in GFAPα+ compared to Control cells.

Most significant genes annotated to probes detecting more than 1.5 fold up or down change induced by GFAPα+ expression. t = t-test statistics, fold change: >1 = GFAPα+ induced expression, <1 = GFAPα+ repressed expression, FDR adj.P.Val = False Discovery Rate controlled p-value.

Supplemental Material 4

Top 50 of most significant probes in GFAPδ+ compared to Control cells.

Most significant genes annotated to probes detecting more than 1.5 fold up or down change induced by GFAPδ+. t = t-test statistics, fold change: >1 = GFAPδ+ induced expression, <1 = GFAPδ+ repressed expression, FDR adj.P.Val = False Discovery Rate controlled p-value.

Supplemental Material 5

Top 50 of most significant probes in GFAPpan- compared to NTC cells.

Most significant genes annotated to probes detecting more than 1.5 fold up or down change induced by GFAPpan-. t = t-test statistics, fold change: >1 = GFAPpan- induced expression, <1 = GFAPpan- repressed expression, FDR adj.P.Val = False Discovery Rate controlled p-value.

Supplemental Material 6

Top 50 of most significant probes in GFAPα- compared to NTC cells.

Most significant genes annotated to probes detecting more than 1.5 fold up or down change induced by GFAPα-. t = t-test statistics, fold change: >1 = GFAPα- induced expression, <1 = GFAPα- repressed expression, FDR adj.P.Val = False Discovery Rate controlled p-value.

Supplemental Material 7

Heat map of genes with an FDR p-value <.1 in at least one knockdown and one recombinant expression condition

Four main patterns were distinguished of either upregulation in both GFAPα- and GFAPδ+ or

downregulation in both GFAPα- and GFAPδ+, or an opposite regulation by GFAPα- and GFAPδ+, as indicated by different colors in the dendrogram (purple, grey, yellow, black). Some genes showed similar behaviour in GFAPα+ as well as in GFAPδ+ cells, whereas GFAPpan- in general didn't show large effects. The observed strongest changes in the GFAPα- and GFAPδ+ condition imply that the change is due to the increase in GFAPδ/GFAPα ratio.

Supplemental Material 8

Top Gene Ontology terms per domain overrepresented by GFAPα+ compared to control.
Annotated genes = number of total microarray probes annotated to this term; Sig genes = number of probes detecting significant change in this term; p-val = parent-child weighted p-value of Fisher's exact test for overrepresentation; GO = Gene Ontology; BP = Biological Process; CC = Cellular Component; MF = Molecular Function.

Supplemental Material 9

Top Gene Ontology terms per domain overrepresented by GFAPδ+ compared to control.
Annotated genes = number of total microarray probes annotated to this term; Sig genes = number of probes detecting significant change in this term; p-val = parent-child weighted p-value of Fisher's exact test for overrepresentation; GO = Gene Ontology; BP = Biological Process; CC = Cellular Component; MF = Molecular Function.

Supplemental Material 10

Top Gene Ontology terms per domain overrepresented by GFAPpan- compared to NTC.
Annotated genes = number of total microarray probes annotated to this term; Sig genes = number of probes detecting significant change in this term; p-val = parent-child weighted p-value of Fisher's exact test for overrepresentation; GO = Gene Ontology; BP = Biological Process; CC = Cellular Component; MF = Molecular Function.

Supplemental Material 11

Top Gene Ontology terms per domain overrepresented by GFAPα- compared to NTC.
Annotated genes = number of total microarray probes annotated to this term; Sig genes = number of probes detecting significant change in this term; p-val = parent-child weighted p-value of Fisher's exact test for overrepresentation; GO = Gene Ontology; BP = Biological Process; CC = Cellular Component; MF = Molecular Function.

Supplemental Material 12

Top Gene Ontology terms per domain overrepresented by comparing GFAPα+ to GFAPδ+.
Annotated genes = number of total microarray probes annotated to this term; Sig genes = number of probes detecting significant change in this term; p-val = parent-child weighted p-value of Fisher's exact test for overrepresentation; GO = Gene Ontology; BP = Biological Process; CC = Cellular

Component; MF = Molecular Function.

Supplemental Material 13

Heatmap of the genes that significantly correlated to either GFAPα or the GFAPδ/α ratio (FDR < 0.01).

The color key indicates the correlation coefficient (R). Hierarchical clustering on the absolute correlation coefficient results into the identification of two main clusters. Cluster 1 consists of genes that positively correlate to GFAPα but negative to the GFAPδ/α ratio, cluster 2 shows the opposite pattern with genes negatively correlating to GFAPα and positively to the GFAPδ/α ratio.

Supplemental Material 14

Linear regression results of the 43 identified anti-tumorigenic genes.

Linear regression results of genes that show a significant positive correlation to GFAPα (α columns), a negative correlation to GFAPδ/α ratio (δ/α columns) and do not correlate to GFAPδ (δ columns). FDR = False Discovery Rate controlled p-value.

Supplemental Material 15

Linear regression results of the 37 identified tumorigenic genes.

Linear regression results of genes that show a significant negative correlation to GFAPα (α columns), a positive correlation to GFAPδ/α ratio (δ/α columns) and do not correlate to GFAPδ (δ columns). FDR = False Discovery Rate controlled p-value

Supplemental Material 16

Kaplan meier survival analysis of GFAP-regulated (anti-)tumorigenic genes in grade III astrocytoma patients.

Results of log rank regression analysis of survival estimates of below and above median expression of genes of interest.

FDR = False Discovery Rate controlled p-value, AT = anti-tumorigenic, TU = tumorigenic, Direction of expression and survival probability = indication whether low or high expression of the gene of interest results in a lower survival probability for grade III astrocytoma patients.

Supplemental Material 17

Linear regression results of final set of GFAP-regulated (anti-)tumorigenic most likely to be regulated by GFAP in patient tumours and are relevant for astrocytoma malignancy.

Linear regression results of genes that show a significant correlation to GFAPα (α columns) or to the GFAPδ/α ratio (δ/α columns) within astrocytoma grade II, III or IV. FDR = False Discovery Rate controlled p-value

Chapter

5

IF deficient glia display distinct molecular profiles linked to ECM and cell-cell interactions

Oscar M.J.A. Stassen
Lieneke Kooijman
A. Marie Orre
Milos Pekny
Willem Kamphuis
Elly M. Hol

Abstract

The intermediate filament (IF) network in glia has mainly been a subject of research in pathology. This has two main reasons: the strong upregulation of IF proteins in astrocytes in pathological conditions, and the lack of a strong phenotype in knockout mouse models of glial IFs. We used a microarray transcriptomics study on microglia and astrocytes acutely isolated from 18 month old mice to investigate the effects of a Gfap knockout and a Vimentin-Gfap double knockout on the transcriptome of glia. Both in the astrocytes and in the microglia, the loss of Gfap and/or Vimentin has profound effects on transcript levels for genes involved in extracellular matrix production and interaction, as well as on genes involved in cell-cell signalling. In microglia this may represent indirect changes induced by the altered IF networks in astrocytes. To address differentially expressed genes that are involved in concrete interactions between astrocytes and microglia, the Dcc / Netrin and components in the Notch signalling pathway are further discussed. This work provides many leads for further investigations into the molecular functions of IFs in cell-cell signalling and ECM interactions.

Introduction

Astrocytes and microglia are two major classes of glial cells in the brain. Astrocytes play important physiological roles in homeostasis by providing energy for neurons, maintaining the integrity of brain vasculature, clearing neurotransmitters from the synaptic cleft, and contributing to the formation and maintenance of the extracellular matrix (ECM) (Christopherson et al., 2005; Sofroniew and Vinters, 2010). In the diseased brain astrocytes become activated, which is hallmarked by a strong increase in their intermediate filament (IF) content, the production of immunoregulatory genes, and a downregulation of the expression of neuron-supporting genes (Hol and Pekny, 2015; Orre et al., 2014a). Microglia are the brain's innate immune system, and as such, are instrumental in dealing with infections and clearing debris after brain damage or during degenerative processes (Hanisch and Kettenmann, 2007). Also in the healthy brain microglia are now recognized to play important roles, such as in the maintenance of functional synapses (Kettenmann et al., 2013). Astrocytes and microglia interact extensively, e.g. through cytokine signalling (Abudara et al., 2015).

Glial fibrillary acidic protein (Gfap) is the signature IF protein of the astrocytes in the central nervous system, in addition also other IFs such as Vimentin (Vim), Nestin, and Synemin are expressed by these cells, and together they form the IF network (Hol and Pekny, 2015). Gfap has also been described in peripheral glia

in the enteric nervous system or in hepatic stellate cells (Clairembault et al., 2014; Knittel et al., 1999). Gfap expression is tightly regulated during CNS development in neural stem cells and differentiation of astrocytes (Mamber et al., 2013; Middeldorp and Hol, 2011). At the cellular level a few functional roles for Gfap have been documented: Gfap modulation influences migration and polarization of astrocytes (Dupin et al., 2011) and alters transport properties of MHC class-II transporting vesicles (Vardjan et al., 2012). Vim is currently emerging as an important protein with cellular roles in epithelial-to-mesenchymal transition, migration and inflammation regulation (Mendez et al., 2010; dos Santos et al., 2015; Virtakoivu et al., 2015). In neuropathological conditions, such as epilepsy and Alzheimer's disease (AD), and upon brain injury, Gfap is highly upregulated in reactive astrocytes (Baldwin and Scheff, 1996; Kamphuis et al., 2014). In a quest to unravel the function of Gfap, Gfap knockout (ko) mice (GFAPko) were made, and studies on these mice so far have revealed a heterogeneous set of data. Four independent groups generated a GFAPko mouse model. One found no obvious phenotype (Pekny et al., 1995), one found white matter instability emerging at old age (Liedtke et al., 1996), and two reported on altered neuronal plasticity (McCall et al., 1996; Shibuki et al., 1996). Later reports also described altered laminin and fibronectin production and distribution, and more subtle differences at cellular level (Menet et al., 2001). The main interacting partner of Gfap is Vim, and Vim deficient astrocytes have been reported to have Gfap-negative astrocytes or astrocytes with an irregular network (Galou et al., 1996). To exclude compensatory mechanisms or redundancy between these two IFs, many studies were done on double ko mice for Gfap and Vim (VIM-GFAPko). These mice showed an increase in large blood vessels in the brain, but this phenotype has not been followed up so far. The observed effects of the IF ko on pathology were not straightforward. Depending on the specific pathology, beneficial or detrimental effects of IF ko have been described, as recently reviewed (Hol and Pekny, 2015). The general effect of an injury to the brain in VIM-GFAPko mice is an early detrimental effect due to larger brain lesions or a more rapid disease progression, contrasted with an increased regenerative potential at a later stage (Li et al., 2008; Menet et al., 2003). Interestingly, the VIM-GFAPko also showed an increased neurogenic permissiveness *in vitro*, as well as an increased success in neural stem cell engraftment *in vivo* (Menet et al., 2001; Widestrand et al., 2007; Wilhelmsson, 2004).

To gain more insight in the molecular pathways that change due to the absence of Gfap and/or Vim in astrocytes and microglia, we compared the transcriptomic profiles of purified cell populations of both cell types acutely isolated from the mouse cortex.

Methods

Microarray Data processing and statistics

Raw microarray data was obtained from GEO dataset GSE74614. For generation of this dataset Vim$^{+/-}$ Gfap$^{+/-}$ AD$^{+/-}$ animals were crossed to generate various genotypes. From these animals cortical cell suspensions were prepared and astrocytes and microglia were sorted by FACS, as described extensively by Kamphuis *et al.* (Kamphuis et al., 2015). Briefly, cell populations were sorted on the basis of specific extracellular markers by initial exclusion of myelin, and the subsequent selection of CD11b (integrin αM) positive cells (microglia) and glutamate transporter (GLT-1: SLC1A2 or EAAT2) positive cells (astrocytes). Only the non-AD animals were incorporated in our analysis, resulting in a comparison of astrocytes and microglia from glia lacking Gfap (GFAPko), both Vim and Gfap (VIM-GFAPko), and wild type (WT) animals. VIMko animals were not included in this study as litters in this genotype were too small to generate enough animals for this study. The data were processed as described before (Bossers et al., 2010a; Orre et al., 2014a, 2014b). Using the limma package in bioconductor (Smyth, 2005), spot intensities were imported into R software for statistical computing (R version 3.1). Spots labelled by the Feature Extraction software as saturated or non-uniformly distributed foregrounds and backgrounds, as well as visually identified artefacts on the array, were omitted. In these cases statistics of differential expression were based on the remaining spots. Backgrounds were subtracted, intensities were quantile normalized between all arrays, and sample intensities were extracted for an intensity-based analysis (Bossers et al., 2010b). Redundant probes with identical sequence were averaged and all genes that had a condition with an average expression intensity of $\log_2 >$ 6 (intensity >64) were included in the analysis. The astrocytes and microglia were analysed separately. This resulted in an inclusion of 22,808 genes for astrocytes and 23,674 genes for microglia in our analysis. Statistical significance for differential expression between conditions was tested using a Bayesian linear model fit with an FDR corrected criterion level of $\alpha = .1$ due to the exploratory nature of this analysis. Microarray probes were considered to report a differentially expressed gene if the statistical test was significant and the absolute $\log_2$ fold change was greater than 1.

Gene ontology and cluster analysis

Differentially expressed genes (DEGs) were analysed using the topGO R package to detect gene ontology (GO) terms that are overrepresented in our dataset, using a Fisher statistical test with a weighted algorithm to correct for dependency between ontology terms (Alexa et al., 2006). As background for the overrepresentation tests we

used all probes considered in the statistical test for differential expression. Databases used to search for overrepresentation were the GO domains 'Cellular compartment' (CC), 'Biological Process' (BP) and 'Molecular Function' (MF). Annotation was performed using an annotation build of 08-Mar-2014 (MmAgilentDesign026655.db v.2.14.0, curated by Bioconductor).

For analysis of GO term overrepresentation in specific IF dependent expression patterns, DEGs were clustered by k-means clustering. DEGs intensities were normalized to an average of 0 and standard deviation of 1 before clustering. The number of clusters required to extract the main expression patterns was determined empirically for astrocytes and microglia to be 8 and 12, respectively. The genes in each cluster were then analysed with topGO as described above. In all cases where genes were represented multiple times in a cluster, duplicates were removed.

Results

Distinct transcriptomes of IF deficient astrocytes and microglia

WT versus GFAPko

The effects of the lack of Gfap (GFAPko) on gene expression in astrocytes and microglia are represented in volcanoplots (Fig. 1). Differentially expressed genes (DEGs) as identified by our criteria are represented in red. The lack of Gfap resulted in 228 DEGs in astrocytes, and surprisingly, as Gfap is an astrocyte-specific gene, in 1165 DEGs in microglia. The 228 DEGs in astrocytes, excluding 3 entries for Gfap, resulted in an average absolute fold change of 3.16, whereas the 1165 DEGs in microglia resulted in an average absolute fold change of 2.74. The top 50 most significantly regulated genes for the GFAPko vs WT astrocytes and microglia are listed in Table 1 and 2.

GFAPko versus VIM-GFAPko

To study the additional effect of a lack of Vim, we compared the transcriptomes of the astrocytes and microglia from the GFAPko with those from the VIM-GFAPko. These data are represented as volcanoplots, with the DEGs in red (Fig. 2). The VIM-GFAPko astrocytes had 314 DEGs compared to the GFAPko astrocytes. The VIM-GFAPko microglia had 731 DEGs compared to the GFAPko microglia. Again it was quite striking that the ko of Vim (in the genetic background of GFAPko) had a larger effect on the microglia than on the astrocytes, as Vim is only lowly expressed in WT microglia. Top 50 most significant DEGs for GFAPko vs VIM-GFAPko astrocytes and microglia are listed in Table 3 and 4.

WT versus VIM-GFAPko

Finally we studied the combined effect of both Gfap and Vim ko by comparing transcriptomes of the astrocytes and microglia from the VIM-GFAPko to the WT transcriptomes. Differential expression profiles of the glia of these two genotypes are represented as volcanoplots, with DEGs in red (Fig. 3). Comparing the VIM-GFAPko astrocytes with WT resulted in 632 DEGs. Comparing the VIM-GFAPko microglia with WT resulted in 634 DEGs. Top 50 most significant DEGs for astrocytes and microglia for the VIM-GFAPko vs WT are listed in Table 5 and 6.

Gene ontology of IF modulated astrocytes and microglia.

WT versus GFAPko GO-analysis

The DEGs found in all comparisons, i.e. WT vs GFAPko, WT vs VIM-GFAPko and GFAPko vs VIM-GFAPko in astrocytes and microglia, were analysed for GO overrepresentation. The top 10 terms for each GO domain
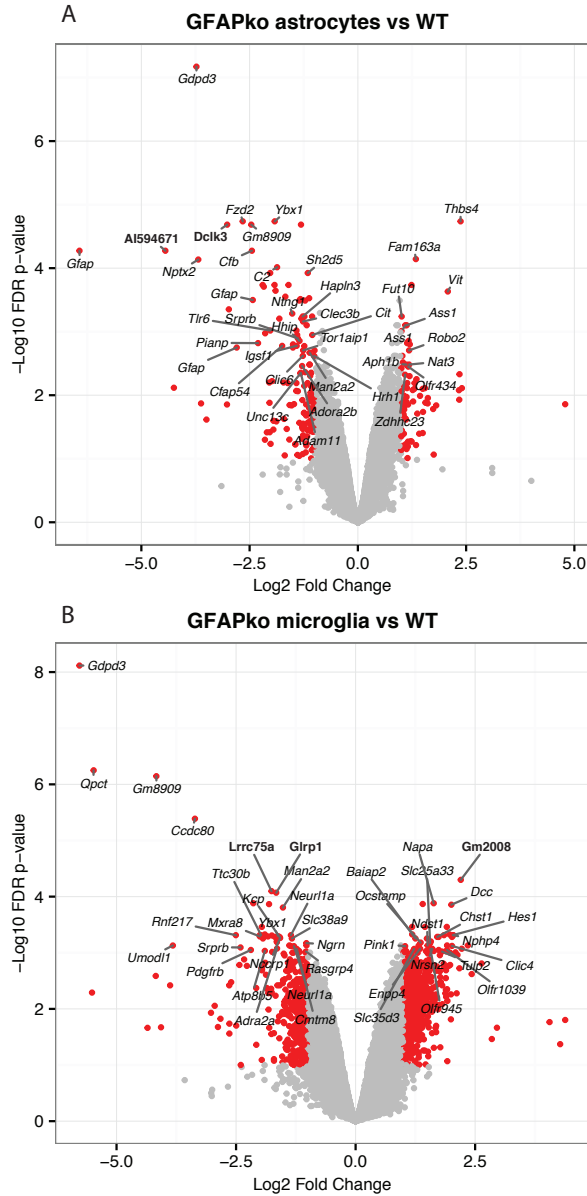
Figure 1. Transcriptomic differences between glia populations from GFAPko and WT adult mice

Volcanoplot representation of transcriptomic changes in astrocytes (A) and microglia (B). DEGs are represented by red dots, and the 40 most significant names of genes annotated to the GO-terms related to ECM interaction or cell-cell signalling are printed in *italics*. The 10 most significant genes, if not in those GO-terms, are printed in bold. 22,808 genes analysed for astrocytes resulted in 228 DEGs (A). 23,674 genes analysed for microglia resulted in 1165 DEGs (B).

(Biological Process, Cellular Compartment and Molecular Function) are given in tables (Tables 7-12). Most remarkable in the GFAPko astrocytes (Table 7) was the overrepresentation of terms related to extracellular proteins and plasma membrane ("Cell periphery", "extracellular region", "integral component of membrane"), as indicated before by Kamphuis et al (Kamphuis et al., 2015). These GO-terms were also strongly overrepresented in the recombinant expression and knockdown studies of GFAP isoforms in glioma cells described in Chapter 4. Also the terms of "blood microparticle" (extracellular vesicles; Cfb, Actg2, Trf, Hspa1a, C4b, Fga) and "microglial cell activation" (Tlr6, Cx3cr1) were overrepresented in the astrocytes. The interaction of Gfap with the other components of the cytoskeleton was shown by overrepresentation of proteins in the GO-term "cytoplasmic microtubule" (Srprb, Mtus2, Sctr, Mid1). In

Figure 2. Transcriptomic differences between cell population from VIM-GFAPko and WT adult mice
Volcanoplot representation of transcriptomic changes in astrocytes (A) and microglia (B). DEGs are represented by red dots, and the 40 most significant names of genes annotated to the GO-terms related to ECM interaction or cell-cell signalling are printed in *italics*. The 10 most significant genes, if not in those GO-terms, are printed in bold. 22,808 genes analysed for astrocytes resulted in 314 DEGs (A). 23,674 genes analysed for microglia resulted in 750 DEGs (B).

5

the GFAPko microglia (Table 8) the most significantly overrepresented GO-terms were "G-protein coupled receptor signalling pathway" and "G-protein coupled receptor activity". Another overrepresented GO-term, which comprises 244 DEGs, was the rather broadly defined "integral component of membrane".

GFAPko versus VIM-GFAPko GO-analysis

The top 10 terms found for each GO domain based on the DEGs between VIM-GFAPko and GFAPko are given in Table 9 (astrocytes) and Table 10 (microglia). Here the additional effect of Vim absence in astrocytes resulted most prominently in overrepresentation of the terms related to angiogenesis and vasculogenesis ("positive regulation of angiogenesis", "vasculogenesis", "patterning of blood vessels"). Again clusters related to extracellular space were overrepresented,
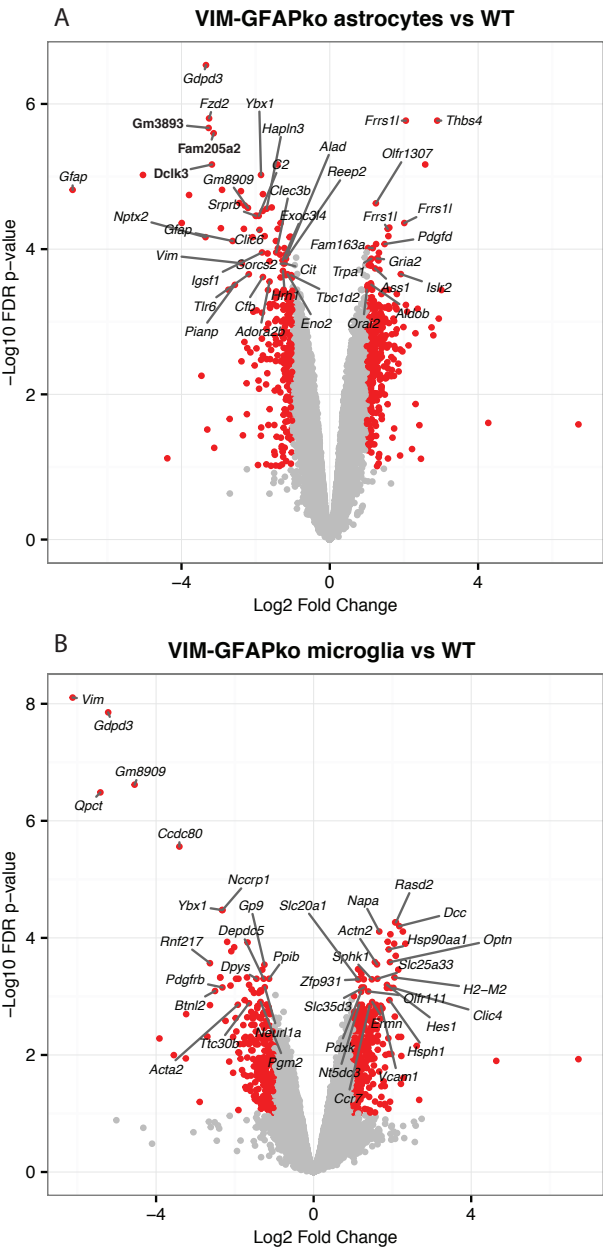
Figure 3. Transcriptomic differences between cell population from VIM-GFAPko and wt

Volcanoplot representation of transcriptomic changes in astrocytes (A) and microglia (B). DEGs are represented by red dots, and the 40 most significant names of genes annotated to the GO-terms related to ECM interaction or cell-cell signalling are printed in *italics*. The 10 most significant genes, if not in those GO-terms, are printed in bold. 22,808 genes analysed for astrocytes resulted in 632 DEGs (A). 23,674 genes analysed for microglia resulted in 634 DEGs (B).

Table 1: Top 50 most significantly regulated genes with more than 2 fold up or down change in GFAPko astrocytes compared to WT astrocytes.

Gene Symbol	FC	Int	t	FDR	GenBank accession	Agilent Probe Name
Gdpd3	0.08	6.5	-22.7	6.7E-08	NM_024228	A_51_P426875
Fzd2	0.16	7.6	-13.9	1.8E-05	NM_020510	A_52_P129428
Ybx1	0.26	8.0	-13.5	1.8E-05	M60419	A_55_P2131379
Thbs4	5.18	9.9	13.3	1.8E-05	NM_011582	A_52_P401504
Dclk3	0.12	6.8	-12.8	2.1E-05	NM_172928	A_51_P419637
NAP000581-003	0.40	9.4	-12.7	2.1E-05	NAP000581-003	A_55_P1959541
Gm8909	0.18	6.2	-12.6	2.1E-05	NM_001081032	A_55_P1956160
AI594671	0.05	4.8	-11.4	5.3E-05	AA711038	A_55_P2295856
Gfap	0.01	5.3	-11.4	5.3E-05	NM_001131020	A_52_P52303
Cfb	0.18	6.6	-11.4	5.3E-05	NM_008198	A_51_P413866
Fam163a	2.53	11.2	11.0	7.2E-05	NM_177838	A_55_P2027421
Nptx2	0.08	6.1	-10.9	7.3E-05	NM_016789	A_52_P187058
C2	0.27	8.7	-10.6	9.7E-05	NM_013484	A_51_P497985
A130040M12Rik	0.25	8.3	-10.3	1.2E-04	NR_002860	A_55_P2116650
Sh2d5	0.45	7.0	-10.3	1.2E-04	NM_001099631	A_52_P571746
Psmc3ip	0.33	6.7	-9.9	1.8E-04	NM_008949	A_52_P238044
LOC100048027	0.22	9.4	-9.9	1.8E-04	XM_001480007	A_55_P2174736
NA	0.26	6.2	-9.8	1.8E-04	A_55_P1990066	A_55_P1990066
Pts	2.36	9.8	9.8	1.8E-04	NM_011220	A_52_P177021
5430410E06Rik	0.22	5.3	-9.7	2.0E-04	XM_001475205	A_55_P1981464
Ccdc24	0.27	8.2	-9.5	2.3E-04	ENSMUST00000106422	A_55_P2177697
Vit	4.22	8.1	9.5	2.3E-04	NM_028813	A_51_P298107
Sfmbt2	0.31	6.8	-9.3	2.8E-04	ENSMUST00000114864	A_55_P1956652
L3hypdh	0.46	7.4	-9.2	3.0E-04	NM_026038	A_51_P408989
Zfp949	0.40	8.6	-9.1	3.1E-04	NM_001142943	A_55_P2170536
Gfap	0.19	6.0	-9.1	3.2E-04	NM_010277	A_55_P2157250
Hapln3	0.39	9.7	-9.0	3.2E-04	ENSMUST00000032827	A_55_P2093553
LOC100046136	0.43	8.7	-9.0	3.2E-04	XM_001476489	A_55_P2143119
OTTMUSG00000002191	0.13	4.9	-8.7	4.4E-04	XM_001474519	A_55_P1997345
Ntng1	0.35	6.2	-8.6	5.2E-04	XM_001479688	A_51_P213099
A230065H16Rik	0.48	7.1	-8.5	5.8E-04	NM_001101503	A_55_P2076916
Hapln3	0.41	9.0	-8.4	5.8E-04	NM_178255	A_51_P244213
Zfp949	0.42	8.1	-8.4	5.8E-04	NM_001142943	A_51_P513244
Fut10	2.02	8.2	8.4	5.8E-04	NM_134161	A_55_P2165011
Mss51	0.41	5.8	-8.3	6.2E-04	NM_029104	A_51_P369426

5

Rem1	0.28	5.3	-8.3	6.2E-04	NM_009047	A_55_P2113078
Clec3b	0.42	6.1	-8.2	6.9E-04	NM_011606	A_51_P486239
Ass1	2.14	10.9	8.1	7.9E-04	NM_007494	A_55_P2004781
A130040M12Rik	0.44	8.9	-8.1	7.9E-04	NR_002860	A_55_P1973347
Ass1	2.18	9.7	8.0	7.9E-04	NM_007494	A_55_P2143070
Tlr6	0.25	6.8	-7.9	9.6E-04	NM_011604	A_52_P117393
5430410E06Rik	0.37	6.1	-7.9	9.6E-04	XM_001475205	A_55_P1981461
Trim12	2.01	7.1	7.8	9.7E-04	NM_023835	A_55_P2064659
NAP114441-1	0.23	4.8	-7.7	1.1E-03	NAP114441-1	A_55_P1992884
Cit	0.48	6.8	-7.7	1.1E-03	NM_007708	A_55_P1999633
Gm3502	0.38	6.5	-7.7	1.1E-03	XM_001477144	A_55_P2018377
Srprb	0.38	8.3	-7.6	1.3E-03	NM_009275	A_52_P131559
Hhip	0.39	8.3	-7.5	1.4E-03	NM_020259	A_55_P1969276
XM_001478398	2.25	7.3	7.5	1.4E-03	XM_001478398	A_55_P2031848
C530028O21Rik	0.20	5.7	-7.4	1.5E-03	NM_175696	A_55_P2004532

FC = fold change (>1 = expression upregulated, <1 = expression downregulated), Int = Mean $\log_2$ intensity, t = t-test statistic, FDR = False Discovery Rate controlled p-value, NA = Not Available

Table 2: Top 50 of most significantly regulated genes with more than 2 fold up or down change in GFAPko microglia compared to WT microglia.

Gene Symbol	FC	Int	t	FDR.	GenBank accession	Agilent Probe Name
Gdpd3	0.02	8.94	-29.29	7.7E-09	NM_024228	A_51_P426875
Qpct	0.02	8.95	-19.76	5.6E-07	NM_027455	A_55_P2140118
Gm8909	0.06	7.62	-18.76	7.2E-07	NM_001081032	A_55_P1956160
Ccdc80	0.10	7.46	-15.94	4.1E-06	NM_026439	A_55_P2169586
Gm2008	4.60	13.78	12.74	5.0E-05	XM_001472097	A_55_P2092831
Fam211a	0.30	11.66	-13.03	8.0E-05	NM_198861	A_55_P2149896
Glrp1	0.32	10.10	-11.86	8.5E-05	NM_008132	A_55_P2042743
Napa	3.10	10.31	11.19	1.3E-04	NM_025898	A_51_P246816
NA	0.23	7.37	-11.28	1.3E-04	XM_001472101	A_55_P1976743
NA	2.65	12.43	11.07	1.4E-04	XM_919542	A_55_P2130575
NA	0.29	8.32	-10.97	1.4E-04	XM_001477916	A_55_P1977920
Dcc	4.01	11.94	10.87	1.4E-04	NM_007831	A_55_P1961761
Man2a2	0.35	7.90	-10.69	1.6E-04	NM_172903	A_52_P659270
Dcaf12l2	2.73	14.66	9.82	3.5E-04	NM_175539	A_55_P1959973

Gpr165	0.26	7.16	-9.75	3.5E-04	NM_029536	A_55_P1987176
NA	3.75	5.93	10.44	3.5E-04	A_55_P2027230	A_55_P2027230
NA	2.27	8.68	9.79	3.5E-04	NM_001113806	A_55_P2157551
Gm14391	2.27	10.68	9.37	4.7E-04	NM_001099308	A_55_P1956807
NA	3.90	9.94	9.41	4.7E-04	XM_001477233	A_55_P1962699
NA	0.27	5.06	-9.36	4.7E-04	XM_485041	A_66_P129469
Rnf217	0.18	4.88	-9.17	4.9E-04	NM_001146349	A_52_P3845
Ttc30b	0.25	7.17	-9.16	4.9E-04	NM_028235	A_52_P96748
Sept1	3.60	8.17	9.09	4.9E-04	NM_017461	A_55_P1963764
Gm3716	0.25	6.19	-9.25	4.9E-04	XM_001478025	A_55_P1964955
Neurl1a	0.39	13.59	-9.09	4.9E-04	NM_021360	A_55_P2023692
Hes1	4.09	9.74	9.20	4.9E-04	NM_008235	A_55_P2046245
Nphp4	4.13	7.95	9.12	4.9E-04	NM_153424	A_55_P2137586
5430410E06Rik	0.30	7.41	-9.05	4.9E-04	XM_001475205	A_55_P1981461
Ybx1	0.33	8.38	-9.00	5.1E-04	M60419	A_55_P2131379
Mxra8	0.25	7.41	-8.97	5.1E-04	NM_024263	A_51_P427476
5430410E06Rik	0.28	6.93	-8.94	5.1E-04	XM_001475205	A_55_P1981464
Zfp69	0.31	7.85	-8.88	5.2E-04	NM_001005788	A_55_P2034385
Chst1	3.27	11.86	8.88	5.2E-04	NM_023850	A_55_P2061620
1700022A21Rik	4.05	7.77	8.82	5.2E-04	NR_003953	A_51_P240723
Kcp	0.33	9.54	-8.83	5.2E-04	NM_001029985	A_55_P2074499
5830444B04Rik	3.33	8.60	8.81	5.2E-04	AK030886	A_55_P2206605
Nccrp1	0.33	8.54	-8.75	5.5E-04	NM_001081115	A_66_P106231
Slc38a9	0.40	7.20	-8.66	5.6E-04	ENSMUST00000091218	A_52_P356228
Hddc3	0.26	7.06	-8.66	5.6E-04	NM_026812	A_52_P521882
Baiap2	2.38	8.32	8.65	5.6E-04	NM_001037755	A_55_P2027788
NA	2.81	9.37	8.69	5.6E-04	XM_001474432	A_55_P2148935
Fam211a	0.32	12.04	-8.55	6.2E-04	NM_198861	A_55_P2090557
NA	2.98	10.58	8.52	6.3E-04	XM_001000635	A_55_P1955244
NA	0.32	5.47	-8.49	6.5E-04	ENSMUST00000114941	A_55_P2131190
Ocstamp	2.57	8.26	8.45	6.6E-04	NM_029021	A_51_P360004
Slc25a33	2.95	11.04	8.41	6.7E-04	NM_027460	A_51_P156438
Ngrn	0.49	11.10	-8.40	6.7E-04	NM_031375	A_55_P2003133
Unc45a	0.49	11.09	-8.27	7.4E-04	NM_133952	A_55_P1970636
Il17d	5.09	9.16	8.30	7.4E-04	NM_145837	A_55_P1980051
Prdm12	2.50	6.09	8.24	7.4E-04	NM_001123362	A_55_P1980134

FC = fold change (>1 = expression upregulated, <1 = expression downregulated),Int = Mean log$_2$ intensity, t = t-test statistic, FDR = False Discovery Rate controlled p-value, NA = Not Available

5

Table 3: Top 50 most significantly regulated genes with more than 2 fold up or down change in VIM-GFAPko astrocytes compared to GFAPko astrocytes

Gene Symbol	FC	Int	t	FDR	GenBank accession	Agilent Probe Name
Gm3892	0.10	7.3	-15.5	5.1E-06	XM_001478587	A_55_P1953273
4933409K07Rik	0.11	7.4	-15.2	5.1E-06	NR_033123	A_55_P2119552
Gm13298	0.11	7.8	-15.0	5.1E-06	NM_001085530	A_55_P2018330
Gm13298	0.07	7.5	-12.0	6.5E-05	NM_001085530	A_55_P2033480
Gm2490	0.11	6.5	-11.5	9.8E-05	XM_001473759	A_55_P2096023
Frrs1l	2.51	7.8	10.4	2.4E-04	NM_001142965	A_55_P2092252
Ccl21a	0.07	8.3	-10.3	2.4E-04	NM_011124	A_55_P2024625
Aldob	2.64	6.4	10.3	2.4E-04	NM_144903	A_51_P337269
9630041G16Rik	3.77	8.7	10.0	2.7E-04	AK079356	A_55_P2330435
Frrs1l	3.44	6.7	9.5	5.1E-04	NM_001142965	A_51_P307559
Kcnk10	0.28	10.1	-8.8	1.0E-03	NM_029911	A_55_P1985544
A230050P20Rik	2.43	9.8	8.7	1.0E-03	NM_175687	A_51_P158073
Vim	0.20	12.2	-8.6	1.1E-03	NM_011701	A_51_P392687
LOC100044738	0.50	5.7	-8.4	1.3E-03	XM_001473138	A_55_P2117594
Krt85	0.29	5.8	-7.6	3.4E-03	NM_016879	A_55_P1999364
Gm6930	0.14	6.6	-7.4	3.9E-03	XM_893705	A_55_P1966774
Gpr116	3.14	9.6	7.3	4.6E-03	NM_001081178	A_55_P1984307
Loxl1	0.45	9.4	-7.1	4.8E-03	NM_010729	A_51_P304239
Atp10a	3.39	7.8	7.1	4.8E-03	NM_009728	A_51_P320022
St3gal1	2.03	8.9	6.9	5.9E-03	NM_009177	A_65_P03728
Frrs1l	2.03	6.6	6.8	6.2E-03	NM_001142965	A_55_P2092251
Ly6c1	2.99	11.2	6.7	6.2E-03	NM_010741	A_55_P1961499
St3gal1	2.09	6.5	6.7	6.2E-03	NM_009177	A_51_P301804
Ttc8	3.24	9.1	6.7	6.2E-03	NM_029553	A_51_P507899
Evi2a	0.44	6.7	-6.7	6.2E-03	NM_001033711	A_55_P2017759
Slc6a6	3.06	10.7	6.6	6.2E-03	NM_009320	A_52_P339996
Col20a1	2.26	6.2	6.6	6.2E-03	NM_028518	A_52_P474902
Irf6	2.66	6.7	6.6	6.4E-03	NM_016851	A_51_P363749
Egfl7	3.06	12.9	6.5	6.6E-03	NM_178444	A_55_P2111355
Crym	0.42	13.0	-6.5	6.9E-03	NM_016669	A_51_P264695
Slco4a1	0.24	6.9	-6.5	6.9E-03	NM_148933	A_55_P1989653
Lsr	3.24	11.2	6.5	7.0E-03	NM_017405	A_55_P1983488
Hspa12b	2.64	9.0	6.5	7.0E-03	NM_028306	A_51_P130332
St8sia4	3.16	9.1	6.4	7.1E-03	NM_009183	A_51_P236267
Arap3	2.84	9.0	6.4	7.1E-03	NM_139206	A_52_P195018

Fn1	3.63	12.0	6.4	7.1E-03	NM_010233	A_55_P2130178
Podxl	3.12	7.5	6.4	7.1E-03	NM_013723	A_52_P380263
Eng	2.56	9.6	6.4	7.1E-03	NM_001146350	A_55_P2040936
Grin3a	2.03	7.5	6.4	7.2E-03	NM_001033351	A_55_P1980471
Paqr5	2.31	6.5	6.3	7.2E-03	NM_028748	A_51_P258768
Gm10601	0.44	6.4	-6.3	7.2E-03	XM_001478493	A_55_P2102998
Prom1	2.10	7.8	6.3	7.3E-03	NM_008935	A_52_P402786
LOC434513	4.42	5.0	6.3	7.3E-03	XM_486348	A_55_P2173210
Cyyr1	2.84	7.2	6.3	7.3E-03	NM_144853	A_55_P2129000
Sema3c	3.47	9.5	6.3	7.4E-03	NM_013657	A_55_P2143025
Ncapg2	0.42	5.8	-6.3	7.4E-03	NM_133762	A_51_P424810
LOC100045191	2.25	10.9	6.2	7.4E-03	XM_001473825	A_55_P2022201
Nkx6-2	0.46	7.2	-6.2	7.4E-03	NM_183248	A_55_P1997569
Tspan13	2.67	11.2	6.2	7.4E-03	NM_025359	A_51_P256246
Kdr	2.66	9.6	6.2	7.4E-03	NM_010612	A_51_P316553

FC = fold change (>1 = expression upregulated, <1 = expression downregulated), Int = Mean $\log_2$ intensity, t = t-test statistic, FDR = False Discovery Rate controlled p-value

Table 4: Top 50 most significantly regulated genes with more than 2 fold up or down change in VIM-GFAPko microglia compared to GFAPko microglia.

Gene Symbol	FC	Int	t	FDR	GenBank accession	Agilent Probe Name
Vim	0.01	9.52	-31.71	2.8E-09	NM_011701	A_51_P392687
Fam193b	2.46	11.19	10.10	1.2E-03	NM_145382	A_51_P407879
Olfr122	0.15	7.32	-9.76	1.2E-03	NM_146288	A_55_P2097814
NA	0.20	8.54	-9.90	1.2E-03	XM_001472454	A_55_P2142724
Pisd	2.52	13.44	10.02	1.2E-03	NM_177298	A_55_P2183735
Hap1	0.17	10.28	-9.38	1.3E-03	NM_010404	A_51_P516728
LOC432842	0.28	6.39	-9.49	1.3E-03	AK163540	A_55_P2162229
Spint2	0.26	10.12	-9.14	1.6E-03	NM_001082548	A_55_P2111713
1700022A21Rik	0.25	7.77	-8.74	2.3E-03	NR_003953	A_51_P240723
NA	0.36	5.17	-8.25	3.9E-03	ENSMUST00000070876	A_55_P2139318
E130119H09Rik	0.37	7.39	-8.03	4.6E-03	AK021396	A_51_P441745
Firre	2.40	8.58	7.93	4.6E-03	NR_026976	A_52_P223508
Pou3f3os	0.35	7.29	-7.95	4.6E-03	NR_027826	A_52_P385736
Lbx1	0.47	5.87	-7.86	4.7E-03	NM_010691	A_55_P2051741

Dmxl2	2.05	6.62	7.69	5.6E-03	NM_172771	A_55_P2179939
Oog2	0.37	7.29	-7.64	5.6E-03	NM_198661	A_55_P2023163
Ttc8	4.21	7.71	7.59	5.7E-03	NM_029553	A_51_P507899
Rprd1b	0.42	10.12	-7.25	5.7E-03	NM_027434	A_51_P229633
Tpgs1	0.41	10.22	-7.42	5.7E-03	NM_148934	A_52_P562593
Mroh2a	0.35	7.47	-7.27	5.7E-03	XM_001475729	A_52_P957031
NA	0.35	7.64	-7.47	5.7E-03	XM_001474573	A_55_P1994173
Pgs1	1.76	13.49	7.17	5.7E-03	NM_133757	A_55_P2002150
Barx2	0.17	7.77	-7.32	5.7E-03	NM_013800	A_55_P2030046
Lrrc45	1.97	12.12	7.44	5.7E-03	NM_153545	A_55_P2040815
Smc5	0.49	10.47	-7.27	5.7E-03	NM_153808	A_55_P2062632
NA	0.27	5.77	-7.16	5.7E-03	XM_987199	A_55_P2088075
Fxyd1	0.20	10.43	-7.30	5.7E-03	NM_052992	A_55_P2137937
Gm9958	0.28	5.92	-7.29	5.7E-03	BQ950205	A_55_P2386742
NA	0.20	10.05	-7.18	5.7E-03	ENSMUST00000101310	A_65_P20683
Agt	0.26	7.00	-7.41	5.7E-03	NM_007428	A_66_P112356
Pisd-ps3	4.24	10.22	7.21	5.7E-03	NR_003518	A_66_P122158
Erbb2	0.32	6.96	-7.12	5.9E-03	NM_001003817	A_52_P49250
NA	0.24	9.78	-7.09	5.9E-03	XM_909126	A_55_P2041910
Nphp4	0.33	7.95	-7.08	5.9E-03	NM_153424	A_55_P2137586
Card14	0.46	7.00	-6.88	5.9E-03	NM_130886	A_51_P137611
Arhgap4	1.78	12.92	6.83	5.9E-03	NM_138630	A_51_P339822
Gm2744	4.07	13.31	6.97	5.9E-03	XM_001475453	A_52_P135873
Olfr1419	0.52	6.51	-6.83	5.9E-03	NM_001011775	A_52_P232438
Troap	0.25	6.12	-6.74	5.9E-03	NM_030159	A_52_P633714
Lhb	0.29	8.90	-6.86	5.9E-03	NM_008497	A_55_P1953991
NA	0.24	6.41	-6.76	5.9E-03	XM_917005	A_55_P1957932
Teddm1	0.52	5.65	-7.00	5.9E-03	NM_178244	A_55_P1970335
Etnk2	0.45	6.06	-6.91	5.9E-03	NM_175443	A_55_P1979019
4932412D23Rik	0.36	9.05	-6.79	5.9E-03	ENSMUST00000099759	A_55_P1990810
Nox1	0.21	7.52	-6.78	5.9E-03	NM_172203	A_55_P1997906
Hhat	0.28	8.30	-6.76	5.9E-03	NM_144881	A_55_P2015143
Hsp90aa1	2.40	14.52	6.81	5.9E-03	NM_010480	A_55_P2057946
Zfp352	0.37	10.22	-6.73	5.9E-03	NM_153102	A_55_P2060343
NA	2.19	7.30	6.73	5.9E-03	ENSMUST00000069459	A_55_P2085727
Dnmt3b	1.86	8.40	6.80	5.9E-03	NM_001003961	A_55_P2130535

t = t-test statistic, fold change: >1 = expression upregulated, <1 = expression downregulated, FDR adj.P.Val = False Discovery Rate controlled p-value, NA = Not Available

Table 5: Top 50 most significantly regulated genes with more than 2 fold up or down change in VIM-GFAPko astrocytes compared to WT astrocytes.

Gene Symbol	FC	Int	t	FDR	GenBank accession	Agilent Probe Name
Gdpd3	0.10	6.5	-20.3	2.9E-07	NM_024228	A_51_P426875
Fzd2	0.10	7.6	-17.0	1.6E-06	NM_020510	A_52_P129428
Thbs4	7.45	9.9	16.3	1.7E-06	NM_011582	A_52_P401504
Frrs1l	4.14	7.8	16.0	1.7E-06	NM_001142965	A_55_P2092252
Gm3892	0.10	7.3	-15.5	2.1E-06	XM_001478587	A_55_P1953273
Gm13298	0.11	7.8	-15.1	2.5E-06	NM_001085530	A_55_P2018330
NAP000581-003	0.38	9.4	-13.7	6.8E-06	NAP000581-003	A_55_P1959541
Dclk3	0.11	6.8	-13.5	6.8E-06	NM_172928	A_51_P419637
9630041G16Rik	5.95	8.7	13.5	6.8E-06	AK079356	A_55_P2330435
Ybx1	0.28	8.0	-13.0	9.5E-06	M60419	A_55_P2131379
AI594671	0.03	4.8	-13.0	9.5E-06	AA711038	A_55_P2295856
Gfap	0.01	5.3	-12.3	1.5E-05	NM_001131020	A_52_P52303
Krt85	0.13	5.8	-12.3	1.5E-05	NM_016879	A_55_P1999364
A_55_P1990066	0.19	6.2	-12.2	1.6E-05	A_55_P1990066	A_55_P1990066
Hapln3	0.29	9.7	-12.0	1.7E-05	ENSMUST00000032827	A_55_P2093553
Gm13298	0.07	7.5	-12.0	1.8E-05	NM_001085530	A_55_P2033480
4933409K07Rik	0.18	7.4	-11.7	2.3E-05	NR_033123	A_55_P2119552
Olfr1307	2.37	7.0	11.6	2.3E-05	NM_001011787	A_51_P362554
Ccdc24	0.20	8.2	-11.5	2.5E-05	ENSMUST00000106422	A_55_P2177697
Tmem181a	0.34	8.6	-11.4	2.7E-05	NM_001033178	A_55_P2021099
Gm8909	0.22	6.2	-11.3	2.7E-05	NM_001081032	A_55_P1956160
Hapln3	0.31	9.0	-11.3	2.8E-05	NM_178255	A_51_P244213
Psmc3ip	0.29	6.7	-11.2	3.0E-05	NM_008949	A_52_P238044
5430410E06Rik	0.25	6.1	-11.0	3.5E-05	XM_001475205	A_55_P1981461
C2	0.26	8.7	-10.9	3.5E-05	NM_013484	A_51_P497985
Srprb	0.25	8.3	-10.9	3.5E-05	NM_009275	A_52_P131559
Frrs1l	4.03	6.7	10.7	4.4E-05	NM_001142965	A_51_P307559
A230065H16Rik	0.40	7.1	-10.6	4.4E-05	NM_001101503	A_55_P2076916
Ccl21a	0.06	8.3	-10.6	4.4E-05	NM_011124	A_55_P2024625
Gm9495	3.04	10.9	10.5	5.0E-05	XM_001475988	A_55_P2054098
Gm2490	0.13	6.5	-10.4	5.1E-05	XM_001473759	A_55_P2096023
LOC100046136	0.38	8.7	-10.4	5.3E-05	XM_001476489	A_55_P2143119
Frrs1l	2.95	6.6	10.3	5.3E-05	NM_001142965	A_55_P2092251
5430410E06Rik	0.20	5.3	-10.3	5.3E-05	XM_001475205	A_55_P1981464
Clic6	0.27	7.6	-10.3	5.4E-05	NM_172469	A_52_P447284

5

XM_001478398	2.99	7.3	10.1	6.6E-05	XM_001478398	A_55_P2031848
LOC547349	0.30	5.4	-10.1	6.6E-05	NM_001025208	A_55_P1966659
LOC100048713	0.48	8.8	-10.0	6.7E-05	XM_001481016	A_55_P1986225
8030453O22Rik	0.24	6.8	-10.0	6.8E-05	AK047163	A_55_P2383897
2610524H06Rik	0.47	7.9	-10.0	6.8E-05	NM_181075	A_65_P09285
Nptx2	0.10	6.1	-9.9	6.8E-05	NM_016789	A_52_P187058
Gfap	0.16	6.0	-9.8	7.7E-05	NM_010277	A_55_P2157250
Atp6ap1l	0.37	6.8	-9.8	7.7E-05	NM_001145879	A_55_P2016139
Trim12a	2.38	7.1	9.7	8.5E-05	NM_023835	A_55_P2064659
Pdgfd	2.79	7.6	9.7	8.5E-05	NM_027924	A_52_P264790
Metap1d	2.04	9.8	9.6	9.7E-05	NM_025633	A_51_P236469
Rnf165	0.43	7.4	-9.5	9.7E-05	NM_001164504	A_55_P2117664
Fam163a	2.23	11.2	9.5	9.7E-05	NM_177838	A_55_P2027421
Zfp949	0.38	8.1	-9.5	9.7E-05	NM_001142943	A_51_P513244
Igsf1	0.28	11.5	-9.4	1.1E-04	NM_177591	A_55_P2059864

Note the absence of Vim in this list, due to our top 50 cutoff, with vimentin at position 66 using our criteria. FC = fold change (>1 = expression upregulated, <1 = expression downregulated), Int = Mean $\log_2$ intensity, t = t-test statistic, FDR = False Discovery Rate controlled p-value

Table 6: Top 50 most significantly regulated genes with more than 2 fold up or down change in VIM-GFAPko microglia compared to WT microglia.

Gene Symbol	FC	Int	t	FDR	GenBank accession	Agilent Probe Name
Vim	0.01	9.52	-29.24	7.8E-09	NM_011701	A_51_P392687
Gdpd3	0.03	8.94	-26.45	1.4E-08	NM_024228	A_51_P426875
Gm8909	0.04	7.62	-20.46	2.4E-07	NM_001081032	A_55_P1956160
Qpct	0.02	8.95	-19.52	3.3E-07	NM_027455	A_55_P2140118
Ccdc80	0.09	7.46	-16.16	2.8E-06	NM_026439	A_55_P2169586
Ybx1	0.20	8.38	-12.95	3.3E-05	M60419	A_55_P2131379
Nccrp1	0.20	8.54	-12.82	3.3E-05	NM_001081115	A_66_P106231
Rasd2	4.26	8.71	12.09	5.4E-05	NM_029182	A_55_P2107155
NA	4.20	9.37	12.06	5.4E-05	XM_001474432	A_55_P2148935
Dcc	4.52	11.94	11.80	6.3E-05	NM_007831	A_55_P1961761
Napa	3.17	10.31	11.42	7.8E-05	NM_025898	A_51_P246816
5830444B04Rik	4.81	8.60	11.49	7.8E-05	AK030886	A_55_P2206605
Ciart	3.86	7.66	11.24	8.7E-05	NM_001033302	A_52_P63343
Gm2008	3.68	13.78	10.89	1.2E-04	XM_001472097	A_55_P2092831

	FC	Int	t	FDR		
NA	0.22	5.06	-10.83	1.2E-04	XM_485041	A_66_P129469
Fam211a	0.31	11.66	-11.50	1.2E-04	NM_198861	A_55_P2149896
Impact	4.13	12.73	10.60	1.3E-04	NM_008378	A_51_P483220
Dennd4a	5.03	11.46	10.59	1.3E-04	ENSMUST00000089035	A_65_P03364
5430410E06Rik	0.25	7.41	-10.42	1.4E-04	XM_001475205	A_55_P1981461
Hsp90aa1	3.75	14.52	10.30	1.6E-04	NM_010480	A_55_P2057946
5430410E06Rik	0.23	6.93	-10.19	1.7E-04	XM_001475205	A_55_P1981464
NA	4.24	9.94	9.99	2.0E-04	XM_001477233	A_55_P1962699
Prdm12	2.94	6.09	9.71	2.6E-04	NM_001123362	A_55_P1980134
Optn	3.83	7.49	9.72	2.6E-04	NM_181848	A_66_P119801
Rnf217	0.16	4.88	-9.64	2.7E-04	NM_001146349	A_52_P3845
Actn2	3.05	5.91	9.57	2.8E-04	ENSMUST00000110616	A_55_P2163438
Gp9	0.42	11.24	-9.52	2.9E-04	NM_018762	A_51_P153995
NA	2.19	8.68	9.35	3.4E-04	NM_001113806	A_55_P2157551
Glrp1	0.41	10.10	-9.30	3.5E-04	NM_008132	A_55_P2042743
A630081D01Rik	4.44	10.78	9.27	3.5E-04	AK042310	A_55_P2249556
Gm14391	2.25	10.68	9.24	3.5E-04	NM_001099308	A_55_P1956807
Mapkapk3	2.32	11.07	9.08	4.1E-04	NM_178907	A_55_P2009762
Rcan2	0.31	7.12	-8.90	4.7E-04	NM_207649	A_55_P1961736
NA	0.19	6.98	-8.93	4.7E-04	A_55_P1990066	A_55_P1990066
H2-M2	4.15	8.34	8.92	4.7E-04	NM_008204	A_55_P2135064
Hist1h1d	0.19	6.22	-8.88	4.7E-04	NM_145713	A_55_P2183508
Slc25a33	3.07	11.04	8.73	5.0E-04	NM_027460	A_51_P156438
Dpys	0.37	6.29	-8.72	5.0E-04	NM_001164466	A_51_P244950
Ppib	0.46	13.27	-8.74	5.0E-04	NM_011149	A_51_P327828
Hddc3	0.26	7.06	-8.80	5.0E-04	NM_026812	A_52_P521882
Gm3716	0.27	6.19	-8.80	5.0E-04	XM_001478025	A_55_P1964955
Depdc5	0.41	6.35	-8.78	5.0E-04	NM_177786	A_55_P1984381
Sphk1	2.79	8.02	8.66	5.1E-04	NM_025367	A_51_P501248
Dcaf12l2	2.42	14.66	8.63	5.1E-04	NM_175539	A_55_P1959973
Slc20a1	2.18	12.18	8.68	5.1E-04	NM_015747	A_55_P2115582
Zfp931	2.21	9.09	8.64	5.1E-04	NM_001162922	A_55_P2173073
Hes1	3.64	9.74	8.43	6.3E-04	NM_008235	A_55_P2046245
NA	0.32	5.47	-8.45	6.3E-04	ENSMUST00000114941	A_55_P2131190
Tagln	0.23	10.49	-8.40	6.5E-04	NM_011526	A_51_P450527
Neurl1a	0.42	13.59	-8.33	7.0E-04	NM_021360	A_55_P2023692

FC = fold change (>1 = expression upregulated, <1 = expression downregulated), Int = Mean log$_2$ intensity, t = t-test statistic, FDR = False Discovery Rate controlled p-value, NA = Not Available

5

Table 7: Top 10 Gene Ontology terms per domain overrepresented by GFAPko astrocytes compared to WT astrocytes.

Domain	GO.ID	Term	# Annot	# Sig	p-val
BP	GO:0016045	detection of bacterium	7	2	2.20E-03
BP	GO:0010575	positive regulation vascular endothelial growth factor production	9	2	3.80E-03
BP	GO:0001774	microglial cell activation	10	2	4.70E-03
BP	GO:0060644	mammary gland epithelial cell differentiation	11	2	5.70E-03
BP	GO:0050919	negative chemotaxis	17	2	1.35E-02
BP	GO:0051781	positive regulation of cell division	49	3	1.49E-02
BP	GO:0045429	positive regulation of nitric oxide biosynthetic process	20	2	1.85E-02
BP	GO:0016485	protein processing	791	7	1.94E-02
BP	GO:0045907	positive regulation of vasoconstriction	21	2	2.04E-02
BP	GO:0045879	negative regulation of smoothened signaling pathway	22	2	2.22E-02
CC	GO:0072562	blood microparticle	59	6	4.50E-05
CC	GO:0005881	cytoplasmic microtubule	47	4	1.70E-03
CC	GO:0071944	cell periphery	2595	41	3.40E-03
CC	GO:0005576	extracellular region	2075	36	1.01E-02
CC	GO:0005578	proteinaceous extracellular matrix	202	9	1.83E-02
CC	GO:0016021	integral component of membrane	3105	47	2.20E-02
CC	GO:0043233	organelle lumen	1379	6	2.35E-02
CC	GO:0034707	chloride channel complex	25	2	3.05E-02
CC	GO:0009925	basal plasma membrane	27	2	3.52E-02
CC	GO:0005604	basement membrane	66	3	3.60E-02
MF	GO:0005518	collagen binding	33	3	5.40E-03
MF	GO:0005247	voltage-gated chloride channel activity	11	2	6.00E-03
MF	GO:0004930	G-protein coupled receptor activity	324	13	6.90E-03
MF	GO:0005540	hyaluronic acid binding	15	2	1.12E-02
MF	GO:0008201	heparin binding	82	4	1.20E-02
MF	GO:0043236	laminin binding	16	2	1.27E-02
MF	GO:0005178	integrin binding	53	3	1.97E-02
MF	GO:0017046	peptide hormone binding	25	2	2.97E-02
MF	GO:0042605	peptide antigen binding	26	2	3.20E-02
MF	GO:0015179	L-amino acid transmembrane transporter activity	27	2	3.43E-02

 # Annot = Total microarray probes annotated to this term; # Sig = number of probes detecting significant change in this term; p-val = parent-child weighted p-value of Fisher's exact test for overrepresentation; GO.ID = Gene Ontology Identifier; BP = Biological Process; CC = Cellular Component; MF = Molecular Function.

Table 8: Top 10 Gene Ontology terms per domain overrepresented by GFAPko microglia compared to WT microglia.

Domain	GO.ID	Term	# Annot	# Sig	p-val
BP	GO:0007186	G-protein coupled receptor signaling pathway	668	81	2.60E-10
BP	GO:0050911	detection of chemical stimulus involved in sensory perception of smell	224	29	2.20E-05
BP	GO:2000288	positive regulation of myoblast proliferation	6	4	1.30E-04
BP	GO:0001886	endothelial cell morphogenesis	7	4	3.00E-04
BP	GO:0045672	positive regulation of osteoclast differentiation	21	6	8.00E-04
BP	GO:0032753	positive regulation of interleukin-4 production	9	4	9.90E-04
BP	GO:0060347	heart trabecula formation	10	4	1.57E-03
BP	GO:0008284	positive regulation of cell proliferation	518	57	2.00E-03
BP	GO:0007200	phospholipase C-activating G-protein coupled receptor signaling pathway	33	7	2.02E-03
BP	GO:0090303	positive regulation of wound healing	11	4	2.36E-03
CC	GO:0016021	integral component of membrane	3323	244	3.30E-05
CC	GO:0009897	external side of plasma membrane	190	24	1.80E-04
CC	GO:0005615	extracellular space	624	54	8.10E-04
CC	GO:0005886	plasma membrane	2725	209	2.19E-03
CC	GO:0045095	keratin filament	20	5	4.33E-03
CC	GO:0005887	integral component of plasma membrane	398	40	5.31E-03
CC	GO:0005576	extracellular region	2164	135	7.82E-03
CC	GO:0009986	cell surface	414	44	2.47E-02
CC	GO:0048471	perinuclear region of cytoplasm	397	32	2.73E-02
CC	GO:0034707	chloride channel complex	21	4	2.81E-02
MF	GO:0004930	G-protein coupled receptor activity	465	69	4.50E-10
MF	GO:0004984	olfactory receptor activity	225	29	2.00E-05
MF	GO:0005179	hormone activity	42	9	2.80E-04
MF	GO:0005550	pheromone binding	16	5	1.37E-03
MF	GO:0008083	growth factor activity	80	12	1.48E-03
MF	GO:0016670	oxidoreductase activity, acting on a sulphur group of donors, oxygen as acceptor	6	3	3.02E-03
MF	GO:0016503	pheromone receptor activity	20	5	4.04E-03
MF	GO:0005200	structural constituent of cytoskeleton	34	6	1.02E-02
MF	GO:0008395	steroid hydroxylase activity	10	3	1.53E-02
MF	GO:0016705	oxidoreductase activity, acting on paired donors, with incorporation or reduction of molecular oxygen	116	11	1.53E-02

Annot = Total microarray probes annotated to this term; # Sig = number of probes detecting significant change in this term; p-val = parent-child weighted p-value of Fisher's exact test for overrepresentation; GO.ID = Gene Ontology Identifier; BP = Biological Process; CC = Cellular Component; MF = Molecular Function.

5

Table 9: Top 10 Gene Ontology terms per domain overrepresented by VIM-GFAPko astrocytes compared to GFAPko astrocytes.

Domain	GO.ID	Term	# Annot	# Sig	p-val
BP	GO:0045766	positive regulation of angiogenesis	75	12	2.70E-08
BP	GO:0001570	vasculogenesis	70	12	6.10E-07
BP	GO:0001569	patterning of blood vessels	36	7	2.50E-06
BP	GO:0014045	establishment of endothelial blood-brain barrier	5	3	5.20E-05
BP	GO:0006855	drug transmembrane transport	15	4	1.10E-04
BP	GO:0001525	Angiogenesis	283	29	1.10E-04
BP	GO:0038084	vascular endothelial growth factor signaling pathway	17	6	1.70E-04
BP	GO:0001701	in utero embryonic development	310	16	4.00E-04
BP	GO:0043129	surfactant homeostasis	9	3	4.10E-04
BP	GO:0048863	stem cell differentiation	219	10	5.00E-04
CC	GO:0016324	apical plasma membrane	151	12	1.70E-05
CC	GO:0005615	extracellular space	574	31	1.90E-05
CC	GO:0005886	plasma membrane	2534	82	6.40E-05
CC	GO:0072562	blood microparticle	59	7	8.30E-05
CC	GO:0046581	intercellular canaliculus	6	3	1.10E-04
CC	GO:0030173	integral component of Golgi membrane	30	5	1.70E-04
CC	GO:0009897	external side of plasma membrane	149	10	3.40E-04
CC	GO:0009986	cell surface	367	22	4.20E-04
CC	GO:0016021	integral component of membrane	3101	83	1.04E-03
CC	GO:0044447	axoneme part	8	2	8.29E-03
MF	GO:0008559	xenobiotic-transporting ATPase activity	5	3	4.90E-05
MF	GO:0045296	cadherin binding	26	5	7.20E-05
MF	GO:0008009	chemokine activity	14	4	7.50E-05
MF	GO:0005021	vascular endothelial growth factor-activity	6	3	9.70E-05
MF	GO:0050431	transforming growth factor beta binding	12	3	9.90E-04
MF	GO:0005539	glycosaminoglycan binding	111	11	1.48E-03
MF	GO:0008373	sialyltransferase activity	16	3	2.40E-03
MF	GO:0005178	integrin binding	55	5	2.52E-03
MF	GO:0008201	heparin binding	81	6	2.73E-03
MF	GO:0001846	opsonin binding	5	2	2.86E-03

Annot = Total microarray probes annotated to this term; # Sig = number of probes detecting significant change in this term; p-val = parent-child weighted p-value of Fisher's exact test for overrepresentation; GO.ID = Gene Ontology Identifier; BP = Biological Process; CC = Cellular Component; MF = Molecular Function.

Table 10: Top 10 Gene Ontology terms per domain overrepresented by VIM-GFAPko microglia compared to GFAPko microglia.

Domain	GO.ID	Term	# Annot	# Sig	p-val
BP	GO:0007186	G-protein coupled receptor signaling pathway	670	48	1.50E-04
BP	GO:0090179	planar cell polarity pathway involved in neural tube closure	10	4	2.30E-04
BP	GO:0043267	negative regulation of potassium ion transport	13	4	7.40E-04
BP	GO:0006936	muscle contraction	139	11	9.80E-04
BP	GO:0048318	axial mesoderm development	7	3	1.23E-03
BP	GO:0018119	peptidyl-cysteine S-nitrosylation	7	3	1.23E-03
BP	GO:0048664	neuron fate determination	7	3	1.23E-03
BP	GO:0030534	adult behavior	94	9	1.32E-03
BP	GO:0007202	activation of phospholipase C activity	8	3	1.92E-03
BP	GO:0048712	negative regulation of astrocyte differentiation	10	3	3.91E-03
CC	GO:0005922	connexon complex	8	5	2.30E-06
CC	GO:0005882	intermediate filament	75	11	4.40E-04
CC	GO:0005929	cilium	257	13	1.64E-03
CC	GO:0030018	Z disc	64	7	5.94E-03
CC	GO:0030673	axolemma	12	3	6.88E-03
CC	GO:0000786	nucleosome	39	5	9.98E-03
CC	GO:0019005	SCF ubiquitin ligase complex	26	4	1.10E-02
CC	GO:0016324	apical plasma membrane	149	11	1.31E-02
CC	GO:0016235	aggresome	16	3	1.58E-02
CC	GO:0005938	cell cortex	150	10	2.13E-02
MF	GO:0004930	G-protein coupled receptor activity	467	38	1.80E-04
MF	GO:0005243	gap junction channel activity	7	3	1.25E-03
MF	GO:0020037	heme binding	70	8	2.59E-03
MF	GO:0004984	olfactory receptor activity	225	16	4.64E-03
MF	GO:0043395	heparan sulfate proteoglycan binding	13	3	8.80E-03
MF	GO:0097110	scaffold protein binding	25	4	9.65E-03
MF	GO:0043121	neurotrophin binding	5	2	1.09E-02
MF	GO:0005179	hormone activity	41	5	1.24E-02
MF	GO:0004540	ribonuclease activity	66	5	1.59E-02
MF	GO:0016615	malate dehydrogenase activity	6	2	1.60E-02

Annot = Total microarray probes annotated to this term; # Sig = number of probes detecting significant change in this term; p-val = parent-child weighted p-value of Fisher's exact test for overrepresentation; GO.ID = Gene Ontology Identifier; BP = Biological Process; CC = Cellular Component; MF = Molecular Function.

5

Table 11: Top 10 Gene Ontology terms per domain overrepresented by VIM-GFAPko astrocytes compared to WT astrocytes.

Domain	GO.ID	Term	# Annot	# Sig	p-val
BP	GO:0051781	positive regulation of cell division	50	7	4.00E-04
BP	GO:0016525	negative regulation of angiogenesis	44	7	9.00E-04
BP	GO:0050901	leukocyte tethering or rolling	7	3	9.60E-04
BP	GO:0010043	response to zinc ion	17	4	1.60E-03
BP	GO:0072203	cell proliferation involved in metanephros development	9	3	2.20E-03
BP	GO:0090023	positive regulation of neutrophil chemotaxis	9	3	2.20E-03
BP	GO:0042416	dopamine biosynthetic process	10	3	3.06E-03
BP	GO:0045907	positive regulation of vasoconstriction	22	4	4.36E-03
BP	GO:0014002	astrocyte development	12	3	5.36E-03
BP	GO:0034114	regulation of heterotypic cell-cell adhesion	9	3	5.56E-03
CC	GO:0072562	blood microparticle	59	8	4.70E-04
CC	GO:0009986	cell surface	374	24	1.62E-03
CC	GO:0005615	extracellular space	577	37	1.69E-03
CC	GO:0016021	integral component of membrane	3122	126	3.36E-03
CC	GO:0005868	cytoplasmic dynein complex	16	3	1.26E-02
CC	GO:0005578	proteinaceous extracellular matrix	205	16	2.74E-02
CC	GO:0005576	extracellular region	2090	88	2.84E-02
CC	GO:0005915	zonula adherens	9	2	3.04E-02
CC	GO:0031528	microvillus membrane	9	2	3.04E-02
CC	GO:0005887	integral component of plasma membrane	387	21	3.71E-02
MF	GO:0008009	chemokine activity	16	5	8.60E-05
MF	GO:0031994	insulin-like growth factor I binding	7	3	9.00E-04
MF	GO:0005247	voltage-gated chloride channel activity	12	3	5.10E-03
MF	GO:0045296	cadherin binding	24	4	5.60E-03
MF	GO:0001968	fibronectin binding	14	3	8.00E-03
MF	GO:0042802	identical protein binding	856	39	8.50E-03
MF	GO:0004060	arylamine N-acetyltransferase activity	5	2	8.80E-03
MF	GO:0003690	double-stranded DNA binding	101	8	1.21E-02
MF	GO:0015643	toxic substance binding	6	2	1.29E-02
MF	GO:0008889	glycerophosphodiester phosphodiesterase activity	6	2	1.29E-02

Annot = Total microarray probes annotated to this term; # Sig = number of probes detecting significant change in this term; p-val = parent-child weighted p-value of Fisher's exact test for overrepresentation; GO.ID = Gene Ontology Identifier; BP = Biological Process; CC = Cellular Component; MF = Molecular Function.

Table 12: Top 10 Gene Ontology terms per domain overrepresented by VIM-GFAPko microglia compared to WT microglia.

Domain	GO.ID	Term	# Annot	# Sig	p-val
BP	GO:0090303	positive regulation of wound healing	11	4	3.40E-04
BP	GO:0010628	positive regulation of gene expression	918	42	3.80E-04
BP	GO:0051491	positive regulation of filopodium assembly	20	5	4.30E-04
BP	GO:0016584	nucleosome positioning	6	3	7.00E-04
BP	GO:0003143	embryonic heart tube morphogenesis	42	4	7.00E-04
BP	GO:0008284	positive regulation of cell proliferation	510	43	7.30E-04
BP	GO:0008217	regulation of blood pressure	104	12	1.47E-03
BP	GO:0042510	regulation of tyrosine phosphorylation of Stat1 protein	8	3	1.86E-03
BP	GO:2000188	regulation of cholesterol homeostasis	8	3	1.86E-03
BP	GO:0001525	angiogenesis	291	23	2.25E-03
CC	GO:0005615	extracellular space	621	40	1.30E-04
CC	GO:0030018	Z disc	65	9	2.90E-04
CC	GO:0005887	integral component of plasma membrane	393	30	6.80E-04
CC	GO:0000786	nucleosome	39	6	1.71E-03
CC	GO:0009897	external side of plasma membrane	189	16	2.26E-03
CC	GO:0031012	extracellular matrix	227	22	2.27E-03
CC	GO:0005614	interstitial matrix	9	3	2.67E-03
CC	GO:0033270	paranode region of axon	10	3	3.72E-03
CC	GO:0005604	basement membrane	60	8	4.92E-03
CC	GO:0005865	striated muscle thin filament	11	3	4.98E-03
MF	GO:0008083	growth factor activity	79	10	2.50E-04
MF	GO:0015026	coreceptor activity	17	4	1.94E-03
MF	GO:0008201	heparin binding	86	9	2.00E-03
MF	GO:0005200	structural constituent of cytoskeleton	33	5	4.13E-03
MF	GO:0004519	endonuclease activity	93	7	7.18E-03
MF	GO:0043565	sequence-specific DNA binding	461	28	7.21E-03
MF	GO:0015185	gamma-aminobutyric acid transmembrane transporter activity	5	2	1.01E-02
MF	GO:0030506	ankyrin binding	15	3	1.19E-02
MF	GO:0005283	sodium:amino acid symporter activity	6	2	1.48E-02
MF	GO:0005114	type II transforming growth factor beta receptor binding	6	2	1.48E-02

Annot = Total microarray probes annotated to this term; # Sig = number of probes detecting significant change in this term; p-val = parent-child weighted p-value of Fisher's exact test for overrepresentation; GO.ID = Gene Ontology Identifier; BP = Biological Process; CC = Cellular Component; MF = Molecular Function.

5

although less terms related to the proteinaceous extracellular matrix (ECM) were present (mainly "sialyltransferase activity"). The term "extracellular space" (everything extracellular except the ECM) or extracellular matrix-interacting related terms were present ("plasma membrane", "cells surface", "glycosaminoglycan binding", "heparin binding"). In the microglia, similar to the GFAPko to WT comparison, the terms of "G-protein coupled receptor signalling pathway" and "G-protein coupled receptor activity" were overrepresented, and the most significantly overrepresented term was "connexon complex" (Gja4, Gjb6, Gjb1, Gjc3, Gjc2). In these microglia, also the term "intermediate filament" was overrepresented (Bfsp2, Vim, Krtap5-1, Gm11567, Krt16, Ina, Fbf1, Krtap19-5, Krtap1-4, Krtap19-4, Krtap5-5).

WT versus VIM-GFAPko GO-analysis

Comparing the VIM-GFAPko with the WT astrocytes (Table 11) again showed a clear effect on extracellular environment, including the term "proteinaceous extracellular matrix". The most significantly overrepresented term in the VIM-GFAPko astrocytes was "chemokine activity" (Pdgfd, Thbs4, Fgf1, Pdgfb, Ybx1, Gkn1, Igf1r). In the VIM-GFAPko microglia, the most significant GO-terms were "extracellular space" (40 DEGs) and "growth factor activity" (Tgfb3, Cxcl12, Hbegf, Osgin1, Il34, Il12b, Gdf15, Csf1, Ptn, Gkn1). Again also "integral component of plasma membrane" and "angiogenesis" were overrepresented.

Highlight: GFAPko specific GPCRs, olfactory and vomeronasal receptor expression

We looked more specifically into a peculiar expression pattern found in the overrepresented GO-terms in the microglia. In the GFAPko vs WT as well as the VIM-GFAPko vs GFAPko, but not the VIM-GFAPko vs WT comparisons, the cluster of G-protein coupled receptor (GPCR) pathway was overrepresented with 81 DEGs in the GFAPko vs WT and 48 DEGs in the VIM-GFAPko vs GFAPko. Interestingly, among the 81 DEGs of the GFAPko vs WT there were 30 olfactory receptors and 12 vomeronasal receptors. For the VIM-GFAPko vs GFAPko this amounts up to 16 olfactory receptors and 7 vomeronasal receptors. Since the G-protein coupled receptor pathway cluster is not overrepresented in the VIM-GFAPko vs WT, this appears to be a GFAPko-specific effect, no longer found when Vim is additionally knocked out. We plotted the expression pattern of these DEGs (Fig. 4A) and the other genes in the GPCR terms (Fig. 4B). This showed that almost all olfactory and vomeronasal receptors in the GPCR terms were upregulated in the GFAPko yet the expression was not changed in the in the VIM-GFAPko vs WT. For the non-olfactory and non-vomeronasal GPCRs, a similar pattern was present, albeit more dispersed

(Fig. 4B).

Cluster analyses showed several patterns of gene expression

This pattern of DEGs - upregulated in the GFAPko and no change in the VIM-GFAPko - could be a more general pattern in the two models. To extract these patterns, all identified DEGs in astrocytes and microglia were analysed by k-means cluster analysis across the three genotypes. For astrocytes this amounted to 893 clustered DEGs. We empirically determined the optimal number of clusters required to extract the different patterns of expression to be 9 clusters for the astrocytes (Fig. 5). For microglia 1882 DEGs were clustered (Fig. 6), that optimally clustered into the different expression patterns when assigned to 12 clusters. Still, 6 of the main clusters (cluster 1, 2, 4, 5, 7 & 12) showed a pattern of upregulation or downregulation by GFAPko, which is partly or completely compensated by VIM-GFAPko, as seen in the olfactory and vomeronasal receptors (Fig. 4A), indicating the olfactory receptor pattern is indeed followed by multiple genes.

To see if there are specific gene groups that are sensitive to a "total IF dose" in astrocytes, we analysed the clusters that have a cumulative change in response to the deletion of single and both IFs (Fig. 5, clusters 6 and 8, total 279 genes) for GO overrepresentation. GO analysis on both these clusters resulted in overrepresentation of "signalling" and "adhesion related"
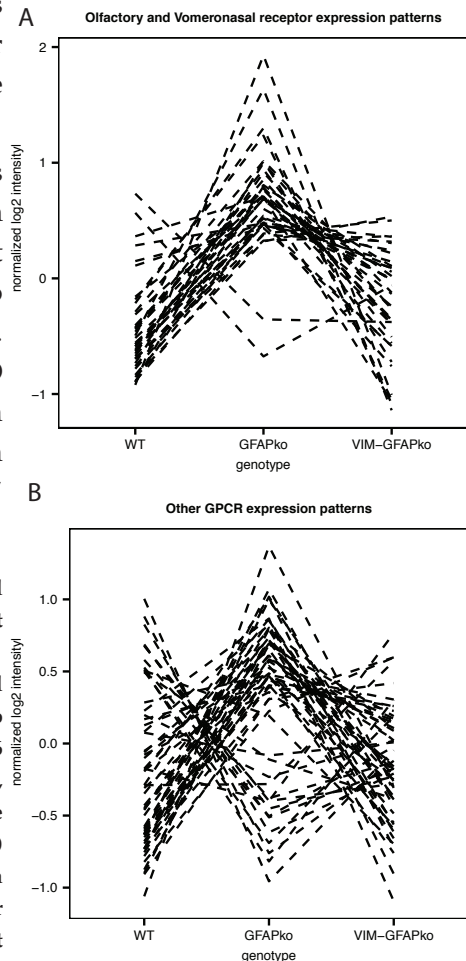
Figure 4. Expression pattern across microglial genotypes for olfactory-related receptors in contrast to general G-protein coupled receptors
Expression patterns for DEGs from the microglial GFAPko vs WT and VIM-GFAPko vs GFAPko contrasts annotated to the GO-term GO:007186 "G-protein coupled receptor signalling pathway", comprising 81 DEG annotations, were split in the olfactory and vomeronasal receptor family (A) and all other DEGs in this term (B). Expression intensities were normalized to log$_2$ intensity = 0 for plotting purposes, but log fold changes were not scaled.

GO-terms (Table 13). All clusters were subsequently individually tested for GO overrepresentation, to identify the expression patterns with the most significant functional clustering. Lowest GO annotation p-values were found in cluster 1 and 7 (Table 13), which corresponds to a pattern for Gfap specific effects or Vim specific effects. These clusters are enriched most strongly for "olfactory receptors" and "blood vessel patterning", respectively.

The microglia were only analysed for the lowest p-value, as the lack of Gfap expression in microglia makes the IF "dose dependent" reinforcing pattern difficult to interpret. The lowest p-value was reported for cluster 4, with "G-protein coupled receptor signalling pathway" (Table 14). This cluster shows the pattern of upregulation by GFAPko, and partial compensation by VIM-GFAPko (Fig. 6).
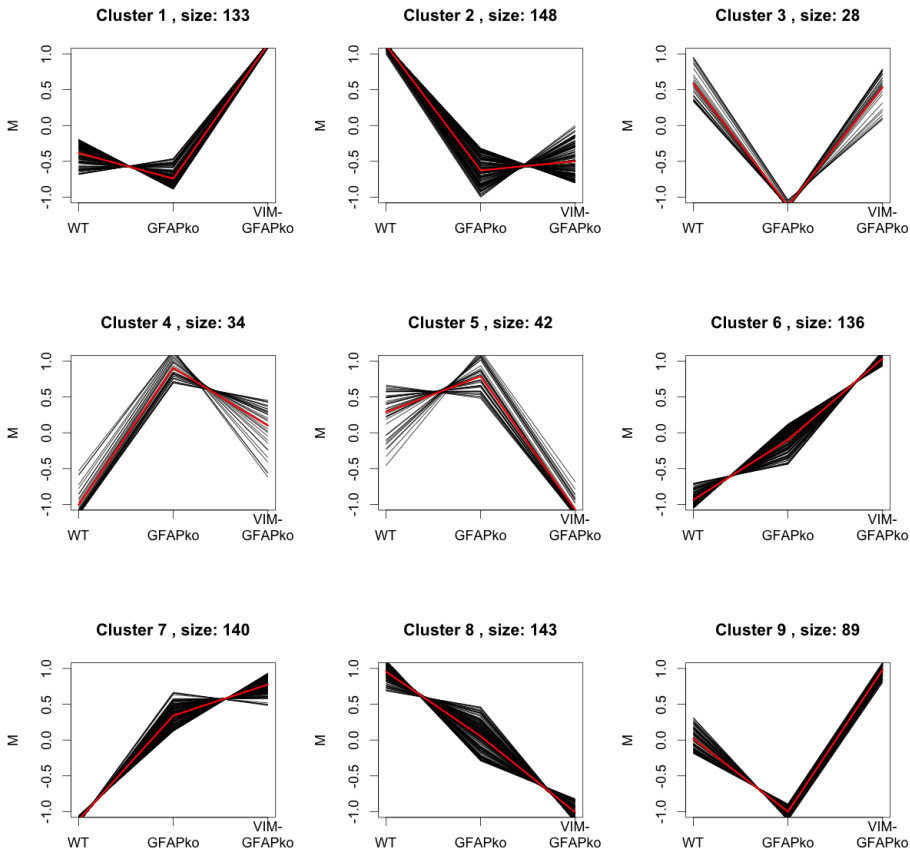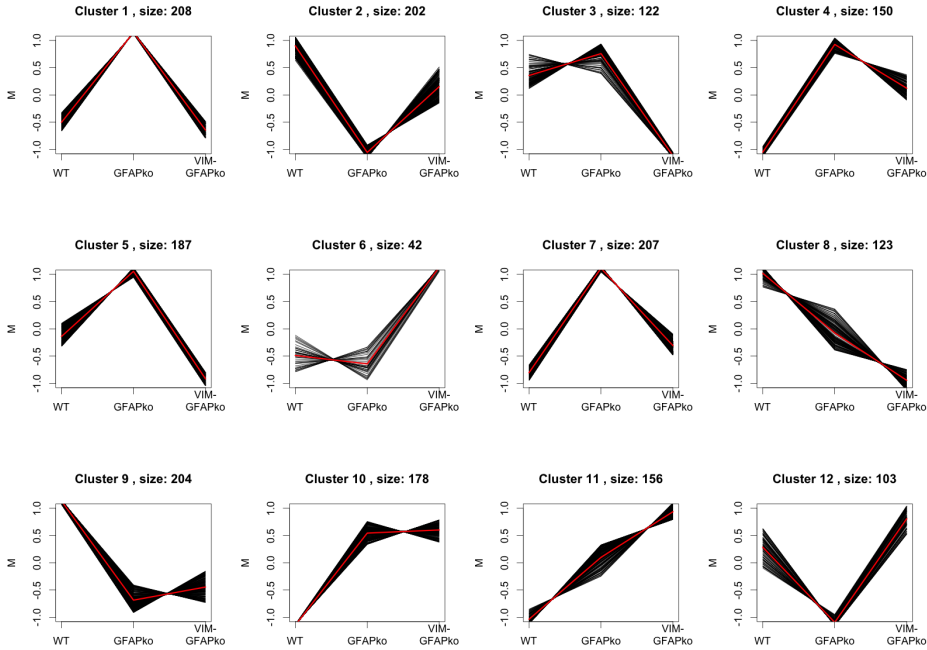

Figure 5. Cluster analysis of DEG patterns in astrocytes across genotypes
K-means clustering analysis of DEGs into 9 clusters extracted the main occurring expression patterns: Vimentin DEGs (Cluster 1 and part of Cluster 5), Gfap DEGs (Cluster 2 & 7 and part of cluster 4), IF-dose DEGs (Cluster 6 & 8). The remaining clusters show an opposite effect induced by Gfap and Vim (Cluster 3 & 9) or show a mixed pattern (Part of cluster 4 and part of cluster 5)

Table 13: Top Gene Ontology terms overrepresented in various clusters of expression patterns induced by GFAPko or VIM-GFAPko in astrocytes.

Domain	GO.ID	Term *Cluster*	# Annot	# Sig	p-val
		Cluster 8 – Positively correlates with both Gfap and Vim			
BP	GO:0008045	motor neuron axon guidance	17	2	5.40E-03
BP	GO:0006958	complement activation, classical pathway	18	2	6.10E-03
CC	GO:0016021	integral component of membrane	3089	33	1.80E-03
MF	GO:0042802	identical protein binding	846	15	4.20E-03
		Cluster 6 – Negatively correlates with both Gfap and Vim			
BP	GO:0050901	leukocyte tethering or rolling	6	2	6.70E-04
CC	GO:0014069	postsynaptic density	106	3	3.40E-02
MF	GO:0031994	insulin-like growth factor I binding	6	2	6.40E-04
MF	GO:0001968	fibronectin binding	14	2	3.78E-03
		Cluster 1 – Negatively correlates with Vim			
BP	GO:0001569	patterning of blood vessels	37	6	4.90E-07
CC	GO:0016324	apical plasma membrane	153	10	5.90E-07
MF	GO:0008559	xenobiotic-transporting ATPase activity	5	3	4.90E-06
		Cluster 7 – Negatively correlates with Gfap			
BP	GO:0050911	detection of chemical stimulus involved in sensory perception of smell	127	7	9.50E-06
CC	GO:0032421	stereocilium bundle	15	2	3.70E-03
MF	GO:0004984	olfactory receptor activity	128	7	9.50E-06

 # Annot = Total microarray probes annotated to this term; # Sig = number of probes detecting significant change in this term; p-val = parent-child weighted p-value of Fisher's exact test for overrepresentation; GO.ID = Gene Ontology Identifier; BP = Biological Process; CC = Cellular Component; MF = Molecular Function.

Discussion

Intermediate filaments in glia functions.

In this study we analysed the gene expression patterns in astrocytes and microglia that lack the IFs Gfap or both Gfap and Vim. The data provides insight into the role of the IFs in the healthy brain, where so far only slight phenotypic alterations have been described for knockout models of Gfap and Vim. To the best of our knowledge, this is the first description of transcriptomic changes induced by Gfap and Vim ko at a cellular population resolution of acutely isolated material.

Gfap and Vim expression

The array data showed a strong reduction in Vim in the VIM-GFAPko in both astrocytes and microglia, and only a reduction in Gfap in the astrocytes in the

Figure 6. Cluster analysis of DEG patterns in microglia across genotypes
K-means clustering analysis of DEGs into 12 clusters extracted the main occurring expression patterns: Vimentin DEGs (Cluster 3 & 6), Gfap DEGs (Cluster 9 & 10), IF-dose DEGs (Cluster 8 & 11). The remaining clusters show an opposite effect induced by Gfap and Vimentin (Cluster 1, 2, 4, 5, 7 & 12).

GFAPko. However, microglia in the healthy brain are traditionally not viewed as Vim expressing cells, although transcripts are detected in mice microglia (Zhang et al., 2014c). In macrophages, Vim has been shown to be present, and to be a factor in the function of the NLRP3 inflammasome (dos Santos et al., 2015). Vim can also be expressed by activated microglia in human (Graeber et al., 1988; Yamada et al., 1992). Therefore, there is a possibility for Vim transcript to be present in the isolated microglia, and if the protein is present in an unpolymerized form Vim is not observed in the immunostainings. This makes astrocyte-induced changes in the microglia hard to separate from innate changes in the microglia by the VIM-GFAPko, but for the GFAPko this should be possible. Still, it was surprising that the transcriptome of microglia appears to be more effected in the GFAPko than the transcriptome of astrocytes, considering microglia do not express Gfap (1165 DEGs in microglia vs 228 DEGs in astrocytes). This could be due to a change in the extracellular environment created by the Gfap deficient astrocytes, which subsequently induces a more dramatic shift in the phenotype of microglia. However, the additional ko of Vim in the VIM-GFAPko restored many DEGs changed in the GFAPko back to WT level (Fig. 6, clusters 1, 2, 4, 5, 7 & 12).

Table 14: Top Gene Ontology terms overrepresented in various clusters of expression patterns induced by GFAPko or VIM-GFAPko in microglia.

Domain (Cluster)	GO.ID	Term	# Annot	# Sig	p-val
BP *(10 – Negatively correlates with Gfap)*	GO:2000379	positive regulation of reactive oxygen species metabolic process	31	4	1.00E-04
BP *(4 – Induced by GFAPko, returned by VIM-GFAPko)*	GO:0007186	G-protein coupled receptor signaling pathway	660	17	1.30E-07
BP *(3 – Positively correlates with Vim)*	GO:0014002	astrocyte development	10	3	2.20E-05
BP *(3 – Positively correlates with Vim)*	GO:0048712	negative regulation of astrocyte differentiation	10	3	2.20E-05

 # Annot = Total microarray probes annotated to this term; # Sig = number of probes detecting significant change in this term; p-val = parent-child weighted p-value of Fisher's exact test for overrepresentation; GO.ID = Gene Ontology Identifier; BP = Biological Process; CC = Cellular Component; MF = Molecular Function.

Potential contamination or true change in phenotypic expression?

The pattern of the GFAPko, but not VIM-GFAPko, induced changes that we initially observed in the olfactory/vomeronasal receptors, also emerged in 6 of the 12 clusters in microglia, as well as in 2 out of 9 clusters in astrocytes. The pattern could be an indication of a contaminating cell population in the isolation procedure. Especially in the microglial isolation, due to high number of genes showing the pattern and the lack of Gfap expression in microglia, we need to consider this possibility. Still, considering the isolation procedures are identical for all genotypes as well as the and yield in cell numbers, and the strong specificity of the CD11b marker for immune cells, these patterns may represent a true difference of the GFAPko, e.g. induced expression of the CD11b marker on a cell population other than the microglia. We tried to identify a contaminating cell population by taking all the DEGs from the clusters that show an effect in GFAPko that is restored in the VIM-GFAPko and analysing these genes for GO overrepresentation (Fig. 6, cluster 1, 2, 4, 5, 7 &12). This resulted in overrepresentation of 'olfactory receptors', which is an unexpected term, as the olfactory receptor genes are considered to be quite uniquely localized to the olfactory neurons, and the transcripts could not be identified in any cell population in a mouse brain expression database (Zhang et al., 2014c). Therefore no clear candidate population responsible for a contamination could be identified, as the olfactory neurons were rigorously removed early in the isolation procedure by cutting of the olfactory bulb and isolating the cortex, and no other functional GO-terms emerged that point towards another cellular population. Screening a number of the Olfr-genes in the Allen brain atlas in situ hybridization data did not result in an indication for widespread expression of Olfr-genes in the

5

cortex, although a few studies report expression of Olfr-signalling genes outside olfactory neurons, with Olfr genes present in the cortex of humans and regulated in Parkinson's Disease (Garcia-Esparcia et al., 2013), as well as present in the kidney (Pluznick et al., 2009). Due to our peculiar, but interesting, observation we decided for now to omit genes with these expression patterns from any further discussion and to focus on DEGs of interest with the highest chance to be GFAPko induced or VIM-GFAPko induced within astrocytes or microglia, reducing the risk of finding effects due to contamination with other cells, e.g. pericytes or endothelial cells. These expression patterns are identified by clusters with a horizontal line in one half of the cluster analysis, or clusters that show an enhanced effect by the VIM-GFAPko of the GFAPko effect (Fig. 5 & 6). Due to the large amount of data generated by this type of study, we will focus on the general emerging pattern of effects on ECM effects and cell-cell signalling, and point attention to a few conspicuous genes for the rest of the discussion.

Plasma membrane and extracellular matrix DEGs responding to Gfap, Vim or both.

A strong and general effect of IF modulation revealed by the GO analysis was the enrichment for plasma membrane and extracellular region related genes, pointing towards a role for IFs in interactions within the multicellular environment. This is in line with earlier findings for the function for Vim and Gfap. Gfap interacts with the glutamate transporter Glast, membrane-cytoskeleton binding protein Ezrin, and a regulator of sodium/hydrogen exchange Nherf1 (Sullivan et al., 2007). Also the distribution of ECM protein Laminin is altered from restricted expression in specific cell groups in WT, to a widespread expression in the GFAPko (Menet et al., 2001). Fibronectin is produced more ubiquitously in the VIMko than in WT, whereas in the GFAPko or the VIM-GFAPko small punctate aggregates of Fibronectin appear (Menet et al., 2001). This last effect may be due to altered trafficking of Fibronectin, as other reports demonstrate that Gfap has an effect on the trafficking of certain classes of vesicles (Potokar et al., 2010). In addition, recent studies demonstrate that the Notch signalling pathway shows altered trafficking and activation of the membrane-presented ligand Jagged1 in the VIM-GFAP ko (Wilhelmsson et al., 2012).

Gfap specific DEGs in ECM and Signalling ontologies

In an effort to give more insight into the genes that show a Gfap-specific clustering, crossed with the ECM and plasma membrane terms, we will now first list the DEG names in relation to the relevant GO terms (underlined = downregulated, *italic* = upregulated). Effects on ECM and signalling are represented in our dataset for Gfap by complement or cytokines related DEGs (C2, Cfb, *C4b*, Clec3b, Scgb3a1, *Fgf1*,

Hhip, *Cxcl5*, *Penk*, Ybx1, *Gkn1*, Agt), receptor or receptor binding DEGs (Lrg1, Ptch1, *Ssc4d*, Fzd2, *Robo2*, Tlr6, Cx3cr1, Cdh22), ECM DEGs or ECM modifying enzymes DEGs (*Csn3*, *Thbs4*, *Col5a2*, Col16a1, Hapln3, Adamtsl2, *Fga*, *Vit*), or Transporter DEGs (Rhcg, Lcn2).

Especially the effect on Thbs4 (517% increase in GFAPko vs WT) is quite prominent, and may be of great relevance functionally. The Thrombospondins (Thbs1-4) have roles in synaptogenesis and synaptic activation (Christopherson et al., 2005; Kim et al., 2012). Thbs4 is also important for astrogenesis in the subventricular zone through direct Notch1 activation after injury (Benner et al., 2013). In addition, Thbs4 affects the migration of neuroblasts through the rostral migratory stream and incorporation of the neuroblasts in the olfactory bulb (Girard et al., 2014). In another recent study investigating indirect-injury-induced expression of plasticity related genes, it was found that Thbs4 and Ezrin were increased after injury in the hippocampus. This injury-induced increase of Thbs4 and Ezrin was attenuated in the VIM-GFAPko mouse, although no increased baseline in expression of Thbs4 was reported in the hippocampal homogenate (Andersson et al., 2013). Note that although we find the largest effect of GFAPko on Thbs4 expression level, the VIM-GFAPko displayed an enhanced increase of Thbs4 expression compared to WT (745% VIM-GFAPko vs WT, or 143% compared to GFAPko vs WT). There can be multiple causes for this discrepancy of VIM-GFAPko induced Thbs4 expression. The origin of the cells (cortical vs hippocampal), the specificity of the examined population (sorted astrocytes vs tissue homogenate), as well as the age of the animals (450-540 days vs 180-450 days) are all different between our study and the study by Andersson et al., hence all are possible contributors to the discrepancy.

Vim specific DEGs in ECM and Signalling ontologies

The Vim specific DEGs identified in our study, by extracting the DEGs only found in the VIM-GFAPko vs GFAPko contrast, also contained a large number of genes assigned to the broad spectrum of ECM and signalling. These again include cytokines (*Edn1*, *Cxcl12*, Vipr2, *Sema3c*, Cxcl10, *Pdgfb*), receptor or receptor binding genes (*Cd34*, *Cd93*, Cd200, *Thbd*, *Tgfbr2*, *Jag2*, *Eltd1*, *Ocln*, *Cdh5*, *Prom1*, *Ctnnb1*, *Nr4a2*, *Ly6c1*, *Grin3a*, *Robo4*, *Sgk1*, *Tek*), ECM or ECM modifying genes (Serpina3n, *Lama4*, Loxl1, *Aldob*, *Flt1*, *Mmrn2*, *Mgp*, Cml5, *Col20a1*, *Ctsh*, *Fbln2*, *Sgms1*, *Papln*, *Srgn*, *St3gal1*, *Mal*, *Tnfaip6*, *Fn1*), or transporters (*Abcb1a*, *Abcb1b*, *Abcb4*, *Abcg2*, *Slco1a4*, *Slc16a4*, *Slc40a1*, *Clic5*, *Slc38a2*, *Nostrin*, Slco4a1, *Slco2b1*, *Cp*). In addition, the GO analysis revealed a specific effect of Vim on angiogenesis. Early investigations into the phenotype of the IFko mice also revealed an increase of large dilated blood

vessels in the GFAPko, VIMko, and the VIM-GFAPko (Pekny et al., 1999). Vim is emerging as an important factor in angiogenesis, and is also expressed in pericytes and endothelial cells of the brain vasculature (Kwak et al., 2012). Some of the targets found may originate from a contaminating source of pericytes or endothelial cells in the astrocytes from the VIM-GFAPko mice, as cluster 1 from the astrocytes showed a very consistent pattern of regulation. Whether these DEGs are actual DEGs in astrocytes or in putative contaminating vascular cells requires further investigation. Three of the targets that were enhanced in the VIM-GFAPko astrocytes are Egfl7, Tek, and Ly6c1. Investigating the expression pattern of these genes on the RNAseq brain database, reveals a 100-1000-fold enrichment of these gene in endothelial cells over astrocytes. Slc1a2 (Glt1) is however not expressed on endothelial cells at all, so if there is contamination, it should either be due to aspecific binding of the antibody, or to Slc1a2 induction in endothelial cells in the VIM-GFAPko. Pericyte data was not available in the RNAseq database, although the paper describing the database does give some of the VIM-GFAPko DEGs as pericyte-enriched (e.g. Cxcl12) (Zhang et al., 2014c). For astrocytoma cells it is known that they can show a behaviour called vascular mimicry, where they obtain an endothelial phenotype, indicating that spurious transdifferentiation of astrocytic lineage to endothelial lineage is possible. Our data, if not caused by contamination of endothelial cells, may hint towards a role for Gfap and Vim in maintaining the stability of the astrocytic phenotype. In support of this idea is that we find increased expression of Rock1 in the VIM-GFAPko astrocytes, a gene which has been associated with an increased potential for vasculogenic mimicry, and thus a form of transdifferentiation, in a hepatocellular carcinoma cell line (Zhang et al., 2014a).

Gfap and Vim DEGs in ECM and Signalling ontologies

DEGs increased or decreased in the GFAPko and enhanced further in the Vim-GFAPko are interesting due to a possible regulatory mechanism depending on IF dose, rather than a specific IF protein. Focussing on the GO-terms involving cell-cell communication ("GO-term Extracellular Region") we found various targets of interest in this cluster, including members of the complement system or cytokines (C1qc, C1qa, *Pdgfd*, Bmp7, Ccl4, Igfbp2, *Igfbp5*), receptors (*Itga4*, Cgref1, Chl1, Trem2, *Gria2*, *Dmd*, *Dcc*), ECM genes or ECM modifying enzymes (*Gcnt1*, *Cpb2*, *Serpinf1*, Ctss, *Cst8*, Optc) or transporters (*Slc38a1*, Clic4, Slc12a9, Clic6, and others (*Hba-a2* (haemoglobin), Hspe1 & *Hspa1a* (heat shock proteins)). In contrast to our finding for C1qc, no difference in was reported before (Andersson et al., 2013). Another relevant target in these DEG clusters is Igfbp2 (insulin growth factor binding protein 2). Igfbp2 has been shown to interact with Vim before (Shen et al., 2015) and

is important for proliferation in astrocytes and glioma (Arscott et al., 2013; Fletcher et al., 2013).

ECM in astrocyte physiology

ECM production by astrocytes is typically associated with pathogenic gliosis. However, in the healthy brain, a healthy ECM is also of the utmost importance. The ECM has an important role in demarcating and functionalizing microdomains and niches in the brain, either by creating local gradients of cytokines, by creating diffusion barriers for solutes and/or cells, and by providing scaffolding for membrane proteins to organize to (Dityatev et al., 2010). The importance of ECM in brain plasticity and the lifecycle of synapses has given rise to the term of the tetrapartite synapse, consisting of a presynaptic neuron, a postsynaptic neuron, astrocytes, and the ECM as functional units (Dityatev and Rusakov, 2011) (although the same term has been used to describe microglia as the fourth functional unit). Astrocytes are an essential contributor to this synaptic ECM (Pyka et al., 2011). Since the data analysed in this study are derived from healthy mice, the ECM and signalling DEGs identified may be most relevant for this physiological function of Gfap and Vim in astrocytes, but this naturally requires further research.

DEG interactions between astrocytes and/or microglia

For the microglia, we investigated whether there were targets in the corresponding Gfap, Vim, or Vim and Gfap correlating clusters that can be connected to genes differentially expressed by the astrocytes. As an initial approach, we manually searched for the most straightforward candidates, although a protein-protein interaction database is needed to reveal more functional interactions. One interacting gene pair that was differentially expressed was the extracellular matrix component Ntn1 (netrin), downregulated in microglia and astrocytes in the GFAPko mice. The netrin receptor Dcc was strongly increased in the microglia in the GFAPko, but not in the astrocytes. In the VIM-GFAPko however, Dcc was increased also in the astrocytes.

Another signalling pathway that we found to be altered on several levels was the Notch pathway. The aforementioned increase in Thbs4 in the GFAPko can have a direct inducing effect on Notch activation, whereas Jag2, a canonical Notch ligand, and Mind bomb (Mib1), a modulator of the pathway, were both upregulated in the VIM-GFAPko. Neurl1a (Neuralized) and Reck, two Notch pathway modulators were downregulated in the microglia in the GFAPko, with Reck upregulated, but Neurl1a downregulated (significantly, but not above the threshold of fold change > 2) in the astrocytes of the VIM-GFAPko. Finally, to indicate this pathway modulation

also results in an effect, in the microglia, Hes5, a direct transcriptional target of Notch, was downregulated in the VIM-GFAPko, whereas Hes1 was upregulated in the GFAPko. The complex interplay between canonical-noncanonical, cis-trans signalling and ligand-receptor modifying pathways are common to the Notch pathway making it difficult to predict what Notch targets will do when multiple components are modulated in the system (Andersson et al., 2011). To illustrate: Reck is both a regulator of Notch, as well as a direct target of Notch (Muraguchi et al., 2007; Pézeron et al., 2014). Similar to this concept, Gfap expression in differentiation of neural stem cells to astrocytes has an inhibiting effect on expression of Notch target genes, whereas Notch activation induces Gfap production (Kanski, 2014). The downregulation of Hes5 in a microglial – neural stem cell (NSC) coculture has been shown before, although the supposed cell population that downregulated Hes5 in this case was suggested to be the NSCs, whereas our data indicate this could also be the microglial population (Gu et al., 2011). The Notch signalling pathway has also been suggested to be central to the effect of enhanced incorporation of grafts in VIM-GFAPko animals and astrocytic inhibition of neurogenesis (Wilhelmsson et al., 2012). In addition, Notch signalling is essential for regulation of vascularization of the brain, and mutations in one receptor, Notch3, cause the infarction disease CADASIL (Cerebral Arteriopathy, Autosomal Dominant, With Subcortical Infarcts and Leukoencephalopathy), possibly linking back to the vascular markers discussed before. A direct interaction between a Gfap isoform and the Presenilin complex, part of the γ–secretase that processes Notch, has been identified before (Nielsen et al., 2002). This warrants further investigation into the molecular mechanisms at play between IFs and Notch signalling to develop therapies for improved recovery after brain injury, and gain better understanding of brain vasculature biology and the neurogenic niche.

Further DEGs of specific interest

Finally we would like to mention a few noticeable genes that may reveal completely new functions of GFAP in the brain. One gene strongly downregulated in both astrocytes and microglia in the GFAPko was Gdpd3 (Glycerophosphodiester phosphodiesterase domain containing 3; in humans also known as GDE7, Fig. 1). The Gdpd family (in humans consisting of GDE1-7, with varying official gene symbols) has been mostly studied in bacteria and plants, but was recently found to be important in mammals for the differentiation of various cell types (Corda et al., 2014). Most members of the family display enzymatic activity towards deacetylated glycerophospholipids, cleaving them into glycerol phosphate and alcohol, but GDE7 and its homolog GDE4, have lysophospholipase D catalytic activity, meaning

they can process lysophosphatidylcholine into choline and lysophosphatidic acid (LPA) (Ohshima et al., 2015). LPA is an important signalling molecule in the CNS, with 6 different direct LPA receptors (LPAR1-6) identified up to date. Effects have been demonstrated on neural progenitor cell function, synaptic function, immune response, myelination and vascularization, as recently reviewed (Yung et al., 2015). Whether this reduction in Gdpd3 is a direct or indirect effect of the GFAPko remains unclear, considering the similar drop in microglial and astrocytic expression. This suggests the change is indirect, via a change in the extracellular environment or cytokines, influencing expression of Gdpd3 in both microglia and astrocytes.

One other strong candidate identified in this study with reported connections to IFs is Rock (Rock1: GFAPko vs WT = 157%, FDR 4E-2; VIM-GFAPko vs WT = 248%, FDR 6E-4 Rock2: VIM-GFAPko vs WT = 183%, FDR 6E-3). Rock is a Rho associated kinase that effects cytoskeletal reorganization, regulating downstream interactions with and the transport of Vim by phosphorylation of Vim (Hyder et al., 2015; Robert et al., 2014). On a cellular level, Rock also regulates transport, migration, and proliferation of astrocytes (Kheirollah et al., 2014; Lau et al., 2011; Racchetti et al., 2012; Yu et al., 2012). So far Vim or Gfap has not been implied in the regulation of Rock activity. Decreased Rock activity has also been linked to increased production of neurite growth-inhibitory ECM production, and thus may also provide a link for the mechanistic effect of the increased neuritogenesis on the VIM-GFAPko astrocytes (Chan et al., 2007; Widestrand et al., 2007). However, in a stroke model, VIM-GFAPko resulted in increased CSPG expression in the injured area, and inhibited functional recovery (Liu et al., 2014b). Although the Rock phosphorylation of Vim is well described, the effect Vim and Gfap have on Rock expression is novel. In addition to this effect on Rock expression, another Rho associated DEG was found in the VIM-GFAPko: *Cdc42ep3*. Cdc42 is an important astrocytic Rho-GTPase and exerts its function through Cdc42 effector proteins, similar to how RhoA is upstream of Rock.

A last DEG we will point attention to here is Qpct, a gene expressed by microglia encoding an enzyme with catalytic functions relevant in pathology for both Alzheimer's Disease (AD) and Huntington's Disease (HD), and a candidate druggable target in both these diseases (Alexandru et al., 2011; Jimenez-Sanchez et al., 2015; Schilling et al., 2008). In addition, the Qpct gene was also identified in GWAS studies as a risk factor for schizophrenia susceptibility, although these SNPs did not affect expression levels of Qpct (Ripke et al., 2013; Zhang et al., 2015). Qpct encodes the protein glutaminyl cyclase (QC), which catalyzes the conversion of glutaminyl peptides (with a glutamine at the N-terminus) into pyro-glutamic acid peptides

5

(with a cyclic-glutamate at the N- terminus) (Busby et al., 1987; Fischer and Spiess, 1987). The QC enzyme is of relevance in AD as the enzyme catalyses the formation of Aβ with a pyroglutamate at the N-terminus, making up 15-20% of total Abeta (Mori et al., 1992). This modification of the Abeta peptide has important effects on pathological properties such as oligomerization of fibrils, cytotoxicity, and disease progression in humans and has been proposed to be the most pathological variant of Abeta (Morawski et al., 2014; Schlenzig et al., 2012; Wittnam et al., 2012). There are two genes with QC activity, Qpct and Qpctl, but whether there is a distinction between these genes on activity of pathogenic target cyclization, cell population of origin, and whether the conversion occurs intracellularly or extracellularly is under close attention at the moment. Where Qpct is the main target in most AD studies, Qpctl has been proposed to be mainly responsible for modification of inflammatory cytokines such as CCL2 (MCP-1) (Hartlage-Rübsamen et al., 2015; Jimenez-Sanchez et al., 2015). Our data indicate Qpct mRNA in microglia is regulated by Gfap expression in Astrocytes. This interesting finding is further spiced up by the upregulation of Qpct in the microglia of the VIM-GFAPko AD model, back to WT-AD level (Kamphuis et al., 2015). Although neurons also express Qpct, astrocytes do not and this microglial Qpct may play a role in the onset or progression of AD.

Although the earliest reports on many different IF knockouts did not indicate gross defects in mouse phenotype, recent studies identified IFs as important players in various biological functions. IFs provide an organism with robustness in the face of cellular stress of diverse natures, such as toxicological or mechanical stress (Asghar et al., 2015; Coulombe and Wong, 2004; Fudge et al., 2008; Ramms et al., 2013; Sahlgren et al., 2006; Toivola et al., 2010). The same goes for Gfap and Vim in the reactive astrocyte. How the IF proteins convey this robustness in molecular detail is now being unravelled. This study provides insight into the molecular changes in glial cell populations affected directly or indirectly by the GFAPko and VIM-GFAPko, generating interesting leads for further investigation. In combination with the transcriptomics studies of GFAP in human astrocytoma cells (Chapter 4) this study may provide a cross species and cell origin profile of GFAP function, which will be further explored in Chapter 7 of this thesis.

Chapter

6

Towards microrheological probing of the effect of GFAP on cell stiffness

Oscar M.J.A. Stassen
Elly M. Hol*
Gijsje H. Koenderink*

* Authors contributed equally

Abstract

Cells in the human body interact with and respond to their mechanical environment. The cells themselves are an important contributor to the mechanical environment, both through tensile forces and remodelling of the extracellular matrix, and through the cell's intrinsic material properties. The intrinsic material properties are mainly determined by the cytoskeleton. One of the cytoskeletal elements in astrocytes, the intermediate filament GFAP, is highly regulated throughout development and disease. To investigate the contribution of GFAP to the stiffness of the cell, we used an intermediate filament network (IFN) extraction method to study the effect of recombinantly expressed GFAP isoforms (GFAPα and GFAPδ) on the mechanical properties of the astrocytoma IFN by multiple particle tracking microrheology (MPTM). We developed a robust IFN extraction method to obtain cell-derived skeletonized networks, a useful technique to study biological influences on network mechanics. The analysis revealed that the stiffness of the IFN is on the edge of what can be reliably measured by MPTM, but by comparing the MSD(τ=10) between conditions, a reduced mobility was found when expressing GFAP isoforms GFAPα and GFAPδ in comparison to control.

Introduction

Cells in the human body interact with and respond to their environment. The mechanical environment influences cell migration, motility, proliferation and differentiation. One of the main players in creating this environment and determining its mechanical properties are the cells themselves. They do this by producing and remodelling the extracellular matrix, and by exerting tensile forces using their actomyosin network (Jansen et al., 2015).

The mechanical properties of the cells themselves are important in cell-cell contact situations, and when cells are migrating through a tissue or extravasating from specific tissue boundaries, in the case of e.g. immune response, cancer metastasis, or angiogenesis (Friedl and Wolf, 2010). The cell's mechanical properties are mainly determined by its cytoskeleton, consisting of actin filaments, microtubules, and intermediate filaments (Huber et al., 2015). Actin filaments and microtubules both provide the cell with structure but are also important for force generation in cell migration and intracellular transport, whereas intermediate filaments are emerging as an integrating hub of cell mechanics and signalling, as described in Chapter 1.

The brain is intuitively not considered the most mechanical of organs, but mechanics also play an important role in this tissue (Tyler, 2012). It is an organ with a highly organised structure. The grey matter contains cell bodies, various

specialized domains and nodes traditionally identified histologically by the difference in cellular densities, whereas white matter contains axonal bundles and the fatty myelin. Recently, it was shown that forces contribute to a constant flow of interstitial fluid through the brain, which is important to clear the brain of debris (Iliff et al., 2012). Where the neurons are the main communicating units in the brain, the glial cells form a crucial supportive cell type important for homeostasis in physiology. Until the intricate and complex biology of glial cells was discovered, glial cells were considered purely as a mechanical filling keeping the neurons together ($\gamma\lambda\iota\alpha$ is Greek for glue). Now it is recognized that glial cells are not only important for structural support, but also for brain functioning. Thus the glial cells are important contributors to the mechanical properties of the brain (Lu et al., 2006), and both neuronal and glial cells are sensitive to these mechanical properties. This mechanical sensitivity of neural cells has been demonstrated in multiple ways: stiffness of the substrate can direct neural stem cell fate (Keung et al., 2011), the presence of rigid implants in the brain induces reactive gliosis (Moshayedi et al., 2014), neuronal firing can be activated by mechanical cues (Coste et al., 2010), and in the extreme case of traumatic brain injury, mechanical trauma can lead to neurodegeneration, loss of consciousness, disability or death (Hemphill et al., 2011; Rosenfeld et al., 2012).

Astrocytes, a glial cell type, have their own unique cytoskeleton due to the presence of an astrocyte-specific intermediate filament (IF): Glial Fibrillary Acidic Protein (GFAP). GFAP forms a network together with the other IFs expressed in astrocytes, i.e. vimentin, nestin, and synemin (Middeldorp and Hol, 2011). Astrocytes increase the production of GFAP when they are faced with a range of pathological conditions, but no clear-cut function has been attributed to the protein yet. We were interested in the effect of increased contents of GFAP on the mechanics of the cell, as a change in these mechanics can have functional consequences for the astrocytes themselves as well as the brain cells around them. GFAP has been shown to affect the mechanics of cells, but contradicting results have been described. In one study, *in vivo* retinal ischemia induced gliosis in Müller cells, and an increased stiffness was reported with increasing GFAP expression, whereas another study, using *in vitro* injury of astrocytes reported a reduction in stiffness with increasing GFAP (Lu et al., 2010; Miller et al., 2009).

Different techniques have been developed to measure the mechanical properties of single cells. These include shear, compression, and tensile tests on whole cells, local nanoindentation by atomic force microscopy (AFM), and local probing of the cytoskeleton by passive microrheology with particle tracking

6

video microscopy, or by active microrheology with optical or magnetic tweezers microscopy (Waigh, 2005). Interpreting measurements on live cells is complicated by the spatial heterogeneity of cells, presence of multiple interacting cytoskeletal networks, and by out of equilibrium activity. An established technique to investigate the IFN is to extract actin and microtubules while retaining the IF cytoskeleton by making use of its insolubility (Lazarides, 1982). Recently, this approach was applied to keratinocytes to probe the role of keratin network changes under shear stress (Sivaramakrishnan et al., 2008). Here, we adopt the same procedure to glial cells, to probe the mechanics of GFAP. To measure the mechanics of the IFN we implemented the technique of multiple particle tracking microrheology (MPTM). One advantage of MPTM over other techniques like AFM, is that in AFM a probe taps on top of the cell and measures the local mechanics on the boundaries of the network, whereas the probes for MPTM are dispersed throughout the network, and thus can give an indication of the local intracellular mechanics of the network. Due to the spatial heterogeneity of cells, MPTM has often been used in living cells, but due to the cell's non-equilibrium state the interpretation of particle motions in terms of the generalized Stokes-Einstein relation is difficult (Guo et al., 2014). At thermal equilibrium, the mechanics of the network determines the magnitude and time dependence of the displacements the particles undergo by Brownian forces. In a purely viscous liquid, the particle displacements are related to the viscosity via the Stokes relation. For viscoelastic networks, this relation can be generalized to a relation of the particle displacements to the complex shear modulus of the network surrounding that particle (Mason and Weitz, 1995).

To probe the effect of IFN modulation, we started with living cells, modified the IFN in these cells by overexpression of GFAP isoforms with molecular biological tools, and then extracted the IFN from these cells to measure its mechanical properties. The networks we measure are in equilibrium, due to the permeabilization of the cell. This approach combines the advantage of retaining the architecture of the IFN synthesized by a cell, thus providing a reliable biological model for the network, with the advantage of no active forces being at work, facilitating a quantitative interpretation of the data in terms of rheological properties (Brangwynne et al., 2008). We were able to develop a robust cell extraction method to produce cell-constructed IFNs amenable for mechanical measurements. Although the networks from cells transduced with GFAP did display reduced mobility of encapsulated particles, our study revealed that the MPTM method is not sensitive enough to quantify the mechanical properties of the extracted IFNs. However, this could be addressed in future studies by implementing active microrheological techniques.

Methods

Cell lines

For our experiments we used a human astrocytoma cell lines U251-MG (U251). Since the expression of GFAP in the U251 cell line varies, we first selected subclones of U251, and continued with a clone with a low/undetectable basal expression of GFAP (clone D10). This clone was subsequently transduced with lentiviral vectors containing recombinant-mCherry (control), recombinant human GFAPα-IRES-eGFP (GFAPα^+) or recombinant human GFAPδ-IRES-mCherry (GFAPδ^+) as described before (Moeton et al., 2016). These transduced populations were again selected for subclones, to obtain 100% transduced populations (control: clone C5, GFAPα^+: clone G1, GFAPδ^+: clone E9). U251 cells were maintained in 1:1 Dulbecco's modified Eagle medium (DMEM) GlutaMAX high glucose: Ham's F-10 nutrient mix, supplemented with 100 U/ml penicillin, 100 μg/ml streptomycin (1% P/S) and 10% (v/v) fetal bovine serum (FBS; all Invitrogen, Bleiswijk NL).

For maintenance, all cells were split twice a week and cultured in uncoated tissue culture plastics at 37°C, under a humidified 5% CO_2 / 95% air atmosphere.

Preparation of IF networks with embedded particles

Glass bottom dishes (#0, Mattek corp) were coated with poly-L-lysine (PLL; Sigma-Aldrich) and laminin (PLL (20μg/ml) at 37°C for 30 minutes (mins) followed by laminin (10 μg/ml) at 37°C for 3 hours. Cells were plated at a density of 25,000 cells/35 mm dish and adhered to the dish over night (o/n). Then yellow/green carboxylate modified microspheres of 0.5 μm diameter (F-8888, Molecular Probes) were sonicated and added to the cells in a concentration of 1.75 * 10^7 particles / ml and incubated with the cells o/n. Cell culture medium was refreshed the next day to wash away the particles that were not internalized by the cells. Other methods using a gene gun or particle delivery system were tested for delivery of particles into the cells (Li et al., 2009), but these procedures were unsuccessful in our hands, due to particle aggregation and/or cell death. The procedure for cell permeabilization and IF skeletonization was adapted from a protocol proposed by Sivaramakrishnan et al (Sivaramakrishnan et al., 2008). Briefly, before microscopy analysis, cells were washed twice with phosphate buffered saline (PBS). Cells were then permeabilized in PPST buffer (100 mM pipes (pH 6.9), 1 mM EGTA, 3.5% (w/v) PEG-35000, 0.4M NaCl, 0.25% triton (v/v)) at room temperature for 10 mins. Permeabilized cells were washed once with buffer G (50 mM MES-NaOH (pH 6.2), 0.1mM $CaCl_2$, 2 mM $MgCl_2$, 0.5 mM DTT) and then incubated with human gelsolin, kindly provided by F. Nakamura (Harvard Medical School), in buffer G at 37°C for 20 mins. Skeletonized

6

IF networks were washed 2x in PBS and fluorescent microspheres were tracked in PBS.

Particle tracking

Skeletonized IF networks in PBS were equilibrated on the microscope at 37°C. Fluorescent microspheres were excited using an MDF-GFP filter set (Thorlabs).

MPTM was performed with a 100x oil immersion objective on a Nikon TE microscope. Videos were captured at a frequency of 50 Hz with a CCD camera (Photron), as higher frequencies and shorter shutter times resulted in too low intensity of the fluorescent particles. The pixel size of the CCD with the 100x objective was measured to be 0.195 µm / pixel.

Post-tracking staining, image correlation and particle annotation

After tracking the mobility of the particles in the IFNs, the networks were fixed in 4% (w/v) paraformaldehyde in PBS (pH 7.4) for 10 mins. Samples were blocked in SuMi (50mM Tris, 150mM NaCl, 0.25 % gelatin, 0.5% Triton X-100, pH 7.4) for 15 mins. To visualize all networks, also the control samples without GFAP, samples were stained with a primary polyclonal chicken anti-Vimentin antibody (1:2000; Chemicon) diluted in SuMi for 1 hour and with a secondary mix of donkey anti chicken-Cy3 and Phalloidin-488 to confirm solubilization of F-actin. Samples were then stored in Mowiol (Calbiochem). Original tracked cells were relocated and imaged using a 40x immersion objective on a confocal microscope (Nikon). A script was written in ImageJ to overlay the positions of the particles in the video tracking to their positions in the immunofluorescence images based on an image transformation calculated based on the coordinates of two distinguishable particles.

Particles were included in the analysis only if they were manually identified as singlets. Particles were then manually annotated to their region within the cell (outside the cell, in the cellular periphery, in contact with the nucleus, or cytoplasmic; an estimation of these boundaries is shown in Fig. 2D). Since the positional overlay of immunofluorescence and the tracking movie was not always 100%, these manual annotation steps were necessary.

Analysis of trajectories

Our particle tracking data was initially analysed with the in-house developed particletracker software, making use of a convenient GUI and based on the Crocker algorithm (Stuhrmann et al., 2012). But as many particles had subpixel displacements, this analysis gave large jumps corresponding to pixel-to-pixel transitions. Therefore, another method was adopted where particle centroids were

determined by a radial symmetry algorithm (Parthasarathy, 2012). This algorithm was reported to be more accurate and less sensitive to a low signal to noise ratio than the Crocker algorithm. The radial symmetry code was implemented into a particle tracking and processing algorithm kindly provided by the Kilfoil group (http:// people.umass.edu/kilfoil/). Briefly, the procedure consisted of identifying particle locations by a local maximum of intensity. Then the direction and steepness of the intensity gradient within a given radius around the center pixel were calculated on the intersections between the pixels surrounding this local maximum of intensity (Roberts cross operator). The centroid was then calculated by algebraically finding the point with a minimized distance to the lines parallel to the direction gradients on each pixel corner surrounding the local maximum. This minimization took into account a weighing factor, which consisted of the distance of the pixel corner to an initial estimate of the centroid and the steepness of the gradient (Parthasarathy, 2012). A slight alteration was made to the weighing factor as proposed by Parthasarathy (Equation (Eq.) 1).

$$w_k = \frac{\left| \vec{\nabla} I_k \right|^2}{d_{k,c}}$$

(Eq. 1)

We used an iteration of the radial symmetry center calculation for the initial estimate of the centroid ($d_{k,c}$) and by making the distance to this estimate a relatively larger contribution to the weighing factor than in the original weighing factor (Eq. 2).

$$w_k = \frac{\left| \vec{\nabla} I_k \right|}{d_{k,c}}$$

(Eq. 2)

Further processing of the individual particles identified per frame were then linked through a tracking algorithm kindly provided by the Kilfoil group, to retain only those features that were present throughout the entire movie (3119 frames), allowing for gaps of at most 1 frame per particle. The coordinates of the feature in this frame were then interpolated from the preceding and the following frame.

The recordings of the particles displayed a drift. Therefore we decided to smoothen the trajectory using a LOESS (LOcal polynomial regrESSion fitting) algorithm in R software for statistical computing (Cleveland et al., 1992). This algorithm calculates a local regression by weighing the distance of datapoints considered in a tricubic fashion. The amount of datapoints per local area considered are based on the spanning parameter α ($0<\alpha<1$), which controls the degree of

6

smoothing. The trajectory was locally fit to a second degree polynomial, with an α of 0.1 (Fig. 3A-F). After subtracting this smoothened trajectory, a small oscillation with a frequency of 2 Hz was still observed (Fig. 3G). This drift was observed in all samples, but was not corrected for, due to the varying amplitude.

The mean square displacements (MSDs) of the features were calculated by (Eq 3.).

$$MSD(\tau) = \langle \Delta r(\tau)^2 \rangle = \langle [r(t+\tau) - r(t)]^2 \rangle \qquad \text{(Eq. 3)}$$

For τ_{max} we used $0.25 * t_{max}$, to allow for sufficient measured displacements for reliable statistics per τ. The procedure was verified on particles dispersed in a mixture of 50% glycerol in water (with a viscosity of 4.5E-3 Ns/m^2 (Cheng, 2008)), and the MSD obtained in this procedure corresponded to the theoretical MSD expected for particles in this mixture.

Statistics

The (further referred to as MSD(τ=10)) was taken to represent the MSD at the point where all the features had a plateau. Statistics on these values were performed in R software for statistical computing. The MSDs between conditions of interest were tested for normality with a Shapiro-Wilk test. Conditions were compared with a nonparametric Kruskal-Wallis test for difference between conditions, and individual contrasts were performed with Dunn's post hoc test, corrected by Benjamini Hochberg's False Discovery Rate.

Results

Intermediate filament network extraction

To reduce variability in IFN expression by our cell lines, the heterogeneous U251 cell line was clonally selected for cells expressing low GFAP, but still expressing vimentin. This clonal line was subsequently transduced with mCherry (control), GFAPα (GFAPα^+) or GFAPδ (GFAPδ^+). These transduced cells were again clonally selected to obtain cell lines with 100% transduction efficiency. This resulted in three cell lines with three different IFNs: either only the native IF network (vimentin), with low almost undetectable GFAP (control), a network consisting of both GFAPα and vimentin, or a network with vimentin and GFAPδ, known to induce a collapsed network (Fig. 1A-C). The IFs are known to interact with actin and microtubules, which can affect the mechanics of the network (Huber et al., 2015). Therefore we extracted these two components from the cells, while retaining the IFN to determine only the changes in the IFN mechanics, in analogy to a recent publication where the keratin IFN of keratinocytes was studied (Sivaramakrishnan et al., 2008). To retain the pure

IFN, the cells were permeabilized by 0.5% triton, to remove all soluble proteins. Microtubules were successfully depolymerized and washed away by this step, but the IFN and actin bundles were retained. In some permeabilizations a condensed microtubule spot positive for staining (anti-acetylated tubulin, T6793, Sigma-Aldrich) was still present in the cell, which is likely the microtubule organizing center (Fig. 1D-E, arrowheads in the figure). The networks were treated with gelsolin, a protein that can cleave actin fibers into smaller pieces, to depolymerize the actin bundles. This treatment resulted in a retained IFN in the case of all three cell lines (Fig. 1F-H). Note that the GFAPδ$^+$ cells in the tracking experiment had a much lower fraction of collapses than the cell line shown in the original generation (Fig. 1C). This may be due to the difference in culturing conditions, since for confirmation of the cell line transduction efficiency different culturing conditions were used as in the experiment (uncoated coverslips vs laminin coated coverslips). Also before permeabilization, GFAPδ$^+$ did not show collapses in cells cultured on laminin coated coverslips, so it is not a permeabilization effect (not shown). For all IFNs extracted, attachment to the glass was very stable, as recording sessions of a single sample would usually take 2-3 hours at 37°C, after which the sample was fixed with 4% PFA. In our experiments no loss of complete cells or networks was observed by the permeabilization procedure (Fig. 1D-F), or during the recording. It is likely that the laminin coating of the glass enhances the stability of cell attachment.

Particle annotation and tracking

The time frame in which particles were endocytosed by the cells was between 10-18 hours (not shown). After incubating the cells with the particles for this time, particle-loaded IFNs were obtained by the extraction described. The particles were then tracked by video imaging at a rate of 50 Hz. To interpret the data obtained from each particle in the context of the local IFN, it was necessary to stain the IFN after the tracking. Since the control cells have only low levels of GFAP, we used a vimentin staining to visualize the networks in all cells and imaged the cells in 3D by confocal microscopy. In our earlier work we have shown that vimentin co-localizes and co-collapses with GFAP (Moeton et al., 2016). The particles that were successfully tracked in the movies were correlated to their corresponding confocal images and annotated to their cellular position. The correlation between video tracking and confocal microscopy was based on two reference particles. This approach did not give a completely correct overlap, possibly due to some displacements of the particles that occurred between tracking and staining. The patterns of particles positioning, however, was reliable enough to correctly identify the tracked particles in the confocal images (Fig. 2A-C). Due to the inaccuracy in assignment of
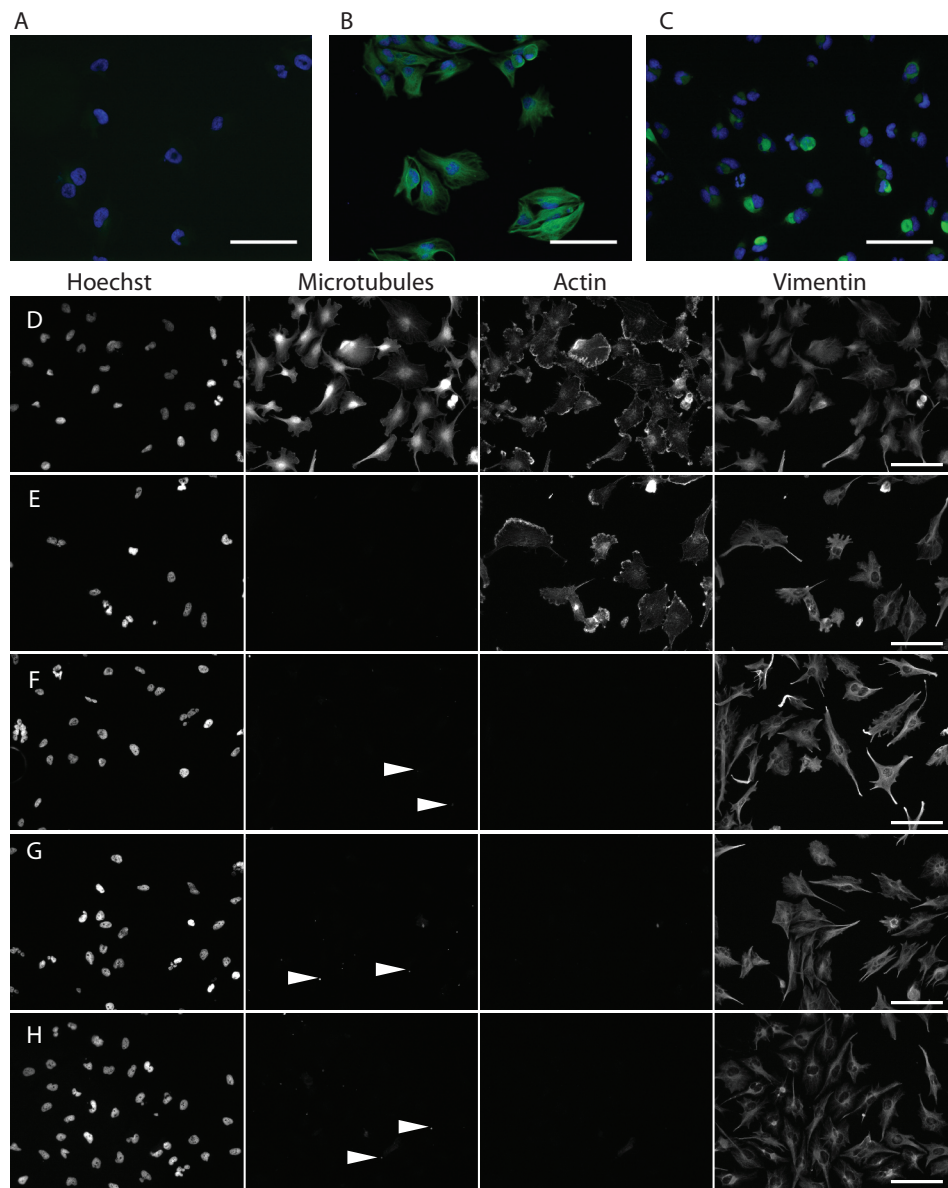
Figure 1. Generation of clonal lines and intermediate filament extraction

(A-C) A cell line was derived of the U251 line by clonal selection. This clonal line was subsequently transduced with mCherry, GFAPα or GFAPδ. These cells were again clonally picked to obtain a 100% transduction efficiency and immunostained for GFAP (green). Nuclei were counterstained with Hoechst (blue). In the control cells, a very faint GFAP network is present (A). In the GFAPα⁺ cells, clear networks of GFAP can be seen extending throughout the cell (B). In the cells transduced with GFAPδ, the GFAP network is collapsed into a juxtanuclear aggregate.

(D-H) To extract the intermediate filament network, the cells were exposed to two subsequent steps to first remove soluble content and then to remove polymerized actin. mCherry cells were fixed by a standard procedure and directly stained or immunostained for nuclei (Hoechst),

position of the particles, the annotation of the position in the local network had to be done manually. To this end, four categories of particles were formed: 1) extracellular: particles outside of the cells (coloured white), 2) cell periphery: cells close by the cell edge, often also based on whether the IFN showed a transition from a more homogeneous network to more aligned fibre-like organization (coloured yellow), 3) nuclear contact: particles on top/below the nucleus or touching the outer edge of the nucleus (coloured blue), 4) center of cytoplasm: particles in the rest of the cellular network (coloured green) (Fig. 2D). For the GFAPδ^+ cells contact with an aggregate (which is the collapsed IF network) was a separate category (not shown).

The trajectories found for the different particles within a single movie all displayed similar shapes signifying drift of the setup (usually in the order of 100 nm / 60 s; Fig. 2E). Therefore a drift correction per particle was performed based on a LOESS smoothing algorithm, resulting in displacements of 10-100 nm over 60 seconds that could be subtracted from the trajectory (Fig. 2F).

The trajectories were smoothened using a LOESS algorithm, with different α values tested for drift extraction. An α of 0.1 resulted in smoothing the displacement over longer time scales and was used for drift correction. This drift correction was calculated per individual particle, as calculating this over the ensemble of particles in a movie where one or two particles were more mobile than the rest, would result in artificially enlarged displacements for the immobile particles. An example is shown of a stable particle with smoothened drift extraction (Fig. 3A-C) compared to a mobile particle drift with smoothened drift extraction (Fig. 3D-F). It is clear that the drift in the x-direction is similar for both particles (Fig. 3A&D), but the mobile particle is less affected by the drift in the y-direction (Fig. 3B&E). After this correction another LOESS fit was performed with an $\alpha = 0.01$ on the individual particles. This revealed a periodically oscillating drift of 2 Hz present in the sample, with an

(Figure 1 continued) microtubules, actin (phalloidin) and vimentin. When cells were fixed before permeabilization, microtubules, actin and vimentin were all present inside the cell (D). When cells were permeabilized before fixation, microtubules were lost with the soluble pool of proteins, but polymerized actin and the intermediate filament network were retained (E). Treating the permeabilized cells with gelsolin resulted in removal of the actin network, keeping the intermediate filament network intact (F). Similar results of the two-step skeletonization procedure were obtained with the GFAPα^+ (G) and GFAPδ^+ (H) cell lines. Curiously in the conditions the experiment was performed, the IF collapse has a much lower frequency than in the conditions the clonal line was verified (possibly due to adhesion to laminin-coated glass vs uncoated glass respectively). Also the particle tracking was performed on laminin-coated glass.
Note that in some cells specks of tubulin immunofluorescence were still present (arrowheads), which likely represented the microtubule organizing center that is not as soluble as the microtubule-forming tubulin.
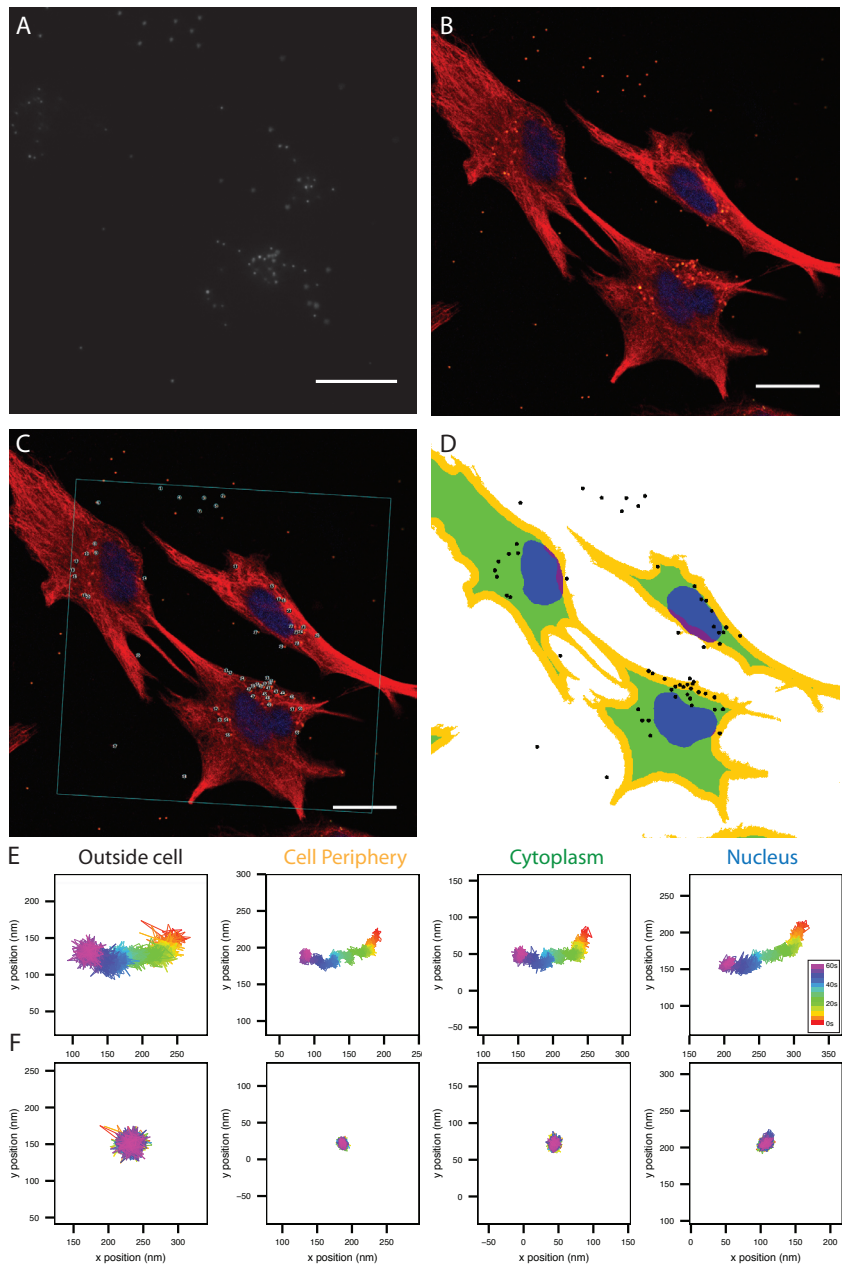
Figure 2. Particle tracking and annotation of particles
Movies were made to track the mobility of fluorescent particles in the cell cultures after o/n incubation with a 100x magnification objective. A frame of a movie (3119 frames, 62.38 s) is shown (A). To be able to assign the location of each particle to a cellular position, IFNs were fixed with PFA, stained for vimentin, and imaged with confocal fluorescence microscopy after tracking the particles (B). The process of finding back the original cells was done by hand, and the cells were imaged in a round petridish, therefore there was a slightly rotated angle in the confocal microscopy

amplitude of ca. 5 nm (Fig. 3G). The trajectories were not corrected for this periodic displacement, as the periodic displacements for particles within the same movie varied in amplitude. Therefore the two options available for correcting, i.e. subtracting the averaged displacement of the ensemble of particles or subtracting individually smoothened displacements with $\alpha = 0.01$, would not improve the data. The periodic displacement is likely imposed by an external force, and the difference in displacements between particles may in principle contain information about the local mechanical properties of the network. The MSDs extracted from two different particles, one immobile (Fig. 3H), the other relative mobile (Fig. 3I), were compared with or without drift correction. The MSDs of both particles were affected by the drift correction. The theoretical line of MSD = 4Dt, representing free 2-dimensional diffusion in water at 315 K, is represented by the dotted line going through the origin of the graph. The difference between this steep curve and the measured MSDs illustrates the highly restricted mobility of the particles (Fig. 3H-I).

A difference in mechanical properties at different locations in the cell has been reported for keratin networks (Sivaramakrishnan et al., 2008). Therefore we first investigated if this was the case in our recordings (Fig. 4A). At first glance the particles displayed a very restricted mobility, but we decided to compare the values of the MSD(τ=10) between cellular regions. For highest statistical power, all network recordings of the 0.5 um beads were included, regardless of the nature of the IFN. Four separate locations of particles were included in the analysis: extracellular (Median = 95.63 nm^2, N=213, IQR: 51.55-275.40), cellular periphery (Median = 99.86 nm^2, N=251, IQR = 60.39-212.00), center of cytoplasm (Median = 86.73 nm^2, N=505, IQR = 49.86 – 158.8), and particles making nuclear contact (Median = 78.18 nm^2, N=316, IQR = 51.17-155.40). Particles that were assigned to multiple location categories were excluded (e.g. a particle attached to the outside of a cell would be in both the "extracellular" and "periphery" categories). The Shapiro-Wilk test for normality rejected the null hypothesis of the normal distribution of the data points

(Figure 2 continued) compared to the particle tracking microscopy. An algorithm was developed in ImageJ to correlate the objects identified in the particle tracking microscopy analysis with the confocal image, based on a comparison between the positions of two recognizable particles in both images. The frame of the tracking camera is outlined with the cyan square, whereas all overlaid particles are encircled and labeled with their identifier from the video analysis (C). All particles that were confirmed to be single particles were manually annotated to their location in the cell based on four main regions: extracellular (white), cellular periphery (yellow), cytoplasmic (green), or nuclear (blue) (D). Sample trajectories were plotted with a rainbow colour code for time, (t_0=red, t_{max}=violet) from the various regions in the cell before correction for drift (E) and after correction for drift (F). The plotted area amounts to approximately 1 pixel size (0.194 um^2), with the vast majority of the particles displaying subpixel mobility. Scale bars: 20 μm.

measured for the samples, therefore non-parametric tests were performed on the data. The hypothesis that different particle mobility occurs in different cellular locations was tested with a Kruskal-Wallis rank sum test. This test reported a significant difference between the subcellular locations, H(3)=12.57, p = 0.0057. To identify the groups that significantly differed from other groups, a Dunn's post hoc test was performed, with a False Discovery Rate correction for multiple testing. This revealed a significant effect of bead location on the MSD(τ=10), with beads in contact with the nucleus and beads in the central cytoplasm being less mobile than beads in the periphery (Fig. 4A). Surprisingly, beads at extracellular locations, which were expected to be stuck to the glass, had a bigger spread in MSD(τ=10) than the intracellular beads. Further analysis of the data implied this spread in the extracellular beads originated solely from a high mobility of extracellular beads in the GFAPα^+ condition compared to the control and GFAPδ^+ conditions (Fig. 4D).

To investigate the effect of the presence of GFAPα or GFAPδ in the IFN, we compared the mobility of beads that were trapped by the cytoskeletal network and were neither in contact with the nucleus nor at the cell periphery. Therefore the beads in the central cytoplasm location were tested for the effect of IFN composition: Control (Median = 102.60 nm^2, N = 168, IQR = 62.58-174.10), GFAPα (Median = 80.30 nm^2, N = 231, IQR = 49.16-171.10), and GFAPδ (Median = 68.95 nm^2, N = 106, IQR = 40.96-127.60). The hypothesis of different mobility in different IFNs was tested with a Kruskal-Wallis rank sum test. This test reported a difference between the different networks, H(2)=15.41, p < .001. To identify which groups differed significantly from the other groups, we performed a Dunn's post hoc test. This reported a different mobility of particles between all groups in the order of GFAPδ < GFAPα < control (Fig. 4B).

We expected to observe many complete IFN collapses in the GFAPδ condition. Surprisingly, the percentage of cells with collapses in the MPTM experiment was a lot lower than the fraction when we initially verified the cell line (38% vs 100%, Fig. 1H vs 1C). Therefore, we were unable to reliably test the effect of collapsed networks on bead mobility. To investigate whether network collapses had an effect on bead mobility, we studied the data for the GFAPδ samples per cellular location. However, the number of beads in contact with aggregate was low (periphery and collapse: N=9, central cytoplasm and collapse: N = 21, nucleus and collapse: N=13). Therefore we pooled all intracellular beads and tested with Wilcoxon's rank sum test for a difference between beads in the network (Median = 76.09 nm^2, N = 235, IQR = 45.56-129.52) versus beads at collapses (Median = 121.46 nm^2, N = 43, IQR = 54.77-229.57). A significantly higher mobility was observed for the beads in contact
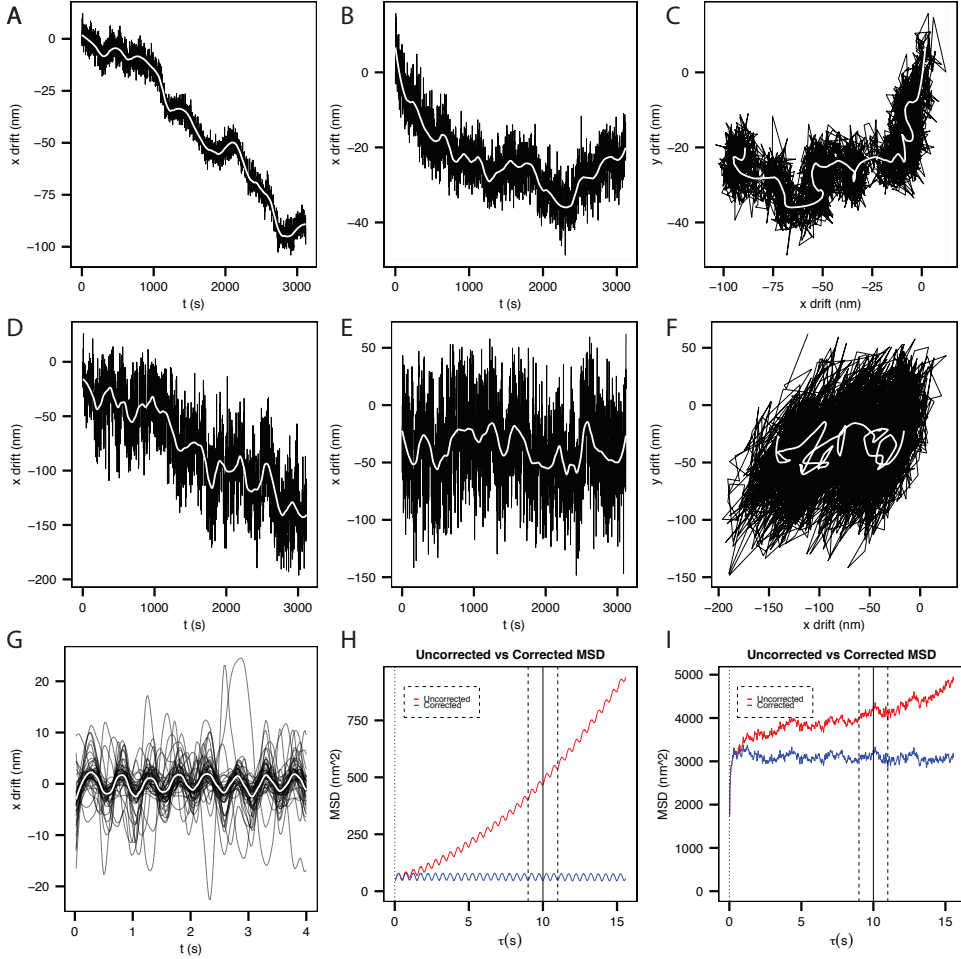
Figure 3. Extraction of the MSD from the trajectories of particles embedded in IFNs

(A-F) Calculation of the drift of two objects based on a trajectory smoothened with a LOESS local regression algorithm (α= 0.1), comparing a relatively static particles (A-C) and a relatively mobile particle (D-F). Shown is the displacement over time for x (A, D) and y (B, E) and the resulting trajectory in x and y (C&F), with the trajectory in black and the calculated drift in white. (G) After correction for this calculated drift per particle, a periodic oscillation of 2 Hz was still observed in the individual particles when smoothened with a LOESS with α= 0.01 (black traces) as well as in the ensemble of the particles (white, mean of all smoothened fits). No correction was performed for this oscillation. (H-I) The extracted MSD was plotted against the lag time extracted for the uncorrected and the corrected data, for either the relatively static particle (H) or the relatively mobile particle (I). The dotted line going through the origin of the graph represents the MSD=4Dt relation expected for Brownian motion of 0.5 um particles in water at 315K, illustrating that both particles display highly restricted displacements. For further statistics the MSD($<\tau$=10s>) (vertical line) was used to compare the amplitude of motion between conditions. MSD($<\tau$=10s>) was calculated by averaging the MSD($<9s\leq\tau<11s>$) (dashed lines), to eliminate the periodic variation found in Fig. 3G.
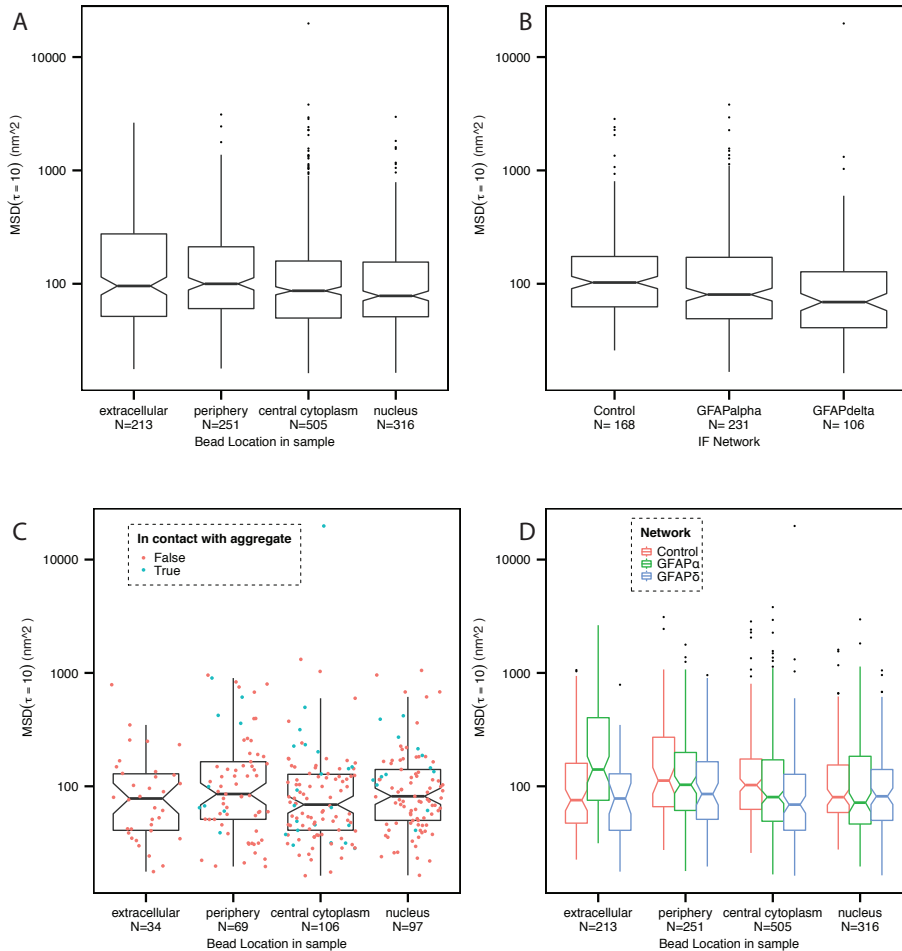
Figure 4. Analysis of the MSD(τ=10s) as a function of cellular location and IF network composition
(A) The MSD(τ=10s)was determined for all particles meeting the inclusion criteria. All the GFAP isoform conditions were pooled to detect if there was an effect of the location of the particle in the cell on the MSD. Particles that could not unambiguously be assigned to a single category were excluded from analysis.

(B) GFAP network effect on the MSD of particles localized in the cytoplasm. Boxplots show the distribution of the MSD(τ=10s) in a cell with a control network, a GFAPα network, or a GFAPδ network. To probe only particles trapped by the network, and not by the nucleus or the cell edge, only particles classified as cytosolic were taken into account. Cells with a GFAPα or GFAPδ network showed a slightly but significantly reduced MSD(τ=10s).

(C) As the GFAPδ cells were in some cases loaded with a collapse of IFs, we separately plotted the effect of location of a particle in a cell with a GFAPδ network and indicated the effect of the particle being in contact with an aggregate (blue dots in contact with aggregate, red dots not in contact with aggregate, boxplots represent all datapoints).

(D) An overview of the effect of particle location per IFN. It shows a decrease in MSD(τ=10s) for GFAPα⁺ and GFAPδ⁺ at the cell periphery and cytoplasm, and an unexpected increase in MSD(τ=10s) for the GFAPα⁺ extracellular particles in contrast to control and GFAPδ⁺.

with a collapse $W_s = 3300$, p = 0.016 (Fig. 4C).

Discussion

GFAP is the signature IF of astrocytes and astrocytoma cells. The protein is highly regulated in development and disease, but the effect it has on cell mechanics has not unequivocally been demonstrated. Two studies investigating this in living cells by AFM probing described either increased or decreased stiffness with increasing GFAP expression (Lu et al., 2010; Miller et al., 2009). Here we implemented a different method based on MPTM to study whether a change in IF composition will result in different mechanics of the IFN extracted from cells. Our data indicate increased stiffness of the IFN with increasing GFAP expression, but the method is not sensitive enough for the IFN and should be supplemented with active probing methods to extend the range of sensitivity. Here we will discuss the technical aspects and challenges met in our approach. Finally we will give some suggestions for further investigation into the effect of IFN composition on IFN mechanics.

In this study we used MPTM as a method to investigate the mechanical properties of different compositions of cell-extracted IFNs of astrocytoma cells. This method has been used in various other studies before to investigate cellular mechanics in living cells (Daniels et al., 2010; Guo et al., 2014; Kole et al., 2004) or in vitro constituted gels of biopolymers (Apgar et al., 2000; Aufderhorst-Roberts et al., 2014). Here we used an approach in between *in vitro* and *in vivo* (in cell), by probing networks constructed by cells and subsequently extracted for mechanical tests, as described before for keratin networks (Sivaramakrishnan et al., 2008). This has the advantage that the complexities originating from 1) the many different proteins contained by the cell and 2) the active forces exerted by the cell are greatly reduced or no longer of concern. The first point is extra relevant in the case of IFs since they do not only have a mechanical function in the cytoskeleton, but are emerging as important signaling platforms with interactions with, and regulatory functions for, actin and microtubule networks (Helfand et al., 2011; Ivaska et al., 2007; Jiu et al., 2015; Sakamoto et al., 2013). A recent study by Guo et al gives a good example of the implications of active forces in cellular microrheology (Guo et al., 2014). They compared particle displacements in normal cells to cells where active transport had been blocked by either ATP depletion or by applying an inhibitor of non-muscle myosin II, the main protein responsible for the active forces in cells (Koenderink et al., 2009). In the cells with active transport, particles showed behaviour reminiscent of unhindered Brownian diffusion. However, inhibition of active transport rendered the MSDs nearly time independent, effectively implying elastic behaviour

6

of the cytosol (Guo et al., 2014). The time independent behaviour we observe in the extracted IFNs seems consistent with this observation of the necessity of active forces for diffusive behaviour in a cytoskeletal network, although we lack of course the microtubules and actin filaments.

The main challenge in the current study was that the displacements of the particles in the IFN networks were small. Although comparable to the trajectory size in the earlier study on keratinocytes, we could not extract viscoelastic behaviour from the data (Sivaramakrishnan et al., 2008). This made the system very sensitive to noise and resulted in difficulties determining the actual trajectories of the particles. In a first approach, centroids were determined using an often used algorithm (Crocker et al., 1996). This method identifies features based on local maxima, meeting the proper criteria expected from the particles under study (e.g. size and brightness). However this method was sensitive to the shifting of a local maximum from one pixel to the next, and this would often result in a calculated displacement larger than the subpixel Brownian motion of the particle. Therefore we switched to a more robust method of particle center determination, based on the calculation of the radial symmetry center (Parthasarathy, 2012). This method is less sensitive to the signal to noise ratio, and in our experience also reduced the jumping behaviour induced by the displacement of the local maximum of a feature. This method indeed reduced the number of artefacts found in particle tracking. With this improved precision of particle localization, displacements remained very small, and were dominated by the drift of the sample (Fig. 2E). After subtraction of the drift, the trajectories of the particles were likely close to the resolution limit of our setup. However, despite these small displacements, differences could still be observed between particles based on location in the cell (Fig. 4A). It is possible that the differences observed between cellular locations are caused by the position of the particles above or below the focal plane. We inspected whether particle intensity, as a measure of out-of-focusness for a particle, had an effect on MSD. Although low particle intensity did result in a narrower distribution of MSD(τ=10), the particles at different cellular locations had a similar distribution across particle intensity (not shown). With the small displacements observed in our experiments, the errors of the measurement become a large contribution of the trajectories measured. For MPTM, there are two main contributions to the error of a measurement, the static error and the dynamic error. The static error depends on the signal to noise ratio of the image of a particle, and determines the effective spatial resolution of the setup, whereas the dynamic error originates from the motion of a particle during the recording of a frame and is shutter time dependent (Savin and Doyle, 2005a).

Cytoskeletal networks were modelled as a Kelvin-Voigt viscoelastic material, where at short time scales particles display diffusive behavior (MSD scales with power 1), whereas at longer time scales they can reach a plateau phase, where elastic properties dominate. Savin and Doyle demonstrated that especially in the case where the shortest lag time is too short to determine the diffusive behavior, the MSD in the plateau phase will be underestimated (Savin and Doyle, 2005b). With the dataset currently available, the dynamic error cannot be determined, as extensive calibrations are required for this. Therefore we cannot extract the viscoelastic modulus from the measured particles trajectories by the methods that have been developed for MPTM. The static error of our measurement could be extracted from immobile particles. Although initially we intended to determine this based on the displacement of particles attached to the glass, we observed smaller MSDs in the case of cells embedded in the network, especially when in contact with the nucleus (Fig. 4). Also the particles that are located extracellularly are not sticking to the glass directly, as this has been coated with a layer of both PLL and laminin before experiments. Laminin is an extracellular matrix protein that can have its own mechanical properties, depending on the thickness of the laminin layer deposited on the glass slide. Without clearly defined immobile particles, it could be an option to determine the resolution based on the least mobile set of beads, but it is better to make a controlled sample with a larger number of beads fixed to a surface and measure the displacements in such a sample as a control for the static error.

To place our measurements into context, we determined values reported in the literature for the mechanical properties of IFNs. For cells without a vimentin component in the cytoskeleton, an elastic modulus of 5 Pa has been determined at 1 Hz by active microrheology, which increased to 9 Pa when a vimentin network was expressed (Guo et al., 2013). This is still in the context of a live cell and thus in a composite network, but also by using *in vitro* constituted networks, elastic moduli of 1-10 Pa have been reported for vimentin networks (Lin et al., 2010a, 2010b; Pawelzyk et al., 2014). If the IFN extracted from our cells has an elastic modulus in the range of 1-10 Pa, then this is indeed above the upper limit of MPTM, as this is around 1 Pa. Methods more suited to probe stiffer networks include active microrheology techniques, such as optical tweezer microrheology or magnetic microrheology (Waigh, 2005).

Apart from this inherent sensitivity limitation of the technique, there were two more limitations to our assay. Although we tried to control the particle-network interaction in a cell-derived network to the best of our abilities, two important factors were not controlled. On the one hand, the exact composition of the network,

6

both in terms of specific IF protein contributions, as well as the insoluble IF-binding proteins that are not released upon permeabilization and washing, are not known. This is clearly illustrated by the fact that the network is staying attached to the coverslip, implying that integrins and other focal adhesion proteins anchoring the network to the extracellular laminin are not washed away. On the other hand the specific interactions of the particles with the network are not controlled. The particles have a surface chemistry of carboxylate groups, which has a lower interaction with proteins than a polystyrene surface, although not as low as particles with a polyethylene glycol (PEG) surface chemistry (Valentine et al., 2004). A test was performed with PEGylated particles, but cells did not endocytose these particles. We expected the carboxylate particles to be endocytosed, and released from the endocytic vesicles by the triton treatment, after which they would be trapped in the IF network. Tests were performed to confirm this through staining for LAMP1 (a marker for late endosomes and lysosomes), but the strong fluorescent signal of the particles and subsequent bleed-through in all other microscopy channels made it difficult to interpret these micrographs (not shown). Although the particles that we observe in the tracking experiment are clearly trapped, it is not clear if this is due to specific interactions with or capture by the IFN or encapsulation by proteins in the endosome that may be linked to the IFs. Particles of 0.2 μm and 1.0 μm size showed a similar limited mobility as described for the 0.5 μm particles (not shown). The fraction of particles that showed displacements larger than pixel size (195 nm) was <1%, and most of these particles were no longer present after fixation and staining.

Although our results cannot be interpreted quantitatively, we made a semi-quantitative comparison between the tested conditions, by using the MSD(τ=10) as a measure for the stiffness of the network. We observed an effect of the intracellular localization of the particles on the apparent MSD, which is in line with earlier findings on the mechanics of keratinocytes, where particles in the periphery of the cell were more mobile than particles near the nucleus. In the keratinocytes this was attributed to the IF network around the nucleus being more dense with smaller mesh sizes, whereas at the periphery of the cell it is more sparse (Sivaramakrishnan et al., 2008). Although our confocal images do not have a high enough spatial resolution to determine mesh size, the distribution of the network can be seen to be heterogeneous (Fig. 2B). The decreased MSD of networks extracted from GFAPα and GFAPδ transduced cells as compared to control networks is intuitive, when considering all IFs to contribute to the overall network stiffness (Lin et al., 2010a). The absence of collapses in the GFAPδ^+ samples was surprising, but an effect of GFAPδ on IFN geometry could be seen, with vimentin immunoreactivity at the periphery

of the cell showing less bundles (not shown) and some collapses occurring (Fig. 1H, arrows).

Future directions

The goal of this study was to investigate the effect of a difference in IFNs with different compositions on network stiffness. In the future this method can be relevant to study IFNs from astrocytes that have been exposed to inflammatory, pathological or pharmacological stimuli to identify the mechanical effect of astrocyte reactivity or neural stem cell differentiation. Although the passive MPTM method is not sensitive enough to reliably describe the mechanical behaviour of the elastic IFN, the goal of characterizing IFN mechanics is an interesting one, as different mechanical properties have been described for different IFNs, attributed to the interactions different IF subunits have with one another (Pawelzyk et al., 2014). Therefore adding GFAPα or GFAPδ to a vimentin-dominated network, can have interesting effects on the total IFN mechanics. Although currently investigations are being done into composite networks of two-component systems containing either actin, microtubules or IFs to identify emerging properties (Jensen et al., 2014; Lin et al., 2011; Pelletier et al., 2009), the composite networks consisting of different IF proteins with their specific side arms and backbone charges, can also deliver interesting insights into network formation and material properties (Kornreich et al., 2015). The method used in this paper to extract IFNs from cells, and potentially composite networks of IFs and actin stress fibers if the gelsolin treatment is skipped, is a robust method for further studies. On the one hand, it offers perspectives for characterizing the network properties of IFNs or actin IF composite networks, polymerized and geometry defined in a cell, allowing for an in-between model for *in vitro* (test-tube network) and *in vivo* (living cell). Although, as mentioned before, the particle interactions should be characterized, by either making the particle non-sticking, or targeting it specifically to a component of interest (Valentine et al., 2004; Wong et al., 2014). For embedding the particles in the network a different technique may be required, which circumvents the endocytosis machinery of the cell. Although this is usually done by microinjection, this is a laborious process, and not very suitable for obtaining large statistics across many cells rapidly. A novel method developed to transduce cells with protein via osmosis-induced macropinocytosis may be an interesting candidate to transduce cells with tracer particles (D'Astolfo et al., 2015). To probe the skeletonized networks obtained in this way, the method should then be switched to the active microrheology procedures, to gain a broader sensitivity.

6

Acknowledgements

Chapter
7

Summary and Discussion

Summary

Astrocytes are brain cells that are essential for the brain's physiological homeostasis and they also respond strongly to a variety of pathologies that affect this homeostasis (Sofroniew and Vinters, 2010). Glioma or astrocytoma are tumours originating from deregulated astrocytes, glia progenitors or neural stem cells (Chen et al., 2012). All cells in the body have a cytoskeleton important for cell shape, motility, scaffolding and signalling processes. A hallmark of the cytoskeleton of astrocytes and glioma cells is that it contains the intermediate filament (IF) protein Glial Fibrillary Acidic Protein (GFAP). The production of GFAP is increased in high quantities in neuropathology. The gene expression of GFAP is tightly regulated in both quantity and splicing during development. Splicing of the GFAP mRNA can generate at least 10 different isoforms, of which GFAPα and GFAPδ are the most prominent isoforms in the brain. GFAPδ is enriched in the neurogenic niche and might therefore also be related to the formation of glioma. Although GFAP is already known since 1970 (Eng et al., 2000), the function of this protein and its later identified isoforms remains an open question. In this thesis we have investigated cell biological, molecular biological, and biophysical aspects of the IF network, in particular of GFAP, in astrocyte and astrocytoma biology.

In Chapter 1 we introduced IFs, more specifically type III IFs, and compared the molecular interactions and biological significance of GFAP with those of Vimentin (Vim). These proteins have a similar structure and are closely related proteins, although the N-terminal head and C-terminal tail domain of GFAP and Vim differ substantially. Despite the low degree of similarity between GFAP and Vim in the head and tail, these IF proteins do appear to be involved in similar global processes in the cell. The head and tail domains are functionally important as these domains interact with other proteins, and their high serine and threonine content make them targets for post-translational modifications. Therefore, it is likely that the two proteins have distinct specific molecular functions within astrocytes.

In Chapter 2 we induced reactive gliosis in an astrocyte cell line (astrocytoma) and in primary human astrocytes, and investigated the changes in whole genome gene expression profiles by a transcriptomics platform. To induce reactive gliosis we used a mechanical injury device that inflicted a short-lasting but severe stretch of the substrate the cells were cultured on. This approach mimics the type of injury the cells would be exposed to in traumatic brain injury. Curiously, both the astrocytoma and the primary cells used in this mechanical injury model did not reveal major changes at a transcriptional level. Several potential causes for this lack in response were investigated by changing the injury protocol. In contrast to the reported

findings of other studies, we were unable to induce astrocytosis, evidenced by GFAP increase or other related genes, by our mechanical stretching protocol, implying a strong resilience of these cultured cells to stretching injury.

In Chapter 3 we determined whether different GFAP isoforms have an effect on the IF dynamics in cultured cells. We observed that the turnover rate between the soluble and filamentous pool of GFAPδ is lower than that of GFAPα. For both isoforms, a higher expression resulted in larger focal adhesions, although this did not affect cell motility. High expression of GFAPδ resulted in a change of cell shape and induced a collapse of the complete IF network but, remarkably, without further apparent effects on cell motility and proliferation.

In Chapter 4 we investigated the role of GFAP in astrocytoma biology. So far, conflicting reports have been published on the relation between GFAP and astrocytoma malignancy. We first analysed the expression of the different isoforms in the Cancer Genome Atlas (TCGA) database. We showed that GFAPα mRNA
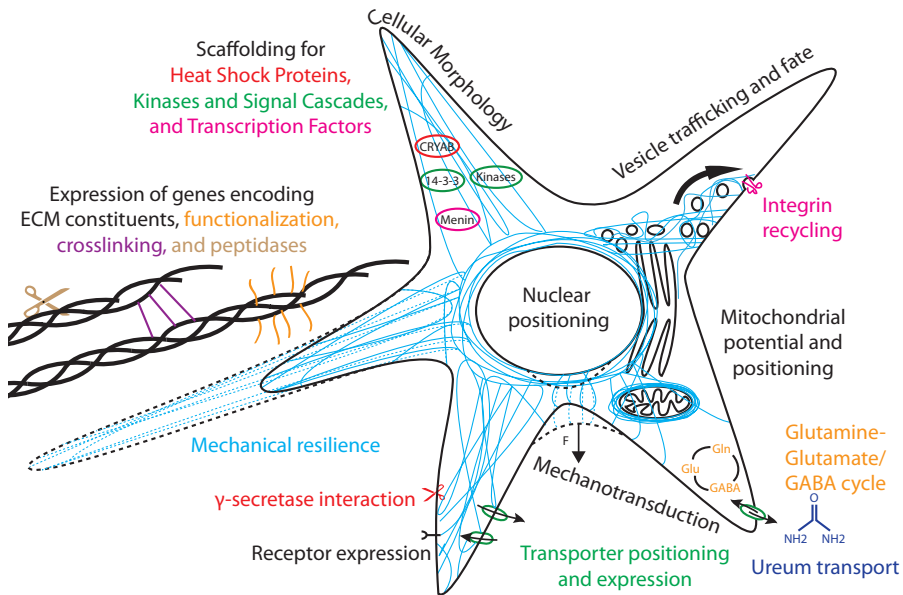
Figure 1. Molecular functions of astrocytic IFs GFAP and Vim
Displayed are various molecular functions reported in literature and discussed more in depth in the introduction, as well as functions emerging from the transcriptome profiling described in this thesis. Some functions are based upon functional interactions at the protein level, whereas others are further downstream as identified by gene expression. For mechanotransduction, integrin recycling, vesicle trafficking and fate, and mitochondrial potential and positioning see Chapter 1. Colour code in the figure text relates to the depictions in the similarly coloured symbol that is closest by.

7

expression declines with increasing malignancy while GFAPδ expression remains at a constant expression level. Together this results in an increase in the GFAPδ/α ratio, which could reflect a measure of stemness, since GFAPδ is highly expressed in neural stem cells. To determine the downstream changes in gene expression induced by an increase in GFAPδ/α ratio, we modulated the GFAP isoform content in different astrocytoma cell lines. By microarray transcriptome analysis we found that changing the GFAPδ/α ratio changes the expression of genes relevant for direct and indirect cell interactions with the external environment, including the extracellular matrix and the interaction with other cells. Projecting this *in vitro* dataset on the TCGA patient data revealed 8 target genes that are involved in tumour malignancy and are regulated by the GFAP isoform ratio. Most importantly, the expression of these genes is prognostic for patient outcome.

In Chapter 5 we analysed mRNA transcript profiles of acutely isolated astrocytes and microglia from GFAPko and VIM-GFAPko mice. Similar to the findings in Chapter 4 it became clear that GFAP and Vim are both involved in cell-environment interactions. For Vim, an added role in angiogenesis emerged as an overrepresented ontology. The analysis of microglia, the brain's innate immune cells, in the GFAPko revealed that prominent transcriptional changes take place in these cells induced by GFAPko in the astrocytes. This supports the finding of a function of GFAP in cell-environment interaction. We generated gene clusters based on their expression patterns and identified genes regulated by GFAP, Vim, or both GFAP and Vim. This approach revealed multiple mRNA downstream targets of GFAP and Vim, as well as transcripts regulated by the modulation of only one of the two IF proteins, implying both distinct and shared pathways downstream of GFAP and Vim.

In Chapter 6 we investigated the contribution of GFAPα and GFAPδ to cell mechanics, a well-established function of IFs. Using skeletonized IF networks stripped from other cytoskeletal components, we were able to probe the pure mechanical contribution of GFAP isoforms to IF network mechanics. This was done by the multiple particle tracking microrheology method, which revealed that the increase of both GFAP isoforms had a stiffening effect on the network.

In conclusion, we found evidence that GFAP is involved in the communication between cells or between cells and the extracellular matrix and that GFAP contributes to the mechanical properties of the cell (Fig. 1). In the following discussion I will focus on a few common themes emerging from the transcriptome analyses and make suggestions for further paths of investigation to take in order to narrow down molecular mechanisms that are regulated by GFAP and other IF proteins in astrocytes.
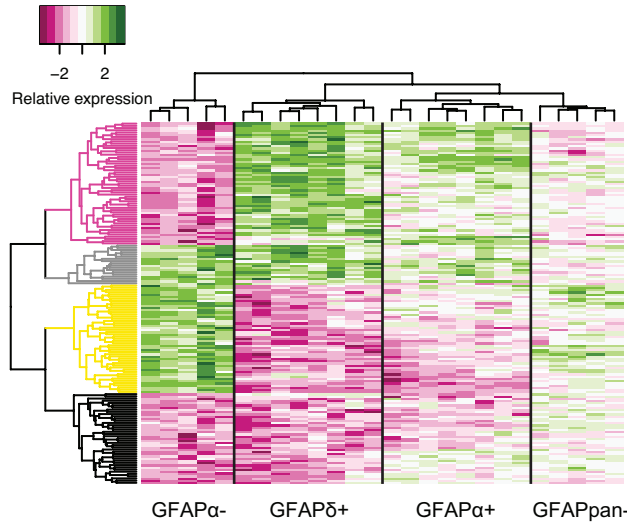
Figure 2. Heatmap of GFAP isoform modulated expression, adapted from Chapter 4.
Clustering of the scaled expression changes revealed 4 main clusters of genes, dominated by parallel or opposite changes in expression of these genes between GFAPδ+ and GFAPα-, as indicated by different colors in the dendrogram (purple, yellow: opposite; gray, black: parallel).

Emerging common molecular mechanisms controlled by GFAP

In Chapters 4 and 5 we modulated the compositions of the GFAP IFs and performed a transcriptomics analysis. Combining these data, that were gathered from *in vitro* in human cell lines and *in vivo* mouse astrocytes, revealed novel common molecular pathways that are regulated by the composition of the IF network.

First, we explored more in depth the consequences of modulating the GFAP network in astrocytoma cells in vitro with either a recombinant expression or a knockdown of GFAP isoforms. This analysis revealed several genes or molecular pathways that were either controlled by GFAP in general or by a change in the GFAPδ/α ratio shift. Then we searched for genes and molecular pathways that were regulated in both the human *in vitro* experiments as well as in the mouse astrocytes with different GFAP networks. The latter genes and pathways imply conserved actions induced by GFAP independent of the model system.

GFAP isoform specific responses observed *in vitro*

In the *in vitro* modulation of the GFAP network in Chapter 4, we identified two main clusters in GFAP induced differentially expressed genes (DEGs; Fig. 2). The first cluster is associated with a change in GFAPδ/GFAPα ratio. Here, we observed similar changes in expression of genes in both the GFAPα- and GFAPδ+ conditions (i.e. up or down in both conditions). This cluster was enriched for genes coding for growth factor

7

GFAPδ/α isoform ratio dependent	Gene Function	GFAP dependent	Gene Function
KDR	GF signalling	**AJAP1**	Adherens Junction
BAIAP2L1	GF signalling	**CRYAB**	Heat Shock Protein
KIAA1217	Unknown	**LEPREL1**	ECM modifier
SLC1A3	Glu transporter	**RAMP1**	CGRP receptor processing
ACP5	ECM modifier	**A2M**	Peptidase
PRKCZ	Kinase	**AKR1C1**	Progesterone metabolism
GGTLC1	Glutathione metabolism	*TRIML2*	P53 regulation
PLEKHS1 (C10orf81)	Pleckstrin domain	*LAMA1*	ECM protein
ERBB2	GF signalling	*OGDHL*	Oxoglutarate dehydrogenase
RNF150	Ubiquitination?	*NRXN3*	Axonal guidance

Table 1: Genes that correlate with either GFAPδ/α ratio or with total GFAP, based on Chapter 4
Genes written in bold correlate positively with GFAPδ/α or GFAP, whereas genes in italics correlate negatively. GF: Growth Factor; Glu: Glutamate; CGRP: Calcitonin-gene-related peptide. Gene functions based on Maglott et al., 2011.

receptors. We expected to find an opposite regulation in the GFAPα[+] condition, but interestingly this was not the case (Fig. 2). A possible cause could be that GFAPδ is sequestered by GFAPα, and that the ratio-dependent genes respond particularly to high unsequestered GFAPδ. Under physiological conditions GFAPα is 10 times higher expressed than GFAPδ, so more GFAPα will not cause a drastic change in IF stoichiometry and GFAPδ sequestering. In contrast more GFAPδ will change the IF network and will lead to a collapse (Chapter 3, Fig. 1). In the GFAPδ[+] and the GFAPα[-] condition another similarity is that the amount of GFAP that is close to the cell membrane is reduced, in the first case due to reduced total GFAPα, in the other case due to the collapse of the network (Chapter 4, Sup. Material 2). The IF network forms a scaffold for phosphatases and kinases, and therefore these enzymes can interact with different targets when the IF network is in close proximity of the cell membrane. In addition, modulation of GFAP in astrocytes, as well as different IFs in other cell types, results in mislocalization of membrane proteins, which may be dependent on the membrane proximity of the IF network (Alam et al., 2013; Hughes et al., 2004; Ivaska et al., 2005). The second cluster contains the GFAP-dependent genes (Fig. 2). These were either positively or negatively correlated to the level of

GFAP expression, regardless of the isoform. Table 1 shows the 10 genes with the most significant changes in these two groups of DEGs, i.e. GFAPδ/α-ratio-dependent and GFAP-dependent genes.

A logical question is whether this list of genes also pops up in the astrocytoma samples from patients. In the analysis of the TCGA data (Chapter 4) we showed that GFAPα expression was significantly downregulated in high-grade tumours. This is mimicked by the GFAPα- condition in the astrocytoma cell line experiment. However, the picture that is emerging from comparing the TCGA and the GFAPα-condition showed that some of the targets identified in the *in vitro* study were not correlated to GFAP in the patient data from the TCGA. As the TCGA data is obtained from RNA-samples taken from a biopsy, this gives very local information of the tumour, whereas the full astrocytoma tumour environment is hallmarked by its pluriformity. Therefore, the expression of genes at the rim of tumour could differ from the core of the tumour. A good analogy of this concept is given by the specific keratin-14 expression of the invasive front of a 3d breast cancer model, which is essential to give the front a basal-epithelial phenotype (Cheung et al., 2013), or the increased expression of Vim at the leading edge in a lens epithelium wound healing (Menko et al., 2014). Hence, our *in vitro* targets are of interest for tumour biology in patients, but the heterogeneity of specific tumour cell populations needs to be taken into account.

GFAP modulation induces gene clusters involved in Extracellular matrix remodelling and cell-cell signalling

In Chapter 5 we isolated astrocytes from mice lacking GFAP. By comparing the gene ontology analysis of Chapter 4 on human astrocytoma cell lines with Chapter 5 on primary mouse astrocytes we observed an overrepresentation of two ontologies relevant for both tumour biology and astrocytes in physiology and pathology. The first is extracellular matrix (ECM) remodelling. This process is essential for brain tumours to grow and metastasize. On the one hand tumours have to degrade the ECM barrier to allow for infiltration. On the other hand the ECM environment of the tumour itself has to meet requirements for maintenance of the various heterogeneous populations of tumour cells present in the tumour, ranging from a tumour stem cell population to the vasculature of the tumour (Wang et al., 2010). A functional analysis in Ingenuity Pathway Analysis (IPA) performed in Chapter 4 predicted an enhancing effect on invasion of tumours in the GFAPδ+ condition, in contrast to a decreased predicted invasion in the GFAPα- condition. The predicted lower invasive capacity of GFAPα knockdown cells is in agreement with the effects

7

Table 2: Typical responder genes for GFAP isoform/Vim modulation based on Gene Ontology or cross referencing the *in vitro* and *in vivo* data.

Gene Symbol human (mouse)	Gene function	FC α+	FC δ+	FC pan-	FC α-	FC Gko	FC GVko	Notes
MMP2	Peptidase	n.s.	0.6	n.s.	1.5	n.d.	n.d.	Role in tumour invasiveness, immune recruitment and vasculogenesis (Tremblay et al., 2011)
CPE	Peptidase	n.s.	0.6	(2.1)	4.9	n.s.	n.s.	Can control switch between migration and proliferation (Höring et al., 2012)
A2M	Peptidase Inhibitor	2.7	3.0	n.s.	0.2	n.d.	n.d.	Inhibits MMP2 (Fears et al., 2005)
PI15	Peptidase Inhibitor	2.3	2.5	(0.5)	0.4	n.d.	n.d.	CAP superfamily (Gibbs et al., 2008)
GLIPR1	Peptidase Inhibitor	1.6	1.4	n.s.	n.s.	n.d.	n.d.	CAP superfamily (Gibbs et al., 2008)
GLIPR2	Peptidase Inhibitor	n.s.	n.s.	0.53	0.69	n.s.	n.s.	CAP superfamily (Gibbs et al., 2008)
FBLN1	*ECM associated*	*n.s.*	*1.43*	*n.s.*	*0.54*	*1.98*	*n.s.*	*Incorporates into ECM, alters higher order structure and can activate peptidases (Twal et al., 2001)*
LAMA1	ECM	0.34	0.41	n.s	9.16	n.d.	n.d.	Component of ECM, highly important for angiogenesis, migration, neurogenesis and invasion (Kawataki et al., 2007)
LAMA4	ECM	n.s.	1.48	n.s.	0.67	n.s.	1.7	Component of ECM, highly important for angiogenesis, migration, neurogenesis and invasion (Kawataki et al., 2007)
SPP1	ECM	n.s.	2.17	n.s.	1.57	n.d.	n.d.	Osteopontin, strongly associated to migration, invasion and stemness (Pietras et al., 2014)
ACP5	ECM Modifyer	n.s.	0.56	n.s.	0.51	0.61	n.s.	Unique phosphatase of SPP1 (Lausch et al., 2011)
LEPREL1	ECM Modifyer	n.s.	1.59	n.s.	0.37	n.s.	n.s.	Collagen IV Prolyl-3-hydroxylation (Hudson et al., 2015)
SULF1	ECM / GF Modifyer	1.90	1.95	n.s.	0.17	1.58	1.53	HSPG sulphate cleavage, GF retention altered (Joy et al., 2015; Rams-bottom et al., 2014)
SULF2	ECM / GF Modifyer	n.s.	n.s.	n.s.	n.s.	1.86	n.s.	HSPG sulphate cleavage, GF retention altered (Kleinschmit et al., 2010; Meyers et al., 2013)

Gene	Category	α+	δ+	pan-	α-	Gko	GVko	Description
ERBB2	GF Signalling	n.s.	n.s.	0.74	0.31	n.s.	0.80	EGF & Neuregulin coreceptor, risk factor in astrocytoma (Gulati et al., 2010)
KDR	GF Signalling	n.s.	n.s.	1.55	1.87	n.s.	1.63	VEGF receptor, crucial for vascularization, possible role in vasculogenic mimicry (Wang et al., 2010; Francescone et al., 2012)
IGFBP5	*GF Signalling*	*n.s.*	*1.57*	*1.51*	*0.32*	*n.s.*	*2.14*	*Binds to Insulin-like Growth factor (IGF), stabilizing it and modulating receptor interactions (Schneider et al., 2002)*
BAIAP2L1	GF Signalling	n.s.	n.s.	1.54	1.62	n.s.	n.s.	Target and Scaffold for Insulin Signalling Cascade (Millard et al., 2007; Wang et al., 2013)
PRKCZ	Signalling	n.s.	n.s.	0.63	0.54	n.s.	0.58	Protein Kinase Downstream of EGFR signalling, inhibition reduces invasion of astrocytoma (Guo et al., 2009)
GABBR2	**Signalling**	**n.s.**	**0.61**	**1.46**	**0.56**	**n.s.**	**0.48**	**Member of a GABA-receptor complex, relevant for astrocyte-neuron interactions**
OGDHL	Signalling / metabolism	0.68	n.s.	0.37	2.27	n.s.	n.s.	Dehydrogenase of oxoglutarate, metabolite relevant as substrate of oncogenes IDH1/IDH2 (Dang et al., 2009)
THSD7A	*Signalling*	*1.36*	*1.59*	*n.s.*	*0.50*	*n.s.*	*1.53*	*Important for angiogenesis (Liu et al, 2016)*
C16orf45 (2900011O08Rik)	*Signalling?*	*n.s.*	*(0.70)*	*0.74*	*0.60*	*n.s.*	*0.56*	*Recently identified as Migration Inhibitory Protein (MINP), involved in radial migration (Zhang et al, 2014)*
NTNG1	*Axonal Guidance*	*0.69*	*0.35*	*0.59*	*1.38*	*n.s.*	*0.49*	*Growth cue for axons, promotes neurite outgrowth (Moore et al., 2012)*
SLC14A1	***Transport***	***0.41***	***1.64***	***n.s.***	***4.11***	***n.s.***	***n.s.***	***Ureum transporter, unknown function in astrocytes/astrocytoma***
CRYAB	Small Heat Shock	n.s.	n.s.	1.79	0.23	n.s.	n.s.	IF associated protein, strongest regulated gene in IDH1 mutated astrocytoma patients (Avliyakulov et al., 2014)

Entries in italics were identified by the meta-analysis. Entries in bold are the most promising targets based on consistent correlation with GFAP.
FC: Fold Change; α+: U251 GFAPα recombinant expression; δ+: U373 GFAPδ recombinant expression; pan-: U373 GFAPpan knockdown; α-: U373 GFAPα knockdown; Gko: GFAP-/- isolated astrocytes; GVko: GFAP-/-Vim-/- isolated astrocytes; Fold changes between parentheses: not significant but trend; n.d.: not detected; n.s.: not significant; ECM: Extracellular Matrix; GF: Growth Factor; CAP: CRISPS, Ag5, and Pr-1; HSPG: heparan sulphate proteoglycan; IDH1: isocitrate dehydrogenase 1, oncogene for astrocytoma

7

observed in *in vitro* studies (Moeton et al., 2014). In contrast, we observed that higher grade and more invasive astrocytoma cells lose their GFAP expression. Thus, more experiments are required on strictly defined GFAP isoform modulations to gain more insight in the specific role of GFAP versus the GFAPδ/GFAPα ratio. This regulation might even be more complex if we take into account the other 8 identified GFAP isoforms (Hol and Pekny, 2015; Middeldorp and Hol, 2011). ECM remodelling is also relevant for astrocytes both in physiology and pathology as the ECM is an essential component in physiological neuronal communication (Dityatev et al., 2010), whereas in pathology ECM remodelling is part of the gliotic response (Sofroniew, 2009). The DEGS in our experiments encompass ECM proteins, ECM protein modifying enzymes, peptidases, and peptidase inhibitors and thus modulating the GFAP network can have a large effect on the composition of the ECM (Table 2).

The second ontology overrepresented in Chapter 4 and Chapter 5 was related to the cell's interaction with its environment, and cell signalling with a focus on growth factors (Table 2). It is tempting to interpret this combination of control over ECM composition and signalling pathways as specifically relevant for multicellular organisms, the group of organisms that cytoskeletal IFs are restricted to (Kollmar, 2015).

GFAP is involved in the Glutamine-Glutamate/GABA cycle

We combined our all our datasets (astrocytoma with an overexpression or knockdown of GFAP and astrocytes isolated from GFAP knockouts) in a meta-analysis (see Box 1). The most consistent genes responding to GFAP were SLC14A1 (negatively correlating with GFAP expression) and GABBR2 (positively correlating with GFAP expression) (Table 2). These targets can either be directly or indirectly regulated by GFAP or can have functional interactions with GFAP. Therefore, SLC14A1 and GABBR2 are the most promising targets for future studies.

SLC14A1 (Solute Carrier 14A, member 1 (Kidd Blood Group)) is a transporter responsible for urea transport, mainly described to be important in kidney and erythrocytes. Urea is the less toxic form of ammonia, and a product of amino acid metabolism. Although urea is mainly considered to be produced in the liver (Weiner et al., 2015), the RNAseq database (www.brainrnaseq.org) of Barres et al. and our microarray data confirm that SLC14A1 is expressed in mouse astrocytes (Cahoy et al., 2008; Orre et al., 2014a). Note that hepatic stellate cells in the liver also express GFAP (Schachtrup et al., 2011), and that GFAP may also play a role in liver amino acid metabolism. In astrocytes metabolism of Glutamine, Glutamate and γ-aminobutyric acid (GABA) takes place, nitrogen rich amino acids. These

three amino acids play an important role in neuronal signalling. Glutamate is an excitatory neurotransmitter and GABA an inhibitory neurotransmitter. Both can be

---

Box 1: Meta-analysis

To determine highly conserved molecular pathways that are regulated by the change in the GFAP network, we investigated the overlap between the datasets in Chapter 4 (human astrocytoma cell lines) and 5 (acutely isolated mouse astrocytes) to identify common denominators. This often used strategy of meta-analysis can lead to novel findings of inconspicuous targets, as the persistent effects between different model systems may not be the same as the top of the single studies. We compared the two transcriptomics studies in this thesis using Fisher's inverse chi-square, where p-values from separate studies can be combined to calculate a combined p-value (Campain and Yang, 2010; Fisher, 1970). We applied this method to our datasets, using as input every separate p-value for GFAPδ$^+$, GFAPα$^+$, GFAPpan$^-$, GFAPα$^-$, GFAPko mouse, and VIM-GFAPko mouse, to come up with the most consistently responding genes to GFAP modulation. First, human and mouse orthologs based on gene names were identified using Ensembl Biomart, resulting in 9,957 genes represented in all datasets. If one human gene resulted in multiple mouse orthologs or if genes were represented on the array multiple times, the lowest p-values of the identified set of similar genes were used for the comparison, not taking into account direction of change. Since Fisher's inverse chi-square is known to be anti-conservative, even more so when samples are not independent (since the U251 recombinant expression, the U373 knockdown and the mouse knockout study all have multiple conditions used as separate inputs in the test), we filtered the genes of interest further for significant change in each of the three GFAP modulations. This resulted in 47 genes that were significantly changed in all paradigms. We excluded genes that were not significantly regulated in the GFAPko to leave out genes regulated by Vim or complete IF-network ablation. By comparing the genes identified in the meta-analysis with the genes identified on basis of functions in ECM or signalling, 7 genes emerged that were not identified before (Table 2, entries in italics). Note that the GFAPpan$^-$ condition is not significantly regulated in most of the genes in Table 2, possibly due to the weak response of GFAP to this knockdown condition. As the direction of change is not taken into account in this p-value based analysis, this was investigated manually, leading to the identification of GABBR2 and SLC14A1 as most promising GFAP responders.

7

taken up by astrocytes and metabolised to Glutamine, which is then transported back to neurons that can recycle it, a process known as the Glutamine-Glutamate/ GABA cycle (Walls et al., 2015). Whether urea or the urea cycle is involved in that has not been described.

GABBR2 (GABA B receptor 2) forms a G-protein coupled receptor complex with GABBR1 (Geng et al., 2013). The GABBR1 gene was also detected in astrocytes in an earlier study by our group (Orre et al., 2014b). Furthermore, GABBR2 in astrocytes binds to the astrocyte specific enzyme converting Glutamate into Glutamine, Glutamine synthethase (GS), thereby affecting localization and stability of GS (Huyghe et al., 2014). A study investigating the role of reactive astrocytes in neuronal signalling found that reactive astrocytes produced less GS. This resulted in reduced GABAergic signalling and subsequent reduced inhibition of neurons, leading to overactivity in neuronal networks, which could be rescued by providing external glutamine (Ortinski et al., 2010). Earlier studies have shown that GFAP positive reactive astrocytes responding to intrastriatal lesions are highly GABBR2 immunoreactive (Rekik et al., 2011), thereby corroborating our finding that GFAP and GABBR2 are co-regulated. In addition, GFAP with the R239C mutation, the most common mutation in Alexander's Disease, causes aggregation of GFAP. *In vitro* and *in vivo* this results in a reduction of Glutamate Transporter 1 (GLT-1) protein levels and attenuated inward glutamate transport (Tian et al., 2010). An earlier study also revealed that GFAPko mouse have altered localization of GLT-1 (Hughes et al., 2004) and that another Glutamate transporter (GLAST) interacts with GFAP (Sullivan et al., 2007), further corroborating the role of GFAP in astrocyte Glutamine-Glutamate-GABA metabolism. Concluding, we and others showed that a change in GFAP leads to changes in proteins involved in the regulation of the Glutamine-Glutamate/ GABA cycle, thereby affecting neuronal communication.

Mechanisms of GFAP regulated gene expression

One question not addressed elsewhere in this thesis is how GFAP regulates the expression of all the other genes that are differentially expressed in our analyses. Therefore we performed an Ingenuity Pathway Analysis (IPA) for regulators upstream of all the DEGs identified in our studies.

The astrocytoma IPA upstream analysis revealed two candidate key regulators: TGFβ and IL6 (interleukin 6). Both signalling pathways were predicted to be significantly activated in the GFAPδ+ cells, and predicted to be significantly inhibited in the GFAPα- cells. TGFβ has both antitumour as well as tumorigenic properties. It is involved in stemness, angiogenesis, invasion, treatment resistance

and immunosuppression as reviewed by Joseph et al (Joseph et al., 2013). Various genes involved in the extensive TGFβ signalling pathway are altered in our GFAPα⁻ cells, with a significant upregulation of NOG (Noggin; 1642%, FDR<.001) and downregulation of BAMBI (BMP and activin membrane-bound inhibitor; 42%, FDR<.001). NOG can bind and inactivate members of the TGFβ family, and BAMBI is a pseudoreceptor for TGF family members, without an intracellular signalling domain. IL6 promotes invasion and angiogenesis in astrocytoma, whereas IL6 or IL6 receptor targeted interventions reduces astrocytoma stem cell survival and tumour size in xenograft studies (Liu et al., 2010; Wang et al., 2009).

An important and interesting question is how GFAP modulation could alter signalling by TGFβ and/or IL-6. GFAPδ can bind to presenilin-1, which is the active enzymatic part of the γ-secretase complex (Li et al., 2006; Nielsen et al., 2002). The γ-secretase enzyme can cleave two TGFβ receptors: TβR1 and betaglycan (Blair et al., 2011; Gudey et al., 2014), as well as process the IL-6 receptor (Chalaris et al., 2010). We hypothesize that turnover of the respective TGFβ and IL-6 receptors can be regulated or coordinated by the presence of GFAP, either through GFAP modulation of the γ-secretase activity, or by GFAP altering receptor endocytosis. From studies on the VIM-GFAPko, it is known that astrocyte IFs play a role in vesicle trafficking, and that Notch signalling is altered due to a reduced Jagged1 vesicle content and reduced Notch endocytosis (Potokar et al., 2010; Vardjan et al., 2012; Wilhelmsson et al., 2012). It is known that Notch signalling strongly interacts with TGFβ signalling pathways, providing an alternative path of GFAP mediated changes downstream of TGFβ (Andersson et al., 2011; Borggrefe et al., 2016).

The genes altered by *in vivo* GFAPko were also analysed by IPA upstream analysis, but here the lowest p-value of upstream regulators was determined to be TNFα, with lower confidence scores. This may represent a difference between tumour versus astrocyte biology, or may be due to the much more complex biology of long-term GFAPko in astrocytes in contrast to the relatively straightforward and direct GFAP modulation in cell lines.

Conclusion

We have found that changes in GFAP have an impact on ECM remodelling and cell-cell signalling genes. Our data provide insight into (1) the mechanisms regulated by GFAP and its isoforms, and (2) the effect of the stoichometry of the GFAP isoforms on the integration of signalling in astrocytoma. Combining this data with the *in vivo* data revealed further evidence for the effects changes in GFAP isoform and/or Vim expression have on cell signalling and the ECM composition.

7

Unexpected candidates emerging from the combination of these datasets were the GABBR2 and SLC14A1 genes, further opening the possibility of a role of GFAP in the regulation of the Glutamine-Glutamate/GABA cycle.

References

Abudara, V., Roux, L., Dallérac, G., Matias, I., Dulong, J., Mothet, J.P., Rouach, N., and Giaume, C. (2015). Activated microglia impairs neuroglial interaction by opening Cx43 hemichannels in hippocampal astrocytes. Glia 63, 795–811.

Ahmed, S.M., Rzigalinski, B.A., Willoughby, K.A., Sitterding, H.A., and Ellis, E.F. (2000). Stretch-induced injury alters mitochondrial membrane potential and cellular ATP in cultured astrocytes and neurons. J. Neurochem. 74, 1951–1960.

Alam, C.M., Silvander, J.S.G., Daniel, E.N., Tao, G.-Z., Kvarnström, S.M., Alam, P., Omary, M.B., Hänninen, A., and Toivola, D.M. (2013). Keratin 8 modulates β-cell stress responses and normoglycaemia. J. Cell Sci. 126, 5635–5644.

Alexa, A., Rahnenführer, J., and Lengauer, T. (2006). Improved scoring of functional groups from gene expression data by decorrelating GO graph structure. Bioinforma. Oxf. Engl. 22, 1600–1607.

Alexandru, A., Jagla, W., Graubner, S., Becker, A., Bauscher, C., Kohlmann, S., Sedlmeier, R., Raber, K.A., Cynis, H., Ronicke, R., et al. (2011). Selective Hippocampal Neurodegeneration in Transgenic Mice Expressing Small Amounts of Truncated A Is Induced by Pyroglutamate-A Formation. J. Neurosci. 31, 12790–12801.

Al-Mutairi, M.S., Cadalbert, L.C., McGachy, H.A., Shweash, M., Schroeder, J., Kurnik, M., Sloss, C.M., Bryant, C.E., Alexander, J., and Plevin, R. (2010). MAP kinase phosphatase-2 plays a critical role in response to infection by Leishmania mexicana. PLoS Pathog. 6, e1001192.

Anderson, M.A., Ao, Y., and Sofroniew, M.V. (2014). Heterogeneity of reactive astrocytes. Neurosci. Lett. 565, 23–29.

Anderson, M.A., Burda, J.E., Ren, Y., Ao, Y., O'Shea, T.M., Kawaguchi, R., Coppola, G., Khakh, B.S., Deming, T.J., and Sofroniew, M.V. (2016). Astrocyte scar formation aids central nervous system axon regeneration. Nature 532, 195–200.

Andersson, D., Wilhelmsson, U., Nilsson, M., Kubista, M., Ståhlberg, A., Pekna, M., and Pekny, M. (2013). Plasticity Response in the Contralesional Hemisphere after Subtle Neurotrauma: Gene Expression Profiling after Partial Deafferentation of the Hippocampus. PLoS ONE 8, e70699.

Andersson, E.R., Sandberg, R., and Lendahl, U. (2011). Notch signaling: simplicity in design, versatility in function. Development 138, 3593–3612.

Andreiuolo, F., Junier, M.-P., Hol, E.M., Miquel, C., Chimelli, L., Leonard, N., Chneiweiss, H., Daumas-Duport, C., and Varlet, P. (2009). GFAPδ immunostaining improves visualization of normal and pathologic astrocytic heterogeneity. Neuropathology 29, 31–39.

Apgar, J., Tseng, Y., Fedorov, E., Herwig, M.B., Almo, S.C., and Wirtz, D. (2000). Multiple-Particle Tracking Measurements of Heterogeneities in Solutions of Actin Filaments and Actin Bundles. Biophys. J. 79, 1095–1106.

Ardini, E., Sporchia, B., Pollegioni, L., Modugno, M., Ghirelli, C., Castiglioni, F., Tagliabue, E., and Ménard, S. (2002). Identification of a Novel Function for 67-kDa Laminin Receptor Increase in Laminin Degradation Rate and Release of Motility Fragments. Cancer Res. 62, 1321–1325.

Arscott, W.T., Tandle, A.T., Zhao, S., Shabason, J.E., Gordon, I.K., Schlaff, C.D., Zhang, G., Tofilon, P.J., and Camphausen, K.A. (2013). Ionizing radiation and glioblastoma exosomes: implications in tumor biology and cell migration. Transl. Oncol. 6, 638–648.

Asghar, M.N., Silvander, J.S.G., Helenius, T.O., Lähdeniemi, I.A.K., Alam, C., Fortelius, L.E., Holmsten, R.O., and Toivola, D.M. (2015). The Amount of Keratins Matters for Stress Protection of the Colonic Epithelium. PLOS ONE 10, e0127436.

Assimakopoulou, M., Kondyli, M., Gatzounis, G., Maraziotis, T., and Varakis, J. (2007). Neurotrophin receptors expression and JNK pathway activation in human astrocytomas. BMC Cancer 7, 202.

Aufderhorst-Roberts, A., Frith, W.J., and Donald, A.M. (2014). A microrheological study of hydrogel kinetics and micro-heterogeneity. Eur. Phys. J. E 37.

Avliyakulov, N.K., Rajavel, K.S., Le, K.M.T., Guo, L., Mirsadraei, L., Yong, W.H., Liau, L.M., Li, S., Lai, A., Nghiemphu, P.L., et al. (2014). C-terminally truncated form of αB-crystallin is associated with IDH1 R132H mutation in anaplastic astrocytoma. J. Neurooncol. 117, 53–65.

Azevedo, F.A.C., Carvalho, L.R.B., Grinberg, L.T., Farfel, J.M., Ferretti, R.E.L., Leite, R.E.P., Jacob Filho, W., Lent, R., and Herculano-Houzel, S. (2009). Equal numbers of neuronal and nonneuronal cells make the human brain an isometrically scaled-up primate brain. J. Comp. Neurol. 513, 532–541.

Badn, W., Hegardt, P., Fellert, M.A., Darabi, A., Esbjörnsson, M., Smith, K.E., Janelidze, S., Salford, L.G., Visse, E., and Siesjö, P. (2007). Inhibition of inducible nitric oxide synthase enhances anti-tumour immune responses in rats immunized with IFN-gamma-secreting glioma cells. Scand. J. Immunol. 65, 289–297.

Baldwin, S.A., and Scheff, S.W. (1996). Intermediate filament change in astrocytes following mild cortical contusion. Glia 16, 266–275.

Bandyopadhyay, U., Sridhar, S., Kaushik, S., Kiffin, R., and Cuervo, A.M. (2010). Identification of Regulators of Chaperone-Mediated Autophagy. Mol. Cell 39, 535–547.

Bär, J., Kumar, V., Roth, W., Schwarz, N., Richter, M., Leube, R.E., and Magin, T.M. (2014). Skin Fragility and Impaired Desmosomal Adhesion in Mice Lacking All Keratins. J. Invest. Dermatol. 134, 1012–1022.

Bauer, N.G., Richter-Landsberg, C., and Ffrench-Constant, C. (2009). Role of the oligodendroglial cytoskeleton in differentiation and myelination. Glia 57, 1691–1705.

Bear, M.D., Liu, T., Abualkhair, S., Ghamloush, M.A., Hill, N.S., Preston, I., Fanburg, B.L., Kayyali, U.S., and Toksoz, D. (2016). Alpha-Catulin Co-Localizes With Vimentin Intermediate Filaments and Functions in Pulmonary Vascular Endothelial Cell Migration via ROCK: α-Catulin Co-localizes with Vimentin. J. Cell. Physiol. 231, 934–943.

Beck, H., Semisch, M., Culmsee, C., Plesnila, N., and Hatzopoulos, A.K. (2008). Egr-1 regulates expression of the glial scar component phosphacan in astrocytes after experimental stroke. Am. J. Pathol. 173, 77–92.

Benito, E., and Barco, A. (2014). The Neuronal Activity-Driven Transcriptome. Mol. Neurobiol.

Benner, E.J., Luciano, D., Jo, R., Abdi, K., Paez-Gonzalez, P., Sheng, H., Warner, D.S., Liu, C., Eroglu, C., and Kuo, C.T. (2013). Protective astrogenesis from the SVZ niche after injury is controlled by Notch modulator Thbs4. Nature 497, 369–373.

Bercury, K.K., and Macklin, W.B. (2015). Dynamics and mechanisms of CNS myelination. Dev. Cell 32, 447–458.

Bershadsky, A.D., Balaban, N.Q., and Geiger, B. (2003). Adhesion-dependent cell

mechanosensitivity. Annu. Rev. Cell Dev. Biol. 19, 677–695.

Bhattacharya, R., Gonzalez, A.M., DeBiase, P.J., Trejo, H.E., Goldman, R.D., Flitney, F.W., and Jones, J.C.R. (2009). Recruitment of vimentin to the cell surface by 3 integrin and plectin mediates adhesion strength. J. Cell Sci. 122, 1390–1400.

Bigner, D., Bigner, S., Pontén, J., Westermark, B., Mahaley, M., Ruoslahti, E., Herschman, H., Eng, L., and Wikstrand, C. (1981). Heterogeneity of Genotypic and phenotypic characteristics of fifteen permanent cell lines derived from human gliomas. J Neuropathol Exp Neurol 40, 201–229.

Blair, C.R., Stone, J.B., and Wells, R.G. (2011). The type III TGF-β receptor betaglycan transmembrane-cytoplasmic domain fragment is stable after ectodomain cleavage and is a substrate of the intramembrane protease γ-secretase. Biochim. Biophys. Acta 1813, 332–339.

Blikstad, I., and Lazarides, E. (1983). Vimentin filaments are assembled from a soluble precursor in avian erythroid cells. J. Cell Biol. 96, 1803–1808.

Block, J., Schroeder, V., Pawelzyk, P., Willenbacher, N., and Köster, S. (2015). Physical properties of cytoplasmic intermediate filaments. Biochim. Biophys. Acta BBA - Mol. Cell Res. 1853, 3053–3064.

Blumenthal, N.R., Hermanson, O., Heimrich, B., and Shastri, V.P. (2014). Stochastic nanoroughness modulates neuron-astrocyte interactions and function via mechanosensing cation channels. Proc. Natl. Acad. Sci. U. S. A.

Boateng, S.Y. (2004). RGD and YIGSR synthetic peptides facilitate identical cellular adhesion as laminin and fibronectin but alter the physiology of neonatal cardiac myocytes. AJP Cell Physiol.

Bolego, C., Ceruti, S., Brambilla, R., Puglisi, L., Cattabeni, F., Burnstock, G., and Abbracchio, M.P. (1997). Characterization of the signalling pathways involved in ATP and basic fibroblast growth factor-induced astrogliosis. Br. J. Pharmacol. 121, 1692–1699.

Borggrefe, T., Lauth, M., Zwijsen, A., Huylebroeck, D., Oswald, F., and Giaimo, B.D. (2016). The Notch intracellular domain integrates signals from Wnt, Hedgehog, TGFβ/BMP and hypoxia pathways. Biochim. Biophys. Acta 1863, 303–313.

Bossers, K., Wirz, K.T.S., Meerhoff, G.F., Essing, A.H.W., van Dongen, J.W., Houba, P., Kruse, C.G., Verhaagen, J., and Swaab, D.F. (2010a). Concerted changes in transcripts in the prefrontal cortex precede neuropathology in Alzheimer's disease. Brain J. Neurol. 133, 3699–3723.

Bossers, K., Ylstra, B., Brakenhoff, R.H., Smeets, S.J., Verhaagen, J., and van de Wiel, M.A. (2010b). Intensity-based analysis of dual-color gene expression data as an alternative to ratio-based analysis to enhance reproducibility. BMC Genomics 11, 112.

Brangwynne, C.P., Koenderink, G.H., MacKintosh, F.C., and Weitz, D.A. (2008). Cytoplasmic diffusion: molecular motors mix it up. J. Cell Biol. 183, 583–587.

Bredel, M., Scholtens, D.M., Harsh, G.R., Bredel, C., Chandler, J.P., Renfrow, J.J., Yadav, A.K., Vogel, H., Scheck, A.C., Tibshirani, R., et al. (2009). A network model of a cooperative genetic landscape in brain tumors. JAMA 302, 261–275.

Brehar, F.M., Arsene, D., Brinduse, L.A., and Gorgan, M.R. (2014). Immunohistochemical analysis of GFAP-δ and nestin in cerebral astrocytomas. Brain Tumor Pathol. 1–9.

Brenner, M., Johnson, A.B., Boespflug-Tanguy, O., Rodriguez, D., Goldman, J.E., and Messing, A. (2001). Mutations in GFAP, encoding glial fibrillary acidic protein, are associated with Alexander disease. Nat.Genet. 27, 117–120.

Buffo, A., Rolando, C., and Ceruti, S. (2010). Astrocytes in the damaged brain: molecular and cellular insights into their reactive response and healing potential. Biochem. Pharmacol. 79, 77–89.

Burda, J.E., Bernstein, A.M., and Sofroniew, M.V. (2015). Astrocyte roles in traumatic brain injury. Exp. Neurol.

Busby, W.H., Quackenbush, G.E., Humm, J., Youngblood, W.W., and Kizer, J.S. (1987). An enzyme(s) that converts glutaminyl-peptides into pyroglutamyl-peptides. Presence in pituitary, brain, adrenal medulla, and lymphocytes. J. Biol. Chem. 262, 8532–8536.

Byun, Y., Chen, F., Chang, R., Trivedi, M., Green, K.J., and Cryns, V.L. (2001). Caspase cleavage of vimentin disrupts intermediate filaments and promotes apoptosis. Cell Death Differ. 8, 443–450.

Cáceres-Marzal, C., Vaquerizo, J., Galán, E., and Fernández, S. (2006). Early mitochondrial dysfunction in an infant with Alexander disease. Pediatr. Neurol. 35, 293–296.

Cahoy, J.D., Emery, B., Kaushal, A., Foo, L.C., Zamanian, J.L., Christopherson, K.S., Xing, Y., Lubischer, J.L., Krieg, P.A., Krupenko, S.A., et al. (2008). A Transcriptome Database for Astrocytes, Neurons, and Oligodendrocytes: A New Resource for Understanding Brain Development and Function. J. Neurosci. 28, 264–278.

Cai, Y., Liu, Y., Yu, D., and Zhang, X. (2003). Down-regulation of transcription of the proapoptotic gene BNip3 in cultured astrocytes by murine coronavirus infection. Virology 316, 104–115.

Campain, A., and Yang, Y. (2010). Comparison study of microarray meta-analysis methods. BMC Bioinformatics 11, 408.

Cancer Genome Atlas Research Network, Brat, D.J., Verhaak, R.G.W., Aldape, K.D., Yung, W.K.A., Salama, S.R., Cooper, L.A.D., Rheinbay, E., Miller, C.R., Vitucci, M., et al. (2015). Comprehensive, Integrative Genomic Analysis of Diffuse Lower-Grade Gliomas. N. Engl. J. Med. 372, 2481–2498.

Chalaris, A., Gewiese, J., Paliga, K., Fleig, L., Schneede, A., Krieger, K., Rose-John, S., and Scheller, J. (2010). ADAM17-mediated shedding of the IL6R induces cleavage of the membrane stub by gamma-secretase. Biochim. Biophys. Acta 1803, 234–245.

Challa, A.A., and Stefanovic, B. (2011). A Novel Role of Vimentin Filaments: Binding and Stabilization of Collagen mRNAs. Mol. Cell. Biol. 31, 3773–3789.

Chan, C.C.M., Wong, A.K., Liu, J., Steeves, J.D., and Tetzlaff, W. (2007). ROCK inhibition with Y27632 activates astrocytes and increases their expression of neurite growth-inhibitory chondroitin sulfate proteoglycans. Glia 55, 369–384.

Charles, N.A., Holland, E.C., Gilbertson, R., Glass, R., and Kettenmann, H. (2012). The brain tumor microenvironment. Glia 60, 502–514.

Chen, W.J., and Liem, R.K. (1994). The endless story of the glial fibrillary acidic protein. J. Cell Sci. 107 (Pt 8), 2299–2311.

Chen, J., McKay, R.M., and Parada, L.F. (2012). Malignant Glioma: Lessons from Genomics, Mouse Models, and Stem Cells. Cell 149, 36–47.

Chen, M., Hagemann, T.L., Quinlan, R.A., Messing, A., and Perng, M. (2013). Caspase cleavage of GFAP produces an assembly-compromised proteolytic fragment that promotes filament aggregation. ASN NEURO 5, 293–308.

Chen, Y.-S., Lim, S.-C., Chen, M.-H., Quinlan, R.A., and Perng, M.-D. (2011). Alexander disease causing mutations in the C-terminal domain of GFAP are deleterious both to assembly and network formation with the potential to both activate caspase 3 and decrease cell viability. Exp. Cell Res. 317, 2252–2266.

Cheng, N.-S. (2008). Formula for the Viscosity of a Glycerol–Water Mixture. Ind. Eng. Chem. Res. 47, 3285–3288.

Chernoivanenko, I.S., Matveeva, E.A., Gelfand, V.I., Goldman, R.D., and Minin, A.A. (2015). Mitochondrial membrane potential is regulated by vimentin intermediate filaments. FASEB J. 29, 820–827.

Chernyatina, A.A., Nicolet, S., Aebi, U., Herrmann, H., and Strelkov, S.V. (2012). Atomic structure of the vimentin central α-helical domain and its implications for intermediate filament assembly. Proc. Natl. Acad. Sci.

Cheung, K.J., Gabrielson, E., Werb, Z., and Ewald, A.J. (2013). Collective Invasion in Breast Cancer Requires a Conserved Basal Epithelial Program. Cell 155, 1639–1651.

Cho, W., and Messing, A. (2009). Properties of astrocytes cultured from GFAP over-expressing and GFAP mutant mice. Exp. Cell Res. 315, 1260–1272.

Choi, K.-C., Kwak, S.-E., Kim, J.-E., Sheen, S.H., and Kang, T.-C. (2009). Enhanced glial fibrillary acidic protein-δ expression in human astrocytic tumor. Neurosci. Lett. 463, 182–187.

Choo, A.M., Miller, W.J., Chen, Y.-C., Nibley, P., Patel, T.P., Goletiani, C., Morrison, B., Kutzing, M.K., Firestein, B.L., Sul, J.-Y., et al. (2013). Antagonism of purinergic signalling improves recovery from traumatic brain injury. Brain 136, 65–80.

Chou, Y.H., Rosevear, E., and Goldman, R.D. (1989). Phosphorylation and disassembly of intermediate filaments in mitotic cells. Proc. Natl. Acad. Sci. U. S. A. 86, 1885–1889.

Chou, Y.H., Opal, P., Quinlan, R.A., and Goldman, R.D. (1996). The relative roles of specific N- and C-terminal phosphorylation sites in the disassembly of intermediate filament in mitotic BHK-21 cells. J. Cell Sci. 109, 817–826.

Christopherson, K.S., Ullian, E.M., Stokes, C.C.A., Mullowney, C.E., Hell, J.W., Agah, A., Lawler, J., Mosher, D.F., Bornstein, P., and Barres, B.A. (2005). Thrombospondins are astrocyte-secreted proteins that promote CNS synaptogenesis. Cell 120, 421–433.

Clairembault, T., Kamphuis, W., Leclair-Visonneau, L., Rolli-Derkinderen, M., Coron, E., Neunlist, M., Hol, E.M., and Derkinderen, P. (2014). Enteric GFAP expression and phosphorylation in Parkinson's disease. J. Neurochem. 130, 805–815.

Cleveland, W.S., Grosse, E., and Shyu, W.M. (1992). Local regression models. Chapter 8 of Statistical Models in S.

Colakoglu, G., and Brown, A. (2009). Intermediate filaments exchange subunits along their length and elongate by end-to-end annealing. J. Cell Biol. 185, 769–777.

Colucci-Guyon, E., Portier, M.M., Dunia, I., Paulin, D., Pournin, S., and Babinet, C. (1994). Mice lacking vimentin develop and reproduce without an obvious phenotype. Cell 79, 679–694.

Corda, D., Mosca, M.G., Ohshima, N., Grauso, L., Yanaka, N., and Mariggiò, S. (2014). The emerging physiological roles of the glycerophosphodiesterase family. FEBS J. 281, 998–1016.

Coste, B., Mathur, J., Schmidt, M., Earley, T.J., Ranade, S., Petrus, M.J., Dubin, A.E., and Patapoutian, A. (2010). Piezo1 and Piezo2 Are Essential Components of Distinct Mechanically Activated Cation Channels. Science 330, 55–60.

Coulombe, P.A., and Wong, P. (2004). Cytoplasmic intermediate filaments revealed as dynamic and multipurpose scaffolds. Nat. Cell Biol. 6, 699–706.

Crocker, J.C., Grier, D.G., and others (1996). Methods of digital video microscopy for colloidal studies. J. Colloid Interface Sci. 179, 298–310.

Cuadrado, E., Jansen, M.H., Anink, J., De Filippis, L., Vescovi, A.L., Watts, C., Aronica, E., Hol, E.M., and Kuijpers, T.W. (2013). Chronic exposure of astrocytes to interferon- reveals molecular changes related to Aicardi-Goutieres syndrome. Brain 136, 245–258.

Dang, L., White, D.W., Gross, S., Bennett, B.D., Bittinger, M.A., Driggers, E.M., Fantin, V.R., Jang, H.G., Jin, S., Keenan, M.C., et al. (2009). Cancer-associated IDH1 mutations produce 2-hydroxyglutarate. Nature 462, 739–744.

Daniels, B.R., Hale, C.M., Khatau, S.B., Kusuma, S., Dobrowsky, T.M., Gerecht, S., and Wirtz, D. (2010). Differences in the Microrheology of Human Embryonic Stem Cells and Human Induced Pluripotent Stem Cells. Biophys. J. 99, 3563–3570.

D'Astolfo, D.S., Pagliero, R.J., Pras, A., Karthaus, W.R., Clevers, H., Prasad, V., Lebbink, R.J., Rehmann, H., and Geijsen, N. (2015). Efficient Intracellular Delivery of Native Proteins. Cell 161, 674–690.

Dave, J.M., and Bayless, K.J. (2014). Vimentin as an Integral Regulator of Cell Adhesion and Endothelial Sprouting. Microcirculation 21, 333–344.

Dave, J.M., Kang, H., Abbey, C.A., Maxwell, S.A., and Bayless, K.J. (2013). Proteomic Profiling of Endothelial Invasion Revealed Receptor for Activated C Kinase 1 (RACK1) Complexed with Vimentin to Regulate Focal Adhesion Kinase (FAK). J. Biol. Chem. 288, 30720–30733.

Davis, S., Bozon, B., and Laroche, S. (2003). How necessary is the activation of the immediate early gene zif268 in synaptic plasticity and learning? Behav. Brain Res. 142, 17–30.

Derouiche, A., Haseleu, J., and Korf, H.-W. (2015). Fine Astrocyte Processes Contain Very Small Mitochondria: Glial Oxidative Capability May Fuel Transmitter Metabolism. Neurochem. Res. 40, 2402–2413.

Desmet, C.J., and Peeper, D.S. (2006). The neurotrophic receptor TrkB: a drug target in anti-cancer therapy? Cell. Mol. Life Sci. CMLS 63, 755–759.

Ding, M., Eliasson, C., Betsholtz, C., Hamberger, A., and Pekny, M. (1998). Altered taurine release following hypotonic stress in astrocytes from mice deficient for GFAP and vimentin. Brain Res. Mol. Brain Res. 62, 77–81.

Dityatev, A., and Rusakov, D.A. (2011). Molecular signals of plasticity at the tetrapartite synapse. Curr. Opin. Neurobiol. 21, 353–359.

Dityatev, A., Seidenbecher, C.I., and Schachner, M. (2010). Compartmentalization from the outside: the extracellular matrix and functional microdomains in the brain. Trends Neurosci. 33, 503–512.

Dmello, C., Sawant, S., Alam, H., Gangadaran, P., Tiwari, R., Dongre, H., Rana, N., Barve, S., Costea, D.E., Chaukar, D., et al. (2016). Vimentin-mediated regulation of cell motility through modulation of beta4 integrin protein levels in oral tumor derived cells. Int. J. Biochem. Cell Biol. 70, 161–172.

Ducray, F., Idbaih, A., de Reyniès, A., Bièche, I., Thillet, J., Mokhtari, K., Lair, S., Marie, Y., Paris, S., Vidaud, M., et al. (2008). Anaplastic oligodendrogliomas with 1p19q codeletion have a proneural gene expression profile. Mol. Cancer 7, 41.

Dupin, I., Sakamoto, Y., and Etienne-Manneville, S. (2011). Cytoplasmic intermediate filaments mediate actin-driven positioning of the nucleus. J. Cell Sci. 124, 865–872.

Eckes, B., Colucci-Guyon, E., Smola, H., Nodder, S., Babinet, C., Krieg, T., and Martin, P. (2000). Impaired wound healing in embryonic and adult mice lacking vimentin. J. Cell Sci. 113, 2455–2462.

Edling, Y., Ingelman-Sundberg, M., and Simi, A. (2007). Glutamate activatesc-fos in glial cells via a novel mechanism involving the glutamate receptor subtype mGlu5 and the transcriptional repressor DREAM. Glia 55, 328–340.

Ellie, E., Loiseau, H., Lafond, F., Arsaut, J., and Demotes-Mainard, J. (1995). Differential expression of inducible nitric oxide synthase mRNA in human brain tumours. Neuroreport 7, 294–296.

Ellis, E.F., McKinney, J.S., Willoughby, K.A., Liang, S., and Povlishock, J.T. (1995). A new model for rapid stretch-induced injury of cells in culture: characterization of the model using astrocytes. J. Neurotrauma 12, 325–339.

Elobeid, A., Bongcam-Rudloff, E., Westermark, B., and Nistér, M. (2000). Effects of inducible glial fibrillary acidic protein on glioma cell motility and proliferation. J. Neurosci. Res. 60, 245–256.

Eng, L.F., Ghirnikar, R.S., and Lee, Y.L. (2000). Glial fibrillary acidic protein: GFAP-thirty-one years (1969-2000). Neurochem. Res. 25, 1439–1451.

Engler, A.J., Sen, S., Sweeney, H.L., and Discher, D.E. (2006). Matrix Elasticity Directs Stem Cell Lineage Specification. Cell 126, 677–689.

Erhardt, J.A., Hynicka, W., DiBenedetto, A., Shen, N., Stone, N., Paulson, H., and Pittman, R.N. (1998). A novel F box protein, NFB42, is highly enriched in neurons and induces growth arrest. J. Biol. Chem. 273, 35222–35227.

Eyler, C.E., Wu, Q., Yan, K., MacSwords, J.M., Chandler-Militello, D., Misuraca, K.L., Lathia, J.D., Forrester, M.T., Lee, J., Stamler, J.S., et al. (2011). Glioma stem cell proliferation and tumor growth are promoted by nitric oxide synthase-2. Cell 146, 53–66.

Fanarraga, M.L., Villegas, J.C., Carranza, G., Castaño, R., and Zabala, J.C. (2009). Tubulin cofactor B regulates microtubule densities during microglia transition to the reactive states. Exp. Cell Res. 315, 535–541.

Fears, C.Y., Grammer, J.R., Stewart, J.E., Annis, D.S., Mosher, D.F., Bornstein, P., and Gladson, C.L. (2005). Low-Density Lipoprotein Receptor–Related Protein Contributes to the Antiangiogenic Activity of Thrombospondin-2 in a Murine Glioma Model. Cancer Res. 65, 9338–9346.

Fischer, W.H., and Spiess, J. (1987). Identification of a mammalian glutaminyl cyclase converting glutaminyl into pyroglutamyl peptides. Proc. Natl. Acad. Sci. U. S. A. 84, 3628–3632.

Fisher, R.A. (1970). Statistical methods for research workers (Edinburgh: Oliver and Boyd).

Fletcher, L., Isgor, E., Sprague, S., Williams, L.H., Alajajian, B.B., Jimenez, D.F., and Digicaylioglu, M. (2013). Spatial distribution of insulin-like growth factor binding protein-2 following hypoxic-ischemic injury. BMC Neurosci. 14, 158.

Floyd, C.L., Rzigalinski, B.A., Weber, J.T., Sitterding, H.A., Willoughby, K.A., and Ellis, E.F. (2001). Traumatic injury of cultured astrocytes alters inositol (1, 4, 5)–trisphosphate-mediated signaling. Glia 33, 12–23.

Floyd, C.L., Rzigalinski, B.A., Sitterding, H.A., Willoughby, K.A., and Ellis, E.F. (2004). Antagonism of group I metabotropic glutamate receptors and PLC attenuates increases in inositol trisphosphate and reduces reactive gliosis in strain-injured astrocytes. J. Neurotrauma 21, 205–216.

Floyd, C.L., Gorin, F.A., and Lyeth, B.G. (2005). Mechanical strain injury increases intracellular sodium and reverses Na+/Ca2+ exchange in cortical astrocytes. Glia 51, 35–46.

Foo, L.C., Allen, N.J., Bushong, E.A., Ventura, P.B., Chung, W.-S., Zhou, L., Cahoy, J.D., Daneman, R., Zong, H., Ellisman, M.H., et al. (2011). Development of a Method for the Purification and Culture of Rodent Astrocytes. Neuron 71, 799–811.

Francescone, R., Scully, S., Bentley, B., Yan, W., Taylor, S.L., Oh, D., Moral, L., and Shao, R. (2012). Glioblastoma-derived Tumor Cells Induce Vasculogenic Mimicry through Flk-1 Protein Activation. J. Biol. Chem. 287, 24821–24831.

Franke, H., Verkhratsky, A., Burnstock, G., and Illes, P. (2012). Pathophysiology of astroglial purinergic signalling. Purinergic Signal. 8, 629–657.

Friedl, P., and Wolf, K. (2010). Plasticity of cell migration: a multiscale tuning model. J. Cell Biol. 188, 11–19.

Fudge, D., Russell, D., Beriault, D., Moore, W., Lane, E.B., and Vogl, A.W. (2008). The Intermediate Filament Network in Cultured Human Keratinocytes Is Remarkably Extensible and Resilient. PLoS ONE 3, e2327.

Galou, M., Colucci-Guyon, E., Ensergueix, D., Ridet, J.-L., Gimenez y Ribotta, M., Privat, A., Babinet, C., and Dupouey, P. (1996). Disrupted glial fibrillary acidic protein network in astrocytes from vimentin knockout mice. J. Cell Biol. 133, 853–863.

Garcia-Esparcia, P., Schlüter, A., Carmona, M., Moreno, J., Ansoleaga, B., Torrejón-Escribano, B., Gustincich, S., Pujol, A., and Ferrer, I. (2013). Functional Genomics Reveals Dysregulation of Cortical Olfactory Receptors in Parkinson Disease: Novel Putative Chemoreceptors in the Human Brain. J. Neuropathol. Exp. Neurol. 72, 524–539.

Garofalo, S., D'Alessandro, G., Chece, G., Brau, F., Maggi, L., Rosa, A., Porzia, A., Mainiero, F., Esposito, V., Lauro, C., et al. (2015). Enriched environment reduces glioma growth through immune and non-immune mechanisms in mice. Nat. Commun. 6, 6623.

Gelfand, V.I., and Bershadsky, A.D. (1991). Microtubule dynamics: mechanism, regulation, and function. Annu. Rev. Cell Biol. 7, 93–116.

Gene Ontology Consortium (2015). Gene Ontology Consortium: going forward. Nucleic Acids Res. 43, D1049–D1056.

Geng, Y., Bush, M., Mosyak, L., Wang, F., and Fan, Q.R. (2013). Structural mechanism of ligand activation in human GABA(B) receptor. Nature 504, 254–259.

Gibbs, G.M., Roelants, K., and O'Bryan, M.K. (2008). The CAP Superfamily: Cysteine-Rich Secretory Proteins, Antigen 5, and Pathogenesis-Related 1 Proteins—Roles in Reproduction, Cancer, and Immune Defense. Endocr. Rev. 29, 865–897.

Gilchrist, S., Gilbert, N., Perry, P., Ostlund, C., Worman, H.J., and Bickmore, W.A. (2004). Altered protein dynamics of disease-associated lamin A mutants. BMC Cell Biol. 5, 46.

Gingold, M.K., Bodensteiner, J.B., Schochet, S.S., and Jaynes, M. (1999). Alexander's Disease: Unique Presentation. J. Child Neurol. 14, 325–329.

Girard, F., Eichenberger, S., and Celio, M.R. (2014). Thrombospondin 4 deficiency in mouse impairs neuronal migration in the early postnatal and adult brain. Mol. Cell. Neurosci. 61, 176–186.

Gitik, M., Reichert, F., and Rotshenker, S. (2010). Cytoskeleton plays a dual role of activation and inhibition in myelin and zymosan phagocytosis by microglia. FASEB J. Off. Publ. Fed. Am. Soc. Exp. Biol. 24, 2211–2221.

Glavey, S.V., Manier, S., Natoni, A., Sacco, A., Moschetta, M., Reagan, M.R., Murillo, L.S., Sahin, I., Wu, P., Mishima, Y., et al. (2014). The sialyltransferase ST3GAL6 influences homing and survival in multiple myeloma. Blood 124, 1765–1776.

Gleize, V., Alentorn, A., Connen de Kérillis, L., Labussière, M., Nadaradjane, A.A., Mundwiller, E., Ottolenghi, C., Mangesius, S., Rahimian, A., Ducray, F., et al. (2015). CIC inactivating mutations identify aggressive subset of 1p19q codeleted gliomas. Ann. Neurol. 78, 355–374.

Goldman, J.E., and Corbin, E. (1988). Isolation of a major protein component of Rosenthal fibers. Am. J. Pathol. 130, 569–578.

Goldman, R.D., Grin, B., Mendez, M.G., and Kuczmarski, E.R. (2008). Intermediate filaments: versatile building blocks of cell structure. Curr. Opin. Cell Biol. 20, 28–34.

Gopalan, S.M., Wilczynska, K.M., Konik, B.S., Bryan, L., and Kordula, T. (2006). Astrocyte-specific Expression of the α1-Antichymotrypsin and Glial Fibrillary Acidic Protein Genes Requires Activator Protein-1. J. Biol. Chem. 281, 1956–1963.

Gordon, W.R., Zimmerman, B., He, L., Miles, L.J., Huang, J., Tiyanont, K., McArthur, D.G., Aster, J.C., Perrimon, N., Loparo, J.J., et al. (2015). Mechanical Allostery: Evidence for a Force Requirement in the Proteolytic Activation of Notch. Dev. Cell 33, 729–736.

Goto, H., Kosako, H., and Inagaki, M. (2000). Regulation of intermediate filament organization during cytokinesis: possible roles of Rho-associated kinase. Microsc. Res. Tech. 49, 173–182.

Graeber, M.B., Streit, W.J., and Kreutzberg, G.W. (1988). The microglial cytoskeleton: vimentin is localized within activated cells in situ. J. Neurocytol. 17, 573–580.

Graf, J., Ogle, R.C., Robey, F.A., Sasaki, M., Martin, G.R., Yamada, Y., and Kleinman, H.K. (1987). A pentapeptide from the laminin B1 chain mediates cell adhesion and binds to 67000 laminin receptor. Biochemistry (Mosc.) 26, 6896–6900.

Gregor, M., Osmanagic-Myers, S., Burgstaller, G., Wolfram, M., Fischer, I., Walko, G., Resch, G.P., Jorgl, A., Herrmann, H., and Wiche, G. (2013). Mechanosensing through focal adhesion-anchored intermediate filaments. FASEB J. 28, 715–729.

Grin, B., Mahammad, S., Wedig, T., Cleland, M.M., Tsai, L., Herrmann, H., and Goldman, R.D. (2012). Withaferin a alters intermediate filament organization, cell shape and behavior.

PloS One 7, e39065.

Gu, F., Wang, J., Fu, L., and Ma, Y.-J. (2011). Co-culture with microglia promotes neural stem cells differentiation into astrocytes. Chin. Med. J. (Engl.) 124, 3394–3398.

Gudey, S.K., Sundar, R., Mu, Y., Wallenius, A., Zang, G., Bergh, A., Heldin, C.-H., and Landstrom, M. (2014). TRAF6 Stimulates the Tumor-Promoting Effects of TGF Type I Receptor Through Polyubiquitination and Activation of Presenilin 1. Sci. Signal. 7, ra2–ra2.

Guelen, L., Pagie, L., Brasset, E., Meuleman, W., Faza, M.B., Talhout, W., Eussen, B.H., de Klein, A., Wessels, L., de Laat, W., et al. (2008). Domain organization of human chromosomes revealed by mapping of nuclear lamina interactions. Nature 453, 948–951.

Guérette, D., Khan, P.A., Savard, P.E., and Vincent, M. (2007). Molecular evolution of type VI intermediate filament proteins. BMC Evol. Biol. 7, 164.

Gulati, S., Ytterhus, B., Granli, U.S., Gulati, M., Lydersen, S., and Torp, S.H. (2010). Overexpression of c-erbB2 is a negative prognostic factor in anaplastic astrocytomas. Diagn. Pathol. 5, 18.

Guo, H., Gu, F., Li, W., Zhang, B., Niu, R., Fu, L., Zhang, N., and Ma, Y. (2009). Reduction of protein kinase C ζ inhibits migration and invasion of human glioblastoma cells. J. Neurochem. 109, 203–213.

Guo, M., Ehrlicher, A.J., Mahammad, S., Fabich, H., Jensen, M.H., Moore, J.R., Fredberg, J.J., Goldman, R.D., and Weitz, D.A. (2013). The Role of Vimentin Intermediate Filaments in Cortical and Cytoplasmic Mechanics. Biophys. J. 105, 1562–1568.

Guo, M., Ehrlicher, A.J., Jensen, M.H., Renz, M., Moore, J.R., Goldman, R.D., Lippincott-Schwartz, J., Mackintosh, F.C., and Weitz, D.A. (2014). Probing the Stochastic, Motor-Driven Properties of the Cytoplasm Using Force Spectrum Microscopy. Cell 158, 822–832.

Hagemann, T.L., Gaeta, S.A., Smith, M.A., Johnson, D.A., Johnson, J.A., and Messing, A. (2005). Gene expression analysis in mice with elevated glial fibrillary acidic protein and Rosenthal fibers reveals a stress response followed by glial activation and neuronal dysfunction. Hum. Mol. Genet. 14, 2443–2458.

Hagemann, T.L., Boelens, W.C., Wawrousek, E.F., and Messing, A. (2009). Suppression of GFAP toxicity by B-crystallin in mouse models of Alexander disease. Hum. Mol. Genet. 18, 1190–1199.

Hahn, C., and Schwartz, M.A. (2009). Mechanotransduction in vascular physiology and atherogenesis. Nat. Rev. Mol. Cell Biol. 10, 53–62.

Hanahan, D., and Weinberg, R.A. (2011). Hallmarks of Cancer: The Next Generation. Cell 144, 646–674.

Hanisch, U.-K., and Kettenmann, H. (2007). Microglia: active sensor and versatile effector cells in the normal and pathologic brain. Nat. Neurosci. 10, 1387–1394.

Hara, A., and Okayasu, I. (2004). Cyclooxygenase-2 and inducible nitric oxide synthase expression in human astrocytic gliomas: correlation with angiogenesis and prognostic significance. Acta Neuropathol. (Berl.) 108, 43–48.

Hara, E., Takahashi, K., Tominaga, T., Kumabe, T., Kayama, T., Suzuki, H., Fujita, H., Yoshimoto, T., Shirato, K., and Shibahara, S. (1996). Expression of heme oxygenase and inducible nitric oxide synthase mRNA in human brain tumors. Biochem. Biophys. Res.

Commun. 224, 153–158.

Hartlage-Rübsamen, M., Waniek, A., Meissner, J., Morawski, M., Schilling, S., Jäger, C., Kleinschmidt, M., Cynis, H., Kehlen, A., Arendt, T., et al. (2015). Isoglutaminyl cyclase contributes to CCL2-driven neuroinflammation in Alzheimer's disease. Acta Neuropathol. (Berl.) 129, 565–583.

Hashimoto, K., Parker, A., Malone, P., Gabelt, B.T., Rasmussen, C., Kaufman, P.S., and Hernandez, M.R. (2005). Long-term activation of c-Fos and c-Jun in optic nerve head astrocytes in experimental ocular hypertension in monkeys and after exposure to elevated pressure in vitro. Brain Res. 1054, 103–115.

Havel, L.S., Kline, E.R., Salgueiro, A.M., and Marcus, A.I. (2015). Vimentin regulates lung cancer cell adhesion through a VAV2–Rac1 pathway to control focal adhesion kinase activity. Oncogene 34, 1979–1990.

Helfand, B.T., Mendez, M.G., Murthy, S.N.P., Shumaker, D.K., Grin, B., Mahammad, S., Aebi, U., Wedig, T., Wu, Y.I., Hahn, K.M., et al. (2011). Vimentin organization modulates the formation of lamellipodia. Mol. Biol. Cell 22, 1274–1289.

Hemphill, M.A., Dabiri, B.E., Gabriele, S., Kerscher, L., Franck, C., Goss, J.A., Alford, P.W., and Parker, K.K. (2011). A Possible Role for Integrin Signaling in Diffuse Axonal Injury. PLoS ONE 6, e22899.

Henrion, D., Terzi, F., Matrougui, K., Duriez, M., Boulanger, C.M., Colucci-Guyon, E., Babinet, C., Briand, P., Friedlander, G., Poitevin, P., et al. (1997). Impaired flow-induced dilation in mesenteric resistance arteries from mice lacking vimentin. J. Clin. Invest. 100, 2909–2914.

Heo, D.H., Kim, S.H., Yang, K.-M., Cho, Y.J., Kim, K.N., Yoon, D.H., and Kang, T.-C. (2012). A histopathological diagnostic marker for human spinal astrocytoma: expression of glial fibrillary acidic protein-δ. J. Neurooncol. 108, 45–52.

Herrmann, H., Häner, M., Brettel, M., Müller, S.A., Goldie, K.N., Fedtke, B., Lustig, A., Franke, W.W., and Aebi, U. (1996). Structure and assembly properties of the intermediate filament protein vimentin: the role of its head, rod and tail domains. J. Mol. Biol. 264, 933–953.

Herrmann, H., Strelkov, S.V., Burkhard, P., and Aebi, U. (2009). Intermediate filaments: primary determinants of cell architecture and plasticity. J. Clin. Invest. 119, 1772–1783.

Ho, V.K.Y., Reijneveld, J.C., Enting, R.H., Bienfait, H.P., Robe, P., Baumert, B.G., and Visser, O. (2014). Changing incidence and improved survival of gliomas. Eur. J. Cancer 50, 2309–2318.

Hobbs, R.P., DePianto, D.J., Jacob, J.T., Han, M.C., Chung, B.-M., Batazzi, A.S., Poll, B.G., Guo, Y., Han, J., Ong, S., et al. (2015). Keratin-dependent regulation of Aire and gene expression in skin tumor keratinocytes. Nat. Genet. 47, 933–938.

Hoffman, B.D., Grashoff, C., and Schwartz, M.A. (2011). Dynamic molecular processes mediate cellular mechanotransduction. Nature 475, 316–323.

Hoffman, S.W., Rzigalinski, B.A., Willoughby, K.A., and Ellis, E.F. (2000). Astrocytes generate isoprostanes in response to trauma or oxygen radicals. J. Neurotrauma 17, 415–420.

Hol, E.M., and Pekny, M. (2015). Glial fibrillary acidic protein (GFAP) and the astrocyte intermediate filament system in diseases of the central nervous system. Curr. Opin. Cell Biol. 32, 121–130.

Höring, E., Harter, P.N., Seznec, J., Schittenhelm, J., Bühring, H.-J., Bhattacharyya, S., von

Hattingen, E., Zachskorn, C., Mittelbronn, M., and Naumann, U. (2012). The "go or grow" potential of gliomas is linked to the neuropeptide processing enzyme carboxypeptidase E and mediated by metabolic stress. Acta Neuropathol. (Berl.) 124, 83–97.

Hsieh, H.-L., Wang, H.-H., Wu, C.-Y., and Yang, C.-M. (2010). Reactive Oxygen Species-Dependent c-Fos/Activator Protein 1 Induction Upregulates Heme Oxygenase-1 Expression by Bradykinin in Brain Astrocytes. Antioxid. Redox Signal. 13, 1829–1844.

Huber, F., Boire, A., López, M.P., and Koenderink, G.H. (2015). Cytoskeletal crosstalk: when three different personalities team up. Curr. Opin. Cell Biol. 32, 39–47.

Hudson, D.M., Joeng, K.S., Werther, R., Rajagopal, A., Weis, M., Lee, B.H., and Eyre, D.R. (2015). Post-translationally abnormal collagens of prolyl 3-hydroxylase-2 null mice offer a pathobiological mechanism for the high myopia linked to human LEPREL1 mutations*. J. Biol. Chem. jbc.M114.634915.

Hughes, E.G., Maguire, J.L., McMinn, M.T., Scholz, R.E., and Sutherland, M.L. (2004). Loss of glial fibrillary acidic protein results in decreased glutamate transport and inhibition of PKA-induced EAAT2 cell surface trafficking. Mol. Brain Res. 124, 114–123.

Huyghe, D., Nakamura, Y., Terunuma, M., Faideau, M., Haydon, P., Pangalos, M.N., and Moss, S.J. (2014). Glutamine Synthetase Stability and Subcellular Distribution in Astrocytes Are Regulated by γ-Aminobutyric Type B Receptors. J. Biol. Chem. 289, 28808–28815.

Hyder, C.L., Kemppainen, K., Isoniemi, K.O., Imanishi, S.Y., Goto, H., Inagaki, M., Fazeli, E., Eriksson, J.E., and Törnquist, K. (2015). Sphingolipids inhibit vimentin-dependent cell migration. J. Cell Sci. 128, 2057–2069.

Iliff, J.J., Wang, M., Liao, Y., Plogg, B.A., Peng, W., Gundersen, G.A., Benveniste, H., Vates, G.E., Deane, R., Goldman, S.A., et al. (2012). A Paravascular Pathway Facilitates CSF Flow Through the Brain Parenchyma and the Clearance of Interstitial Solutes, Including Amyloid. Sci. Transl. Med. 4, 147ra111–ra147ra111.

Ingber, D.E. (1993). Cellular tensegrity: defining new rules of biological design that govern the cytoskeleton. J. Cell Sci. 104 (Pt 3), 613–627.

Ishikawa, H., Bischoff, R., and Holtzer, H. (1968). Mitosis and intermediate-sized filaments in developing skeletal muscle. J. Cell Biol. 38, 538–555.

Ivaska, J., Vuoriluoto, K., Huovinen, T., Izawa, I., Inagaki, M., and Parker, P.J. (2005). PKCε-mediated phosphorylation of vimentin controls integrin recycling and motility. EMBO J. 24, 3834–3845.

Ivaska, J., Pallari, H.-M., Nevo, J., and Eriksson, J.E. (2007). Novel functions of vimentin in cell adhesion, migration, and signaling. Exp. Cell Res. 313, 2050–2062.

Iwaki, T., Kume-Iwaki, A., Liem, R.K.H., and Goldman, J.E. (1989). αB-crystallin is expressed in non-lenticular tissues and accumulates in Alexander's disease brain. Cell 57, 71–78.

Izawa, I., and Inagaki, M. (2006). Regulatory mechanisms and functions of intermediate filaments: a study using site- and phosphorylation state-specific antibodies. Cancer Sci. 97, 167–174.

Janke, C., Ortiz, J., Lechner, J., Shevchenko, A., Shevchenko, A., Magiera, M.M., Schramm, C., and Schiebel, E. (2001). The budding yeast proteins Spc24p and Spc25p interact with Ndc80p and Nuf2p at the kinetochore and are important for kinetochore clustering and checkpoint control. EMBO J. 20, 777–791.

Jansen, K.A., Donato, D.M., Balcioglu, H.E., Schmidt, T., Danen, E.H.J., and Koenderink, G.H. (2015). A guide to mechanobiology: Where biology and physics meet. Biochim. Biophys. Acta BBA - Mol. Cell Res. 1853, 3043–3052.

Jensen, M.H., Morris, E.J., Goldman, R.D., and Weitz, D.A. (2014). Emergent properties of composite semiflexible biopolymer networks. BioArchitecture 4, 138–143.

Jiang, S.X., Slinn, J., Aylsworth, A., and Hou, S.T. (2012). Vimentin participates in microglia activation and neurotoxicity in cerebral ischemia: Vimentin controls microglia activation. J. Neurochem. 122, 764–774.

Jimenez-Sanchez, M., Lam, W., Hannus, M., Sönnichsen, B., Imarisio, S., Fleming, A., Tarditi, A., Menzies, F., Ed Dami, T., Xu, C., et al. (2015). siRNA screen identifies QPCT as a druggable target for Huntington's disease. Nat. Chem. Biol. 11, 347–354.

Jin, Z., Fu, Z., Yang, J., Troncosco, J., Everett, A.D., and Van Eyk, J.E. (2013). Identification and characterization of citrulline-modified brain proteins by combining HCD and CID fragmentation. PROTEOMICS 13, 2682–2691.

Jiu, Y., Lehtimäki, J., Tojkander, S., Cheng, F., Jäälinoja, H., Liu, X., Varjosalo, M., Eriksson, J.E., and Lappalainen, P. (2015). Bidirectional Interplay between Vimentin Intermediate Filaments and Contractile Actin Stress Fibers. Cell Rep. 11, 1511–1518.

Johnson, C.P., Tang, H.-Y., Carag, C., Speicher, D.W., and Discher, D.E. (2007). Forced unfolding of proteins within cells. Science 317, 663–666.

Johnston, J.A., Ward, C.L., and Kopito, R.R. (1998). Aggresomes: a cellular response to misfolded proteins. J. Cell Biol. 143, 1883–1898.

Joseph, J.V., Balasubramaniyan, V., Walenkamp, A., and Kruyt, F.A.E. (2013). TGF-β as a therapeutic target in high grade gliomas – Promises and challenges. Biochem. Pharmacol. 85, 478–485.

Joy, M.T., Vrbova, G., Dhoot, G.K., and Anderson, P.N. (2015). Sulf1 and Sulf2 expression in the nervous system and its role in limiting neurite outgrowth in vitro. Exp. Neurol. 263, 150–160.

Jungblut, M., Tiveron, M.C., Barral, S., Abrahamsen, B., Knöbel, S., Pennartz, S., Schmitz, J., Perraut, M., Pfrieger, F.W., Stoffel, W., et al. (2012). Isolation and characterization of living primary astroglial cells using the new GLAST-specific monoclonal antibody ACSA-1. Glia 60, 894–907.

Kachar, B., Behar, T., and Dubois-Dalcq, M. (1986). Cell shape and motility of oligodendrocytes cultured without neurons. Cell Tissue Res. 244, 27–38.

Kamphuis, W., Mamber, C., Moeton, M., Kooijman, L., Sluijs, J.A., Jansen, A.H.P., Verveer, M., de Groot, L.R., Smith, V.D., Rangarajan, S., et al. (2012). GFAP Isoforms in Adult Mouse Brain with a Focus on Neurogenic Astrocytes and Reactive Astrogliosis in Mouse Models of Alzheimer Disease. PLoS ONE 7, e42823.

Kamphuis, W., Middeldorp, J., Kooijman, L., Sluijs, J.A., Kooi, E.-J., Moeton, M., Freriks, M., Mizee, M.R., and Hol, E.M. (2014). Glial fibrillary acidic protein isoform expression in plaque related astrogliosis in Alzheimer's disease. Neurobiol. Aging 35, 492–510.

Kamphuis, W., Kooijman, L., Orre, M., Stassen, O., Pekny, M., and Hol, E.M. (2015). GFAP and vimentin deficiency alters gene expression in astrocytes and microglia in wild-type mice and changes the transcriptional response of reactive glia in mouse model for Alzheimer's disease: GFAP and Vimentin in Alzheimer's Disease. Glia 63, 1036–1056.

Kaneko, N., Miura, K., Gu, Z., Karasawa, H., Ohnuma, S., Sasaki, H., Tsukamoto, N., Yokoyama, S., Yamamura, A., Nagase, H., et al. (2009). siRNA-mediated knockdown against CDCA1 and KNTC2, both frequently overexpressed in colorectal and gastric cancers, suppresses cell proliferation and induces apoptosis. Biochem. Biophys. Res. Commun. 390, 1235–1240.

Kanski, R. (2014). From stem cell to astrocyte: Decoding the regulation of GFAP -PhD-Thesis (BoxPress).

Kawataki, T., Yamane, T., Naganuma, H., Rousselle, P., Andurén, I., Tryggvason, K., and Patarroyo, M. (2007). Laminin isoforms and their integrin receptors in glioma cell migration and invasiveness: Evidence for a role of α5-laminin(s) and α3β1 integrin. Exp. Cell Res. 313, 3819–3831.

Kettenmann, H., Kirchhoff, F., and Verkhratsky, A. (2013). Microglia: New Roles for the Synaptic Stripper. Neuron 77, 10–18.

Keung, A.J., de Juan-Pardo, E.M., Schaffer, D.V., and Kumar, S. (2011). Rho GTPases Mediate the Mechanosensitive Lineage Commitment of Neural Stem Cells. STEM CELLS 29, 1886–1897.

Khachigian, L.M., Lindner, V., Williams, A.J., and Collins, T. (1996). Egr-1-induced endothelial gene expression: a common theme in vascular injury. Science 271, 1427–1431.

Kheirollah, A., Nagayasu, Y., Ueda, H., Yokoyama, S., Michikawa, M., and Ito, J. (2014). Involvement of cdc42/Rho kinase in ApoA-I-mediated cholesterol efflux through interaction between cytosolic lipid-protein particles and microtubules in rat astrocytes: ApoA-I Activates cdc42/Rho Kinase for HDL Generation. J. Neurosci. Res. 92, 455–463.

Kim, D.-S., Li, K.-W., Boroujerdi, A., Peter Yu, Y., Zhou, C.-Y., Deng, P., Park, J., Zhang, X., Lee, J., Corpe, M., et al. (2012). Thrombospondin-4 Contributes to Spinal Sensitization and Neuropathic Pain States. J. Neurosci. 32, 8977–8987.

Kim, R.-K., Suh, Y., Cui, Y.-H., Hwang, E., Lim, E.-J., Yoo, K.-C., Lee, G.-H., Yi, J.-M., Kang, S.-G., and Lee, S.-J. (2013). Fractionated radiation-induced nitric oxide promotes expansion of glioma stem-like cells. Cancer Sci. 104, 1172–1177.

Kleinschmit, A., Koyama, T., Dejima, K., Hayashi, Y., Kamimura, K., and Nakato, H. (2010). Drosophila heparan sulfate 6-O endosulfatase regulates Wingless morphogen gradient formation. Dev. Biol. 345, 204–214.

Klioueva, N.M., Rademaker, M.C., Dexter, D.T., Al-Sarraj, S., Seilhean, D., Streichenberger, N., Schmitz, P., Bell, J.E., Ironside, J.W., Arzberger, T., et al. (2015). BrainNet Europe's Code of Conduct for brain banking. J. Neural Transm.

Klotzsch, E., Smith, M.L., Kubow, K.E., Muntwyler, S., Little, W.C., Beyeler, F., Gourdon, D., Nelson, B.J., and Vogel, V. (2009). Fibronectin forms the most extensible biological fibers displaying switchable force-exposed cryptic binding sites. Proc. Natl. Acad. Sci. U. S. A. 106, 18267–18272.

Knittel, T., Kobold, D., Piscaglia, F., Saile, B., Neubauer, K., Mehde, M., Timpl, R., and Ramadori, G. (1999). Localization of liver myofibroblasts and hepatic stellate cells in normal and diseased rat livers: distinct roles of (myo-)fibroblast subpopulations in hepatic tissue repair. Histochem. Cell Biol. 112, 387–401.

Koenderink, G.H., Dogic, Z., Nakamura, F., Bendix, P.M., MacKintosh, F.C., Hartwig, J.H., Stossel, T.P., and Weitz, D.A. (2009). An active biopolymer network controlled by molecular motors. Proc. Natl. Acad. Sci. 106, 15192–15197.

Kole, T.P., Tseng, Y., Huang, L., Katz, J.L., and Wirtz, D. (2004). Rho kinase regulates the intracellular micromechanical response of adherent cells to rho activation. Mol. Biol. Cell 15, 3475–3484.

Kollmar, M. (2015). Polyphyly of nuclear lamin genes indicates an early eukaryotic origin of the metazoan-type intermediate filament proteins. Sci. Rep. 5, 10652.

Kornreich, M., Avinery, R., Malka-Gibor, E., Laser-Azogui, A., and Beck, R. (2015). Order and disorder in intermediate filament proteins. FEBS Lett. 589, 2464–2476.

Kostourou, V., Cartwright, J.E., Johnstone, A.P., Boult, J.K.R., Cullis, E.R., Whitley, G., and Robinson, S.P. (2011). The role of tumour-derived iNOS in tumour progression and angiogenesis. Br. J. Cancer 104, 83–90.

Kouklis, P.D., Papamarcaki, T., Merdes, A., and Georgatos, S.D. (1991). A potential role for the COOH-terminal domain in the lateral packing of type III intermediate filaments. J. Cell Biol. 114, 773–786.

Kreft, K.L., van Meurs, M., Wierenga-Wolf, A.F., Melief, M.-J., van Strien, M.E., Hol, E.M., Oostra, B.A., Laman, J.D., and Hintzen, R.Q. (2014). Abundant kif21b is associated with accelerated progression in neurodegenerative diseases. Acta Neuropathol. Commun. 2, 144.

Kreplak, L., and Fudge, D. (2007). Biomechanical properties of intermediate filaments: from tissues to single filaments and back. BioEssays News Rev. Mol. Cell. Dev. Biol. 29, 26–35.

Kreplak, L., Aebi, U., and Herrmann, H. (2004). Molecular mechanisms underlying the assembly of intermediate filaments. Exp. Cell Res. 301, 77–83.

Kreplak, L., Bär, H., Leterrier, J.F., Herrmann, H., and Aebi, U. (2005). Exploring the Mechanical Behavior of Single Intermediate Filaments. J. Mol. Biol. 354, 569–577.

Ku, N.O., Liao, J., Chou, C.F., and Omary, M.B. (1996). Implications of intermediate filament protein phosphorylation. Cancer Metastasis Rev. 15, 429–444.

Kumar, V., Bouameur, J.-E., Bär, J., Rice, R.H., Hornig-Do, H.-T., Roop, D.R., Schwarz, N., Brodesser, S., Thiering, S., Leube, R.E., et al. (2015). A keratin scaffold regulates epidermal barrier formation, mitochondrial lipid composition, and activity. J. Cell Biol. 211, 1057–1075.

Kwak, H.-I., Kang, H., Dave, J.M., Mendoza, E.A., Su, S.-C., Maxwell, S.A., and Bayless, K.J. (2012). Calpain-mediated vimentin cleavage occurs upstream of MT1-MMP membrane translocation to facilitate endothelial sprout initiation. Angiogenesis 15, 287–303.

Kwiatkowska, A., Didier, S., Fortin, S., Chuang, Y., White, T., Berens, M.E., Rushing, E., Eschbacher, J., Tran, N.L., Chan, A., et al. (2012). The small GTPase RhoG mediates glioblastoma cell invasion. Mol. Cancer 11, 65.

Lariviere, R.C., and Julien, J.-P. (2004). Functions of intermediate filaments in neuronal development and disease. J. Neurobiol. 58, 131–148.

Lau, C.L., O'Shea, R.D., Broberg, B.V., Bischof, L., and Beart, P.M. (2011). The Rho kinase inhibitor Fasudil up-regulates astrocytic glutamate transport subsequent to actin remodelling in murine cultured astrocytes. Br. J. Pharmacol. 163, 533–545.

Lausch, E., Janecke, A., Bros, M., Trojandt, S., Alanay, Y., De Laet, C., Hübner, C.A., Meinecke, P., Nishimura, G., Matsuo, M., et al. (2011). Genetic deficiency of tartrate-resistant acid phosphatase associated with skeletal dysplasia, cerebral calcifications and autoimmunity.

Nat. Genet. 43, 132–137.

Lazarides, E. (1980). Intermediate filaments as mechanical integrators of cellular space. Nature 283, 249–256.

Lazarides, E. (1982). Intermediate filaments: a chemically heterogeneous, developmentally regulated class of proteins. Annu. Rev. Biochem. 51, 219–250.

Leduc, C., and Etienne-Manneville, S. (2015). Intermediate filaments in cell migration and invasion: the unusual suspects. Curr. Opin. Cell Biol. 32, 102–112.

Lepekhin, E.A., Eliasson, C., Berthold, C.H., Berezin, V., Bock, E., and Pekny, M. (2001). Intermediate filaments regulate astrocyte motility. J. Neurochem. 79, 617–625.

Leube, R.E., Moch, M., and Windoffer, R. (2015). Intermediate filaments and the regulation of focal adhesion. Curr. Opin. Cell Biol. 32, 13–20.

Li, H., Guo, Y., Teng, J., Ding, M., Yu, A.C.H., and Chen, J. (2006). 14-3-3 affects dynamics and integrity of glial filaments by binding to phosphorylated GFAP. J. Cell Sci. 119, 4452–4461.

Li, L., Lundkvist, A., Andersson, D., Wilhelmsson, U., Nagai, N., Pardo, A.C., Nodin, C., Ståhlberg, A., Aprico, K., Larsson, K., et al. (2008). Protective role of reactive astrocytes in brain ischemia. J. Cereb. Blood Flow Metab. Off. J. Int. Soc. Cereb. Blood Flow Metab. 28, 468–481.

Li, Y., Vanapalli, S.A., and Duits, M.H.G. (2009). Dynamics of ballistically injected latex particles in living human endothelial cells. Biorheology 46, 309–321.

Liedtke, W., Edelmann, W., Bieri, P.L., Chiu, F.C., Cowan, N.J., Kucherlapati, R., and Raine, C.S. (1996). GFAP is necessary for the integrity of CNS white matter architecture and long-term maintenance of myelination. Neuron 17, 607–615.

Lin, Y.-C., Yao, N.Y., Broedersz, C.P., Herrmann, H., MacKintosh, F.C., and Weitz, D.A. (2010a). Origins of Elasticity in Intermediate Filament Networks. Phys. Rev. Lett. 104.

Lin, Y.-C., Broedersz, C.P., Rowat, A.C., Wedig, T., Herrmann, H., MacKintosh, F.C., and Weitz, D.A. (2010b). Divalent Cations Crosslink Vimentin Intermediate Filament Tail Domains to Regulate Network Mechanics. J. Mol. Biol. 399, 637–644.

Lin, Y.-C., Koenderink, G.H., MacKintosh, F.C., and Weitz, D.A. (2011). Control of non-linear elasticity in F-actin networks with microtubules. Soft Matter 7, 902–906.

Lin, Y.-M., Jan, H.-J., Lee, C.-C., Tao, H.-Y., Shih, Y.-L., Wei, H.-W., and Lee, H.-M. (2008). Dexamethasone reduced invasiveness of human malignant glioblastoma cells through a MAPK phosphatase-1 (MKP-1) dependent mechanism. Eur. J. Pharmacol. 593, 1–9.

Liu, J.K., Lubelski, D., Schonberg, D.L., Wu, Q., Hale, J.S., Flavahan, W.A., Mulkearns-Hubert, E.E., Man, J., Hjelmeland, A.B., Yu, J., et al. (2014a). Phage display discovery of novel molecular targets in glioblastoma-initiating cells. Cell Death Differ. 21, 1325–1339.

Liu, L.Y.-M., Lin, M.-H., Lai, Z.-Y., Jiang, J.-P., Huang, Y.-C., Jao, L.-E., and Chuang, Y.-J. (2016). Motor neuron-derived Thsd7a is essential for zebrafish vascular development via the Notch-dll4 signaling pathway. J. Biomed. Sci. 23, 59.

Liu, Q., Li, G., Li, R., shen, J., He, Q., Deng, L., Zhang, C., and Zhang, J. (2010). IL-6 promotion of glioblastoma cell invasion and angiogenesis in U251 and T98G cell lines. J. Neurooncol. 100, 165–176.

Liu, Z., Li, Y., Cui, Y., Roberts, C., Lu, M., Wilhelmsson, U., Pekny, M., and Chopp, M. (2014b). Beneficial effects of gfap/vimentin reactive astrocytes for axonal remodeling and motor behavioral recovery in mice after stroke. Glia 62, 2022–2033.

Lopez-Egido, J.R., Cunningham, J., Berg, M., Oberg, K., Bongcam-Rudloff, E., and Gobl, A.E. (2002). Menin's Interaction with Glial Fibrillary Acidic Protein and Vimentin Suggests a Role for the Intermediate Filament Network in Regulating Menin Activity. Exp. Cell Res. 278, 175–183.

Louis, D.N., Ohgaki, H., Wiestler, O.D., Cavenee, W.K., Burger, P.C., Jouvet, A., Scheithauer, B.W., and Kleihues, P. (2007). The 2007 WHO classification of tumours of the central nervous system. Acta Neuropathol. (Berl.) 114, 97–109.

Lowery, J., Kuczmarski, E.R., Herrmann, H., and Goldman, R.D. (2015). Intermediate Filaments Play a Pivotal Role in Regulating Cell Architecture and Function. J. Biol. Chem. 290, 17145–17153.

Lu, X. (1993). Network Incorporation of Intermediate Filament Molecules Differs between Preexisting and Newly Assembling Filaments. Exp. Cell Res. 208, 218–225.

Lu, Y.B., Franze, K., Seifert, G., Steinhäuser, C., Kirchhoff, F., Wolburg, H., Guck, J., Janmey, P., Wei, E.Q., Käs, J., et al. (2006). Viscoelastic properties of individual glial cells and neurons in the CNS. Proc. Natl. Acad. Sci. 103, 17759–17764.

Lu, Y.-B., Iandiev, I., Hollborn, M., Korber, N., Ulbricht, E., Hirrlinger, P.G., Pannicke, T., Wei, E.-Q., Bringmann, A., Wolburg, H., et al. (2010). Reactive glial cells: increased stiffness correlates with increased intermediate filament expression. FASEB J. 25, 624–631.

Lynch, C.D., Lazar, A.M., Iskratsch, T., Zhang, X., and Sheetz, M.P. (2012). Endoplasmic spreading requires coalescence of vimentin intermediate filaments at force-bearing adhesions. Mol. Biol. Cell 24, 21–30.

Maas, A.I., Stocchetti, N., and Bullock, R. (2008). Moderate and severe traumatic brain injury in adults. Lancet Neurol. 7, 728–741.

Maglott, D., Ostell, J., Pruitt, K.D., and Tatusova, T. (2011). Entrez Gene: gene-centered information at NCBI. Nucleic Acids Res. 39, D52–D57.

Mamber, C., Kozareva, D.A., Kamphuis, W., and Hol, E.M. (2013). Shades of gray: The delineation of marker expression within the adult rodent subventricular zone. Prog. Neurobiol. 111, 1–16.

Manthorpe, M., Adler, R., and Varon, S. (1979). Development, reactivity and GFA immunofluorescence of astroglia-containing monolayer cultures from rat cerebrum. J. Neurocytol. 8, 605–621.

Margiotta, A., and Bucci, C. (2016). Role of Intermediate Filaments in Vesicular Traffic. Cells 5, 20.

Martinian, L., Boer, K., Middeldorp, J., Hol, E.M., Sisodiya, S.M., Squier, W., Aronica, E., and Thom, M. (2009). Expression patterns of glial fibrillary acidic protein (GFAP)-delta in epilepsy-associated lesional pathologies. Neuropathol. Appl. Neurobiol. 35, 394–405.

Mason, T.G., and Weitz, D.A. (1995). Optical measurements of frequency-dependent linear viscoelastic moduli of complex fluids. Phys. Rev. Lett. 74, 1250–1253.

Massa, P.T., Szuchet, S., and Mugnaini, E. (1984). Cell-cell interactions of isolated and cultured oligodendrocytes: formation of linear occluding junctions and expression of peculiar

intramembrane particles. J. Neurosci. Off. J. Soc. Neurosci. 4, 3128–3139.

Massia, S.P., Rao, S.S., and Hubbell, J.A. (1993). Covalently immobilized laminin peptide Tyr-Ile-Gly-Ser-Arg (YIGSR) supports cell spreading and co-localization of the 67-kilodalton laminin receptor with alpha-actinin and vinculin. J. Biol. Chem. 268, 8053–8059.

McCall, M.A., Gregg, R.G., Behringer, R.R., Brenner, M., Delaney, C.L., Galbreath, E.J., Zhang, C.L., Pearce, R.A., Chiu, S.Y., and Messing, A. (1996). Targeted deletion in astrocyte intermediate filament (Gfap) alters neuronal physiology. Proc. Natl. Acad. Sci. 93, 6361.

McCormick, M.B., Kouklis, P., Syder, A., and Fuchs, E. (1993). The roles of the rod end and the tail in vimentin IF assembly and IF network formation. J. Cell Biol. 122, 395–407.

McLean, W.H., Sultan, N., Parfitt, E., and Lane, E.B. (1994). Polymorphisms in the keratin 8 gene detected by PCR. Hum. Mol. Genet. 3, 1031.

Mendez, M.G., Kojima, S.-I., and Goldman, R.D. (2010). Vimentin induces changes in cell shape, motility, and adhesion during the epithelial to mesenchymal transition. FASEB J. 24, 1838–1851.

Mendez, M.G., Restle, D., and Janmey, P.A. (2014). Vimentin Enhances Cell Elastic Behavior and Protects against Compressive Stress. Biophys. J. 107, 314–323.

Menet, V., y Ribotta, M.G., Chauvet, N., Drian, M.J., Lannoy, J., Colucci-Guyon, E., and Privat, A. (2001). Inactivation of the glial fibrillary acidic protein gene, but not that of vimentin, improves neuronal survival and neurite growth by modifying adhesion molecule expression. J. Neurosci. 21, 6147–6158.

Menet, V., Prieto, M., Privat, A., and Ribotta, M.G. y. (2003). Axonal plasticity and functional recovery after spinal cord injury in mice deficient in both glial fibrillary acidic protein and vimentin genes. Proc. Natl. Acad. Sci. 100, 8999–9004.

Menko, A.S., Bleaken, B.M., Libowitz, A.A., Zhang, L., Stepp, M.A., and Walker, J.L. (2014). A central role for vimentin in regulating repair function during healing of the lens epithelium. Mol. Biol. Cell 25, 776–790.

Meyers, J.R., Planamento, J., Ebrom, P., Krulewitz, N., Wade, E., and Pownall, M.E. (2013). Sulf1 modulates BMP signaling and is required for somite morphogenesis and development of the horizontal myoseptum. Dev. Biol. 378, 107–121.

Middeldorp, J., and Hol, E.M. (2011). GFAP in health and disease. Prog. Neurobiol. 93, 421–443.

Middeldorp, J., Kamphuis, W., Sluijs, J.A., Achoui, D., Leenaars, C.H.C., Feenstra, M.G.P., van Tijn, P., Fischer, D.F., Berkers, C., Ovaa, H., et al. (2009). Intermediate filament transcription in astrocytes is repressed by proteasome inhibition. FASEB J. 23, 2710–2726.

Milanese, M., Bonifacino, T., Zappettini, S., Usai, C., Tacchetti, C., Nobile, M., and Bonanno, G. (2009). e. In International Review of Neurobiology, (Elsevier), pp. 295–318.

Milde-Langosch, K., Karn, T., Schmidt, M., zu Eulenburg, C., Oliveira-Ferrer, L., Wirtz, R.M., Schumacher, U., Witzel, I., Schütze, D., and Müller, V. (2014). Prognostic relevance of glycosylation-associated genes in breast cancer. Breast Cancer Res. Treat. 145, 295–305.

Millard, T.H., Dawson, J., and Machesky, L.M. (2007). Characterisation of IRTKS, a novel IRSp53/MIM family actin regulator with distinct filament bundling properties. J. Cell Sci. 120, 1663–1672.

Miller, W.J., Leventhal, I., Scarsella, D., Haydon, P.G., Janmey, P., and Meaney, D.F. (2009). Mechanically induced reactive gliosis causes ATP-mediated alterations in astrocyte stiffness. J. Neurotrauma 26, 789–797.

Moeton, M., Kanski, R., Stassen, O.M.J.A., Sluijs, J.A., Geerts, D., van Tijn, P., Wiche, G., van Strien, M.E., and Hol, E.M. (2014). Silencing GFAP isoforms in astrocytoma cells disturbs laminin-dependent motility and cell adhesion. FASEB J. Off. Publ. Fed. Am. Soc. Exp. Biol. 28, 2942–2954.

Moeton, M., Stassen, O.M.J.A., Sluijs, J.A., van der Meer, V.W.N., Kluivers, L.J., van Hoorn, H., Schmidt, T., Reits, E.A.J., van Strien, M.E., and Hol, E.M. (2016). GFAP isoforms control intermediate filament network dynamics, cell morphology, and focal adhesions. Cell. Mol. Life Sci. CMLS.

Moir, R.D., Yoon, M., Khuon, S., and Goldman, R.D. (2000). Nuclear lamins A and B1: different pathways of assembly during nuclear envelope formation in living cells. J. Cell Biol. 151, 1155–1168.

Moore, S.W., Zhang, X., Lynch, C.D., and Sheetz, M.P. (2012). Netrin-1 Attracts Axons through FAK-Dependent Mechanotransduction. J. Neurosci. 32, 11574–11585.

Morawski, M., Schilling, S., Kreuzberger, M., Waniek, A., Jäger, C., Koch, B., Cynis, H., Kehlen, A., Arendt, T., Hartlage-Rübsamen, M., et al. (2014). Glutaminyl Cyclase in Human Cortex: Correlation with (pGlu)-Amyloid-β Load and Cognitive Decline in Alzheimer's Disease. J. Alzheimeraposs Dis. 385–400.

Mori, H., Takio, K., Ogawara, M., and Selkoe, D.J. (1992). Mass spectrometry of purified amyloid beta protein in Alzheimer's disease. J. Biol. Chem. 267, 17082–17086.

Moshayedi, P., Ng, G., Kwok, J.C.F., Yeo, G.S.H., Bryant, C.E., Fawcett, J.W., Franze, K., and Guck, J. (2014). The relationship between glial cell mechanosensitivity and foreign body reactions in the central nervous system. Biomaterials 35, 3919–3925.

Mosmann, T. (1983). Rapid colorimetric assay for cellular growth and survival: application to proliferation and cytotoxicity assays. J.Immunol.Methods 65, 55–63.

Mostowy, S., and Cossart, P. (2012). Septins: the fourth component of the cytoskeleton. Nat. Rev. Mol. Cell Biol.

Movilla, N., and Bustelo, X.R. (1999). Biological and regulatory properties of Vav-3, a new member of the Vav family of oncoproteins. Mol. Cell. Biol. 19, 7870–7885.

Muraguchi, T., Takegami, Y., Ohtsuka, T., Kitajima, S., Chandana, E.P.S., Omura, A., Miki, T., Takahashi, R., Matsumoto, N., Ludwig, A., et al. (2007). RECK modulates Notch signaling during cortical neurogenesis by regulating ADAM10 activity. Nat. Neurosci. 10, 838–845.

Murray, M.E., Mendez, M.G., and Janmey, P.A. (2014). Substrate stiffness regulates solubility of cellular vimentin. Mol. Biol. Cell 25, 87–94.

Nakamura, Y., Takeda, M., Aimoto, S., Hojo, H., Takao, T., Shimonishi, Y., Hariguchi, S., and Nishimura, T. (1992). Assembly regulatory domain of glial fibrillary acidic protein. A single phosphorylation diminishes its assembly-accelerating property. J. Biol. Chem. 267, 23269–23274.

Naldini, L., Blomer, U., Gallay, P., Ory, D., Mulligan, R., Gage, F.H., Verma, I.M., and Trono, D. (1996a). In vivo gene delivery and stable transduction of nondividing cells by a lentiviral vector. Science 272, 263–267.

Naldini, L., Blomer, U., Gage, F.H., Trono, D., and Verma, I.M. (1996b). Efficient transfer, integration, and sustained long-term expression of the transgene in adult rat brains injected with a lentiviral vector. Proc.Natl.Acad.Sci.U.S.A 93, 11382–11388.

Neary, J.T., Kang, Y., Tran, M., and Feld, J. (2005). Traumatic Injury Activates Protein Kinase B/Akt in Cultured Astrocytes: Role of Extracellular ATP and P2 Purinergic Receptors. J. Neurotrauma 22, 491–500.

Nekrasova, O.E., Mendez, M.G., Chernoivanenko, I.S., Tyurin-Kuzmin, P.A., Kuczmarski, E.R., Gelfand, V.I., Goldman, R.D., and Minin, A.A. (2011). Vimentin intermediate filaments modulate the motility of mitochondria. Mol. Biol. Cell 22, 2282–2289.

Nielsen, A.L., and Jørgensen, A.L. (2004). Self-assembly of the Cytoskeletal Glial Fibrillary Acidic Protein Is Inhibited by an Isoform-specific C Terminus. J. Biol. Chem. 279, 41537–41545.

Nielsen, A.L., Holm, I.E., Johansen, M., Bonven, B., Jørgensen, P., and Jørgensen, A.L. (2002). A New Splice Variant of Glial Fibrillary Acidic Protein, GFAPε, Interacts with the Presenilin Proteins. J. Biol. Chem. 277, 29983–29991.

Nobuhara, Y., Nakahara, K., Higuchi, I., Yoshida, T., Fushiki, S., Osame, M., Arimura, K., and Nakagawa, M. (2004). Juvenile form of Alexander disease with GFAP mutation and mitochondrial abnormality. Neurology 63, 1302–1304.

Oberheim, N.A., Wang, X., Goldman, S., and Nedergaard, M. (2006). Astrocytic complexity distinguishes the human brain. Trends Neurosci. 29, 547–553.

Oberheim, N.A., Takano, T., Han, X., He, W., Lin, J.H.C., Wang, F., Xu, Q., Wyatt, J.D., Pilcher, W., Ojemann, J.G., et al. (2009). Uniquely Hominid Features of Adult Human Astrocytes. J. Neurosci. 29, 3276–3287.

Oberheim, N.A., Goldman, S.A., and Nedergaard, M. (2012). Heterogeneity of astrocytic form and function. Methods Mol. Biol. Clifton NJ 814, 23–45.

Ogrodnik, M., Salmonowicz, H., Brown, R., Turkowska, J., redniawa, W., Pattabiraman, S., Amen, T., Abraham, A. -c., Eichler, N., Lyakhovetsky, R., et al. (2014). Dynamic JUNQ inclusion bodies are asymmetrically inherited in mammalian cell lines through the asymmetric partitioning of vimentin. Proc. Natl. Acad. Sci. 111, 8049–8054.

Ohgaki, H., and Kleihues, P. (2013). The Definition of Primary and Secondary Glioblastoma. Clin. Cancer Res. 19, 764–772.

Ohira, K., Kumanogoh, H., Sahara, Y., Homma, K.J., Hirai, H., Nakamura, S., and Hayashi, M. (2005). A truncated tropomyosin-related kinase B receptor, T1, regulates glial cell morphology via Rho GDP dissociation inhibitor 1. J. Neurosci. Off. J. Soc. Neurosci. 25, 1343–1353.

Ohira, K., Homma, K.J., Hirai, H., Nakamura, S., and Hayashi, M. (2006). TrkB-T1 regulates the RhoA signaling and actin cytoskeleton in glioma cells. Biochem. Biophys. Res. Commun. 342, 867–874.

Ohshima, N., Kudo, T., Yamashita, Y., Mariggiò, S., Araki, M., Honda, A., Nagano, T., Isaji, C., Kato, N., Corda, D., et al. (2015). New Members of the Mammalian Glycerophosphodiester Phosphodiesterase Family: GDE4 and GDE7 produce lysophosphatidic acid by lysophospholipase D activity. J. Biol. Chem. 290, 4260–4271.

Omary, M.B., Ku, N.-O., Tao, G.-Z., Toivola, D.M., and Liao, J. (2006). "Heads and tails" of intermediate filament phosphorylation: multiple sites and functional insights. Trends

Biochem. Sci. 31, 383–394.

Opal, P., and Goldman, R.D. (2013). Explaining intermediate filament accumulation in giant axonal neuropathy. Rare Dis. Austin Tex 1, e25378.

Orre, M., Kamphuis, W., Osborn, L.M., Jansen, A.H.P., Kooijman, L., Bossers, K., and Hol, E.M. (2014a). Isolation of glia from Alzheimer's mice reveals inflammation and dysfunction. Neurobiol. Aging 35, 2746–2760.

Orre, M., Kamphuis, W., Osborn, L.M., Melief, J., Kooijman, L., Huitinga, I., Klooster, J., Bossers, K., and Hol, E.M. (2014b). Acute isolation and transcriptome characterization of cortical astrocytes and microglia from young and aged mice. Neurobiol. Aging 35, 1–14.

Ortinski, P.I., Dong, J., Mungenast, A., Yue, C., Takano, H., Watson, D.J., Haydon, P.G., and Coulter, D.A. (2010). Selective induction of astrocytic gliosis generates deficits in neuronal inhibition. Nat. Neurosci. 13, 584–591.

O'Shea, R.D., Lau, C.L., Zulaziz, N., Maclean, F.L., Nisbet, D.R., Horne, M.K., and Beart, P.M. (2015). Transcriptomic analysis and 3D bioengineering of astrocytes indicate ROCK inhibition produces cytotrophic astrogliosis. Front. Neurosci. 9.

Ostrow, L.W., Suchyna, T.M., and Sachs, F. (2011). Stretch induced endothelin-1 secretion by adult rat astrocytes involves calcium influx via stretch-activated ion channels (SACs). Biochem. Biophys. Res. Commun. 410, 81–86.

Palani, M., Arunkumar, R., and Vanisree, A.J. (2014). Methylation and expression patterns of tropomyosin-related kinase genes in different grades of glioma. Neuromolecular Med. 16, 529–539.

Park, A.L., Lin, H.-K., Yang, Q., Sing, C.W., Fan, M., Mapstone, T.B., Gross, N.L., Gumerlock, M.K., Martin, M.D., Rabb, C.H., et al. (2010). Differential expression of type 2 3α/type 5 17β-hydroxysteroid dehydrogenase (AKR1C3) in tumors of the central nervous system. Int. J. Clin. Exp. Pathol. 3, 743–754.

Parsons, J.T., Horwitz, A.R., and Schwartz, M.A. (2010). Cell adhesion: integrating cytoskeletal dynamics and cellular tension. Nat. Rev. Mol. Cell Biol. 11, 633–643.

Parthasarathy, R. (2012). Rapid, accurate particle tracking by calculation of radial symmetry centers. Nat. Methods 9, 724–726.

Patel, A.P., Tirosh, I., Trombetta, J.J., Shalek, A.K., Gillespie, S.M., Wakimoto, H., Cahill, D.P., Nahed, B.V., Curry, W.T., Martuza, R.L., et al. (2014). Single-cell RNA-seq highlights intratumoral heterogeneity in primary glioblastoma. Science 344, 1396–1401.

Pawelzyk, P., Mücke, N., Herrmann, H., and Willenbacher, N. (2014). Attractive interactions among intermediate filaments determine network mechanics in vitro. PloS One 9, e93194.

Pecchio, A.R.A., Gizzi, A.M.C., Renner, M.L., Molina-Calavita, M., and Caputto, B.L. (2011). c-Fos activates and physically interacts with specific enzymes of the pathway of synthesis of polyphosphoinositides. Mol. Biol. Cell 22, 4716–4725.

Pekny, M. (2001). Astrocytic intermediate filaments: lessons from GFAP and vimentin knock-out mice. Prog. Brain Res. 132, 23–30.

Pekny, M., Leveen, P., Pekna, M., Eliasson, C., Berthold, C.H., Westermark, B., and Betsholtz, C. (1995). Mice lacking glial fibrillary acidic protein display astrocytes devoid of intermediate filaments but develop and reproduce normally. EMBO J. 14, 1590.

Pekny, M., Johansson, C.B., Eliasson, C., Stakeberg, J., Wallén, \AA, Perlmann, T., Lendahl, U., Betsholtz, C., Berthold, C.H., and Frisén, J. (1999). Abnormal reaction to central nervous system injury in mice lacking glial fibrillary acidic protein and vimentin. J. Cell Biol. 145, 503–514.

Pekny, M., Pekna, M., Messing, A., Steinhäuser, C., Lee, J.-M., Parpura, V., Hol, E.M., Sofroniew, M.V., and Verkhratsky, A. (2016). Astrocytes: a central element in neurological diseases. Acta Neuropathol. (Berl.) 131, 323–345.

Pelletier, V., Gal, N., Fournier, P., and Kilfoil, M.L. (2009). Microrheology of Microtubule Solutions and Actin-Microtubule Composite Networks. Phys. Rev. Lett. 102.

Pérez-Sala, D., Oeste, C.L., Martínez, A.E., Carrasco, M.J., Garzón, B., and Cañada, F.J. (2015). Vimentin filament organization and stress sensing depend on its single cysteine residue and zinc binding. Nat. Commun. 6, 7287.

Perlson, E., Hanz, S., Ben-Yaakov, K., Segal-Ruder, Y., Seger, R., and Fainzilber, M. (2005). Vimentin-Dependent Spatial Translocation of an Activated MAP Kinase in Injured Nerve. Neuron 45, 715–726.

Perng, M.D., Cairns, L., van den IJssel, P., Prescott, A., Hutcheson, A.M., and Quinlan, R.A. (1999). Intermediate filament interactions can be altered by HSP27 and alphaB-crystallin. J. Cell Sci. 112 (Pt 13), 2099–2112.

Perng, M.D., Su, M., Wen, S.F., Li, R., Gibbon, T., Prescott, A.R., Brenner, M., and Quinlan, R.A. (2006). The Alexander disease-causing glial fibrillary acidic protein mutant, R416W, accumulates into Rosenthal fibers by a pathway that involves filament aggregation and the association of alpha B-crystallin and HSP27. Am. J. Hum. Genet. 79, 197–213.

Perng, M.-D., Wen, S.-F., Gibbon, T., Middeldorp, J., Sluijs, J., Hol, E.M., and Quinlan, R.A. (2008). Glial Fibrillary Acidic Protein Filaments Can Tolerate the Incorporation of Assembly-compromised GFAP- , but with Consequences for Filament Organization and B-Crystallin Association. Mol. Biol. Cell 19, 4521–4533.

Pézeron, G., Millen, K., Boukhatmi, H., and Bray, S. (2014). Notch directly regulates the cell morphogenesis genes Reck, talin and trio in adult muscle progenitors. J. Cell Sci. 127, 4634–4644.

Pietras, A., Katz, A.M., Ekström, E.J., Wee, B., Halliday, J.J., Pitter, K.L., Werbeck, J.L., Amankulor, N.M., Huse, J.T., and Holland, E.C. (2014). Osteopontin-CD44 Signaling in the Glioma Perivascular Niche Enhances Cancer Stem Cell Phenotypes and Promotes Aggressive Tumor Growth. Cell Stem Cell 14, 357–369.

Pluznick, J.L., Zou, D.-J., Zhang, X., Yan, Q., Rodriguez-Gil, D.J., Eisner, C., Wells, E., Greer, C.A., Wang, T., Firestein, S., et al. (2009). Functional expression of the olfactory signaling system in the kidney. Proc. Natl. Acad. Sci. 106, 2059–2064.

Portal, M.M., Ferrero, G.O., and Caputto, B.L. (2007). N-Terminal c-Fos tyrosine phosphorylation regulates c-Fos/ER association and c-Fos-dependent phospholipid synthesis activation. Oncogene 26, 3551–3558.

Potokar, M., Stenovec, M., Gabrijel, M., Li, L., Kreft, M., Grilc, S., Pekny, M., and Zorec, R. (2010). Intermediate filaments attenuate stimulation-dependent mobility of endosomes/ lysosomes in astrocytes. Glia NA – NA.

Prabhakar, S., Asuthkar, S., Lee, W., Chigurupati, S., Zakharian, E., Tsung, A.J., and Velpula, K.K. (2014). Targeting DUSPs in glioblastomas - wielding a double-edged sword? Cell Biol. Int. 38, 145–153.

Prust, M., Wang, J., Morizono, H., Messing, A., Brenner, M., Gordon, E., Hartka, T., Sokohl, A., Schiffmann, R., Gordish-Dressman, H., et al. (2011). GFAP mutations, age at onset, and clinical subtypes in Alexander disease. Neurology 77, 1287–1294.

Puschmann, T.B., Dixon, K.J., and Turnley, A.M. (2010). Species Differences in Reactivity of Mouse and Rat Astrocytes in vitro. Neurosignals 18, 152–163.

Puschmann, T.B., Zandén, C., De Pablo, Y., Kirchhoff, F., Pekna, M., Liu, J., and Pekny, M. (2013). Bioactive 3D cell culture system minimizes cellular stress and maintains the in vivo -like morphological complexity of astroglial cells. Glia 61, 432–440.

Pyka, M., Wetzel, C., Aguado, A., Geissler, M., Hatt, H., and Faissner, A. (2011). Chondroitin sulfate proteoglycans regulate astrocyte-dependent synaptogenesis and modulate synaptic activity in primary embryonic hippocampal neurons: Proteoglycans regulate synaptogenesis. Eur. J. Neurosci. 33, 2187–2202.

Racchetti, G., D'Alessandro, R., and Meldolesi, J. (2012). Astrocyte stellation, a process dependent on Rac1 is sustained by the regulated exocytosis of enlargeosomes. Glia 60, 465–475.

Ragel, B.T., Couldwell, W.T., Gillespie, D.L., and Jensen, R.L. (2007). Identification of hypoxia-induced genes in a malignant glioma cell line (U-251) by cDNA microarray analysis. Neurosurg. Rev. 30, 181–187; discussion 187.

Ramms, L., Fabris, G., Windoffer, R., Schwarz, N., Springer, R., Zhou, C., Lazar, J., Stiefel, S., Hersch, N., Schnakenberg, U., et al. (2013). Keratins as the main component for the mechanical integrity of keratinocytes. Proc. Natl. Acad. Sci. U. S. A. 110, 18513–18518.

Ramsbottom, S.A., Maguire, R.J., Fellgett, S.W., and Pownall, M.E. (2014). Sulf1 influences the Shh morphogen gradient during the dorsal ventral patterning of the neural tube in Xenopus tropicalis. Dev. Biol. 391, 207–218.

Rekik, L., Daguin-Nerrière, V., Petit, J.-Y., and Brachet, P. (2011). γ-Aminobutyric acid type B receptor changes in the rat striatum and substantia nigra following intrastriatal quinolinic acid lesions. J. Neurosci. Res. 89, 524–535.

Ridge, K.M., Shumaker, D., Robert, A., Hookway, C., Gelfand, V.I., Janmey, P.A., Lowery, J., Guo, M., Weitz, D.A., Kuczmarski, E., et al. (2016). Methods for Determining the Cellular Functions of Vimentin Intermediate Filaments. In Methods in Enzymology, (Elsevier), pp. 389–426.

Rihani, A., Van Maerken, T., Pattyn, F., Van Peer, G., Beckers, A., De Brouwer, S., Kumps, C., Mets, E., Van der Meulen, J., Rondou, P., et al. (2013). Effective Alu Repeat Based RT-Qpcr Normalization in Cancer Cell Perturbation Experiments. PLoS ONE 8, e71776.

Ripke, S., O'Dushlaine, C., Chambert, K., Moran, J.L., Kähler, A.K., Akterin, S., Bergen, S.E., Collins, A.L., Crowley, J.J., Fromer, M., et al. (2013). Genome-wide association analysis identifies 13 new risk loci for schizophrenia. Nat. Genet. 45, 1150–1159.

Robert, A., Herrmann, H., Davidson, M.W., and Gelfand, V.I. (2014). Microtubule-dependent transport of vimentin filament precursors is regulated by actin and by the concerted action of Rho- and p21-activated kinases. FASEB J. fj.14–250019.

Roelofs, R.F., Fischer, D.F., Houtman, S.H., Sluijs, J.A., Van Haren, W., Van Leeuwen, F.W., and Hol, E.M. (2005). Adult human subventricular, subgranular, and subpial zones contain astrocytes with a specialized intermediate filament cytoskeleton. Glia 52, 289–300.

Rosenfeld, J.V., Maas, A.I., Bragge, P., Morganti-Kossmann, M.C., Manley, G.T., and Gruen,

R.L. (2012). Early management of severe traumatic brain injury. The Lancet 380, 1088–1098.

Ruijter, J.M., Thygesen, H.H., Schoneveld, O.J., Das, A.T., Berkhout, B., and Lamers, W.H. (2006). Factor correction as a tool to eliminate between-session variation in replicate experiments: application to molecular biology and retrovirology. Retrovirology. 3, 2.

Russell, D., Andrews, P.D., James, J., and Lane, E.B. (2004). Mechanical stress induces profound remodelling of keratin filaments and cell junctions in epidermolysis bullosa simplex keratinocytes. J. Cell Sci. 117, 5233–5243.

Rutka, J.T., and Smith, S.L. (1993). Transfection of human astrocytoma cells with glial fibrillary acidic protein complementary DNA: analysis of expression, proliferation, and tumorigenicity. Cancer Res. 53, 3624–3631.

Rutka, J.T., Hubbard, S.L., Fukuyama, K., Matsuzawa, K., Dirks, P.B., and Becker, L.E. (1994). Effects of antisense glial fibrillary acidic protein complementary DNA on the growth, invasion, and adhesion of human astrocytoma cells. Cancer Res. 54, 3267–3272.

Rutka, J.T., Ackerley, C., Hubbard, S.L., Tilup, A., Dirks, P.B., Jung, S., Ivanchuk, S., Kurimoto, M., Tsugu, A., and Becker, L.E. (1998). Characterization of glial filament-cytoskeletal interactions in human astrocytomas: an immuno-ultrastructural analysis. Eur. J. Cell Biol. 76, 279–287.

Rutka, J.T., Ivanchuk, S., Mondal, S., Taylor, M., Sakai, K., Dirks, P., Jun, P., Jung, S., Becker, L.E., and Ackerley, C. (1999). Co-expression of nestin and vimentin intermediate filaments in invasive human astrocytoma cells. Int. J. Dev. Neurosci. 17, 503–515.

Sahlgren, C.M., Pallari, H.-M., He, T., Chou, Y.-H., Goldman, R.D., and Eriksson, J.E. (2006). A nestin scaffold links Cdk5/p35 signaling to oxidant-induced cell death. EMBO J. 25, 4808–4819.

Sakamoto, Y., Boëda, B., and Etienne-Manneville, S. (2013). APC binds intermediate filaments and is required for their reorganization during cell migration. J. Cell Biol. 200, 249–258.

Salhia, B., Tran, N.L., Chan, A., Wolf, A., Nakada, M., Rutka, F., Ennis, M., McDonough, W.S., Berens, M.E., Symons, M., et al. (2008). The guanine nucleotide exchange factors trio, Ect2, and Vav3 mediate the invasive behavior of glioblastoma. Am. J. Pathol. 173, 1828–1838.

Sanbe, A., Osinska, H., Saffitz, J.E., Glabe, C.G., Kayed, R., Maloyan, A., and Robbins, J. (2004). Desmin-related cardiomyopathy in transgenic mice: a cardiac amyloidosis. Proc. Natl. Acad. Sci. U. S. A. 101, 10132–10136.

Sankar, S., Tanner, J.M., Bell, R., Chaturvedi, A., Randall, R.L., Beckerle, M.C., and Lessnick, S.L. (2013). A Novel Role for Keratin 17 in Coordinating Oncogenic Transformation and Cellular Adhesion in Ewing Sarcoma. Mol. Cell. Biol. 33, 4448–4460.

dos Santos, G., Rogel, M.R., Baker, M.A., Troken, J.R., Urich, D., Morales-Nebreda, L., Sennello, J.A., Kutuzov, M.A., Sitikov, A., Davis, J.M., et al. (2015). Vimentin regulates activation of the NLRP3 inflammasome. Nat. Commun. 6, 6574.

Satoh, K., Hata, M., Takahara, S., Tsuzaki, H., Yokota, H., Akatsu, H., Yamamoto, T., Kosaka, K., and Yamada, T. (2006). A novel membrane protein, encoded by the gene covering KIAA0233, is transcriptionally induced in senile plaque-associated astrocytes. Brain Res. 1108, 19–27.

Savin, T., and Doyle, P.S. (2005a). Static and Dynamic Errors in Particle Tracking Microrheology. Biophys. J. 88, 623–638.

Savin, T., and Doyle, P.S. (2005b). Role of a finite exposure time on measuring an elastic modulus using microrheology. Phys. Rev. E 71.

Schachtrup, C., Le Moan, N., Passino, M.A., and Akassoglou, K. (2011). Hepatic stellate cells and astrocytes: Stars of scar formation and tissue repair. Cell Cycle 10, 1764–1771.

Scheiman, J., Jamieson, K.V., Ziello, J., Tseng, J.-C., and Meruelo, D. (2010). Extraribosomal functions associated with the C terminus of the 37/67 kDa laminin receptor are required for maintaining cell viability. Cell Death Dis. 1, e42.

Schilling, S., Zeitschel, U., Hoffmann, T., Heiser, U., Francke, M., Kehlen, A., Holzer, M., Hutter-Paier, B., Prokesch, M., Windisch, M., et al. (2008). Glutaminyl cyclase inhibition attenuates pyroglutamate Abeta and Alzheimer's disease-like pathology. Nat. Med. 14, 1106–1111.

Schlenzig, D., Rönicke, R., Cynis, H., Ludwig, H.-H., Scheel, E., Reymann, K., Saido, T., Hause, G., Schilling, S., and Demuth, H.-U. (2012). N-Terminal pyroglutamate formation of Aβ38 and Aβ40 enforces oligomer formation and potency to disrupt hippocampal long-term potentiation. J. Neurochem. 121, 774–784.

Schneider, M.R., Wolf, E., Hoeflich, A., and Lahm, H. (2002). IGF-binding protein-5: flexible player in the IGF system and effector on its own. J. Endocrinol. 172, 423–440.

Schuelke, M., Smeitink, J., Mariman, E., Loeffen, J., Plecko, B., Trijbels, F., Stöckler-Ipsiroglu, S., and van den Heuvel, L. (1999). Mutant NDUFV1 subunit of mitochondrial complex I causes leukodystrophy and myoclonic epilepsy. Nat. Genet. 21, 260–261.

Shaulian, E., and Karin, M. (2002). AP-1 as a regulator of cell life and death. Nat. Cell Biol. 4, E131–E136.

Shen, X., Xi, G., Wai, C., and Clemmons, D.R. (2015). The coordinate cellular response to insulin-like growth factor-I (IGF-I) and insulin-like growth factor-binding protein-2 (IGFBP-2) is regulated through vimentin binding to receptor tyrosine phosphatase β (RPTPβ). J. Biol. Chem. 290, 11578–11590.

Shibuki, K., Gomi, H., Chen, L., Bao, S., Kim, J.J., Wakatsuki, H., Fujisaki, T., Fujimoto, K., Katoh, A., Ikeda, T., et al. (1996). Deficient cerebellar long-term depression, impaired eyeblink conditioning, and normal motor coordination in GFAP mutant mice. Neuron 16, 587–599.

Sihag, R.K., Inagaki, M., Yamaguchi, T., Shea, T.B., and Pant, H.C. (2007). Role of phosphorylation on the structural dynamics and function of types III and IV intermediate filaments. Exp. Cell Res. 313, 2098–2109.

Sivaramakrishnan, S., DeGiulio, J.V., Lorand, L., Goldman, R.D., and Ridge, K.M. (2008). Micromechanical properties of keratin intermediate filament networks. Proc. Natl. Acad. Sci. 105, 889–894.

Skalli, O., Chou, Y.H., and Goldman, R.D. (1992). Intermediate filaments: not so tough after all. Trends Cell Biol. 2, 308–312.

Smyth, G.K. (2004). Linear Models and Empirical Bayes Methods for Assessing Differential Expression in Microarray Experiments. Stat. Appl. Genet. Mol. Biol. 3.

Smyth, G.K. (2005). Limma: linear models for microarray data. In: "Bioinformatics and Computational Biology Solutions using R and Bioconductor" (New York: Springer).

Snider, N.T., and Omary, M.B. (2014). Post-translational modifications of intermediate

filament proteins: mechanisms and functions. Nat. Rev. Mol. Cell Biol. 15, 163–177.

Soellner, P., Quinlan, R.A., and Franke, W.W. (1985). Identification of a distinct soluble subunit of an intermediate filament protein: tetrameric vimentin from living cells. Proc. Natl. Acad. Sci. 82, 7929–7933.

Sofroniew, M.V. (2009). Molecular dissection of reactive astrogliosis and glial scar formation. Trends Neurosci. 32, 638–647.

Sofroniew, M.V., and Vinters, H.V. (2010). Astrocytes: biology and pathology. Acta Neuropathol. (Berl.) 119, 7–35.

Song, S., Landsbury, A., Dahm, R., Liu, Y., Zhang, Q., and Quinlan, R.A. (2009). Functions of the intermediate filament cytoskeleton in the eye lens. J. Clin. Invest. 119, 1837–1848.

Sosunov, A.A., Guilfoyle, E., Wu, X., McKhann, G.M., and Goldman, J.E. (2013). Phenotypic conversions of "protoplasmic" to "reactive" astrocytes in Alexander disease. J. Neurosci. Off. J. Soc. Neurosci. 33, 7439–7450.

Souady, J., Hülsewig, M., Distler, U., Haier, J., Denz, A., Pilarsky, C., Senninger, N., Dreisewerd, K., Peter-Katalinic, J., and Müthing, J. (2011). Differences in CD75s- and iso-CD75s-ganglioside content and altered mRNA expression of sialyltransferases ST6GAL1 and ST3GAL6 in human hepatocellular carcinomas and nontumoral liver tissues. Glycobiology 21, 584–594.

Starr, D.A., and Fridolfsson, H.N. (2010). Interactions Between Nuclei and the Cytoskeleton Are Mediated by SUN-KASH Nuclear-Envelope Bridges. Annu. Rev. Cell Dev. Biol. 26, 421–444.

Steele, M.L., Fuller, S., Maczurek, A.E., Kersaitis, C., Ooi, L., and Münch, G. (2012). Chronic Inflammation Alters Production and Release of Glutathione and Related Thiols in Human U373 Astroglial Cells. Cell. Mol. Neurobiol.

Strelkov, S.V., Herrmann, H., and Aebi, U. (2003). Molecular architecture of intermediate filaments. BioEssays News Rev. Mol. Cell. Dev. Biol. 25, 243–251.

van Strien, M.E., Sluijs, J.A., Reynolds, B.A., Steindler, D.A., Aronica, E., and Hol, E.M. (2014). Isolation of Neural Progenitor Cells From the Human Adult Subventricular Zone Based on Expression of the Cell Surface Marker CD271. Stem Cells Transl. Med. 3, 470–480.

Stuhrmann, B., Soares e Silva, M., Depken, M., MacKintosh, F.C., and Koenderink, G.H. (2012). Nonequilibrium fluctuations of a remodeling in vitro cytoskeleton. Phys. Rev. E 86.

Styers, M.L. (2004). The Endo-Lysosomal Sorting Machinery Interacts with the Intermediate Filament Cytoskeleton. Mol. Biol. Cell 15, 5369–5382.

Suchyna, T.M., Tape, S.E., Koeppe, R.E., Andersen, O.S., Sachs, F., and Gottlieb, P.A. (2004). Bilayer-dependent inhibition of mechanosensitive channels by neuroactive peptide enantiomers. Nature 430, 235–240.

Sullivan, S.M., Lee, A., Björkman, S.T., Miller, S.M., Sullivan, R.K.P., Poronnik, P., Colditz, P.B., and Pow, D.V. (2007). Cytoskeletal Anchoring of GLAST Determines Susceptibility to Brain Damage An identified role for GFAP. J. Biol. Chem. 282, 29414–29423.

Swift, J., Ivanovska, I.L., Buxboim, A., Harada, T., Dingal, P.C.D.P., Pinter, J., Pajerowski, J.D., Spinler, K.R., Shin, J.-W., Tewari, M., et al. (2013). Nuclear Lamin-A Scales with Tissue Stiffness and Enhances Matrix-Directed Differentiation. Science 341, 1240104–1240104.

Tanaka, H., Goto, H., Inoko, A., Makihara, H., Enomoto, A., Horimoto, K., Matsuyama, M., Kurita, K., Izawa, I., and Inagaki, M. (2015). Cytokinetic Failure-induced Tetraploidy Develops into Aneuploidy, Triggering Skin Aging in Phosphovimentin-deficient Mice. J. Biol. Chem. 290, 12984–12998.

Tang, G., Xu, Z., and Goldman, J.E. (2006). Synergistic Effects of the SAPK/JNK and the Proteasome Pathway on Glial Fibrillary Acidic Protein (GFAP) Accumulation in Alexander Disease. J. Biol. Chem. 281, 38634–38643.

Tang, G., Perng, M.D., Wilk, S., Quinlan, R., and Goldman, J.E. (2010). Oligomers of Mutant Glial Fibrillary Acidic Protein (GFAP) Inhibit the Proteasome System in Alexander Disease Astrocytes, and the Small Heat Shock Protein αB-Crystallin Reverses the Inhibition. J. Biol. Chem. 285, 10527–10537.

Thiele, C.J., Li, Z., and McKee, A.E. (2009). On Trk--the TrkB signal transduction pathway is an increasingly important target in cancer biology. Clin. Cancer Res. Off. J. Am. Assoc. Cancer Res. 15, 5962–5967.

Thiery, J.P., Acloque, H., Huang, R.Y.J., and Nieto, M.A. (2009). Epithelial-Mesenchymal Transitions in Development and Disease. Cell 139, 871–890.

Thurston, G., Jaggi, B., and Palcic, B. (1988). Measurement of cell motility and morphology with an automated microscope system. Cytometry 9, 411–417.

Tian, R., Gregor, M., Wiche, G., and Goldman, J.E. (2006). Plectin Regulates the Organization of Glial Fibrillary Acidic Protein in Alexander Disease. Am. J. Pathol. 168, 888–897.

Tian, R., Wu, X., Hagemann, T.L., Sosunov, A.A., Messing, A., McKhann, G.M., and Goldman, J.E. (2010). Alexander disease mutant glial fibrillary acidic protein compromises glutamate transport in astrocytes. J. Neuropathol. Exp. Neurol. 69, 335–345.

Toivola, D.M., Tao, G.-Z., Habtezion, A., Liao, J., and Omary, M.B. (2005). Cellular integrity plus: organelle-related and protein-targeting functions of intermediate filaments. Trends Cell Biol. 15, 608–617.

Toivola, D.M., Strnad, P., Habtezion, A., and Omary, M.B. (2010). Intermediate filaments take the heat as stress proteins. Trends Cell Biol. 20, 79–91.

Tomokane, N., Iwaki, T., Tateishi, J., Iwaki, A., and Goldman, J.E. (1991). Rosenthal fibers share epitopes with alpha B-crystallin, glial fibrillary acidic protein, and ubiquitin, but not with vimentin. Immunoelectron microscopy with colloidal gold. Am. J. Pathol. 138, 875–885.

Tran, M.D., and Neary, J.T. (2006). Purinergic signaling induces thrombospondin-1 expression in astrocytes. Proc. Natl. Acad. Sci. 103, 9321–9326.

Tran, M.D., Wanner, I.B., and Neary, J.T. (2008). Purinergic receptor signaling regulates N-cadherin expression in primary astrocyte cultures. J. Neurochem. 105, 272–286.

Trappmann, B., Gautrot, J.E., Connelly, J.T., Strange, D.G.T., Li, Y., Oyen, M.L., Cohen Stuart, M.A., Boehm, H., Li, B., Vogel, V., et al. (2012). Extracellular-matrix tethering regulates stem-cell fate. Nat. Mater. 11, 642–649.

Tremblay, P., Beaudet, M.-J., Tremblay, E., Rueda, N., Thomas, T., and Vallières, L. (2011). Matrix metalloproteinase 2 attenuates brain tumour growth, while promoting macrophage recruitment and vascular repair. J. Pathol. 224, 222–233.

Tsuruta, D., and Jones, J.C.R. (2003). The vimentin cytoskeleton regulates focal contact size

and adhesion of endothelial cells subjected to shear stress. J. Cell Sci. 116, 4977–4984.

Twal, W.O., Czirok, A., Hegedus, B., Knaak, C., Chintalapudi, M.R., Okagawa, H., Sugi, Y., and Argraves, W.S. (2001). Fibulin-1 suppression of fibronectin-regulated cell adhesion and motility. J. Cell Sci. 114, 4587–4598.

Tyler, W.J. (2012). The mechanobiology of brain function. Nat. Rev. Neurosci. 13, 867–878.

Tzivion, G., Luo, Z.J., and Avruch, J. (2000). Calyculin A-induced vimentin phosphorylation sequesters 14-3-3 and displaces other 14-3-3 partners in vivo. J. Biol. Chem. 275, 29772–29778.

Valentine, M.T., Perlman, Z.E., Gardel, M.L., Shin, J.H., Matsudaira, P., Mitchison, T.J., and Weitz, D.A. (2004). Colloid Surface Chemistry Critically Affects Multiple Particle Tracking Measurements of Biomaterials. Biophys. J. 86, 4004–4014.

Van Den Berge, S.A., Middeldorp, J., Zhang, C.E., Curtis, M.A., Leonard, B.W., Mastroeni, D., Voorn, P., Van De Berg, W.D.J., Huitinga, I., and Hol, E.M. (2010). Longterm quiescent cells in the aged human subventricular neurogenic system specifically express GFAP-δ. Aging Cell 9, 313–326.

Vardjan, N., Gabrijel, M., Potokar, M., Švajger, U., Kreft, M., Jeras, M., de Pablo, Y., Faiz, M., Pekny, M., and Zorec, R. (2012). IFN-γ-induced increase in the mobility of MHC class II compartments in astrocytes depends on intermediate filaments. J. Neuroinflammation 9, 144.

Velasco, M.E., Dahl, D., Roessmann, U., and Gambetti, P. (1980). Immunohistochemical localization of glial fibrillary acidic protein in human glial neoplasms. Cancer 45, 484–494.

Verhaak, R.G.W., Hoadley, K.A., Purdom, E., Wang, V., Qi, Y., Wilkerson, M.D., Miller, C.R., Ding, L., Golub, T., Mesirov, J.P., et al. (2010). Integrated genomic analysis identifies clinically relevant subtypes of glioblastoma characterized by abnormalities in PDGFRA, IDH1, EGFR, and NF1. Cancer Cell 17, 98–110.

Vincent, P.A., Xiao, K., Buckley, K.M., and Kowalczyk, A.P. (2004). VE-cadherin: adhesion at arm's length. Am. J. Physiol. Cell Physiol. 286, C987–C997.

Virtakoivu, R., Mai, A., Mattila, E., Franceschi, N.D., Imanishi, S.Y., Corthals, G., Kaukonen, R., Saari, M., Cheng, F., Torvaldson, E., et al. (2015). Vimentin-ERK signaling uncouples Slug gene regulatory function. Cancer Res. canres.2842.2014.

Vuoriluoto, K., Haugen, H., Kiviluoto, S., Mpindi, J.-P., Nevo, J., Gjerdrum, C., Tiron, C., Lorens, J.B., and Ivaska, J. (2011). Vimentin regulates EMT induction by Slug and oncogenic H-Ras and migration by governing Axl expression in breast cancer. Oncogene 30, 1436–1448.

Waha, A., Felsberg, J., Hartmann, W., von dem Knesebeck, A., Mikeska, T., Joos, S., Wolter, M., Koch, A., Yan, P.S., Endl, E., et al. (2010). Epigenetic downregulation of mitogen-activated protein kinase phosphatase MKP-2 relieves its growth suppressive activity in glioma cells. Cancer Res. 70, 1689–1699.

Waigh, T.A. (2005). Microrheology of complex fluids. Rep. Prog. Phys. 68, 685–742.

Walls, A.B., Waagepetersen, H.S., Bak, L.K., Schousboe, A., and Sonnewald, U. (2015). The glutamine-glutamate/GABA cycle: function, regional differences in glutamate and GABA production and effects of interference with GABA metabolism. Neurochem. Res. 40, 402–409.

Wang, H., Lathia, J.D., Wu, Q., Wang, J., Li, Z., Heddleston, J.M., Eyler, C.E., Elderbroom, J., Gallagher, J., Schuschu, J., et al. (2009). Targeting Interleukin 6 Signaling Suppresses Glioma Stem Cell Survival and Tumor Growth. Stem Cells 27, 2393–2404.

Wang, R., Chadalavada, K., Wilshire, J., Kowalik, U., Hovinga, K.E., Geber, A., Fligelman, B., Leversha, M., Brennan, C., and Tabar, V. (2010). Glioblastoma stem-like cells give rise to tumour endothelium. Nature 468, 829–833.

Wang, Y.-P., Huang, L.-Y., Sun, W.-M., Zhang, Z.-Z., Fang, J.-Z., Wei, B.-F., Wu, B.-H., and Han, Z.-G. (2013). Insulin receptor tyrosine kinase substrate activates EGFR/ERK signalling pathway and promotes cell proliferation of hepatocellular carcinoma. Cancer Lett. 337, 96–106.

Wanner, I.-B. (2012). An In Vitro Trauma Model to Study Rodent and Human Astrocyte Reactivity. In Astrocytes, R. Milner, ed. (Totowa, NJ: Humana Press), pp. 189–219.

Wanner, I.B., Deik, A., Torres, M., Rosendahl, A., Neary, J.T., Lemmon, V.P., and Bixby, J.L. (2008). A new in vitro model of the glial scar inhibits axon growth. Glia 56, 1691–1709.

Weiner, I.D., Mitch, W.E., and Sands, J.M. (2015). Urea and Ammonia Metabolism and the Control of Renal Nitrogen Excretion. Clin. J. Am. Soc. Nephrol. 10, 1444–1458.

Weinstein, D.E., Shelanski, M.L., and Liem, R.K. (1991). Suppression by antisense mRNA demonstrates a requirement for the glial fibrillary acidic protein in the formation of stable astrocytic processes in response to neurons. J. Cell Biol. 112, 1205–1213.

Wen, H., Kim, N., Fuentes, E.J., Mallinger, A., Gonzalez-Alegre, P., and Glenn, K.A. (2010). FBG1 is a promiscuous ubiquitin ligase that sequesters APC2 and causes S-phase arrest. Cell Cycle Georget. Tex 9, 4506–4517.

West, G., Gullmets, J., Virtanen, L., Li, S.P., Keinänen, A., Shimi, T., Mauermann, M., Heliö, T., Kaartinen, M., Ollila, L., et al. (2016). Deleterious assembly of mutant p.S143P lamin A/C causes ER stress in familial dilated cardiomyopathy. J. Cell Sci.

Widestrand, Å., Faijerson, J., Wilhelmsson, U., Smith, P.L.P., Li, L., Sihlbom, C., Eriksson, P.S., and Pekny, M. (2007). Increased Neurogenesis and Astrogenesis from Neural Progenitor Cells Grafted in the Hippocampus of GFAP −/− Vim −/− Mice. Stem Cells 25, 2619–2627.

Wilhelmsson, U. (2004). Absence of Glial Fibrillary Acidic Protein and Vimentin Prevents Hypertrophy of Astrocytic Processes and Improves Post-Traumatic Regeneration. J. Neurosci. 24, 5016–5021.

Wilhelmsson, U., Eliasson, C., Bjerkvig, R., and Pekny, M. (2003). Loss of GFAP expression in high-grade astrocytomas does not contribute to tumor development or progression. Oncogene 22, 3407–3411.

Wilhelmsson, U., Bushong, E.A., Price, D.L., Smarr, B.L., Phung, V., Terada, M., Ellisman, M.H., and Pekny, M. (2006). Redefining the concept of reactive astrocytes as cells that remain within their unique domains upon reaction to injury. Proc. Natl. Acad. Sci. U. S. A. 103, 17513–17518.

Wilhelmsson, U., Faiz, M., de Pablo, Y., Sjöqvist, M., Andersson, D., Widestrand, Å., Potokar, M., Stenovec, M., Smith, P.L.P., Shinjyo, N., et al. (2012). Astrocytes Negatively Regulate Neurogenesis Through the Jagged1-Mediated Notch Pathway. STEM CELLS 30, 2320–2329.

Williams, E.C., Zhong, X., Mohamed, A., Li, R., Liu, Y., Dong, Q., Ananiev, G.E., Mok,

J.C.C., Lin, B.R., Lu, J., et al. (2014). Mutant astrocytes differentiated from Rett syndrome patients-specific iPSCs have adverse effects on wild-type neurons. Hum. Mol. Genet. 23, 2968–2980.

Wippold, F.J., Perry, A., and Lennerz, J. (2006). Neuropathology for the neuroradiologist: Rosenthal fibers. AJNR Am. J. Neuroradiol. 27, 958–961.

Witt, N., Rodger, G., Vandesompele, J., Benes, V., Zumla, A., Rook, G.A., and Huggett, J.F. (2009). An assessment of air as a source of DNA contamination encountered when performing PCR. J. Biomol. Tech. JBT 20, 236–240.

Wittnam, J.L., Portelius, E., Zetterberg, H., Gustavsson, M.K., Schilling, S., Koch, B., Demuth, H.-U., Blennow, K., Wirths, O., and Bayer, T.A. (2012). Pyroglutamate amyloid β (Aβ) aggravates behavioral deficits in transgenic amyloid mouse model for Alzheimer disease. J. Biol. Chem. 287, 8154–8162.

Wolfenson, H., Henis, Y.I., Geiger, B., and Bershadsky, A.D. (2009). The heel and toe of the cell's foot: a multifaceted approach for understanding the structure and dynamics of focal adhesions. Cell Motil. Cytoskeleton 66, 1017–1029.

Wolfenson, H., Bershadsky, A., Henis, Y.I., and Geiger, B. (2011). Actomyosin-generated tension controls the molecular kinetics of focal adhesions. J. Cell Sci. 124, 1425–1432.

Wong, L.H., Kurniawan, N.A., Too, H.-P., and Rajagopalan, R. (2014). Spatially resolved microrheology of heterogeneous biopolymer hydrogels using covalently bound microspheres. Biomech. Model. Mechanobiol. 13, 839–849.

Xiong, J., Zhou, L.I., Lim, Y., Yang, M., Zhu, Y.-H., Li, Z.-W., Fu, D.-L., and Zhou, X.-F. (2015). Mature brain-derived neurotrophic factor and its receptor TrkB are upregulated in human glioma tissues. Oncol. Lett. 10, 223–227.

Xiong, W., Zhao, J., Yu, H., Li, X., Sun, S., Li, Y., Xia, Q., Zhang, C., He, Q., Gao, X., et al. (2014). Elevated expression of AKR1C3 increases resistance of cancer cells to ionizing radiation via modulation of oxidative stress. PloS One 9, e111911.

Yamada, T., Kawamata, T., Walker, D.G., and McGeer, P.L. (1992). Vimentin immunoreactivity in normal and pathological human brain tissue. Acta Neuropathol. (Berl.) 84, 157–162.

Yang, D.-I., Chen, S.-D., Yang, Y.-T., Ju, T.-C., Xu, J.-M., and Hsu, C.Y. (2004). Carbamoylating chemoresistance induced by cobalt pretreatment in C6 glioma cells: putative roles of hypoxia-inducible factor-1. Br. J. Pharmacol. 141, 988–996.

Yang, J., Dominguez, B., de Winter, F., Gould, T.W., Eriksson, J.E., and Lee, K.-F. (2011). Nestin negatively regulates postsynaptic differentiation of the neuromuscular synapse. Nat. Neurosci. 14, 324–330.

Yang, X., Wang, J., Liu, C., Grizzle, W.E., Yu, S., Zhang, S., Barnes, S., Koopman, W.J., Mountz, J.D., Kimberly, R.P., et al. (2005). Cleavage of p53-vimentin complex enhances tumor necrosis factor-related apoptosis-inducing ligand-mediated apoptosis of rheumatoid arthritis synovial fibroblasts. Am. J. Pathol. 167, 705–719.

Yasui, Y., Amano, M., Nagata, K., Inagaki, N., Nakamura, H., Saya, H., Kaibuchi, K., and Inagaki, M. (1998). Roles of Rho-associated kinase in cytokinesis; mutations in Rho-associated kinase phosphorylation sites impair cytokinetic segregation of glial filaments. J. Cell Biol. 143, 1249–1258.

Yen, S.H., Dahl, D., Schachner, M., and Shelanski, M.L. (1976). Biochemistry of the filaments of brain. Proc. Natl. Acad. Sci. U. S. A. 73, 529–533.

Yin, J.H., Yang, D.I., Chou, H., Thompson, E.M., Xu, J., and Hsu, C.Y. (2001). Inducible nitric oxide synthase neutralizes carbamoylating potential of 1,3-bis(2-chloroethyl)-1-nitrosourea in c6 glioma cells. J. Pharmacol. Exp. Ther. 297, 308–315.

Yoon, K.H., Yoon, M., Moir, R.D., Khuon, S., Flitney, F.W., and Goldman, R.D. (2001). Insights into the dynamic properties of keratin intermediate filaments in living epithelial cells. J. Cell Biol. 153, 503–516.

Yoon, M., Moir, R.D., Prahlad, V., and Goldman, R.D. (1998). Motile properties of vimentin intermediate filament networks in living cells. J. Cell Biol. 143, 147–157.

Yoshida, T., Tomozawa, Y., Arisato, T., Okamoto, Y., Hirano, H., and Nakagawa, M. (2007). The functional alteration of mutant GFAP depends on the location of the domain: morphological and functional studies using astrocytoma-derived cells. J HumGenet 52, 362–369.

Yoshida, T., Sasayama, H., and Nakagawa, M. (2009). The process of inducing GFAP aggregates in astrocytoma-derived cells is different between R239C and R416W mutant GFAP. A time-lapse recording study. Neurosci. Lett. 458, 11–14.

Yoshida, Y., Chiba, T., Tokunaga, F., Kawasaki, H., Iwai, K., Suzuki, T., Ito, Y., Matsuoka, K., Yoshida, M., Tanaka, K., et al. (2002). E3 ubiquitin ligase that recognizes sugar chains. Nature 418, 438–442.

Yu, Z., Liu, M., Fu, P., Xie, M., Wang, W., and Luo, X. (2012). ROCK inhibition with Y27632 promotes the proliferation and cell cycle progression of cultured astrocyte from spinal cord. Neurochem. Int. 61, 1114–1120.

Yung, Y.C., Stoddard, N.C., Mirendil, H., and Chun, J. (2015). Lysophosphatidic Acid Signaling in the Nervous System. Neuron 85, 669–682.

Zamanian, J.L., Xu, L., Foo, L.C., Nouri, N., Zhou, L., Giffard, R.G., and Barres, B.A. (2012). Genomic Analysis of Reactive Astrogliosis. J. Neurosci. 32, 6391–6410.

Zeisel, A., Muñoz-Manchado, A.B., Codeluppi, S., Lönnerberg, P., La Manno, G., Juréus, A., Marques, S., Munguba, H., He, L., Betsholtz, C., et al. (2015). Brain structure. Cell types in the mouse cortex and hippocampus revealed by single-cell RNA-seq. Science 347, 1138–1142.

Zhang, J.-G., Li, X.-Y., Wang, Y.-Z., Zhang, Q.-D., Gu, S.-Y., Wu, X., Zhu, G.-H., Li, Q., and Liu, G.-L. (2014a). ROCK is involved in vasculogenic mimicry formation in hepatocellular carcinoma cell line. PloS One 9, e107661.

Zhang, Q.-Q., Jiang, T., Gu, L.-Z., Zhu, X.-C., Zhao, H.-D., Gao, Q., Zhu, H.-Q., Zhou, J.-S., and Zhang, Y.-D. (2015). Common Polymorphisms Within QPCT Gene Are Associated with the Susceptibility of Schizophrenia in a Han Chinese Population. Mol. Neurobiol.

Zhang, S., Kanemitsu, Y., Fujitani, M., and Yamashita, T. (2014b). The newly identified migration inhibitory protein regulates the radial migration in the developing neocortex. Sci. Rep. 4.

Zhang, Y., Chen, K., Sloan, S.A., Bennett, M.L., Scholze, A.R., O'Keeffe, S., Phatnani, H.P., Guarnieri, P., Caneda, C., Ruderisch, N., et al. (2014c). An RNA-Sequencing Transcriptome and Splicing Database of Glia, Neurons, and Vascular Cells of the Cerebral Cortex. J. Neurosci. 34, 11929–11947.

Zhu, P., Jin, J., Liao, Y., Li, J., Yu, X.-Z., Liao, W., and He, S. (2015). A novel prognostic biomarker SPC24 up-regulated in hepatocellular carcinoma. Oncotarget 6, 41383–41397.

Nederlandse samenvatting

Dankwoord

List of publications

Curriculum vitae

Nederlandse Samenvatting

De hersenen zijn een zeer complex orgaan, bestaande uit verscheidene neuronale en niet-neuronale cellen. Elk celtype heeft zijn eigen rol, zo zijn neuronen gespecialiseerd in snelle communicatie, voorzien oligodendrocyten de hersenen van het vette myeline, en zijn astrocyten betrokken bij het in stand houden van de bloed-brein barrière, homeostase van energie en neurotransmitters en modulatie van neuronale signalen. Daarnaast zijn er ook nog niet-neurale cellen, zoals de microglia, die het immuunsysteem van het brein vormen.

Dit proefschrift gaat over astrocyten. Astrocyten spelen een belangrijke rol in de communicatie tussen de verschillende celtypes in het brein en worden wel beschouwd als integratoren van informatie in het brein, door hun grote oppervlak en contacten met vele verschillende neuronen en andere cellen. Ook in het zieke of beschadigde brein zijn deze cellen van belang, doordat de astrocyten dan reactieve astrocytose ondergaan, een breed omschreven proces van moleculaire, structurele en functionele veranderingen van de cel. Er zijn verschillende soorten astrocyten geidentificeerd, en één subtype wordt gevonden in de neurogene niche, waar ze kenmerken hebben van de stamcellen van het volwassen brein. Er wordt gedacht dat mutaties in deze cellen aanleiding kan zijn voor het ontwikkelen van hersentumoren van astrocytorigine.

Een van de eiwitten aan de hand waarvan we astrocyten herkennen en karakteriseren is het celskeleteiwit Gliaal Fibrilair Zuur Eiwit (GFAP). Dit eiwit is een lid van de intermediaire filament (IF) familie van eiwitten, waartoe ook bijvoorbeeld de haar- en huideiwitten keratines toe behoren. Het GFAP gen kan in de cel door post-transcriptionele veranderingen (mRNA splicing) in ten minste 10 verschillende isovormen voorkomen. Éen van deze isovormen, GFAPδ, is verrijkt in de stamcelniches in het menselijke brein, terwijl de standaardvariant GFAPα in astrocyten in het hele brein voorkomt en in grote hoeveelheden geproduceerd wordt bij ziekte. Beide isovormen zijn beschreven in astrocytoma tumoren en worden gerelateerd aan de kwaadaardigheid van de tumor. Dit proefschrift beschrijft de rol van GFAP in astrocytbiologie van het gezonde en zieke brein vanuit een celbiologische, moleculair biologische en biofysische invalshoek.

In **Hoofdstuk 1** hebben we IFs geintroduceerd, en dan specifiek type III IFs waaronder GFAP en Vimentine, en hebben we de bekende kennis over de biologische betekenis en moleculaire interacties van GFAP vergeleken met die van vimentine. De eiwitten hebben een vergelijkbare structuur en zijn nauw verwant, ondanks dat het N-terminale hoofd en de C-terminale staart van de twee eiwitten

juist veel verschillen vertonen. Ondanks de lage overeenkomst in structuur, blijken de eiwitten wel betrokken te zijn bij vergelijkbare processen in de cel. Op deze variabele N- en C-terminale domeinen zijn veel serine en threonine aminozuren aanwezig die gefosforyleerd kunnen worden, en die vaak betrokken zijn bij de specifieke interacties met andere eiwitten in de cel. Hierdoor is het waarschijnlijk dat de eiwitten GFAP en Vimentine bij vergelijkbare cellulaire processen een rol spelen, maar wel door met verschillende betrokken eiwitten interacties aan te gaan.

In **Hoofdstuk 2** hebben we reactive astrocytose in een astrocyt-cellijn (astrocytoom) en in primaire humane astrocyten geinduceerd door een mechanische schade aan de cellen toe te brengen. Dit is gedaan door cellen te kweken op een rekbaar membraan en dit met een luchtdrukpuls kort maar hevig uit te rekken. Deze benadering bootst het soort mechanische schade na die hersen cellen in traumatisch hersenletsel zouden ervaren. Daarna zijn de mRNA veranderingen van het genoom in de cellen in kaart gebracht met een microarray-transcriptoom platform. Interessant genoeg bleek dat zowel de astrocytoom als de primaire astrocyten gebruikt in dit model geen grote veranderingen ondergingen op transcriptioneel niveau. Verschillende oorzaken van dit onverwachte gebrek aan reactie werden onderzocht door het beschadigingsprotocol aan te passen. Maar in tegenstelling tot eerder gepubliceerde studies waren wij niet in staat om reactieve astrocytose te induceren. Dit was af te leiden uit een gebrek aan productie van mRNAs die veelal als indicatie van reactieve astrocytose worden gebruikt. Deze resultaten impliceren dat deze gekweekte cellen een groot incasseringsvermogen hebben van mechanische schade.

In **Hoofdstuk 3** hebben we aangetoond dat verschillende GFAP isovormen een verschillend effect hebben op de dynamische eigenschappen van het IF netwerk. We hebben waargenomen dat de omzetsnelheid tussen de oplosbare en de filamenteuze fractie van GFAPδ lager is dan die van GFAPα. Wanneer er meer van een van beide isovormen in de cel werd geintroduceerd, namen de focal adhesions, eiwitcomplexen waarmee de cel aan het substraat hecht, in grootte toe, al leidde dit niet tot een verandering in de beweeglijkheid van de cel. Hoge expressie van GFAPδ leidde wel tot een verandering van celvorm en zorgde voor een instorten van het IF netwerk, maar opmerkelijk was dat dit geen effect had op de beweeglijkheid of proliferatie van de cel.

In **Hoofdstuk 4** hebben we een analyse uitgevoerd op aanwezigheid van GFAP isovormen in verhouding tot astrocytoma kwaadaardigheid, gebaseerd op de Kanker Genoom Atlas patiëntendatabase. Deze analyse onthulde dat de GFAPδ/α verhouding toeneemt als de gradatie van de astrocytoom toeneemt. Om vast

te stellen of deze verhouding genexpressie beïnvloedt in astrocytomen, hebben we GFAP isovormen in een astrocytoom cellijn gemoduleerd door recombinante expressie of door 'knockdown' experimenten, gevolgd door transcriptoom analyse op een microarray platform. Door de genen die daar uit kwamen te vergelijken met de genen die in de patiëntendatabase correleerden met de GFAPδ/α verhouding, hebben we 8 genen geidentificeerd die gereguleerd worden door de GFAPδ/α verhouding en die relevant zijn voor tumor biologie en/of prognose.

In **Hoofdstuk 5** hebben we de GFAP- en Vimentinefunctie in het gezonde brein bestudeerd. Hiertoe hebben we de mRNA transcriptie profielen gekarakteriseerd van astrocyten en microglia die we acuut geisoleerd hebben uit wildtype muizen (WT), muizen zonder GFAP (GFAPko) of muizen zonder GFAP en Vimentine (VIM-GFAPko). Vergelijkbaar met bevindingen in Hoofdstuk 4 werd het duidelijk dat zowel GFAP als Vimentine betrokken zijn bij interacties tussen de cel en zijn omgeving. Uit een ontologiestudie bleek Vimentine daarnaast ook nog een rol te hebben in de regulatie van angiogenese gerelateerde genen. In de microglia geïsoleerd uit de GFAPko muis vonden er grote transcriptieveranderingen plaats, geïnduceerd door het verlies van GFAP in de astrocyten aangezien microglia geen GFAP maken. Dit ondersteunt de bevinding dat GFAP een functie heeft in cel-omgevings interacties. We hebben genen gegroepeerd gebaseerd op hun expressiepatronen en op die manier genen geïdentificeerd die alleen op GFAP modulatie reageren, die alleen op Vimentine modulatie reageren of die zowel op GFAP als op Vimentine modulatie reageren in dezelfde richting (een versterkend effect). Deze benadering onthulde meerdere mRNA transcripten stroomafwaarts van zowel GFAP en Vimentine, alsmede transcripten die alleen reageren op de modulatie van één van de twee IF eiwitten. Dit impliceert zowel unieke als gedeelde routes stroomafwaarts van GFAP en Vimentine.

In **Hoofdstuk 6** hebben we de bijdrage van GFAPα en GFAPδ aan de mechanica van de cel bestudeerd, een functie die van oudsher aan IFs wordt toegekend. Door gebruik te maken van een techniek waarbij cellen ontdaan worden van alle componenten behalve het IF skelet, waren we in staat om de bijdrage van alleen de verschillende GFAP isovormen aan de mechanica van het IF netwerk te meten. Dit meten werd uitgevoerd met de meerdere deeltjes-volgen microrheologie methode en hoewel deze methode niet gevoelig genoeg bleek voor deze nauwkeurige kwantitatieve metingen, wees het uit dat de IF netwerken stijver werden als er meer van beide GFAP isovormen in werd gebracht.

Tot slot hebben we in **Hoofdstuk 7**, nadat we bewijzen hebben gevonden dat GFAP betrokken is bij de communicatie tussen cellen of tussen cellen en de

extracellulaire matrix en dat GFAP een bijdrage levert aan de mechanische eigenschappen van cellen, verschillende uitkomsten op een rijtje gezet en een laatste analyse uitgevoerd om interessante overeenkomsten te destilleren. Hierbij vonden we door de vergelijking van transcriptoomanalyses van verschillende GFAP modulaties in verschillende modellen de eerder genoemde overeenkomsten van cel-omgevings interacties, maar ook onverwachte overeenkomsten van twee genen mogelijk betrokken bij het verwerken van glutamaat. Tot slot bediscussieren we nog aanknopingspunten voor toekomstig onderzoek, waarbij het mechanisme van regulatie van al deze genen door GFAP en Vimentine een belangrijk doel zal vormen.

Dankwoord

Nu dat alle puzzelstukjes voor mijn promotie eindelijk op hun plek zijn gekomen, ga ik een poging wagen enigszins volledig te blijven en iedereen te bedanken die mijn promotie mogelijk en/of een stuk aangenamer heeft gemaakt. In het bijzonder:

Elly, uiteraard! Dat ik met jou als supervisor en later ook promotor op een project kon beginnen waar ik vanuit het biologisch oogpunt van de hersenen naar de mechanica van de cel kon kijken was voor mij een waargeworden droom. Uiteraard is dat tijdens de promotie niet altijd een droom gebleven en heb ik (en jij misschien ook) regelmatig met de handen in het (bij mij steeds minder) haar gezeten. Toch heb ik dit proefschrift kunnen produceren, dankzij jouw diepe interesse in de fundamentele kennis over GFAP en dankzij de tijd die je nog beschikbaar maakte nadat ik alweer naar Eindhoven was vertrokken. Je bent altijd erg behulpzaam geweest om je ervaringen en contacten binnen de wetenschap te delen en dit is een bron van inspiratie, realisme, volhardendheid en soms ook relativisme geweest. Dank daarvoor!

Gijsje, als 2e promotor. Bedankt voor de gelegenheid om op het AMOLF experimenten te doen en cellen en eiwitten vanuit een heel ander perspectief te bestuderen. Ook zeker bedankt voor de flexibiliteit in het snelle lezen van m'n uiteindelijke manuscript en je kritische blik op de experimenten.

Willem, als copromotor ben je onmisbaar geweest voor het opzetten en uitvoeren van verscheidene experimenten. Bedankt ook voor alle tekstuele verbeteringen en nauwkeurige formuleringen van wat ik eigenlijk bedoelde. Daarnaast was je er als één van de drie achterblijvers voor discussies en gezelligheid toen er steeds minder astro's in het NIN rondliepen, ook daarvoor: bedankt!

Daarnaast ook zeker:

Dr.bulls&Dr.balls, PhD, thanks for giving me a standard to live up to, finally I have earned the right to join your sophisticated club.

Martina, "petite moeton", we zijn de halve wereld afgereisd en hebben samen veel leuke mensen ontmoet. Dank voor de A2M, de reacties op tandenstokergelen, het uit de brand helpen bij het last-second vinden van prachtige kadootjes en voor het zo veel leuker maken van onderzoek doen! Sorry dat je bijna Andrea moest bellen om te zeggen dat ik op een archeologische site verloren was geraakt.

Carlyn, thank you for being a creative inspiration in so many ways, always ready to correct my English, to have a coffee in the fresh air (science needs it) and to provide hugs when they were most needed. Also big thanks for your help on the

final finishing moments of this thesis.

Eloy, always optimistic and cheerful, you really know how to be a ray of sunshine in the life of scientists lucky enough to work with you, especially in thought provoking discussions. Thanks for that.

Regina, thanks for always making sure we have lunch on time and sharing music with me. Walking through the snowy center of Amsterdam to a performance of Winterreise was a great experience.

Marie, thanks for sharing and solving troubles in analysing sometimes complex transcriptomics data, and bringing a Scandinavian wind to the astro lab. I hope I will have many more conferences and visits to Stockholm in the future!

Ook alle andere sterren van de astro-groep:

Simone en Jinte, bedankt voor het stellen van een voorbeeld om naar op te leven vroeg in mijn project en voor het introduceren tot de hitchhikers guide.

Paula, bedankt voor alle adviezen van jou als wijze post-doc toen ik als jong aio-studentje kwam kijken, en dat je na je werk bij de astros pas echt m'n collega werd door bij FOM te gaan werken.

Lana en Anne, omdat jullie, net zoals ikzelf aan het eind, een beetje diaspora van Elly waren, zagen we elkaar helaas niet veel vaker dan op de groepsuitjes, maar bedankt voor alle gezelligheid daar!

Jacqueline, bedankt voor de enorme ervaring die je hebt overgedragen op het lab, voor het onderscheid tussen noodzaak en bijzaak op moleculair niveau en voor simpele oplossingen voor problemen die je hebt als je PCRs alleen maar in machines hebt gedraaid.

Lieneke, bedankt voor al je tips over IHC en microscopie en daaruit volgende mooie plaatjes, voor de gezelligheid en voor het samen in stand houden van het astro-gevoel in een lab vol veranderingen.

Miriam, bedankt voor alle wetenschappelijke en niet-wetenschappelijke steun die je hebt gegeven, we hebben aardig wat lief en leed gedeeld. Voor de toekomst stel ik voor dat we het leed schrappen en ons alleen maar op het lief richten! Veel geluk met Paul, Naomi en het aanstormend geluk.

Alle nieuwe leden van de astro-groep in Utrecht, bedankt voor het doorzetten van de groep.

Alle studenten die ik begeleid heb, Daniel, Astrid, Tim, Andi en Diana bedankt voor jullie bijdrage aan dit proefschrift en voor alle leerzame momenten aan zowel jullie als aan mijn zijde.

Emma, bedankt voor het oppakken van verscheidene uitkomsten van het onderzoek in dit proefschrift. Ik vond het super om met je op de IF-meeting in de VS te zijn en hoop dat je het GFAP-virus te pakken hebt en wellicht ook weer door gaat geven. Superleuk dat je op m'n promotie aan m'n zijde staat om daar dit werk te verdedigen.

De groep van Joost Verhaagen, bedankt voor vele discussies en gezellige momenten en voor het verwelkomen van mij in de werkbesprekingen op het moment dat de astrogroep al naar Utrecht was verhuisd. Koen nog in het bijzonder bedankt voor het introduceren tot de wondere wereld van R, en alle adviezen en beantwoorde vragen over microarray analyse.

De groep van Inge Huitinga en de Hersenbank, dank voor alle overheerlijke baksels en de gezelligheid op de vele momenten dat we een kamer deelden. Valeria, unfortunately the experiments didn't make it into this thesis, but thank you for your help with the TBI experiments.

Joop en Joris op het NIN en Marco op het AMOLF, dank voor het mogelijk maken van alle microscoopexperimenten en het oplossen van alle tegengekomen problemen.

De dames van het NIN, Jenneke, Wilma en Tini, dank voor alle gezellige lunches en de inzichten in het reilen en zeilen van het instituut en Jenneke ook nog voor alle obscure literatuur die je hebt kunnen vinden.

Everybody at AMOLF and in particular the Biological Soft Matter group of Gijsje, it was great to be a guest of your institute and group. After spending quite some time with you I realized I'm more of a biologist than I thought, but still I was able to enrich my experience with some solid biophysics.

Karin, bedankt voor alle gezelligheid, discussies, hulp en advies bij mijn experimenten en microscoopge –of ver-bruik.

Marjolein, bedankt voor het mogelijk maken van de kweekexperimenten op het AMOLF en gezelligheid bij de espressoautomaat. Ik hoop dat we in de toekomst elkaar nog eens bij een koor/orkestproject tegenkomen!

Everybody of the Mechanobiology consortium, thanks for inspiring meetings from the most fundamental networking models up to our brain biology. Especially Hedde and Thomas, thanks for the beautiful micrographs you were able to make in your lab. I hope to encounter all of you across science or elsewhere in the future.

The Intermediate Filament research community, that I was able to meet every year of my PhD on the biennial European and Gordon meetings. It was a great

inspiration to be able to discuss our favourite proteins in this open and friendly scientific community.

Jan Ruijter, bedankt voor hulp met en discussie over statistische problemen.

Berend Hooijbrink, bedankt voor het uitvoeren van de FACS experimenten.

Carlie de Vries en Vivian de Waard, dank voor de mogelijkheid om mechanische rekexperimenten uit te voeren met onze hersencellen in jullie vasculaire lab.

Joke, bedankt voor het altijd snel kunnen regelen van werkplekken en oplossen van andere problemen in Utrecht als ik hulpeloos bij je langs kwam.

Alle mensen met wie ik voor langer, kortere, of flexibele tijd een kamer heb gedeeld: Joost, Debbie, Nicholas, Roeland, Oscar, en iedereen die ik vergeet te noemen.

Mijn nieuwe collega's in Eindhoven: Cecilia, Carlijn, Rob, Nicole, Bart, Mariëlle, Ariane, Noortje en alle andere STBE-ers, dank voor de steun tijdens het schrijven van dit boekje naast m'n nieuwe project. 180° gedraaid van de hersens naar het hart, maar net zo'n leuke groep en onderzoek als in dit proefschrift beschreven.

DOT-groepers, Steven, Steven, Joost, Chantal, Ingeborg en Marscha, hoewel we het in de toekomst waarschijnlijk alleen maar weer drukker gaan krijgen, valt er met het afronden van dit proefschrift in ieder geval een obstakel weg om elkaar vaker te zien. Ik ben voor!

Sextet Douce Mémoire, Marleen, Allard, Sander, Sari, jullie hebben alle ups en downs meegemaakt tijdens repetities en daarna toen het zingen niet meer ging tijdens gezelligheid. Dank voor het zijn van vrienden in muziek en daarbuiten!

Mannen van het échte-manneneten, Jurriaan, Benjamin, Sander, Allard en David, dank voor alle discussies over de belangrijke dingen in het leven, zoals op welke temperatuur je je wollen truien moet wassen

Zangvrienden, spelletjesvrienden, en andere verwaarloosde vrienden: sorry!

Jurriaan en Yasemien, bedankt voor het blijven proberen om af te spreken! Wellicht moet ik spoedig weer een wat ruimer telefoonabonnement afsluiten als ik in de trein ineens niet meer hoef te schrijven, maar weer 50 minuten per rit kan bijpraten.

Martiene, bedankt voor de hulp met layouten van het proefschrift en voor de tips die me op cruciale momenten weer de organisatie en structuur in m'n project lieten herkennen.

Iedereen die ik toch vergeten ben: Sorry en bij deze alsnog bedankt!

En tot slot nog de familie die mij zo gesteund heeft:

Heleen, jou moet ik voor zoveel bedanken! Niet alleen heb je regelmatig op Sef opgepast om het Andrea en mij mogelijk te maken met onze studieprojecten bezig te blijven, maar ook zorgde je af en toe voor wat ontspanning voor Andrea. Hoe je de omslag van het boekje na wat losse-flodderideeën van mij ontworpen hebt als waar kunstwerk was een enorme inspiratie om het geheel weer met hernieuwde moed af te schrijven.

Mijn schoonfamilie, Evert en Anneke, bedankt voor de flexibiliteit met het oppassen op Sef en Anna, het steeds vaker verrassen met onverwachte gezonde maaltijden en het op de wereld zetten van Andrea (kom ik zo nog op terug)

Miriam, Lourens, Jeroen, Bart, Sanne en Chantal bedankt voor de gezelligheid, interesse en het steeds verder uitbreiden van de Tanges.

Al m'n zussen, Renée, Jeanine, Paula en Carola, jullie onafgebroken steun en luisterend oor zorgde ervoor dat ik regelmatig weer met hernieuwde energie en met georganiseerde gedachten door kon gaan. Jullie zijn de beste Sister Act die ik me maar kan wensen. Jeanine nog in het bijzonder bedankt voor het bijstaan bij de verdediging als paranimf, kan je toch nog even proberen hoe het is om een proefschrift te verdedigen.

Pap en mam, bedankt voor alle interesse, steun, trots en onwrikbaar vertrouwen in mijn vermogen om dit proefschrift af te ronden. En bedankt dat jullie tijdens mijn veel te enthousiaste reactie op het verzoek om iets meer over m'n promotie uit te leggen (>2 uur huiskamercollege) wakker zijn gebleven en ook daarna me nog steunden!

Andrea, mijn dank voor jou is moeilijk hier te verwoorden, want op elke dag van deze hele periode kan ik je voor minstens tien verschillende dingen bedanken (zo'n slordige 20.000 bedankjes). Maar om een tipje van de sluier te lichten: dank voor alle flexibiliteit, dank voor de muziek, dank voor het steunen in de moeilijkste momenten, dank voor het functionerend houden van ons gezin, waarvan onze reusachtige, vrolijke en lieve Anna en Sef het springlevende bewijs zijn, en ondanks dat het onze natuur is, bovenal dank voor de liefde.

List of Publications

Moeton, M., Stassen, O.M.J.A., Sluijs, J.A., van der Meer, V.W.N., Kluivers, L.J., van Hoorn, H., Schmidt, T., Reits, E.A.J., van Strien, M.E., and Hol, E.M. (2016). GFAP isoforms control intermediate filament network dynamics, cell morphology, and focal adhesions. Cell. Mol. Life Sci. CMLS.

Kamphuis, W., Kooijman, L., Orre, M., Stassen, O., Pekny, M., and Hol, E.M. (2015). GFAP and vimentin deficiency alters gene expression in astrocytes and microglia in wild-type mice and changes the transcriptional response of reactive glia in mouse model for Alzheimer's disease: GFAP and Vimentin in Alzheimer's Disease. Glia 63, 1036–1056.

Moeton, M., Kanski, R., Stassen, O.M.J.A., Sluijs, J.A., Geerts, D., van Tijn, P., Wiche, G., van Strien, M.E., and Hol, E.M. (2014). Silencing GFAP isoforms in astrocytoma cells disturbs laminin-dependent motility and cell adhesion. FASEB J. Off. Publ. Fed. Am. Soc. Exp. Biol. 28, 2942–2954.

Stassen, O.M.J.A., Jorna, R.J.J., Berg, B.A., Haghi, R., Ehtemam, F., Flipse, S.M., de Groot, M.J.L., Kiers, J.A., Nikerel, I.E., and Bellomo, D. (2011). Toward tunable RNA thermo-switches for temperature dependent gene expression. ArXiv Prepr. ArXiv11095402.

de Vrij, J., van den Hengel, S.K., Uil, T.G., Koppers-Lalic, D., Dautzenberg, I.J.C., Stassen, O.M.J.A., Bárcena, M., Yamamoto, M., de Ridder, C.M.A., Kraaij, R., Kwappenberg, K.M., Schilham, M.W., Hoeben, R.C. (2011). Enhanced transduction of CAR-negative cells by protein IX-gene deleted adenovirus 5 vectors. Virology 410, 192–200.

Curriculum Vitae

Oscar Stassen is geboren op dinsdag 26 maart 1985 te Venlo. Hij behaalde zijn diploma aan het Sint Willibrord Gymnasium te Deurne in 2003. In datzelfde jaar begon hij met zijn studie Life Science & Technology aan de Universiteit Leiden en de Technische Universiteit Delft. Hij behaalde zijn Bachelor of Science in 2008. Hiervoor deed hij stageonderzoek naar interacties tussen DNA Ligase I en Replicatie Factor C in het Leiden Institute for Chemistry onder begeleiding van Dr. Gregg Siegal en Dr. Hendrie de Groote. In de Master specialiseerde hij zich in de richting van Functional Genomics. In het kader hiervan nam hij deel aan het eerste team van de TUDelft in de international Genetically Engineered Machine competitie (iGEM). Daarna liep hij stage op de moleculaire celbiologie afdeling van het Leids Universitair Medisch Centrum, onder begeleiding van Prof. Dr. Rob Hoeben en Dr. Jeroen de Vrij, waar hij de mogelijke functies en toepassingen van proteïne IX in adenovirale vectoren bestudeerde. Hiermee behaalde hij in 2010 zijn ingenieurstitel. Daarna kon hij aan zijn promotie beginnen bij Prof. Dr. Elly Hol in de Astrocytebiologie en Neurodegeneratie groep op het Nederlands Instituut voor Neurowetenschappen, binnen het Nederlands Mechanobiologie programma. Het resultaat van dat werk vindt u in dit proefschrift.

Momenteel zet hij met veel plezier zijn onderzoek voort in de Soft Tissue Biomechanics & Engineering groep bij Prof. Dr. Carlijn Bouten en Prof. Dr. Cecilia Sahlgren aan de Technische Universiteit Eindhoven.